Journal of Research of the National Bureau of Standards Vol. 45, No. 6, December 1950 Research Paper 2155

Mass Spectra of the Deuteromethanes

By Vernon H. Dibeler and Fred L. Mohler

The four deuteromethanes have been synthesized and their mass spectra obtained with a Consolidated mass spectrometer. The sensitivities of the molecule ions of CH_4 and of CD_4 are equal within the estimated uncertainty. The total ionization is the same for CH_4, CH_3D, and CH_2D_2 but is significantly low for CD_4. The mass spectra of the deuteromethanes are not predictable from CH_4 by statistical considerations alone. In agreement with previously published data on CH_3D, probability factors of 1.18 and 0.45 were observed for the dissociation of an H atom or a D atom compared with the dissociation of an H atom from CH_4. Whereas these factors remain approximately constant for subsequent dissociations in the same molecule, they differ markedly for the three protiodeuteromethanes. Wide divergence is observed for some probability factors obtained in dissociations of two or more atoms.

I. Introduction

The use of deuterium and deuterated molecules in tracer experiments has given much information on reaction mechanisms, kinetics, and catalysis. One of the most rewarding methods of observing isotope exchanges and analyzing the reaction products of tracer experiments is that of mass spectroscopy. In all but the simplest experiments, however, this method requires calibration patterns of the substances encountered in the investigation, and it is obvious that eventually a complete catalog of mass spectra of deuterated and other isotopic molecules will be required. In addition to their practical value, mass spectra of isotopic molecules are of considerable theoretical interest. Studies of a few simple deuterated hydrocarbons have been reported by Delfosse and Hipple [1],[1] Evans, Bauer, and Beach [2], Mohler and Dibeler [3], and Turkevich, Friedman, Solomon, and Wrightson [4]. These studies indicate that although the sensitivity (ion current per unit of pressure) of the molecule ion and the total ion current for all dissociation processes is the same for isotopic molecules, the effect of deuterium substitution on the relative probabilities of the various dissociation processes is not predictable from statistical considerations alone. Appropriate corrections must be made for differences in dissociation probability of C—H and C—D bonds, as well as the difference in behavior of H atoms in normal hydrocarbons and H atoms in deuterohydrocarbons.

Although information has been published on the Raman [5] and infrared [6] spectra of all of the deuteromethanes, mass spectra of only CH_3D [2, 4] and CD_4 [4], and a partial spectrum of CHD_3 [4] have been reported. Accordingly, we report the complete mass spectra of all of the deuteromethanes to extend the published data on this group of molecules. Also, we wish to reexamine the statistical relationship of CH_4 to the deuteromethanes for the complete series now available.

II. Experimental Details

The mass spectra were obtained with a Consolidated mass spectrometer by using conventional techniques. The energy of the ionizing electrons was nominally 50 v. The temperature of the ionization chamber was about 245° C. Possible traces of hydrogen were pumped off of all samples at liquid hydrogen temperature, and the sample storage bulbs were cooled to liquid nitrogen temperature before samples were admitted to the mass spectrometer. The pressure of the sample in the inlet reservoir was measured with a diaphragm-type micromanometer [7].

Methane was "research grade" material obtained from Phillips Petroleum Co. and used without further purification. The purity, as stated by the manufacturer, was 99.7 mole percent. The most probable impurities were nitrogen, ethane, and carbon dioxide.

Mono-, di-, and trideuteromethane were prepared by the reaction of lithium aluminum deuteride on the appropriate bromo-methane, according to the method of Finholt, Bond, and Schlesinger [8]. The apparatus and techniques were similar to those previously used in the reduction of halomethanes with lithium aluminum hydride [9].

In addition to the methanes, small amounts of heavier hydrocarbons and hydrogen were observed in the products. These were effectively removed as described above before the sample was admitted to the mass spectrometer. As the attainment of high isotopic purity became more difficult with increasing numbers of D atoms in the molecule, no attempt was made to prepare tetradeuteromethane by this method. The CD_4 was very kindly given by Leo A. Wall. It was prepared by the reduction of carbon dioxide with deuterium over a supported nickel catalyst. The product contained 1.8 mole percent of CHD_3. Hydrocarbons heavier than CD_4 were not detected by the mass spectrometer.

The observed sensitivity of CH_4 (31.2 div/micron) and of CD_4 (31.9 div/micron) were considered equal within the estimated experimental uncertainty. The average value (31.5) was assumed for the sensitivities of CH_3D, CH_2D_2, and CHD_3, and on this basis the mass spectra of the deuteromethanes were corrected for isotopic impurities. After correcting the mass spectrum of "CH_3D" for the contribution of ions containing carbon-13, a residual peak on mass 18 above the normal H_2O background indicated the presence of 1 percent of CH_2D_2. The sum of the partial pressures of CH_3D and CH_2D_2 (obtained from the mass 17 and 18 peak heights and the sensitivities)

[1] Figures in brackets indicate the literature references at the end of this paper.

subtracted from the total sample pressure indicated 1 percent of CH_4 also present. An exact correction of the mass spectrum was made for the latter, and an approximate correction was made for the CH_2D_2.

Similarly, the mass spectrum of the sample of dideuteromethane showed a trace of CHD_3. The total partial pressures of the CHD_3 and CH_2D_2 subtracted from the sample pressure indicated the presence of 10 percent of CH_3D plus CH_4. Approximate corrections were made to the mass spectrum assuming the amount of CH_4 to be negligible.

The isotopic purity of the trideuteromethane was the least satisfactory of the group. The product obtained from the reaction of lithium aluminum deuteride with bromoform was only 60 percent of CHD_3. The partial pressures of the CD_4 impurity (obvious from the mass spectrum) and the CHD_3 subtracted from the total pressure gave a partial pressure assumed to be CH_2D_2. The corrected mass spectrum was in good agreement with the spectrum derived from a second sample of CD_4 obtained from Wall, containing 30 percent of CHD_3. This sample contained only a small amount of CH_2D_2, as indicated by the partial pressure computations. Finally, the mass spectra summarized in the following section were obtained by successive approximations, as indicated above. With the possible exception of CHD_3, this process should give satisfactory results. Fortunately, CHD_3 was not an appreciable impurity in any of the preparations. The estimated uncertainty in the principal ions of the spectra of CH_4, CH_3D, and CD_4 is about 1 percent. It is probably somewhat higher for CH_2D_2 and is estimated as 5 percent for CHD_3.

III. Results

The relative ion intensities obtained for methane, and the four deuteromethanes are given in Table 1. Correction has been made for ions containing carbon-13. The sum of the carbon-group ions for each molecule is given near the bottom of the appropriate column. The measured sensitivity (molecule-ion current per unit of pressure) is also given for CH_4 and CD_4. No doubly charged ions were observed. One ion due to a metastable transition was observed in the spectrum of CD_4. This ion observed at $m/e=16.2$ was only 0.05 percent of the abundance of the molecule ion and was attributed to the delayed dissociation $CD_4^+ \rightarrow CD_3^+ + D$. No independent check on the isotopic composition of the methanes was employed. However, the mass spectrum of CH_3D is in excellent agreement with previously published data from two different laboratories [2, 4]. Also, the mass spectrum of CD_4 and the odd-mass ions of CHD_3 are in good agreement with the spectrum of CD_4 and the partial spectrum of CHD_3 previously reported by Turkevich et al. [4].

In the dissociation patterns of CH_3D and CH_2D_2, some of the mass peaks come from two different ions; for example, mass 14 is CH_2^+ and CD^+. In order to obtain information on the relative probabilities of dissociating H atoms and D atoms from various isotopic configurations, some assumption must be made to derive the relative amounts of each contributing ion obtained in the dissociation processes. In the case of CHD_3, this problem does not arise, as each peak comes from a single type of ion. It is unfortunate that experimental errors are greatest in this spectrum. In the computations for CH_3D and CH_2D_2, it will be assumed that the probability of removing one atom (either H or D) is equal to the probability of removing one H from CH_4; the probability of removing two atoms is equal to that of removing two H atoms from CH_4, and so forth. This assumption is consistent with the fact that the sums of the ions in CH_4, CH_3D, and CH_2D_2 are nearly equal, as shown in the following computations. Starting from the low-mass end of the CH_3D spectrum, the contribution of each type of ion is computed in the following manner: Mass 13 results from CH^+ only and is equal to 4.90 (table 1). As CH^+ and CD^+ are both formed by the dissociation of three atoms, the above assumption permits us to calculate the CD^+ abundance as the difference: CH^+ in CH_4 (8.21) minus CH^+ in CH_3D (4.90) equals 3.31. Further, the total abundance of ions of mass 14 in CH_3D is 8.80; consequently, the CH_2^+ abundance is given by $8.80-3.31=5.49$. Continuing in this manner, one computes the abundance of CH_2D^+ as 76.0 instead of the observed value 77.2. There is a residual error, because the sum of masses 13, 14, and 15 in CH_4 is not exactly equal to the sum of masses 13 to 16 in CH_3D. If the values for CH_4 are multiplied by 1.01, the sums are exactly equal, and no residual error occurs. This device merely distributes any error in the experimental data or in the assumptions. Similarly, for CH_2D_2 a factor of 1.013 eliminates the residual error. In this manner the ion abundances listed in table 2 were derived.

There are included in table 2, the *a priori* probabilities of removing H or D atoms from the three molecules to give the various ions. The abundances of the various ions are not in the ratios of the *a priori* probabilities. In CH_3D, for example, the observed abundance of the CH_2D^+ ion is not $\frac{3}{4}\times 87.0=65.2$, but 1.183 times 65.2 (77.2), where 87.0 is the corrected abundance of CH_3^+ in CH_4. On the other hand, the CH_3^+ ion in CH_3D is $0.45\times\frac{1}{4}\times 87.0=9.8$. The factors 1.18 and 0.45 are a measure of the prob-

TABLE 1. *Mass spectra of methane and the deuteromethanes for 50-v electrons*

m/e	CH_4	CH_3D	CH_2D_2	CHD_3	CD_4
1	7.05	5.92	4.40	2.05	.....
2	0.34	0.68	1.24	1.86	3.09
3	.....	.11	0.18	0.11	.....
4	.....	.....	.04	.09	0.22
12	2.57	2.46	2.39	2.30	2.19
13	8.21	4.90	2.80	1.42	.....
14	16.3	8.80	6.39	6.41	7.23
15	86.1	20.9	9.79	6.75	.....
16	100.0	77.2	30.7	13.2	12.5
17	.....	100.0	62.4	51.1	.....
18	.....	.....	100.0	27.7	83.0
19	.....	.....	.....	100.0	.....
20	.....	.....	.....	.....	100.0
Total C-group ions	213.2	214.3	214.5	208.9	208.9
Sensitivity	31.2	.....	.....	.....	31.9

TABLE 2. *Computed ion abundance in isotopic methanes*

CH_3D			CH_2D_2			CHD_3		
Ion	Abundance	A priori probability	Ion	Abundance	A priori probability	Ion	Abundance	A priori probability
CH_2D	77.2	3/4	CHD_2	62.4	1/2	CD_3	27.7	1/4
CH_3	9.8	3/4	CH_2D	24.9	1/2	CHD_2	51.1	3/4
CHD	11.1	1/2	CD_2	5.84	1/6	CD_2	13.2	1/2
CH_2	5.40	1/2	CHD	9.79	1/3	CHD	6.75	1/2
CD	3.40	1/4	CH_2	0.87	1/6	CD	6.41	3/4
CH	4.90	3/4	CD	5.52	1/3	CH	1.42	1/4
			CH	2.80	1/2			

ability of dissociating an H atom or a D atom from CH_3D compared with the dissociation of an H atom from CH_4. These probability factors are denoted by the symbols H (H_2D) and D (H_2D) in table 3. The letter outside the parenthesis indicates the atom dissociated, while the letters inside the parenthesis indicate the configuration before the dissociation, the presence of a carbon atom being understood. One can similarly compute H (H_2D_2) and D (H_2D_2). In CHD_3, one uses the observed sum of CD_3^+ and CHD_2^+ without reference to CH_4 to compute the corresponding factors H (HD_3) and D (HD_3).

Removal of two H atoms from CH_3D has an *a priori* probability of one-half compared with CH_4, and the probability factor can be expressed as the product of the probabilities H (H_2D) and H (H_2D). There is an assumption involved in expressing the probability of removing several atoms as the product of the independent probabilities, and it is of interest to see if the assumption leads to consistent results. There are two ways of removing H+D atoms from these molecules; removing H first or removing D first. For CH_3D, the probability for the observed CH_2^+ compared with the *a priori* value can be expressed as:

$$\frac{CH_2^+ \text{ from } CH_3D}{CH_2^+ \text{ from } CH_4} = 1/4 \times H(H_2D) \times D(H_2D) + 1/4 \times D(H_2D).$$

All terms are known except $D(H_2D)$, which can be computed from the above. There are three ways of removing 2H+D atoms to give CH^+, and all constants are known except D(HD), which can be derived in a manner similar to the above.

TABLE 3. *Probabilities of dissociating* H *or* D *atoms from deuteromethane ions*

CH_3D	CH_2D_2	CHD_3
$H(H_2D)=1.18$	$H(H_2D_2)=1.43$	$H(HD_2)=1.41$
$D(H_2D)=0.45$	$D(H_2D_2)=0.57$	$D(HD_2)=0.87$
$H(H_2D)=1.14$	$H(HD_2)=1.49$	$D(HD_2)=.78$
$H(HD)=1.21$	$(D(H_2D)=0.54)$	$(D(HD)=1.07)$
$D(H_2D)=0.73$	[a] $H(H_2D)=1.16$	$H(HD_2)=1.43$
$D(HD)=.78$	[b] $D(HD_2)=0.79$	$(H(HD)=0.95)$
	$(H(HD)=1.05)$	
	$(D(HD)=0.90)$	

[a] Derived by using value of $D(HD_2)$ from CHD_3 spectrum.
[b] Derived by using $H(H_2D)$ from CH_3D spectrum.

Computations for the dissociation of CHD_3 can be carried out in the same manner by using only the data from the CHD_3 spectrum. In CH_2D_2 more constants are involved, and data from CHD_3 or CH_3D must be used to derive one of the constants.

IV. Discussion

The constants derived from the three spectra are not entirely consistent. It should be noted that errors are necessarily cumulative in computing probabilities of removing successive atoms from the methanes, consequently computational errors are greatly magnified. $H(H_2D)$ can be derived either from CH_3D or CH_2D_2, but in the latter case the value of $D(HD_2)$ from CHD_3 must be used. The pairs of values derived for $H(H_2D)$ or for $D(HD_2)$ are entirely consistent in the three spectra. Values for $H(HD_2)$ from CH_2D_2 and CHD_3 are equal within experimental error. Other values do not check well. The values for $D(H_2D)$ are 0.73 from CH_3D and 0.54 from CH_2D_2. The former is probably more reliable, as the CH_2^+ ion in CH_2D_2 (table 2) is very small and any uncertainty in computing table 2 makes more uncertain the value derived from CH_2D_2. Values for H(HD) and D(HD) can be derived from all three spectra, and the values are quite divergent. Computations involve products of three probabilities, and thus errors are magnified. The values derived from the CHD_3 spectrum, $D(HD)=1.07$ and $H(HD)=.95$, are definitely contrary to expectations, as it seems to be quite generally true that the probability of removing H from a radical containing D is greater than 1, and the probability of removing D from a radical containing H is less than 1. In table 3 values that are considered less reliable are inclosed in parentheses.

It is concluded that the assumptions used to derive the probability constants are at least approximately true. The inconsistencies shown in table 3 are no greater than are to be expected if there are experimental uncertainties amounting to several percent of the maximum peak, and this is very likely true in the CH_2D_2 and CHD_3 spectra.

In criticism it can be said that it is probably not accurately true that the probability of removing one, two, or three atoms from these molecules is equal to the probability in CH_4. If one uses CD_4 as the basis of comparison, somewhat different values are derived. There is also reason to doubt whether the probability of removing two or three atoms is accurately equal to the product of the probabilities of removing single atoms, for appearance potential measurements show that H atoms can be removed in pairs to give H_2 and not 2H. However, L. G. Smith has shown [10] that most ions in methane are formed by the dissociation of H atoms. In any event, the assumption seems to be approximately true, and without this assumption there is little possibility of extending data on probability constants observed in one molecule to another. It has been pointed out by E. J. Wells that there are enough interrelations between constants to derive all the constants without the

assumptions that probabilities of removing atoms are equal to those found in methane. Unfortunately, one must base such a derivation on the values derived from CHD_3 that are considered least reliable experimentally.

V. Conclusions

The sensitivities of CH_4 and CD_4 differ by about 2 percent and are probably equal within the experimental uncertainty. The total ionization is apparently the same for CH_4, CH_3D, and CH_2D_2. The low value for CHD_3 is not significant in view of the uncertainty in this spectrum. The difference in the total ionization of CH_4 and CD_4, however, is greater than the estimated error; and since the number of dissociation processes remains the same, the difference is probably a result of the lower probability of dissociating C–D bonds.

Although our experimental results for CH_3D are in good agreement with Turkevich et al. and with Evans, Bauer, and Beach, the different authors have used somewhat different assumptions in the interpretation of results. Although the assumptions used by Evans, Bauer, and Beach lead to nearly the same results in CH_3D, their assumptions did not seem to be generally applicable to the three spectra CH_3D, CH_2D_2, and CHD_3, necessitating the different approach used in this work.

VI. References

[1] J. Delfosse and J. A. Hipple, Phys. Rev. **54,** 1060 (1938).
[2] M. W. Evans, N. Bauer, and J. Y. Beach, J. Chem. Phys. **14,** 701 (1946).
[3] F. L. Mohler and V. H. Dibeler, Phys. Rev. **72,** 158A (1947).
[4] J. Turkevich, L. Friedman, E. Solomon, and F. M. Wrightson, J. Am. Chem. Soc. **70,** 2638 (1948).
[5] G. E. MacWood and H. C. Urey, J. Chem. Phys. **4,** 402 (1936).
[6] W. S. Benedict, K. Morikawa, R. B. Barnes, and H. S. Taylor, J. Chem. Phys. **5,** 1 (1937).
[7] V. H. Dibeler and F. Cordero, J. Research NBS, publication pending.
[8] A. E. Finholt, A. C. Bond, Jr., and H. I. Schlesinger, J. Am. Chem. Soc. **69,** 1199 (1947).
[9] V. H. Dibeler, J. Research NBS **44,** 363 (1950) RP2083.
[10] L. G. Smith, Phys. Rev. **51,** 263 (1937).

WASHINGTON, May 5, 1950

Journal of Research of the National Bureau of Standards Vol. 45, No. 6, December 1950 Research Paper 2156

First Dissociation Constant of Succinic Acid from 0° to 50° C and Related Thermodynamic Quantities

By Gladys D. Pinching and Roger G. Bates

The first dissociation constant, K_1, of succinic acid was determined at intervals of 5 degrees from 0° to 50° C from measurements of the electromotive force between hydrogen and silver–silver-chloride electrodes in cells without liquid junction. In order to reduce the correction for "overlapping" of the two acid groups, which are of nearly equal strengths, the 10 solutions studied contained twice as much succinic acid as acid succinate ion. The residual correction of about 0.02 in log K_1 was made with the aid of values of the second dissociation constant from an earlier determination.

The first dissociation constant between 0° and 50° can be expressed by

$$-\log K_1 = 1206.25/T - 3.3266 + 1.011697\,T,$$

where T is the absolute temperature. The changes of free energy, heat content, entropy, and heat capacity for the first dissociation step of succinic acid in the standard state were calculated from the dissociation constant and its temperature coefficient.

I. Introduction

A determination of the second dissociation constant of succinic acid from 0° to 50° was recently reported by the authors [1].[1] The two acid groups of this dicarboxylic acid are of nearly equal strengths, and there is considerable overlapping, or simultaneous dissociation. Hence, it was necessary to estimate the first dissociation constant, K_1, in order to compute the ionic concentrations required for an accurate determination of the second dissociation constant, K_2. Values of K_1 were therefore calculated from electromotive-force measurements of solutions of sodium acid succinate with added sodium chloride from 0° to 50° by means of a determination of the product of the two constants [2].

Although adequate for correcting the determination of K_2, these values of log K_1 were estimated to have an uncertainty of ± 0.01. Hence, it is doubtful if the earlier results for K_1 are of sufficient accuracy to warrant the calculation of the heat-content and entropy changes that are of considerable theoretical interest. It seemed desirable to undertake an accurate redetermination of the first dissociation constant in order to obtain reliable information concerning the thermodynamic quantities associated with the first dissociation step.

Ten mixtures of hydrochloric acid and sodium acid succinate were prepared, each containing the

[1] Figures in brackets indicate the literature references at the end of this paper.

TABLE 1. *Electromotive force of cell* I *from 0° to 50°*

m	Temperature, °C										
	0	5	10	15	20	25	30	35	40	45	50
	E	E	E	E	E	E	E	E	E	E	E
0.09959	0.50441	0.50572	0.50693	0.50818	0.50929	0.51035	0.51145	0.51250	0.51351	0.51448	0.51537
.09062	.50586	.50812	.50940	.51057	.51172	.51290	.51399	.51503	.51620	.51715	.51804
.08029	.50964	.51107	.51242	.51375	.51500	.51622	.51740	.51853	.51958	.52073	.52165
.07054	.51290	.51414	.515 4	.51697	.51831	.51954	.52078	.52182	.52302	.52408	.52523
.06035	.52112	.52272	.52424	.52574	.52725	.52861	.52999	.53133	.53262	.53392	.53500
.04983	.52118	.52288	.52441	.52592	.52735	.52868	.53022	.53160	.53292	.53418	.53547
.02977	.53364	.53555	.53737	.53913	.54086	.54248	.54410	.54569	.54724	.54878	.55024
.019875	.54350	.54558	.54751	.54945	.55131	.55320	.55498	.55670	.55836	.56007	.56171
.015114	.55020	.55243	.55446	.55655	.55846	.56054	.56238	.56430	.56623	.56804	.56969
.009890	.56023	.56265	.56499	.56728	.56953	.57174	.57383	.57593	.57797	.57991	.58190

latter at one and one-half times the molality, m, of the former, and the electromotive force of the cell,

$$\text{Pt; } H_2(g,\ 1\text{ atm}),\ \text{NaH succinate } (1.5\ m),\ \text{HCl } (m),\ \text{AgCl; Ag,} \qquad \text{(I)}$$

was measured at intervals of 5 degrees from 0° to 50°. The first dissociation constant of succinic acid was calculated from the experimental data. Corrections were applied for the amount of bivalent succinate ion formed in the solutions by dissociation of the acid succinate ion. The changes of free energy, heat content, entropy, and heat capacity for the dissociation of 1 mole of succinic acid in the standard state were evaluated from the dissociation constant and its temperature coefficient.

II. Experimental Procedures and Results

The stock solution of hydrochloric acid was prepared by dilution of a portion of redistilled acid. The mean deviation of five gravimetric analyses from the mean molality was less than 0.02 percent.

Sodium acid succinate, prepared from reagent-grade succinic acid and a standard solution of sodium hydroxide, was recrystallized from water with the addition of sufficient sodium hydroxide to bring the salt to the proper composition. After samples of the salt were dried at 110°, they were found to neutralize 100.03 percent of the theoretical amount of standard alkali. The titration was carried to pH 8.7 with the use of phenolphthalein and a color standard.

Nitrogen was passed through each buffer solution for 2 hr to remove dissolved oxygen. The cells were filled and placed in the water thermostat where they were kept at 25° for about 6 hr to insure initial equilibrium. The emf measurements from near 0° to 25° were made on the second day, and from 25° to 50° on the third, after which the temperature of the thermostat was lowered to 25° for a final measurement. The average difference between the initial and final emf of the 10 cells was less than 0.08 mv, or 0.0013 in log K_1. The electrodes were prepared in the same manner as for the determination of the second dissociation constant [1].

Each emf value, E, given in table 1 is the mean of the potentials between two pairs of electrodes in the same cell. The molality, m, of hydrochloric acid appears in the first column.

III. Calculation of the Dissociation Constant

Withdrawal of electrical energy from cell I causes the following electrochemical reaction to take place:

$$\tfrac{1}{2}\,H_2(g,\ 1\text{ atm}) + AgCl(s) = Ag(s) + H^+ + Cl^- \qquad (1)$$

The initial, reversible potential of the cell depends upon the extent to which the system is displaced from the equilibrium condition, that is, upon the difference between the reaction quotient, Q, and equilibrium constant, Q_e, for reaction 1. If the usual conventions regarding the standard state with respect to which activity, $\boldsymbol{a}$, is measured are observed, we may write

$$Q = \boldsymbol{a}_H \boldsymbol{a}_{Cl}, \qquad (2)$$

and

$$\Delta F = RT \ln Q/Q_e = \Delta F^\circ + RT \ln Q. \qquad (3)$$

In eq 3, ΔF is the molal free-energy change in reaction 1 for any particular state of the system and ΔF° is the corresponding quantity for unit activities of reactants and products.

Inasmuch as the solution is well buffered, the hydrogen ion formed by reaction 1 is largely utilized in converting acid succinate ion ($HSuc^-$) into molecular succinic acid (H_2Suc). The equilibrium between these constituents of the solution is the first dissociation of succinic acid:

$$H_2Suc = H^+ + HSuc^-;\ K_1. \qquad (4)$$

The activity of hydrogen ion is fixed by the activities of the two succinate species and by the first dissociation constant, K_1, of succinic acid. Hence, Q can be written

$$Q = K_1 \boldsymbol{a}_{H_2Suc} \boldsymbol{a}_{Cl} / \boldsymbol{a}_{HSuc^-}. \qquad (2a)$$

As only electrical work is of concern here,

$$\Delta F = -E\boldsymbol{F}, \qquad (5)$$

and

$$\Delta F^\circ = -E^\circ \boldsymbol{F}. \qquad (5a)$$

In eq 5a, E° is the standard potential of reaction 1 [3, 4] [2], and F is the faraday. Substitution of eq 2a, 5, and 5a in eq 3 and rearranging gives

$$-\log K_1=\left[\frac{(E-E^\circ)F}{2.3026RT}+\log m_{Cl}\right]+\log\frac{m_{H_2Suc}}{m_{HSuc^-}}+\log\frac{f_{H_2Suc}f_{Cl}}{f_{HSuc^-}}, \quad (6)$$

where f is an activity coefficient on the molal scale. In cell I, $m_{Cl}=m$.

If eq 6 is compared with the mass-law expression for the first dissociation (eq 4) in logarithmic form, it is seen that the portion of eq 6 enclosed in brackets actually represents the value of $-\log(f_H f_{Cl} m_H)$ in the particular solution for which the emf, E, was measured. For convenience, this experimental quantity will be called pwH.

The last term of eq 6 cannot be evaluated exactly without a knowledge of K_1. However, in agreement with the predictions of the Hückel equation [5], similar activity-coefficient terms for a number of weak monobasic acids have been found to be small and to vary linearly with ionic strength. By definition, this term is zero at infinite dilution. Hence, log K_1 at zero ionic strength was evaluated by extrapolation of log K_1', the value of log K_1 calculated by eq 6 with the last term set equal to zero.

The computation of the next to the last term on the right of eq 6 may be quite difficult for systems with two or more overlapping equilibria. The difficulty is aggravated if one group is moderately strong and the concentration of hydrogen ion is consequently an appreciable fraction of the ionic strength. Although the ratio of K_1 to K_2 for succinic acid is only 26 and overlapping is considerable, neither dissociation constant exceeds 10^{-4}, and the hydrogen-ion correction was readily evaluated.

When sodium acid succinate is dissolved in a solution of hydrochloric acid, as in the preparation of the buffer solutions used in this study, the reaction between hydrogen ion and acid succinate ion does not go to completion because of the small (but appreciable) dissociation of the molecular succinic acid formed (eq 4). Furthermore, the second dissociation constant is not small enough, nor the hydrogen-ion concentration large enough, to prevent the dissociation of a part of the acid succinate ion,

$$HSuc^- = H^+ + Suc^=;\ K_2. \quad (7)$$

It can be shown that the molalities of succinic acid and acid succinate ion remaining at equilibrium are given by the following equations:

$$m_{H_2Suc}=m-m_H+m_{Suc^=}, \quad (8)$$

and

$$m_{HSuc^-}=0.5\ m+m_H-2\ m_{Suc^=}. \quad (9)$$

The concentrations of the constituents of the cell solutions were so chosen that the concentration of succinic acid was about twice that of the acid succinate ion. In this way overlapping, as evidenced by the magnitude of $m_{Suc^=}$, was reduced. It should be emphasized, however, that this device is not always advantageous, for m_H, which usually cannot be measured accurately, is inevitably increased.

Values of m_H', a quantity that approaches the true hydrogen-ion molality, m_H, as the ionic strength decreases, were computed from pwH by

$$-\log m_H' \equiv \text{pwH}-2A\sqrt{\mu}/(1+7B\sqrt{\mu}). \quad (10)$$

The coefficient 7 in the denominator of the last term is the value found most suitable to describe the activity-coefficient term in mixtures of primary and secondary sodium succinates [1], and A and B are constants of the Debye-Hückel theory.

An exact expression for $m_{Suc^=}$ is the following:

$$m_{Suc^=}=K_2 m_{HSuc^-}\ (\text{antilog pwH})\ (f_{HSuc^-}f_{Cl}/f_{Suc^=}). \quad (11)$$

If the activity coefficients are again estimated by the the Debye-Hückel equation, an expression for $m_{Suc^=}'$ is obtained:

$$\log m_{Suc^=}' \equiv \log K_2+\log m_{HSuc^-}+\text{pwH}+2A\sqrt{\mu}/(1+7B\sqrt{\mu}). \quad (12)$$

Inasmuch as the dissociation constant is obtained by extrapolation to infinite dilution where uncertainties in the estimation of activity coefficients disappear, m_H' and $m_{Suc^=}'$ were used for m_H and $m_{Suc^=}$ in eq 8 and 9. The ionic strength is given by

$$\mu=1.5m+m_H'+m_{Suc^=}'. \quad (13)$$

The ionic concentrations required in eq 6 were accordingly calculated by eq 8, 9, 10, and 12 with the aid of the values of K_2 obtained in the earlier study [1]. The ionic strength needed to compute m_H' and $m_{Suc^=}'$ was obtained by arithmetic approximations. Both acid groups of succinic acid are fairly weak, and m_H' was only 1.6 percent of m for the most dilute solution studied. The extent of overlapping was greatest for the most concentrated solution, in which $m_{Suc^=}'$ amounted to about 1.5 percent of m.

Figure 1 illustrates the effect of the K_2 correction and of the method of estimating the activity coefficients on the determination of K_1. The circles and upper solid line (drawn by inspection) represent the final corrected values of pK_1' ($-\log K_1'$). If the correction for bivalent succinate ion had been omitted, the lower solid line would have resulted, and the value of pK_1 found would have been about 0.02 unit too low. If 4 had been chosen instead of 7 as the coefficient of the $B\sqrt{\mu}$ term in the denominator of eq 10 and 12, the extrapolation would have followed the broken line. However, the two upper lines converge satisfactorily, and the value of pK_1 at zero ionic strength would not have been altered.

The slopes, $-\beta$, of the plots of pK_1' *versus* μ were measured for each temperature and $\beta\mu$ added to pK_1'

[2] Reference [4] lists E° and 2.3026RT/F in absolute volts.

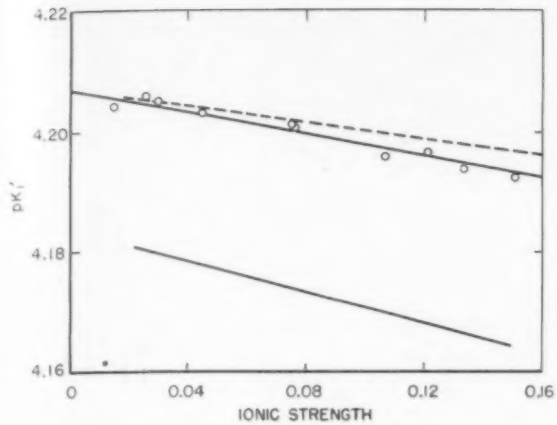

FIGURE 1. *Extrapolation of* pK_1' *to zero ionic strength at 25°.*

The broken line represents the best fit of the experimental values of pK_1' if 4 is used instead of 7 in the denominator of eq 10 and 12. Similarly, the position of the lower solid line illustrates the effect of omitting the correction for overlapping of the first and second acid groups.

computed from each experimental point. The resulting values of pK_1 were averaged. The mean pK_1 is listed in the fourth column of table 2, together with the average deviation of the 10 individual values from the mean at each temperature. The uncertainty in log K_1 is estimated to be less than ± 0.003 unit. The dissociation constant is given in the last column of the table. The values of log K_2 used to compute the correction for overlapping are given in the second column, and log K_1 derived from a measurement of K_1K_2 in the earlier study [1] appears in the third. The distribution of the individual results for pK_1' on either side of the mean at 0°, 25°, and 50° is shown in figure 2.

Earlier determinations of the first dissociation constant are summarized in table 3. No recalculation of any of the data has been attempted. Unfortunately, Jones and Soper [23], who also used the hydrogen–silver-chloride cell but a different method of calculation, do not list their emf values. Hence,

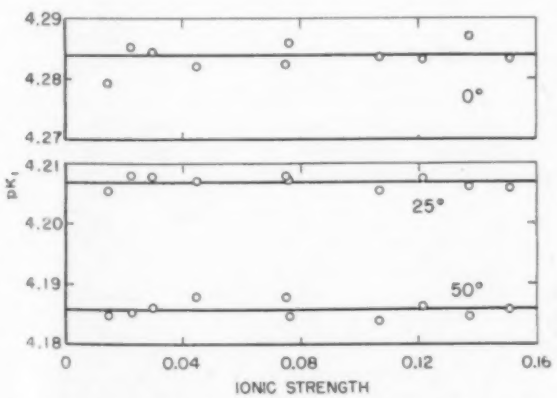

FIGURE 2. *Distribution of values of* pK_1 *at 0°, 25°, and 50°.*

TABLE 2. *Values of log* K_2, *log* K_1, *and* K_1 *from 0° to 50°*

Temperature	$-\log K_2$ (ref. 1)	$-\log K_1$ (ref. 1)	$-\log K_1$	$K_1 \times 10^6$
°C				
0	5.674	4.28_8	4.2845 ± 0.0018	5.20
5	5.661	4.26_8	4.2631 ± 0.0011	5.46
10	5.649	4.24_7	4.2449 ± 0.0008	5.70
15	5.643	4.23_9	4.2316 ± 0.0008	5.88
20	5.639	4.22_3	4.2176 ± 0.0008	6.07
25	5.636	4.20_8	4.2066 ± 0.0009	6.21
30	5.642	4.20_9	4.1980 ± 0.0008	6.34
35	5.648	4.19_4	4.1914 ± 0.0013	6.45
40	5.654	4.19_4	4.1878 ± 0.0012	6.50
45	5.670	4.19_9	4.1869 ± 0.0015	6.51
50	5.680	4.18_8	4.1863 ± 0.0010	6.52

TABLE 3. *Summary of determinations of Log* K_1

Reference	Method	t	$-\log K_1$
Conductance			
		°C	
1889, Ostwald [6]		25	4.177
1891, Crum Brown and Walker [7]		25	4.17
1891, Walden [8]		25	4.168
1904, Voerman [9]		25	4.186
1910, White and Jones [10]		0	4.250
		25	4.184
		35	4.181
1916, Böeseken and Verkade [11]		25	4.186
1935, Jeffery and Vogel [12]		25	4.179
Reaction rate			
1924, Duboux and Tsamados [24]	Sucrose inversion.	73	4.25
1928, Dawson, Hall, and Key [25]	I_2-acetone	25	4.201
Emf, cells with liquid junction			
1924, Auerbach and Smolczyk [13]	Q-cal	20	4.164
1925, Britton [14]	H-cal	18	4.036
1926, Mizutani [15]	H-cal	18, 20	4.09
1928, Simms [16]	H-cal	25	4.195
1928, Kolthoff and Bosch [17]	H-cal	18	4.18
1928, Gane and Ingold [18]	H-cal	25	4.133
1929, Ölander [19]	H-Q; Q at 18°	18	4.22
		50	4.219
1931, Gane and Ingold [20]	H-cal	25	4.193
1934, Ashton and Partington [21]	H-cal	25	4.060
1936, German and Vogel [22]	Q-cal	25	4.196
Emf, cells without liquid junction			
1936, Jones and Soper [23]	H-AgCl	25	4.162
		50	4.135
		74	4.132
1950, This investigation	H-AgCl	20	4.218
		25	4.207
		35	4.191
		50	4.186

* H = hydrogen electrode, Q = quinhydrone, cal = calomel.

the difference of 0.045 at 25° and 0.054 at 50° between the two determinations cannot be explained.

IV. Thermodynamic Functions

By the method of least squares, the following two equations were found to represent the values of log K_1 given in table 2:

$$-\log K_1 = A/T + B + CT = 1206.25/T - 3.3266 + 0.011697\,T, \qquad (14)$$

and

$$-\log K_1 = A^*/T + B^* + C^* \log T$$

$$= 2462.9/T - 47.9882 + 17.755 \log T. \quad (15)$$

The first has the form of the equation proposed by Harned and Robinson [26] to express dissociation constants as a function of temperature. It is based upon the observation that ΔF° is a quadratic function of T, whereas the second equation presupposes that ΔH° is a linear function of T. By differentiation of eq 14 and 15 with respect to temperature, two expressions for the temperature coefficient of log K_1 are obtained:

$$d \log K_1/dT = 1206.25/T^2 - 0.011697, \quad (14a)$$

and

$$d \log K_1/dT = 2462.9/T^2 - 7.7108/T. \quad (15a)$$

The corresponding second derivatives are:

$$d^2 \log K_1/dT^2 = -2412.5/T^3, \quad (14b)$$

and

$$d^2 \log K_1/dT^2 = 7.7108/T^2 - 4925.8/T^3. \quad (15b)$$

The changes of free energy, (ΔF°), heat content (ΔH°), entropy (ΔS°), and heat capacity (ΔC_p°) for the ionization process in the standard state were calculated by the following formulas:

$$\Delta F^\circ = -2.3026 RT \log K_1, \quad (16)$$

$$\Delta H^\circ = 2.3026 RT^2 (d \log K_1/dT), \quad (17)$$

$$\Delta S^\circ = 2.3026 R[\log K_1 + T(d \log K_1/dT)], \quad (18)$$

$$\Delta C_p^\circ = 2.3026 R[2T(d \log K_1/dT) + T^2(d^2 \log K_1/dT^2)]. \quad (19)$$

The values of these functions at 0°, 25°, and 50° C computed from the two empirical representations of the relationship between log K_1 and T are compared in table 4. Cottrell and Wolfenden [27] have combined their calorimetric data for ΔH° and its temperature coefficient with the dissociation constant found by Jones and Soper [23] to calculate the thermodynamic constants at 25° C. Their results, labeled (C and W) are included in table 4.

The two empirical equations, 14 and 15, evidently lead to appreciably different results for the thermodynamic functions at the extremes of the temperature range. Unfortunately, the only basis for a choice between them is the fit of the "observed" data. The mean departure of the calculated log K_2 from the observed is 0.0005 unit for eq 14 and 0.0011 unit for eq 15. Indeed, eq 14 usually provides the better fit of the observed dissociation constants

TABLE 4. *Comparison of thermodynamic functions derived from two different empirical equations (eq 14 and 15) for the variation of log K_1 with T*

Equation	ΔF°	ΔH°	ΔS°	ΔC_p°
		0° C		
	j mole^{-1}	*j mole*$^{-1}$	*j deg*$^{-1}$ *mole*$^{-1}$	*j deg*$^{-1}$ *mole*$^{-1}$
14	22,407	6,384	−58.6	−122
15	22,417	6,828	−57.1	−148
		25° C		
14	24,013	3,186	−69.8	−134
15	24,007	3,138	−70.0	−148
(C and W)	* 23,765	2,519	−71.1	−132
		50° C		
14	25,900	−293	−81.0	−145
15	25,908	−553	−81.9	−148

* From the value of K_1 found by Jones and Soper [23].

for weak electrolytes. Hence, eq 14, 14a, and 14b were used to compute the thermodynamic quantities listed in table 5. The estimated uncertainty in ΔF° is 18 j; in ΔH°, 300 j; in ΔS°, 1.0 j; and in ΔC_p°, 15 j.

TABLE 5. *Thermodynamic functions for the first dissociation of succinic acid*

Temperature	ΔF°	ΔH°	ΔS°	ΔC_p°
°C	*j mole*$^{-1}$	*j mole*$^{-1}$	*j deg*$^{-1}$ *mole*$^{-1}$	*j deg*$^{-1}$ *mole*$^{-1}$
0	22,407	6,384	−58.6	−122
5	22,706	5,767	−60.9	−125
10	23,016	5,138	−63.1	−127
15	23,337	4,499	−65.4	−129
20	23,669	3,848	−67.6	−131
25	24,013	3,186	−69.8	−134
30	24,367	2,513	−72.1	−136
35	24,734	1,828	−74.3	−138
40	25,111	1,132	−76.6	−140
45	25,500	425	−78.8	−142
50	25,900	−283	−81.0	−145

Cottrell and Wolfenden [27] estimated that ΔH° becomes zero at about 45° C. The dissociation constants found by Jones and Soper [23], on the other hand, appear to reach a maximum (and −log K_1 a minimum) between 50° and 74°. The temperature, T_{min}, at which −log K_1 passes through the minimum is readily calculated in terms of the constants of eq 14 and 15 by setting the first derivative equal to zero. Hence, from eq 14,

$$T_{min} = A/C, \quad (20)$$

and from eq 15,

$$T_{min} = 2.3026\ A^*/C^*. \quad (21)$$

The data of this investigation place the minimum value of −log K_1 at 47.9° C (eq 20) and 46.2° C (eq 21).

V. References

[1] G. D. Pinching and R. G. Bates, J. Research NBS **45,** 322 (1950) RP2142.
[2] R. G. Bates, J. Am. Chem. Soc. **70,** 1579 (1948).
[3] H. S. Harned and R. W. Ehlers, J. Am. Chem. Soc. **55,** 2179 (1933).
[4] R. G. Bates and G. D. Pinching, J. Research NBS **42,** 419 (1949) RP1982.
[5] E. Hückel, Physik. Z. **26,** 93 (1925).
[6] W. Ostwald, Z. physik. Chem. **3,** 241 (1889).
[7] A. Crum Brown and J. Walker, Ann. **261,** 107 (1891).
[8] P. Walden, Z. physik. Chem. **8,** 433 (1891).
[9] G. L. Voerman, Rec. trav. chim. **23,** 265 (1904).
[10] G. F. White and H. C. Jones, Am. Chem. J. **44,** 159 (1910).
[11] J. Böeseken and P. E. Verkade, Rec. trav. chim. **36,** 167 (1916).
[12] G. H. Jeffery and A. I. Vogel, J. Chem. Soc., 21 (1935).
[13] F. Auerbach and E. Smolczyk, Z. physik. Chem. **110,** 65 (1924).
[14] H. T. S. Britton, J. Chem. Soc. **127,** 1896 (1925).
[15] M. Mizutani, Z. physik. Chem. **118,** 318 (1926).
[16] H. S. Simms, J. Phys. Chem. **32,** 1121 (1928).
[17] I. M. Kolthoff and W. Bosch, Rec. trav. chim. **47,** 861 (1928).
[18] R. Gane and C. K. Ingold, J. Chem. Soc. 1594 (1928).
[19] A. Ölander, Z. physik. Chem. **A144,** 49 (1929).
[20] R. Gane and C. K. Ingold, J. Chem. Soc. 2153 (1931).
[21] H. W. Ashton and J. R. Partington, Trans. Faraday Soc. **30,** 598 (1934).
[22] W. L. German and A. I. Vogel, J. Am. Chem. Soc. **58,** 1546 (1936).
[23] I. Jones and F. G. Soper, J. Chem. Soc. 133 (1936).
[24] M. Duboux and D. Tsamados, Helv. chim. Acta **7,** 855 (1924).
[25] H. M. Dawson, G. V. Hall, and A. Key, J. Chem. Soc. 2844 (1928).
[26] H. S. Harned and R. A. Robinson, Trans. Faraday Soc. **36,** 973 (1940).
[27] T. L. Cottrell and J. H. Wolfenden, J. Chem. Soc. 1019 (1948).

WASHINGTON, JULY 6, 1950.

Journal of Research of the National Bureau of Standards Vol. 45, No. 6, December 1950 Research Paper 2157

Effects of Prior Static and Dynamic Stresses on the Fatigue Strength of Aluminum Alloys

By John A. Bennett and James L. Baker

Tests made on specimens of Alclad 24S–T sheet showed that prior static load had a marked effect on the fatigue strength in unidirectional bending when the stress amplitude was relatively small. From tests on bare 24S–T sheet, it was found that a few cycles at a stress amplitude of 17,000 lb/in.^{2} resulted in a large increase in the fatigue life at 20,000 lb/in.^{2} Damage tests for other combinations of stress amplitudes indicated that the damage was nearly a linear function of ratio of the number of cycles at a given stress to the number that would cause failure at that stress. A new design of specimen and a new form of stress versus number of cycles to fracture (S-N) diagram are described.

I. Introduction

The phenomenon of fatigue failure in metals remains incompletely understood, despite the extensive research that has been done on the subject. In particular, the mechanism by which a small volume of metal is damaged by repeated stressing until a crack forms may be considered one of the outstanding mysteries in the mechanical behavior of materials. The purpose of the work reported in this paper was to evaluate some of the factors involved in this damaging process by using aluminum alloy specimens. As there appears to be no reliable means of measuring fatigue damage except by a fatigue test, this evaluation was carried out largely by means of tests at two stress levels.

Many investigators have reported experimental data showing the effect of dynamic stressing at one amplitude on the fatigue strength at a second amplitude, but the data for aluminum alloys are not in good agreement. Miner [1] [1] found in testing 24S-T that the damage was proportional to the cycle ratio [2] within the experimental error. On the other hand, Stickley [2, 3] reported that the fatigue strength of 17S-T rod could be increased by prestressing at a stress amplitude slightly below the test stress. Likewise, Work & Dolan [4] found an increase in fatigue life due to stressing at small amplitudes. However, Dolan, Richart, and Work [5] found for 17S-T that the fatigue life under gradually varying load cycles was greater when the minor stress amplitude was 18,000 lb/in.^{2} than when it was decreased to 16,000 lb/in.^{2}

These results do not give any consistent picture of the progress of fatigue damage in aluminum alloys, and it was the purpose of this work to evaluate this progress in much the same way that it was done for SAE X4130 steel in the investigation reported in [6].

One of the most interesting phenomena associated with fatigue is the improvement due to understressing. In ferrous materials this improvement increases as the amplitude of the understress approaches the fatigue limit. Aluminum alloys have no fatigue limit, and the effect of understressing is not so marked, but it is known to cause an increase in fatigue strength under certain conditions. It seemed reasonable that during the course of a fatigue test at relatively low stress there must be a reversal in the

[1] Figures in brackets indicate the literature references at the end of this paper.
[2] Cycle ratio is defined as the ratio of the number of cycles at a given stress amplitude to the number necessary to cause failure at that amplitude. Failure may be defined as either the beginning of a crack or complete fracture.

type of process taking place, with improvement occurring during the early part of the test, and damage later. In order to investigate this, one of the prestress amplitudes chosen was low enough so that the number of cycles to fracture would be very large.

When a metal is subjected to fluctuating stress, there are presumably two opposing processes taking place, namely, work-hardening and fatigue damage. While the mechanism of fatigue damage may involve repeated plastic deformation of a microscopic volume of the metal, this is apparently distinct from the process that is usually referred to as work-hardening. It is to be expected that the greater part of this over-all hardening would be completed in a relatively few cycles at the start of the dynamic stressing. For this reason, it was decided to make tests after a very small number of cycles in order to detect changes due to work-hardening.

A few tests were made to determine the changes in fatigue properties caused by static stressing, prior to testing, for comparison with the changes caused by dynamic stressing prior to testing. In order to make the effect as pronounced as possible, the tests were made on Alclad 24S-T; the soft cladding would be expected to deform plastically at a lower stress than the core, producing a residual stress that would influence the fatigue properties.

Fatigue tests usually are performed by applying the fluctuating load until the specimen fractures. The life of the specimen, as determined by such a test, includes both the period of increasing damage, which culminates in the formation of a crack, and the period of crack growth, which ends with the fracture of the specimen. In order to study the first period without having the results confused by the second, it is necessary to determine as nearly as possible the point at which the crack forms.

II. Materials and Test Methods

All of the tests reported here were made on Krouse sheet bending fatigue testing machines. These machines are designed to load the specimen as a cantilever, the range of deflection being determined by the setting of an adjustable eccentric and the mean load by the adjustment of the movable vise. The amplitude of deflection remains constant during the course of the test, so that any change in the resilience of the specimen results in a change in the applied stress.

The materials used in this investigation were bare and Alclad 24S-T sheet. For the tests reported in sections III and IV, the materials were obtained commercially. For the study of damage reported in section V, the 24S-T sheet was obtained from the NACA Langley Aeronautical Laboratory from a stock maintained especially for fatigue research.

The two types of specimens used are shown in figure 1, a and b. The first is the standard type of specimen recommended by the testing machine manufacturer, while the second is a modification adopted for the reasons given in section IV. The over-all dimensions of the two specimens were the same, and the methods of test were identical. The specimens were cut with the long dimension parallel to the direction of rolling.

There is a possibility of confusion of terms in referring to the various surfaces and lines that bound a specimen cut from sheet material; in this report the term face will be used to refer to the surfaces of the original sheet. The surfaces at right angles to the faces and roughly parallel to the long dimension of the specimen will be called the sides, and the intersection of a face and a side will be termed an edge.

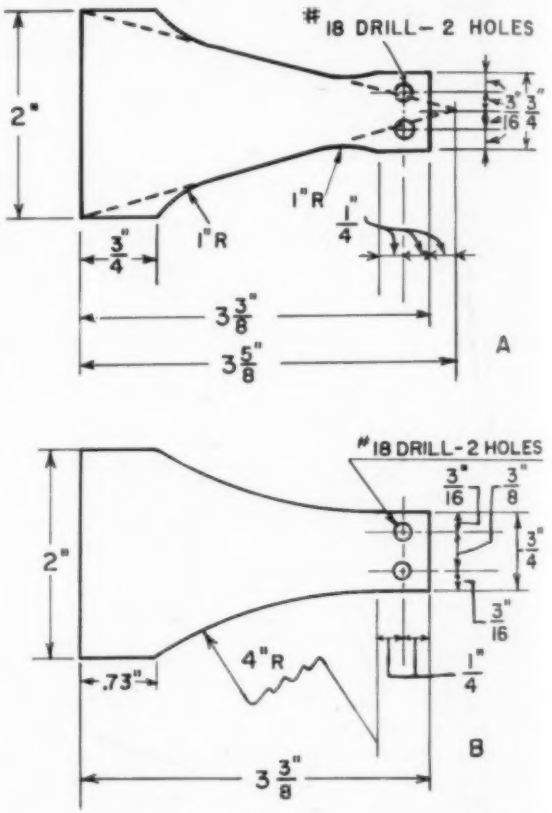

FIGURE 1. *Types of specimen used for bending fatigue tests on sheet materials.*

a, Standard specimen; b, modified specimen.

The edges of all specimens were manually polished with No. 400 Aloxite paper, the direction of polishing being parallel to the edge.

In both types of specimens the maximum stress in the reduced section was only about 25 percent greater than that at the point where the specimen was clamped in the vise. For this reason, there was some difficulty at first with the specimens breaking at the vise. This trouble was almost entirely eliminated by placing several thicknesses of greased paper between the specimen and the clamp-

ing plates to distribute the load. However, it is felt that in any future work with these machines it would be advisable to increase the width of the specimen at the vise to eliminate the need for this precaution.

The load necessary to produce a given stress in the specimen was calculated from the usual cantilever formula

$$P=\frac{Sd^2b}{6L},$$

where P is the load necessary to produce a given stress in the specimen; S is the nominal stress in the extreme fibers; d is the thickness of the specimen; b is the width of the specimen at a given point; and L is the distance from the point where the width is measured to the point at which the load is applied. The standard specimens had a reduced section that tapered toward the crank pin where the load was applied. This resulted in a constant nominal stress in the reduced section, as both the width of the specimen and the bending moment are proportional to the distance from the point of application of the load.

The specimens of 4-in. radius had no straight side, so it was necessary to use a special jig to determine the minimum value of the ratio b/L in the above formula. The jig is shown in figure 2. The pivot on which the vanes turn was at the same distance from the end of the specimen as the crank pin of the machine, and the extended edges of the vanes passed through this pivot. Therefore, if the vanes were rotated until they were tangent to the edges of the specimen, the point of tangency was the point of minimum b/L ratio. In use the jig was clamped to the table of a toolmaker's microscope and the length of the jig alined with the longitudinal measuring screws. Then the vanes were rotated until only a narrow gap remained between each vane and the corresponding edge of the specimen. The width of the specimen was measured near the center of this gap by using the transverse measuring screw, and the distance to the center of the pivot was measured with the longitudinal screw. In the figure a broken specimen is shown in place on the jig to indicate how the typical fracture occurred near the point of minimum b/L ratio.

III. Effect of Prior Static Load on the Fatigue Strength of Alclad 24S–T

The material used in this investigation was obtained commercially, and the surface was badly scratched and dented. These defects, however, did not appear to influence the fatigue test results. All of the tests were made in unidirectional bending with the mean load equal to half the maximum. The stress values given in this section refer to the maximum nominal stress in the cycle. The standard type of specimen (fig. 1, a) was used.

In order to obtain the basic S-N curve, 24 specimens were tested at the following nominal stresses; 20,000, 25,000, 30,000, and 35,000 lb/in.^{2} These results are shown in the first line of table 1 and are represented by the curve (not the points) on figures 3 and 4.

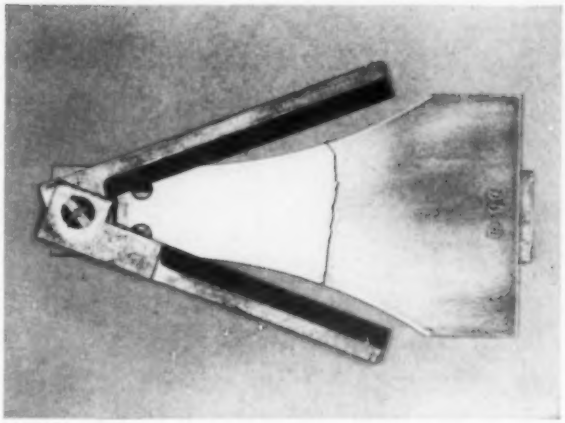

FIGURE 2. *Four-inch radius specimen in place on measuring jig.*

A broken specimen is shown in order to illustrate how the fractures occurred near the point of minimum b/L ratio.

The effect of prior static load was then determined for four conditions of loading, as follows: (1) static load corresponding to a nominal stress of 30,000 lb/in.^{2} applied in the same direction as the subsequent fatigue test load; (2) the same load applied in the direction opposite to that of the subsequent fatigue test load; (3) static load corresponding to a nominal stress of 40,000 lb/in.^{2} applied in the same direction as the subsequent fatigue test load; and (4) the same load applied in the opposite direction. In each case the prior static load was allowed to remain on the specimen for approximately 1 minute, then the fatigue test was started as soon afterward as possible. In most cases two specimens were tested for each load condition, the values given in table 1 being

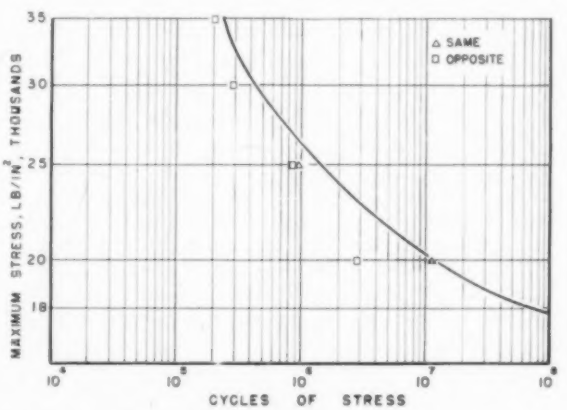

FIGURE 3. *Effect of prior static stress (nominal maximum value 30,000 lb/in.^{2}) on the fatigue properties of Alclad 24S–T sheet in unidirectional bending.*

Solid curve represents data for original material; squares are averages for specimens prestressed in direction opposite to test stress, triangles are averages for specimens prestressed in same direction as test stress.

TABLE 1. *Effect of prior static stress on the fatigue strength of Alclad 24S-T sheet*

(Fatigue test in unidirectional bending. Minimum stress=0, maximum nominal stress is listed)

Nominal static prestress	Direction of loading [a]	Average number of cycles to fracture at test stresses listed										
		No. of tests	20,000 lb/in.²	Range of values	No. of tests	25,000 lb/in.²	Range of values	No. of tests	30,000 lb/in.²	Range of values	No. of tests	35,000 lb/in.²	Range of values
lb/in.²													
None		6	$11,723\times10^3$	$13,693\times10^3$	4	$1,489\times10^3$	$1,002\times10^3$	8	461×10^3	221×10^3	6	253×10^3	26×10^3
30,000	Same	4	10,763	6,628	1	927							
40,000	do	2	23,660	2,885	2	920	284	2	357	64	3	222	49
30,000	Opposite	3	2,788	1,024	2	878	75	2	286	15	1	207	
40,000	do	2	2,166	448	2	677	34	2	508	149	2	255	76

[a] Direction of prior static load relative to fatigue test load.

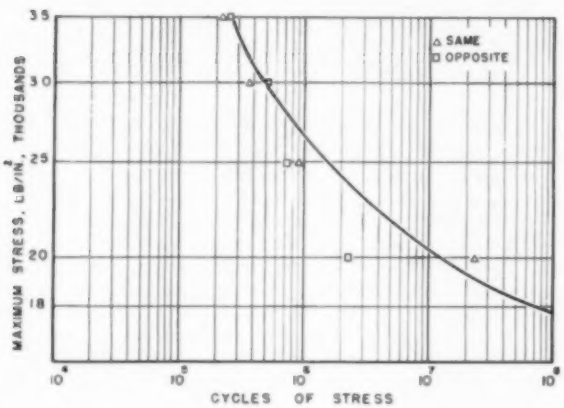

FIGURE 4. *Effect of prior static stress (nominal maximum value 40,000 lb/in.²) on the fatigue properties of Alclad 24S–T sheet in unidirectional bending.*

Solid curve represents data for original material; squares are averages for specimens prestressed in direction opposite to test stress, triangles are averages for specimens prestressed in same direction as test stress.

the averages of the number of cycles to failure for the specimens tested under identical conditions. In figure 3 the results for the specimens tested after a static stress of 30,000 lb/in.² are shown as individual points for comparison with the curve representing the fatigue properties of the original material, while the points in figure 4 represent the data for a prior static stress of 40,000 lb/in.² It should be emphasized that the stress values given here are calculated on the basis of elastic bending of the specimen. As there is considerable plastic deformation, particularly at the higher loads, these nominal values of stress are undoubtedly considerably different from the true stress. However, these values do indicate the magnitude of the bending moments applied to the specimens, which are significant from a practical standpoint.

The results indicate that there was little or no effect except at the lowest test stress used (20,000 lb/in.²). At this stress (20,000 lb/in.²) the effect was quite marked; for example, with a prior static stress of 40,000 lb/in.² the specimens loaded in the same direction as the fatigue test load endured 10 times as many cycles before fracture as those loaded in the opposite direction.

IV. Effect of Specimen Geometry on Results of Bending Fatigue Tests

As a result of the tests reported in the preceding section and other bending fatigue tests made previously, it was thought that the form of specimen commonly used in this type of machine had certain disadvantages. Although it is designed to have a section in which the stress is nominally constant, this section is bounded by fillets that raise the actual stress sufficiently to cause most of the failures to originate at the bottom of one of the fillets. Accordingly, it was thought better to make the specimens with each side formed by a single circular arc of large radius, and the design finally adopted is shown in figure 1, b. The reasons for selecting the value of 4 in. for the radius were as follows: (1) This is the largest radius that could be used with essentially the same over-all dimensions as the standard specimen; (2) it is sufficiently large so that the stress concentration due to the radius is negligible; (3) a sheet specimen having the reduced section formed by an arc of 4-in. radius on each side is being used for axial load fatigue tests in the Engineering Mechanics section of this Bureau, and it was thought that future comparisons of data would be simplified by having a similar reduced section on the sheet bending specimens; (4) it was desirable to have a radius that could be used also for R. R. Moore and axial load fatigue specimens, and new type specimens for these machines have been designed with a 4-in. radius; (5) 8-in. diameter milling cutters are readily available, so that the specimens could be milled with a single traverse of the cutter on each side. This factor is important in reducing the cost of the specimens.

In order to compare the results obtained with the two designs, 20 specimens of each type were prepared from a sheet of 24S–T nominally 0.102-in. thick. The results of fatigue tests made on these specimens are shown in table 2 and figure 5. All tests were made in completely reversed bending. Three specimens of each shape were tested at each of the four test stresses to determine the approximate relationship of the fatigue strengths, then seven additional specimens of each design were tested at a stress amplitude[3] of

[3] To avoid confusion it should be pointed out that the term *amplitude* is used here to mean the value of A in the equation for the stress at any time, t,

$$S = A\ (\sin 2\pi ft + B,$$

where f is the frequency of the testing machine, and B is the mean stress.

25,000 lb/in.^{2} in order to obtain a more accurate comparison of the dispersion of the data.

The fatigue strength of the 4-in. radius specimens was consistently higher than that of the standard specimens, although the difference was not large. The stress to cause fracture in a given number of cycles was, on the average, 5 percent higher for the new type specimens than for the straight tapered ones, the difference being greater the larger the stress amplitude. This difference might be ascribed either to the lower stress concentration in the 4-in. radius specimen or to an effect analogous to size effect, considering that the new specimen has a smaller volume of metal to which maximum stress is applied. If the latter factor were the chief consideration, it would be expected that the dispersion of the results for the tapered specimens would be less than that of the 4-in. radius type. However the coefficients of variation in table 2 indicate that the opposite is true, and that there is quite a difference in favor of the latter type. On the basis of these results it was concluded that the 4-in. radius specimen was a more satisfactory design than the tapered one, both as regards elimination of stress concentration and reduction of scatter of the results. Accordingly, specimens of this type were used in all of the subsequent work reported in the following sections.

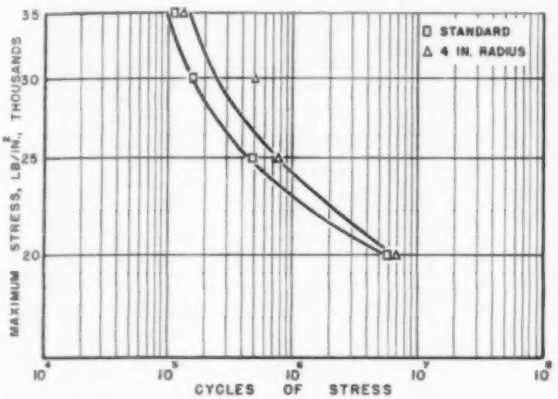

FIGURE 5. *Comparison of fatigue properties of 24S–T sheet obtained with standard and 4-in. radius specimens.*

TABLE 2.

A. Effect of specimen shape on fatigue strength of 24S–T sheet

Stress amplitude	Standard specimen		4-inch radius specimen	
	Number of tests	Average number of cycles to failure	Number of tests	Average number of cycles to failure
lb/in.^{2}				
20,000	3	$5,871\times10^3$	3	$6,644\times10^3$
25,000	10	493	10	743
30,000	3	146	3	536
35,000	3	113	3	132

B. Dispersion of data for a stress of 25,000 lb/in.^{2}

	Standard specimen	4-inch radius specimen
Average number of cycles to fracture $\overline{N}_F$	493×10^3	743×10^3
Standard deviation, σ[a]	319	289
Coefficient of variation, $100\sigma/\overline{N}_F$ (%)	65	39

[a] The values of standard deviation given here were computed by using the formula given on p. 14 of [9].

$$\sigma=\sqrt{\frac{\Sigma(X_i-\overline{X})^2}{n}}.$$

The more common form of the equation is

$$\sigma=\sqrt{\frac{\Sigma(X_i-\overline{X})^2}{n-1}},$$

and this difference should be kept in mind in comparing these data with those reported by other investigators.

V. Evaluation of Fatigue Damage in 24S–T Sheet

It was intended that this study of fatigue damage would follow approximately the same course as that described in the latter part of [6]. However, the data proved to be much less reproducible than the R. R. Moore tests on steel, so the results could not be so readily analyzed and only limited general conclusions could be drawn from them.

The determination of the point at which a crack starts in a fatigue specimen requires two techniques not ordinarily employed in fatigue testing, namely, stopping the test when a small crack has formed, and measuring the growth of the crack with increasing numbers of cycles. This provides information for estimating the number of cycles between the start of cracking and the first observation of the crack. The method used for stopping the test when a small crack had formed was that described by Foster [8]. This involved cementing a small diameter wire on to the surface adjacent to the critical sections of the specimen. The wire carried the operating current to a relay controlling the testing machine motor, so that when the wire was broken the machine would be stopped. It was reported in the reference cited that the wire did not break until a crack had formed under it. This was not found to be the case with the sheet specimens in bending, although the conditions reported by Foster were duplicated as nearly as possible. Wires cemented onto the face of the specimens broke in as little as one-fourth the number of cycles required to start a crack in the specimen. This caused a considerable delay for inspection of the specimen and cementing another wire in place. Accordingly, the wires were usually cemented onto the side of the specimen, a short distance away from the edge where the strain amplitude was not so great. This had the disadvantage that a somewhat larger crack was required to break the wire than when it was on the face, but the sensitivity was considered adequate.

After a small crack had been detected with the fracture wire, measurements of the growth of the crack were made at intervals until final fracture.

Figure 6 shows typical curves of crack length (expressed in terms of the ratio of the crack length to the width of the specimen at that point) versus number of cycles for three specimens tested with a nominal stress amplitude of 30,000 lb/in.^{2} The crack length was measured on the face of the specimen that had the longest crack, and the differences in the shapes of the curves in figure 6 are presumably due to differences in the development of cracks on the other face. The crack growth curves were extrapolated back to 0.01 crack-length ratio, and this was arbitrarily taken as the start of the crack. While this is obviously a rather approximate process for determining the start of cracking, the accuracy was considered adequate in view of the fact that the number of cycles from cracking to fracture was small in comparison to the number of cycles required to start the crack.

Several specimens were tested in the manner described above to determine the average number of cycles from cracking to fracture $\overline{(N_F-N_C)}$ (where N_F is the number of cycles at which the specimen fractured completely, and N_C is the number of cycles at which a crack first formed) at each of four stress amplitudes, 20,000, 25,000, 30,000, 35,000 lb/in.^{2} These values were then subtracted from the average number of cycles to fracture for all specimens tested at the corresponding stress amplitude in order to arrive at the average number of cycles to form a crack, N_C. Both of these sets of data are shown in figure 7 and also are given in table 3. Three tests were made at a stress amplitude of 18,000 lb/in.^{2} in order to obtain a better idea of the general shape of the *S-N* curve, but no determination of the start of cracking was made at this stress, as it was not to be used as a test stress in the evaluation of damage.

The evaluation of fatigue damage was carried out by stressing a specimen for a predetermined number of cycles at one stress amplitude, then testing it to fracture at a second amplitude. The damage was defined as the percentage decrease in the number of

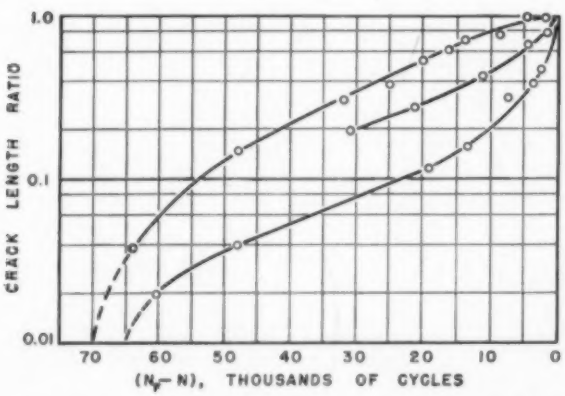

FIGURE 6. *Crack growth curves for 24S–T specimens tested at a nominal stress amplitude of 30,000 lb/in.^{2}*

Crack length ratio is equal to the crack length divided by the specimen width.

TABLE 3. *Data for S–N curve, 24 S–T sheet*

Stress amplitude	Number of specimens	Average number of cycles from beginning of crack to fracture (N_F-N_C)	Number of specimens tested	Average number of cycles to fracture, N_F	Calculated number of cycles to produce crack $N_C^*=N_F-\overline{(N_F-N_C)}$
lb./in.^{2}					
35,000	4	27×10^3	9	141×10^3	114×10^3
30,000	5	70	7	336	266
25,000	4	135	11	919	784
20,000	3	300	8	4,524	4,224
18,000	.....	.....	3	22,266	.....

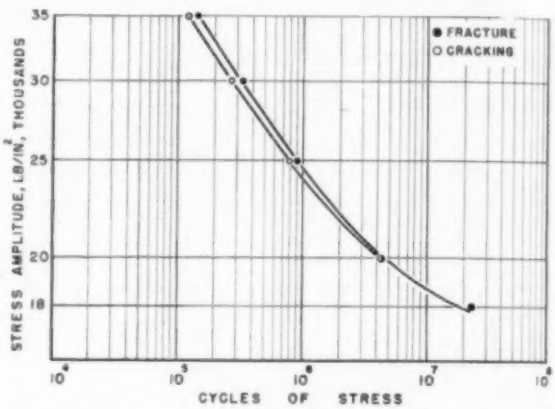

FIGURE 7. *S-N curves for cracking and fracture in 24S–T sheet specimens.*

cycles required to form a crack in the prestressed specimen as compared with the original material,

$$D=\frac{N_C-N_{CP}}{N_C}\times100,$$

where D is the percentage damage, and N_{CP} is the number of cycles at which a crack first formed in a prestressed specimen. None of the tests for the determination of N_C^* (calculated number of cycles to crack) had been made at the stress amplitudes chosen for the prestress, so the number of cycles to start of cracking had to be obtained by interpolation. To make this interpolation as accurate as possible, it was desirable to find a method of plotting the data that would give a straight line. As shown in figure 8, this condition was satisfied very closely by plotting the logarithm of N_C^* against the reciprocal of the stress, so the interpolation was performed on this basis.

Three prestress amplitudes were used, 17,000, 22,500, and 32,500 lb/in^2. For the lowest value, the number of cycles to start a crack was not known, so the numbers of cycles of prestress were arbitrarily selected as 2×10^3, 2×10^6 and 2×10^7. For the two higher stresses it was intended to apply the prestress for cycle ratios of 0.1, 50, and 90 percent. However, the number of cycles corresponding to the intended values of cycle ratio were determined on the basis of a group of tests made prior to starting the two-

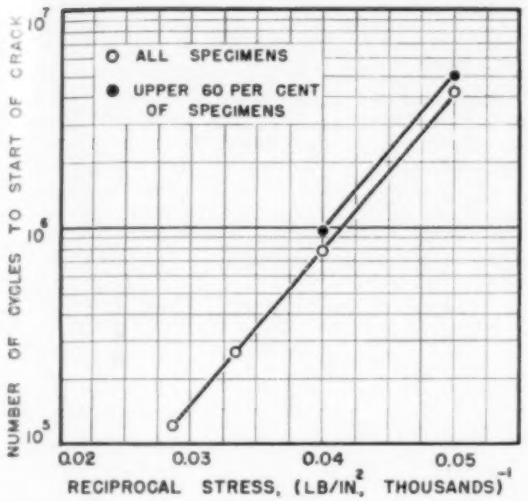

FIGURE 8. *Graph illustrating the linear relationship obtained when log N_C is plotted against the reciprocal of the stress amplitude.*

stress-level tests. Single-stress-amplitude tests were made of additional specimens after the damage tests had been started, and these changed the average values of N_C^*, so that the final values of cycle ratio were somewhat different from the intended ratios. The value of N_C^* originally obtained at 32,500 lb/in.^{2} was too low, so that the final cycle ratios are smaller than the intended values, whereas the reverse was true at 22,500 lb/in^2. In addition, the highest ratio at 22,500 lb/in^2. was altered as a result of specimens that failed before the prestressing was completed, as explained below. The final interpolated values of N_C^* which were used in determining cycle ratios were

Stress amplitude	N_C^*, 10^6 cycles
lb/in.^{2}	
22,500	1,650
32,500	175

The results of the damage tests are shown in figures 9, 10, and 11 and are listed in table 4. A negative value of damage indicates that the average life of the specimens that had been prestressed was greater than that of the original material at the same stress amplitude. There are two values of damage that exceed 100 percent; these are possible because the calculation of damage is based on N_C^*. If the average value of N_P for the prestressed specimens is less than the number of cycles from start of cracking to fracture, then the average N_{CP} will be negative, and the calculated damage will exceed 100 percent.

TABLE 4. *Summary of damage data, 24S–T sheet*

Test stress	2×10^5 cycles prestress		2×10^6 cycles prestress		2×10^7 cycles prestress	
	Number of specimens	Damage	Number of specimens	Damage	Number of specimens	Damage
	Prestress amplitude 17,000 lb/in.^{2}					
lb/in.^{2}		*Percent*		*Percent*		*Percent*
20,000	2	−448	3	−427	3	−33
25,000	3	65	3	−33	3	32
30,000	3	29	3	−3	3	43
35,000	3	14	3	26	3	11
	Prestress amplitude 22,500 lb/in.^{2}					
	0.1-percent cycle ratio		54-percent cycle ratio		80-percent cycle ratio	
20,000	4	−3	6	77	2	42
25,000	3	17	4	73	2	35
30,000	3	−9	3	62	5	−141
35,000	3	41	3	47	5	67
	Prestress amplitude 32,500 lb/in.^{2}					
	0.1-percent cycle ratio		42-percent cycle ratio		75-percent cycle ratio	
20,000	2	−8	3	48	3	77
25,000	5	58	3	57	4	105
30,000	3	−14	3	79	2	79
35,000	3	25	3	45	5	102

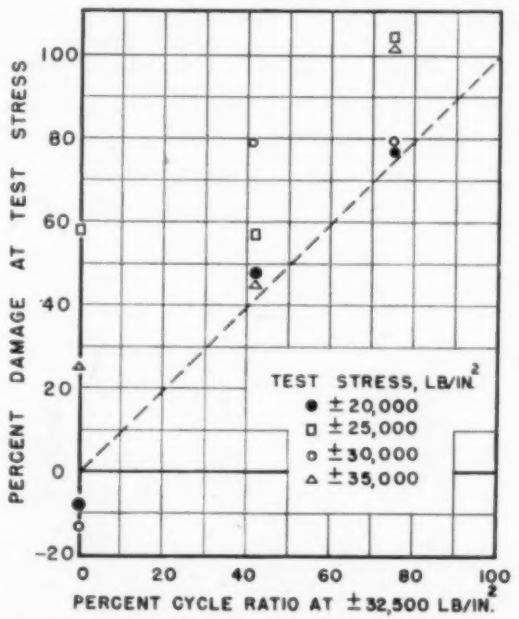

FIGURE 9. *Evaluation of fatigue damage due to prestressing at an amplitude of 32,500 lb/in^2.*

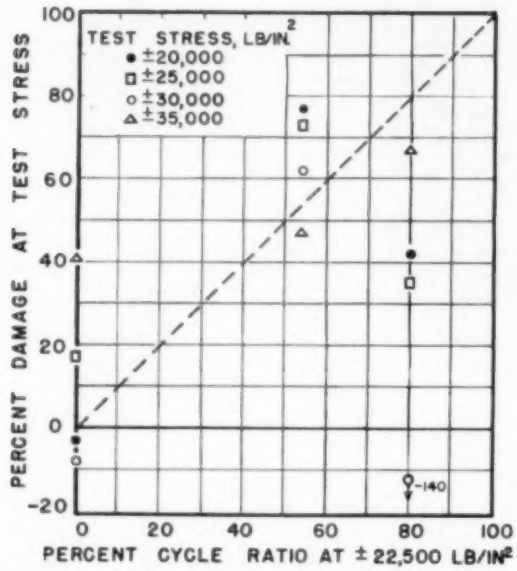

FIGURE 10. *Evaluation of fatigue damage due to prestressing at an amplitude of 22,500 lb/in².*

For the tests involving high cycle ratios, some of the specimens broke before the prestressing was completed. The corrections applied to the data to account for these failures are explained in the appendix.

It can be seen from the figures that the data were somewhat scattered. No attempt has been made to draw curves illustrating the trends of the data on figures 9 and 10, but a dashed line at 45° (representing a constant rate of damage) has been put on the figures for reference. While most of the points lie above this line, there is no consistency as to the relative position of the points representing the different test stresses. It appears also that the method of computing the cycle ratio for the largest number of cycles at ±22,500 lb/in.² introduced an appreciable error, as these results are quite out of line with the others for this prestress amplitude.

The effect of prestress at an amplitude of 17,000 lb/in.² was more pronounced, and the scatter therefore less important. As shown in figure 11, there was an increase in fatigue life as a result of this prestressing, which was particularly marked at the lowest test stress. The effect at all of the other test stresses was of approximately the same magnitude, so that only a single curve has been drawn on the figure to represent these data.

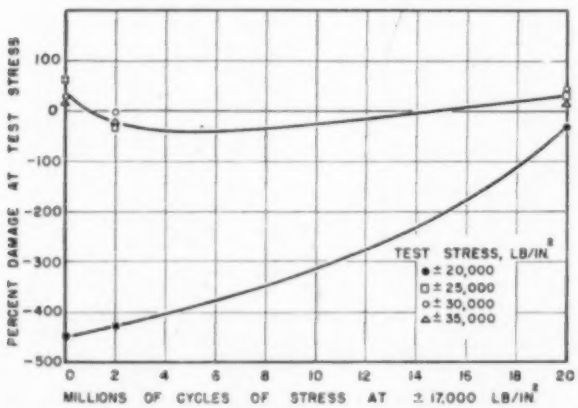

FIGURE 11. *Evaluation of fatigue damage due to prestressing at an amplitude of 17,000 lb/in².*

VI. Discussion of Results

The results of the tests described above indicate that both static and dynamic stress applied prior to the start of a fatigue test can have a marked effect on the fatigue life at relatively low stresses. In the case of the Alclad material tested in unidirectional bending, the changes caused by static bending were probably largely due to residual stress in the outer fibers of the sheet. In the case of the bare material tested in reversed bending, the improvement caused by a small number of cycles of stress slightly below the test stress was probably caused by cold-working. In both cases it appeared that the beneficial effect was eliminated by the fatigue stressing at all amplitudes above the lowest value used in the tests.

The dispersion of the data was so great that it would have been impossible to obtain results as precise as those reported previously for steel [6] without using an unreasonable number of specimens. It is not known how much of the difference in the scatter of the data was due to inherent difference in the material and how much was caused by the specimen geometry, but certainly the latter factor would be important. It is much more difficult to obtain reproducible conditions on the edge of a sheet than on the surface of a cylindrical specimen.

VII. Conclusions

As a result of flexural fatigue tests made on 24S-T aluminum alloy specimens the following conclusions were reached.

1. The application of a static bending load to the specimens had a significant effect on the fatigue life of the specimens under unidirectional bending, if the stress amplitude in the fatigue test was small. For a large static load in the same direction as the fatigue load, the fatigue life was increased, while the reverse was true if the directions were opposite.

2. A new design of specimen, having each side formed by a circular arc of 4-in. radius, was found to be more satisfactory than the straight tapered design. The new specimens were cheaper to manufacture, had less stress concentration in the test section, and gave more-reproducible results than the standard type.

3. Fracture wires were found to be a satisfactory means of stopping these tests when a small fatigue

crack had formed, but their use involved some difficulties.

4. The dispersion of the results of flexural fatigue tests on aluminum alloys was much greater than that of rotating beam test results on steel previously reported.

5. The relation between the reciprocal of the stress and the logarithm of the number of cycles to the start of cracking was found to be linear.

6. For prestress amplitudes of 32,500 and 22,500 lb/in.^{2}, the precision of the data was not sufficient to justify an exact statement regarding the progress of fatigue damage. The assumption of a linear relation between cycle ratio and damage was within the experimental error.

7. Prestressing at a stress amplitude of 17,000 lb/in.^{2} resulted in an improvement in fatigue life, that is, the damage was negative. For specimens subsequently tested at a stress amplitude of 20,000 lb/in.^{2}, the improvement in fatigue life after either 2,000 or 2,000,000 cycles of prestress was more than 400 percent.

IX. References

[1] Milton A. Miner, Cumulative damage in fatigue, Trans. ASME **67,** A-159 to 164 (1945).

[2] G. W. Stickley, Effect of alternately high and low repeated stresses upon the fatigue strength of 25S-T aluminum alloy, NACA Tech. Note 792 (1941).

[3] G. W. Stickley, Improvement of fatigue life of an aluminum alloy by overstressing, NACA Tech. Note 857 (1942).

[4] C. E. Work and T. J. Dolan, The influence of fluctuations in stress amplitude on the fatigue of metals (Part II), Ninth Progress Report, Office of Naval Research Contract N 6-ori-71-T.O. IV, Project N R 031-005 (University of Illinois, Sept. 1948).

[5] T. J. Dolan, R. E. Richart, Jr. and C. E. Work, The influence of fluctuations in stress amplitude on the fatigue of metals (Part I), Seventh Progress Report, Office of Naval Research Contract N 6-ori-71-T.O. IV, Project N R 031-005 (University of Illinois, July 1948).

[6] J. A. Bennett, A study of the damaging effect of fatigue stressing on X4130 steel, Proc. Am. Soc. Testing Mat. **46,** 693 to 711 (1946); also J. Research NBS **37,** 123 (1946) RP 1733.

[7] F. E. Richart, Jr. and N. M. Newmark, An hypothesis for the determination of accumulative damage in fatigue, Proc. Am. Soc. Testing Mat. **48,** pp. 767 to 800 (1948).

[8] H. W. Foster, A Method of detecting incipient fatigue failure, Proc. Soc. Exp. Stress Anal. IV [II], 25 (1947).

[9] ASTM Manual on presentation of data, Am. Soc. Testing Mat. (Philadelphia, Pa., 1947).

VIII. Appendix

1. Correction for Premature Failures

The proportion of premature failures for the four conditions in which they occur are

Stress amplitude	Cycle ratio or number of cycles	Premature failures
lb/in.^{2}		*Percent*
17,000	2×10^7	14
22,500	54%	14
22,500	98%	40
32,500	75%	7

For the first, second, and fourth conditions listed, the data were corrected for the premature failures by considering that these specimens had a value of $N_F=0$ at the test stress. As the values were actually less than zero, this assumption had the effect of making the average N_F at the test stress too high. However, for the conditions mentioned, where the proportion of premature fractures was small, this error was not considered significant.

For the third condition in this tabulation, the proportion of premature failures was so large that the method used in handling the data for the other three conditions was not considered satisfactory. Accordingly, a new value of cycle ratio was determined from the following considerations; as 40 percent of the specimens broke before the prestress was completed, those that were tested might be considered to be the strongest 60 percent of the population, and the average N_C for this portion is larger than that of the whole population. This new value, N_C, was determined by interpolation between the values for the top 60 percent of the specimens tested at $\pm25{,}000$ and $\pm20{,}000$ lb/in.^{2} (upper line on fig. 8). On this basis the cycle ratio of the specimens tested was 80 percent.

WASHINGTON, March 27, 1950.

Journal of Research of the National Bureau of Standards Vol. 45, No. 6, December 1950 Research Paper 2158

Boiling Points of Aqueous Solutions of Dextrose Within the Pressure Range of 200 to 1,500 Millimeters

By John L. Torgesen,[1] Vincent E. Bower, and Edgar R. Smith

By using twin ebulliometers of the Swietoslawski type, with water as the reference standard, data were obtained on the vapor-pressure–temperature relationship for aqueous solutions of dextrose. The pressures ranged from 200 to 1,500 millimeters and the concentrations of the solutions from 10 to 60 percent of dextrose by weight. The vapor-pressure–temperature relationship is expressed by equations of the form

$$\log_{10} p = A - \frac{B}{C+t},$$

in which p is the vapor pressure in standard millimeters of mercury exerted by a solution of a given concentration at the temperature, t, in degrees Celsius. A, B, and C are constants. The boiling-point elevations of aqueous dextrose solutions at a given pressure are expressed by equations of the form

$$\log_{10} \Delta t = \alpha + \beta c + \gamma c^2 + \delta c^3,$$

in which Δt represents the boiling-point elevation in degrees Celsius at a given pressure, c is the concentration in weight percentage of dextrose, and α, β, γ, and δ are constants.

I. Introduction

The boiling points and boiling-point elevations of aqueous solutions of dextrose within the pressure range of 200 to 1,500 mm and the concentration range of 10 to 60 percent of dextrose by weight are reported in this paper. This work is part of a program sponsored by the Corn Industries Research Foundation to obtain physical data for materials of importance in the manufacture of various corn products.

The method used was a comparative dynamic one for measuring successively, with the same thermometer, the boiling point of a given solution and that of water in twin ebulliometers connected to a manostat. A series of corresponding boiling points of the solutions and of water at various pressures was thus obtained. The values of t_s, the boiling point of a solution of dextrose, and t_w, the corresponding boiling point of water at the various pressures were related by equations of the form

$$t_s = a + b\, t_w + c\, t_w^2, \tag{1}$$

in which the constants a, b, and c for each concentration of dextrose were evaluated by the method of least squares. The values of t_w and the corresponding pressures taken as reference standards were selected from the compilation of Osborne, Stimson and Ginnings [1] [2] and have previously been tabulated in convenient form [2].

No equation was found to relate the boiling points of the solutions to their concentrations, at a given pressure, with the precision of the experimental data. For this reason the boiling points of solutions of even values of concentration were obtained graphically by plotting Δt, the boiling point elevation given by the difference between t_s and t_w, with respect to the concentration (or Δt/concentration versus concentration). From the resultant series of curves, one for each of the standard reference pressures, the values of Δt for even concentrations of dextrose were obtained, and the boiling points of the solutions were evaluated by adding the corresponding boiling point of water. These boiling points of the solutions were tabulated with their corresponding pressures and the constants A, B, and C in the Antoine equation [3]

$$\log p = A - \frac{B}{C+t}, \tag{2}$$

were evaluated to obtain the relationship between vapor pressure and temperature for each of the several even concentrations. (The symbol "log" is used in this paper to denote the logarithm to the base 10.) Equation 2 is explicit in temperature when written in the form $t = B/(A - \log p) - C$. Also

$$\frac{dp}{dt} = \frac{p(A - \log p)^2}{B \log e}. \tag{3}$$

The best equation that was found to represent the relationship between the measured boiling point elevations and the concentrations is of the form [4]

$$\log \Delta t = \alpha + \beta c + \gamma c^2 + \delta c^3, \tag{4}$$

in which the constants α, β, γ, and δ were evaluated by the method of least squares. But a comparison of the computed with the observed values of the boiling point elevation at a given pressure shows deviations that are several times larger than the precision of the original data.

[1] Research Associate at the National Bureau of Standards, representing the Corn Industries Research Foundation.

[2] Figures in brackets indicate the literature references at the end of this paper.

II. Apparatus and Materials

Except for minor changes, the apparatus was the same as described in a previous paper [2]. Two simple barometric ebulliometers, of the type developed by Swietoslawski [5], were sealed to a manostat. In the case of the solution ebulliometer, a flask containing water was interposed to inhibit the loss of water vapor from the solution to the manostat. Pressures below atmospheric were obtained with a mechanical pump, and those above were obtained by the addition of nitrogen from a cylinder.

The solutions of dextrose were prepared from NBS Standard Sample dextrose previously dried in a vacuum oven at 60° to 70° C for 6 hours and weighed into known weights of water. All concentrations, expressed in weight percentage on a vacuum basis, are corrected for the vapor and liquid hold-up that prevailed in the ebulliometer during the boiling procedure. Crystalline α-dextrose undergoes mutarotation in aqueous solution to form an equilibrium mixture of α- and β-dextrose [6]. The rate of the conversion is dependent on the temperature and pH of the solution, and the equilibrium amounts of α- and β-dextrose present depend on the temperature and concentration of the solution. Hence the solutions studied contained a mixture of α- and β-dextrose. However, since both forms possess identical molecular weights, no effect on the boiling point or the vapor pressure of a solution is to be expected as a result of different ratios of the two isomeric forms at different temperatures and concentrations.

The solution ebulliometer was charged with a known weight and volume of solution, the water ebulliometer with the proper volume of distilled water and the filling tubes sealed off. Boiling temperatures were measured at as near the same boiling rate as could conveniently be achieved, the rate being controlled to return approximately 20 drops of condensate per minute to the boiler as observed in the drop-counter placed in the return tube. This boiling rate approximates the midpoint of the flat constant-temperature portion of the curve obtained by plotting boiling temperature with respect to boiling rate [5] and was determined by initial experiments. The comparative measurements of temperature were made with a platinum resistance thermometer (coiled filament type) and a Mueller thermometer bridge by the method described in another paper from this laboratory [7]. The temperatures were measured to 0.001 deg C, with an average reproducibility of 0.002 to 0.003 deg C and an estimated accuracy of 0.005 deg C on the International Temperature Scale. It was not necessary to hold the bridge at constant temperature, as the temperature corrections to the resistances were practically identical for the temperatures of the reference and measured substances in these comparative measurements.

The ratios of the boiling points of the solutions to those of water at normal atmospheric pressure taken at the beginning and end of a series of measurements did not differ by more than 0.008 percent in the extreme case of the most concentrated solution. The average difference for the several concentrations studied was 0.003 percent. Refractive index measurements on the original and boiled solutions were practically identical. It is believed that no significant change in concentration occurred during the boiling procedure, although the solutions of higher concentration assumed a slight yellowish tint, particularly after boiling at the higher pressures. Specific rotations were not measured.

III. Experimental Results

The correction for the water vapor and liquid hold-up in the ebulliometer, to be applied to the concentrations of the solutions as originally prepared, was determined experimentally by using solutions of sodium chloride. For this purpose, a stopcock was sealed temporarily at the bottom of the solution ebulliometer for rapid withdrawal of samples while boiling. Solutions of sodium chloride of different known concentrations were placed in the solution ebulliometer and boiled in the usual fashion at normal atmospheric pressure. When boiling equilibrium had become established, as evidenced by steady boiling temperatures, a 25-ml sample was quickly withdrawn into a flask that was surrounded by ice water to minimize the loss of water vapor.

TABLE 1. *Determination of ebulliometer hold-up*

Charge	Original concentration of NaCl	Boiling rate	Boiling concentration of NaCl	Hold-up
g	*Percent*	*Drops/min*	*Percent*	*g*
65.086	11.760	12	11.873	0.62
65.119	11.760	20	11.891	.71
65.135	11.760	30	11.898	.75
70.008	22.195	12	22.391	.61
69.963	22.195	20	22.413	.68
70.087	22.195	30	22.440	.76

The samples were analyzed for sodium chloride by evaporation to dryness in platinum dishes on a steam bath, followed by heating to incipient fusion and weighing the sodium-chloride residue. The difference in concentration between the original and the boiling solution, together with the knowledge of the amount of original charge in the ebulliometer, provided data for the calculation of the hold-up of liquid and vapor while boiling was taking place at normal atmospheric pressure. It was assumed that the liquid hold-up remains essentially constant at all pressures involved. The vapor hold-up, which depends on the pressure and temperature, could be closely estimated from the knowledge of the free volume of the ebulliometer. Since this method of determining the hold-up may be of interest, the results are given in table 1. From these results, the amount of liquid and vapor hold-up at 20 drops a minute, which was the boiling rate employed in this work, was taken as 0.68 g, of which 0.61 g is attributed to liquid hold-up on the walls of the apparatus, and 0.07 g is a calculated value for the

TABLE 2. *Corresponding boiling points of dextrose solutions and water*

10.54-percent solution	Water	21.26-percent solution	Water	32.50-percent solution	Water	40.31-percent solution	Water	50.54-percent solution	Water	59.60-percent solution	Water	63.23-percent solution	Water
°C	°C	°C	°C	°C	°C	°C	°C	°C	°C	°C	°C	°C	°C
100.054	99.724	100.567	99.788	101.286	99.860	101.686	99.686	103.237	100.063	104.806	100.059	105.386	99.867
100.063	99.732	100.563	99.783	101.293	99.876	101.685	99.684	103.246	100.072	104.813	100.066	101.163	95.745
94.182	93.863	94.267	93.514	95.533	94.163	95.258	93.330	99.271	96.170	98.302	93.711	96.579	91.272
94.200	93.881	94.273	93.520	87.802	86.490	87.725	85.879	103.323	100.140	90.880	86.462	91.387	86.222
86.414	86.109	86.927	86.207	81.624	80.356	80.303	78.523	99.134	96.044	80.696	76.489	84.844	79.869
86.433	86.128	86.940	86.220	92.864	91.513	93.033	91.122	94.684	91.673	69.077	65.092	76.686	71.771
75.946	75.652	76.675	75.902	101.389	99.965	101.483	99.472	89.448	86.522	90.914	86.488	105.293	99.742
75.977	75.684	76.704	76.021	101.653	100.229	101.701	99.686	82.844	80.011	104.634	99.882	110.639	104.931
100.261	99.929	64.876	64.232	101.653	100.233	101.698	99.688	75.432	72.705	111.295	106.362	115.148	109.315
100.281	99.928	64.940	64.292	106.877	105.417	106.970	104.898	103.161	99.985	117.229	112.147	119.269	113.303
105.559	105.218	78.142	77.455	111.307	109.798	111.431	109.306	103.162	99.990	122.262	117.038	122.863	116.788
105.562	105.220	87.363	86.638	115.220	113.683	115.416	113.248	108.270	105.011	125.670	120.369	126.482	120.304
109.860	109.507	94.550	93.793	118.782	117.212	119.115	116.895	112.778	109.442	116.143	111.123	105.324	99.795
109.862	109.511	100.616	99.832	122.419	120.805	122.526	120.264	116.880	113.457	104.542	99.828		
113.867	113.508	100.791	100.007	101.522	100.098	116.730	114.542	120.461	116.972				
113.873	113.512	105.904	105.186			110.091	107.987	123.864	120.324				
117.356	116.998	110.293	109.463			101.731	99.722	103.191	100.031				
117.364	116.994	114.495	113.649										
120.838	120.461	117.897	117.030										
120.844	120.462	121.007	120.118										
118.216	117.843												
118.224	117.850	117.891	117.023										
114.205	113.843	114.405	113.556										
114.214	113.851	110.298	109.469										
110.450	110.095	105.852	105.044										
110.458	110.104	100.689	99.907										
106.190	105.844												
106.200	105.855												
100.296	99.934												
100.230	99.896												
100.235	99.902												
94.021	93.609												
94.034	93.712												
86.212	85.905												
86.228	85.922												
76.098	75.799												
76.124	75.825												
62.585	62.297												
62.641	62.344												
77.031	76.732												
86.288	85.982												
94.084	93.763												
100.080	99.747												

vapor hold-up at 760-mm pressure and the boiling temperature. At 200- and 1,500-mm pressure the calculated vapor hold-up is 0.02 and 0.12 g, respectively, giving a total hold-up at these extreme pressures of 0.63 and 0.71 g, respectively, assuming that the liquid hold-up remains constant over this pressure range.

The comparative boiling points of dextrose solutions of several concentrations and water, in the order as actually measured, are given in table 2. The concentrations listed are those prevailing during the boiling procedure at 760-mm pressure. The change in concentration accompanying the change in vapor hold-up with variation of the pressure is small but can be significant, particularly for the more concentrated solutions. For example, a 10-percent solution changes in concentration by −0.01 percent at 200 mm and by +0.01 percent of dextrose at 1,500 mm. A 60-percent solution changes by −0.04 and +0.04 percent at these extreme pressures.

By means of eq 1 the boiling points of the dextrose solutions were expressed as functions of the boiling points of water over the pressure range involved. The constants a, b, and c for each of the solutions are given in table 3. The average and maximum deviations of the experimental points from those calculated by eq 1 with the appropriate constants are given in the last two columns. The average deviations increase from ±0.002 deg C in the case of the more dilute solutions to ±0.013 deg C for the most concentrated solution. An explanation for the increasing experimental deviations at higher concentrations of dextrose is that the boiling equilibrium in the latter cases is established with less certainty. The pumping action in the ebulliometers is probably less efficient because of the increased viscosity of the solutions and, also, the concentration of the solution in the boiler may vary due to incomplete mixing of the condensate with the highly concentrated solution.

The boiling temperatures of the solutions at the standard reference pressures were calculated by means of eq 1 with the constants from table 3. The difference between the boiling temperatures of solution and water at a given pressure represents the boiling-point elevation, Δt, at that pressure. For each reference pressure, Δt was plotted with respect to the concentration on a scale that permitted the plotting and reading of temperatures to ±0.005 deg C and of concentrations to ±0.01 percent of dextrose.

Values of Δt at even concentrations were read from the curves and added to the corresponding boiling points of water to obtain the boiling temperatures of the solutions listed in table 4 at the reference pressures. A separate set of the constants A, B, and C in eq 2 was evaluated to fit the data for each solution given in table 4. Values of the constant C were determined by the method of averages, followed by an evaluation of constants A and B by the method of least squares. The values of the constants are given in table 5. The over-all average deviation of the vapor-pressure–temperature relationships expressed by eq 2 is ± 0.04 mm. The larger maximum deviations shown in the last column of table 5 were at the highest pressure, 1489.14 mm, in every case. Values of the temperature and rates of change of pressure with temperature at even values of the pressure are given in table 6.

The relationship between boiling point elevation and concentration was obtained by using the data in table 3 to calculate the boiling points of the solutions and boiling point elevations at the reference pressures. From the tabulations of Δt and concentration at a given pressure the constants α, β, γ, and δ in eq 4 were evaluated by the method of least squares. These constants are given in table 7 for several reference pressures over the range 200 to 1,500 mm. As the deviations given in the last two columns are considerably larger than the experimental precision, these equations were not used to evaluate Δt. They

TABLE 3. *Boiling points of dextrose solutions in terms of the boiling points of water*

$t_s = a + bt_w + ct_w^2$

Concentration of dextrose	a	b	c	Average deviation	Maximum deviation
Percent				°C	°C
10.34	0.3376	0.997929	0.2011×10^{-4}	±0.002	±0.003
21.26	.5516	.999929	.2377	±.002	±.004
32.50	.9815	1.000342	.4030	±.003	±.005
40.31	1.2027	1.004451	.3925	±.004	±.007
50.54	1.9000	1.007593	.5115	±.007	±.012
59.69	3.2872	1.003518	1.0454	±.009	±.026
63.23	4.7004	.988355	2.0042	±.013	±.023

TABLE 4. *Boiling points of dextrose solutions at standard reference pressures*

Pressure	Boiling point of water	Boiling point of solutions					
		10%	20%	30%	40%	50%	60%
mm Hg	°C	°C	°C	°C	°C	°C	°C
187.57	65	65.277	65.600	66.047	66.624	67.355	69.045
233.72	70	70.280	70.615	71.073	71.670	72.625	74.137
289.13	75	75.284	75.631	76.101	76.718	77.097	79.235
355.22	80	80.289	80.648	81.130	81.767	82.772	84.338
433.56	85	85.295	85.666	86.161	86.818	87.849	89.446
525.86	90	90.302	90.685	91.194	91.871	92.929	94.560
633.99	95	95.310	95.705	96.229	96.926	98.011	99.680
760.00	100	100.319	100.726	101.265	101.983	103.096	104.804
906.06	105	105.329	105.748	106.303	107.042	108.183	109.935
1,074.58	110	110.340	110.771	111.343	112.102	113.273	115.070
1,268.03	115	115.352	115.793	116.385	117.163	118.365	120.212
1,489.14	120	120.365	120.819	121.428	122.225	123.400	125.359

TABLE 5. *Vapor-pressure–temperature relationships of dextrose solutions*

$$\log p = A - \frac{B}{C+t}$$

Concentration of dextrose	A	B	C	Average deviation	Maximum deviation
Percent				mm Hg	mm Hg
10	7.912637	1636.365	224.883	±0.03	+0.08
20	7.902317	1633.713	224.618	±.05	−.14
30	7.900496	1637.294	224.907	±.05	+.25
40	7.888662	1636.304	224.764	±.01	+.02
50	7.853013	1622.430	223.205	±.05	−.11
60	7.779591	1587.450	219.244	±.04	+.17

TABLE 6. *Values of pressure, temperature, and rates of change of pressure with temperature for dextrose solutions*

Pressure	Concentration of dextrose solutions											
	10 Percent		20 Percent		30 Percent		40 Percent		50 Percent		60 Percent	
	Temperature	dp/dt	Temperature	dp/dt	Temperature	dp/dt	Temperature	dp/dt	Temperature	dp/dt	Temperature	dp/dt
mm Hg	°C	mm/°C	°C	mm/°C	°C	mm/°C	°C	mm/°C	°C	mm/°C	°C	mm/°C
*100	51.87	4.92	52.17	4.91	52.58	4.90	53.11	4.88	53.99	4.86	55.42	4.85
200	66.72	8.86	67.05	8.84	67.50	8.82	68.08	8.79	69.02	8.75	70.51	8.71
300	76.17	12.47	76.52	12.45	76.99	12.41	77.61	12.36	78.59	12.31	80.14	12.24
400	83.25	15.87	83.62	15.84	84.11	15.79	84.76	15.73	85.77	15.65	87.36	15.55
500	88.98	19.13	89.36	19.08	89.87	19.03	90.54	18.95	91.58	18.85	93.21	18.72
600	93.82	22.26	94.21	22.20	94.73	22.14	95.42	22.05	96.50	21.93	98.16	21.77
700	98.03	25.30	98.43	25.23	98.96	25.16	99.67	25.06	100.77	24.92	102.46	24.72
760	100.32	27.08	100.73	27.01	101.27	26.93	101.98	26.82	103.10	26.67	104.81	26.46
800	101.77	28.25	102.18	28.18	102.72	28.10	103.44	27.98	104.56	27.82	106.29	27.59
900	105.14	31.14	105.55	31.06	106.11	30.97	106.85	30.84	107.99	30.65	109.74	30.40
1,000	108.21	33.96	108.64	33.87	109.20	33.77	109.95	33.63	111.11	33.43	112.89	33.14
1,100	111.04	36.73	112.47	36.63	112.05	36.53	112.81	36.37	113.99	36.14	115.79	35.82
1,200	113.67	39.45	114.11	39.34	114.69	39.23	115.46	39.06	116.65	38.81	118.48	38.46
1,300	116.12	42.12	116.57	42.01	117.15	41.89	117.94	41.71	119.15	41.44	121.00	41.05
1,400	118.42	44.76	118.87	44.64	119.47	44.50	120.26	44.31	121.49	44.02	123.36	43.60
1,500	120.59	47.35	121.05	47.22	121.65	47.08	122.46	46.88	123.70	46.57	125.59	46.11
*1,600	122.65	49.91	123.11	49.78	123.72	49.63	124.54	49.41	125.79	49.08	127.70	48.59

* Extrapolated values.

TABLE 7. *Boiling-point elevation of dextrose solutions*

$\log \Delta t = \alpha + \beta C + \gamma C^2 + \delta C^3$

Pressure	α	β	γ	δ	Average deviation	maximum deviation
mm Hg					°C	°C
233.72	−0.989843	5.113375×10^{-3}	-7.377463×10^{-4}	5.526503×10^{-6}	±0.017	+0.032
355.22	−.982743	5.191070	−7.435453	5.463234	±.023	+.045
525.86	−.967871	5.239106	−7.477459	5.427242	±.028	+.055
760.00	−.944029	5.235447	−7.427223	5.345987	±.031	+.061
1,074.58	−.918243	5.251193	−7.490898	5.396036	±.033	+.067
1,489.14	−.885843	5.225459	−7.476027	5.404016	±.033	+.067

are useful, however, in calculating the boiling point elevations of dextrose solutions to within 0.05° to 0.1° C.

Molal boiling point elevations of aqueous solutions of dextrose have been measured by Juettner [8], but only at normal atmospheric pressure. A comparison of his values with those of this investigation is given in table 8. Apparently, there are no other published measurements of the vapor pressures of aqueous solutions of dextrose in the range reported in this paper.

TABLE 8. *Molal boiling-point elevation of dextrose solutions (760 mm Hg)*

Molality	Juettner [8]	This paper
	°C/mole	°C/mole
1	0.53	0.520
2	.53	.525
3	.53	.531
4	----------	.537
5	----------	.544
6	----------	.552
7	----------	.561
8	----------	.570
9	----------	.580

IV. References

[1] N. S. Osborne, H. F. Stimson, and D. C. Ginnings, J. Research NBS **23,** 261 (1939) RP1229.
[2] E. R. Smith, J. Research NBS **24,** 229 (1940) RP1280.
[3] G. W. Thomson, Chem. Rev. **38,** 1 (1946).
[4] F. J. Bates and Associates, Polarimetry, saccharimetry, and the sugars, NBS Circular C440, p. 365 (1942).
[5] W. Swietoslawski, Ebulliometry (Reinhold Publishing Corp., New York, N. Y., 1945).
[6] H. S. Isbell and W. W. Pigman, J. Research NBS **18,** 178 (1937) RP969.
[7] E. R. Smith and H. Matheson, J. Research NBS **20,** 641 (1938) RP1097.
[8] F. Juettner, Z. physik. Chem. **38, 76** (1901); Int. Crit. Tables **III,** 327 (1928).

WASHINGTON, July 17, 1950.

Journal of Research of the National Bureau of Standards Vol. 45, No. 6, December 1950 Research Paper 2159

Wavelengths for Calibration of Prism Spectrometers

By Earle K. Plyer and C. Wilbur Peters [1]

Several absorption bands of polystyrene, 1,2,4-trichlorobenzene, and other compounds have been measured in the infrared region from 1.5 to 24 μ on grating spectrometers. These bands have been determined with sufficient accuracy for use in calibration of prism instruments. A table is included that gives the cell thicknesses used in the measurements. The emission lines of mercury for the region from 0.5 to 2.4 μ are included. In order that the table may be of most value, a number of bands that have been determined by previous observers have also been included.

Many infrared absorption bands have been carefully measured, and their reported wavelengths [1] [2] are useful for calibrating spectrometers. Techniques of calibration utilizing vibrational bands with resolved rotational structures, including those of ammonia, carbon dioxide, and water vapor, have been described by Oetjen, Kao, and Randall [2]. When one undertakes to calibrate an infrared spectrometer he soon finds that additional reference lines or bands would be extremely helpful and that the information available has some serious disadvantages. In certain regions there are an insufficient number of standards. In some cases where a band has a rotational fine structure that is not resolved by a prism, it is not possible to locate any individual band with sufficient precision to justify its use for calibration. Furthermore, some absorbing materials require impractically long absorption cells. To avoid these disadvantages and increase the number of calibration points, additional lines and bands in the region from the visible to 24 μ have been measured by using sources or absorbers convenient for the calibration of prism instruments. These include: (1) polystyrene films and trichlorobenzene, which provide standards between 15 and 24 μ; (2) AH–4 mercury lamp in the region visible to 24 μ; (3) toluene at 21.5 μ;

[1] University of Michigan.
[2] Figures in brackets indicate the literature references at the end of this paper.

(4) methylcyclohexane [3], 7 to 12 μ. Wavelength data on all except the mercury source were obtained in order to meet the objectives of this investigation.

This information, combined with previously reported values for carbon dioxide, methane, water vapor [1], and methanol [4], form a reasonably complete set of secondary calibration points, supplementing the bands of ammonia and water vapor now in use.

All the measurements recorded in table 1 and marked on the characteristic spectra that follow were made with grating instruments. Those in the region 1 to 3 μ were made at the National Bureau of Standards with a 15,000-line-per-inch grating and lead sulfide detector. The polystyrene bands in the 3.4-μ region were measured for the authors on the Ohio State University grating spectrometer by John S. Burgess. The bands from 3.6 to 24 μ were measured by the authors at the University of Michigan. These grating measurements are the basis for the values marked on the characteristic spectra shown in figures 2 to 8. The characteristic spectra as shown in figures 1 to 6 were taken with an appropriate prism instrument.

In making the grating measurements, the resolution was adjusted to be of the same order as that obtained from good prism spectrometers for the region appropriate to a given optical material. Fairly wide slits were therefore required. The band positions were determined with a constant-energy background continuum to avoid the confusing shift that occurs when the background is not constant, that is if the spectral energy record shows a steep slope, the apparent positions of absorption minima may be shifted from the correct wavelength.

The bands shown in figures 2 and 4 have been measured with high resolution, so that an accuracy to ± 2A could be obtained. For the calibration of instruments using lithium fluoride prisms, this degree of accuracy is desirable.

In the spectral region from 4 to 14 μ, the grating measurements have been made to 0.001 μ of the wavelength value, and from 14 to 24 μ to 0.01 μ. The following paragraphs give a more detailed account of the procedures in handling the experimental materials and an explanation of specific features of the graphic and tabular data.

Figure 1 shows the mercury lines, and the wavelengths recorded in table 1 have been supplied by Curtis J. Humphreys of this Bureau from his measurements and those of other investigators [5]. These spectra were recorded with a Perkin-Elmer 12–A spectrometer with a lithium fluoride prism. The lines were measured with different slit widths, but the drum readings of the maximum intensity of a line did not vary appreciably with the slit width when the lines were not complex. In the table, lines that were not resolved are joined by brackets, and the wavelengths given on the curve are the average values for these groups of lines.

The polystyrene films are made by first preparing a 10-percent solution of polystyrene in toluene and pouring some of this solution on a smooth, clean piece of fairly fine plate glass, which is resting on a level surface. A doctor blade (number 15 for a film of 25 μ in thickness) is drawn over the solution to make the film more nearly uniform in thickness. The film is then allowed to dry at room temperature; the surface should be protected from dust and other particles while drying. To remove the dried film

TABLE 1. *Calibration wavelengths for prism spectrometers*

Wavelength	Wave number vac. cm^{-1}	State	Description	Substance
μ				
0.54607	18307.8	Emission	AH–4 lamp	Mercury.
.57696	17327.5	do	do	Do.
.57907	17264.4	do	do	Do.
1.01398	9859.4	do	do	Do.
1.12866	8857.7	do	do	Do.
1.35703	7367.0	do	do	Do.
1.36728	7311.0	do	do	Do.
1.39506	7166.3	do	do	Do.
1.52952	6536.2	do	do	Do.
1.6606	6020.3	Liquid	0.5 mm cell	1,2,4-Trichlorobenzene.
1.69202	5908.5	Emission	AH–4 lamp	Mercury.
1.69419	5900.9	do	do	Do.
1.70727	5855.7	do	do	Do.
1.71099	5843.0	do	do	Do.
1.81307	5514.0	do	do	Do.
1.97009	5074.5	do	do	Do.
2.1526	4644.2	Liquid	0.5-mm cell	1,2,4-Trichlorobenzene.
2.24929	4444.6	Emission	AH–4 lamp	Mercury.
2.3126	4322.9	Liquid	0.5-mm cell	1,2,4-Trichlorobenzene.
2.32542	4299.1	Emission	AH–4 lamp	Mercury.
2.4030	4160.3	Liquid	0.5-mm cell	1,2,4-Trichlorobenzene.
2.4374	4101.6	do	do	Do.
2.4944	4007.9	do	do	Do.
2.5434	3930.6	do	do	Do.
2.7144	3683.0	Vapor	5.0-cm cell	Methanol.
3.2204	3104.4	Solid	25-μ film	Polystyrene.
3.2432	3082.6	do	do	Do.
3.2666	3060.5	do	do	Do.
3.3033	3026.5	do	do	Do.
3.3293	3002.8	do	do	Do.
3.3101	3020.3	Gas	5.0-cm cell	Methane.
3.4188	2924.2	Solid	25-μ film	Polystyrene.
3.5078	2850.0	do	do	Do.
4.258	2349.3	Gas	Atmospheric	Carbon dioxide.
4.866	2054	Vapor	5-cm cell	Methanol.
5.138	1945.8	Solid	50-μ film	Polystyrene.
5.549	1801.6	do	do	Do.
6.238	1602.7	do	do	Do.
6.692	1494.9	do	do	Do.
7.268	1375.5	Liquid	0.05-mm cell	Methylcyclohexane.
9.672	1034.2	Vapor	5-cm cell	Methanol.
9.724	1028.1	Solid	50-μ film	Polystyrene.
11.035	906.0	do	do	Do.
11.475	871.3	Liquid	0.05-mm cell	Methylcyclohexane.
11.862	842.8	do	do	Do.
13.883	720.5	Gas	Atmospheric	Carbon dioxide.
[a]14.29	699.6	Solid	50-μ film	Polystyrene.
14.98	667.3	Gas	Atmospheric	Carbon dioxide.
15.48	645.8	Liquid	0.05 mm (1:4 CS_2)	Unknown in technical grade of 1,2,4-trichlorobenzene.
[a]17.40	574.5	do	.025-mm cell	1,2,4-Trichlorobenzene.
18.16	550.5	do	do	Do.
20.56	486.3	do	0.05-mm cell (sat. sol. in CS_2).	1,2,3-Trichlorobenzene.
21.52	464.6	do	0.05-mm cell	Toluene.
21.80	458.6	do	.025-mm cell	1,2,4-Trichlorobenzene.
[a]22.76	439.3	do	do	Do.
23.85	419.2	Vapor	Atmospheric	Water.

[a] Broad bands.

from the glass plate water is applied, and the film readily floats off the glass. After the film is redried, it is ready for use. The thickness may be checked with either a Swedish gauge or a micrometer. In figure 2 are shown the bands of polystyrene in the region of 3.4 μ as recorded with the lithium fluoride prism. Seven bands are observed in this region, and six have been selected for use in calibration. In figure 3 is shown the spectrum of a film of polystyrene from 2 to 16 μ. The grating instrument wavelength values of the bands selected for calibration have been marked on the curve, which was a record obtained from a Baird infrared spectrophotometer.

The trichlorobenzene samples, both highly purified and technical grades, were obtained from Hooker Electrochemical Co., Niagara Falls, N. Y. The authors are indebted to R. H. Kimball of that company for furnishing highly purified samples of both 1,2,3- and 1,2,4-trichlorobenzene. In figure 4 the spectrum from 1.5 to 2.5 μ of highly purified 1,2,4-trichlorobenzene as obtained from the Perkin-Elmer 12–A spectrometer with a lithium fluoride prism is shown. The seven bands that have been selected for the calibration have the wavelengths marked on the curve. These bands were not very broad even when measured on the grating instrument, and the region of maximum absorption could be determined to the fourth decimal place of wavelength in microns. Original grating instrument recorder traces of two bands of 1,2,4-trichlorobenzene in the 2-μ region are given in figures 7 and 8. The wavelength of the band at 1.6606 μ was determined from the mercury emission lines superimposed on the spectrum. To achieve this a Cetron mercury lamp, similar to the S–1 sun lamp, was used as the source. By focussing one of the hot electrodes on the entrance slit, the absorption and emission spectra could be measured simultaneously. In the determination of a second band in this region, figure 8, water vapor lines that appear on both sides of the band were used as standards. On these two figures the wavelengths of the reference lines have been indicated as well as the, wavelengths of the two bands of 1,2,4-trichlorobenzene.

The spectrum of technical grade 1,2,4-trichlorobenzene from 14 to 24 μ as recorded by the Perkin-Elmer 12–A spectrometer is shown with the wavelengths noted in figure 5. The technical grade contains some 1,2,3-trichlorobenzene, and some of the bands in the spectrum are due to the 1,2,3-isomer. In order to distinguish the bands that arise from the 1,2,4-trichlorobenzene and those from the 1,2,3-trichlorobenzene, the spectra of highly purified samples of each of these isomers are shown in figure 6. The band at 20.56 μ is seen to be due to 1,2,3-trichlorobenzene. However, the band at 15.48 μ does not appear in the spectra of either of the purified samples and thus probably arises from another chlorobenzene contained in the technical grade 1,2,4-trichlorobenzene. Although the results are not shown here, a mixture of about 85 percent of 1,2,4-trichlorobenzene and about 15 percent of 1,2,3-trichlorobenzene was also measured from 14 to 24 μ. No changes in the positions of the bands that were selected for calibration points were observed in the prism measurements when the spectrum of the mixture was compared with that of the technical grade 1,2,4-trichlorobenzene. The value of 22.76 μ is a prism instrument determination and is probably accurate to ± 0.02 μ. As the path from the source to the detector for the grating instrument is greater than that for the prism instrument, the atmospheric water vapor absorption is also greater. This absorption in the region of the 22.76-μ band makes it difficult to determine the position of the band, and thus the prism spectrometer value is given. The bands that are broad and not as accurately determined are listed in the table and are denoted as broad bands.

In table 1 is given a list of bands and emission lines that extend from 0.5 to 24 μ. All data not obtained in the current set of experiments are quoted from the sources listed. The absorption band of water vapor at 23.85 μ is made up of several lines, and the listed value was obtained with low resolution of the grating spectrometer. The wavelengths are given in microns and the wave numbers in vacuum in cm^{-1}. The reduction of the values of wave number to vacuum was accomplished by using 1.0002706 as the index of refraction of air. The index of refraction of air is not a constant, but the variation in the value is small and would introduce inappreciable changes in the wave number. The list includes bands measured in this work and other bands, which should give sufficient points for calibration of prism instruments. Additional wavelengths beyond those shown in the table are needed in some regions, and it is hoped that further measurements will be made in the future. This work has not included any measurements beyond 25 μ, but there are a large number of water vapor lines that are very well suited for calibration in this region [6, 7].

[1] G. Herzberg, Infrared and Raman spectra of polyatomic molecules (D. Van Nostrand Co., Inc., New York, N. Y., 1945).
[2] R. A. Oetjen, Chao-Lou Kao, and H. M. Randall, Rev. Sci. Instr. **13,** 515 (1942).
[3] API Project No. 44, Spectrogram No. 369.
[4] Avis Borden and E. F. Barker, J. Chem. Phys. **6,** 553 (1938).
[5] Curtis J. Humphreys, J. Opt. Soc. Am. **40,** 255 (1950).
[6] H. M. Randall, D. M. Dennison, N. Ginsburg, and L. R. Weber, Phys. Rev. **52,** 160 (1937).
[7] Earle K. Plyler, J. Research NBS **41,** 125 (1948) RP 1911.

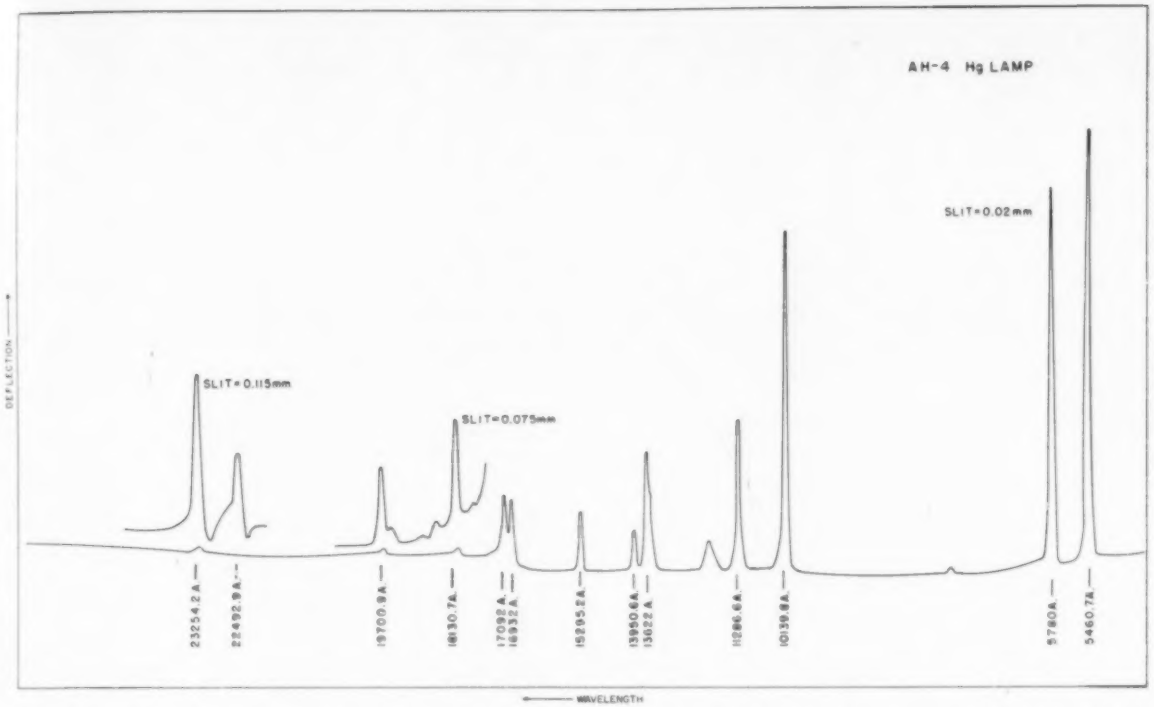

FIGURE 1. *Mercury emission spectra in the region from 0.5 to 2.4 μ as obtained from an AH–4 mercury lamp and a 12–A Perkin-Elmer spectrometer with a lithium fluoride prism.*

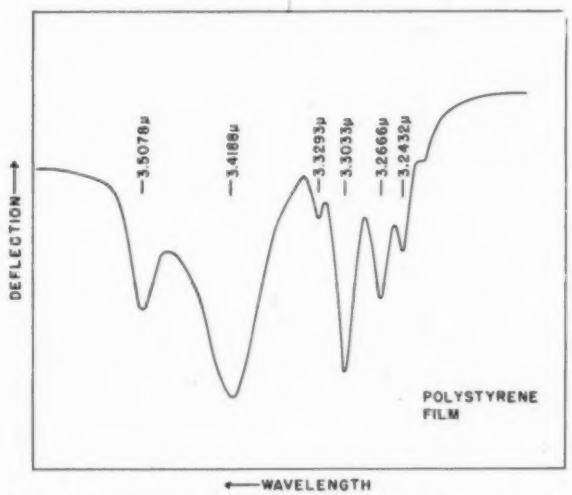

FIGURE 2. *Infrared absorption bands of polystyrene in the region of 3.4 μ for a film of about 25 μ in thickness.*

A lithium fluoride prism was used.

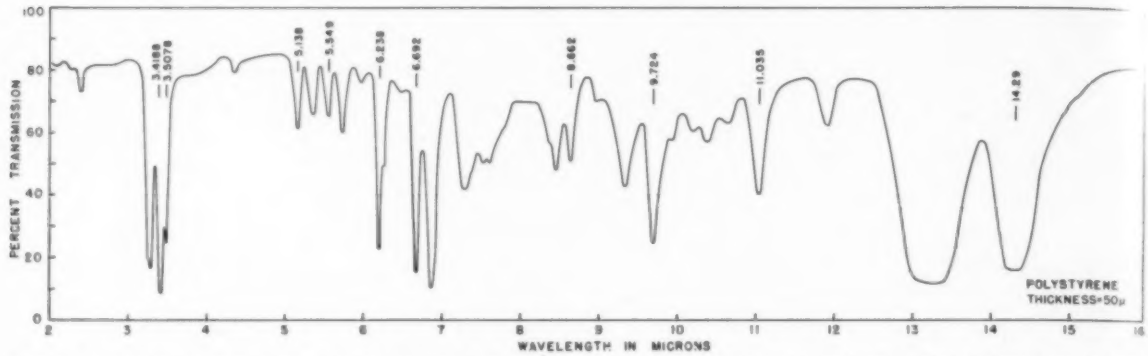

FIGURE 3. *Infrared absorption spectrum from 2 to 16μ of a polystyrene film measured on a Baird Associates infrared spectrophotometer.*

The bands that have been measured on a grating instrument are marked on the figure.

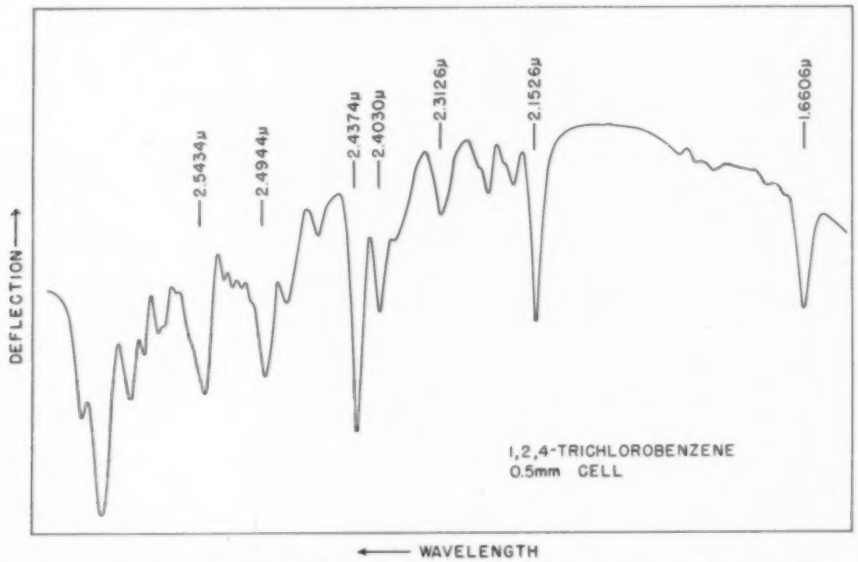

FIGURE 4. *Infrared absorption spectrum of highly purified 1,2,4-trichlorobenzene as measured with the lithium fluorid prisme.*

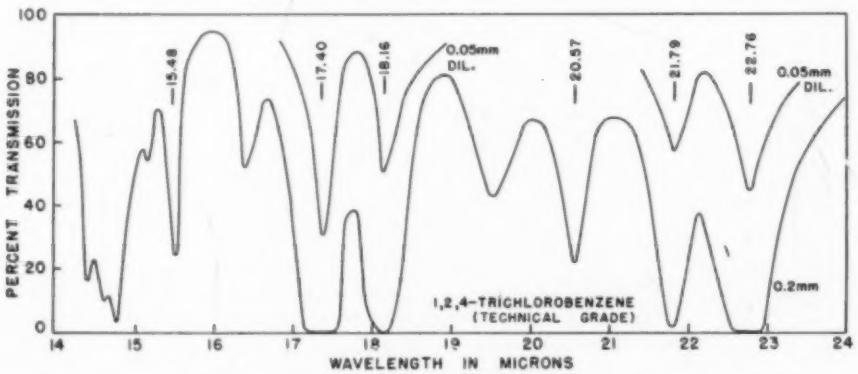

FIGURE 5. *Infrared absorption spectrum of 1,2,4-trichlorobenzene from 14 to 24 μ.*

The inserts were obtained by diluting the trichlorobenzene 1:4 in carbon disulfide.

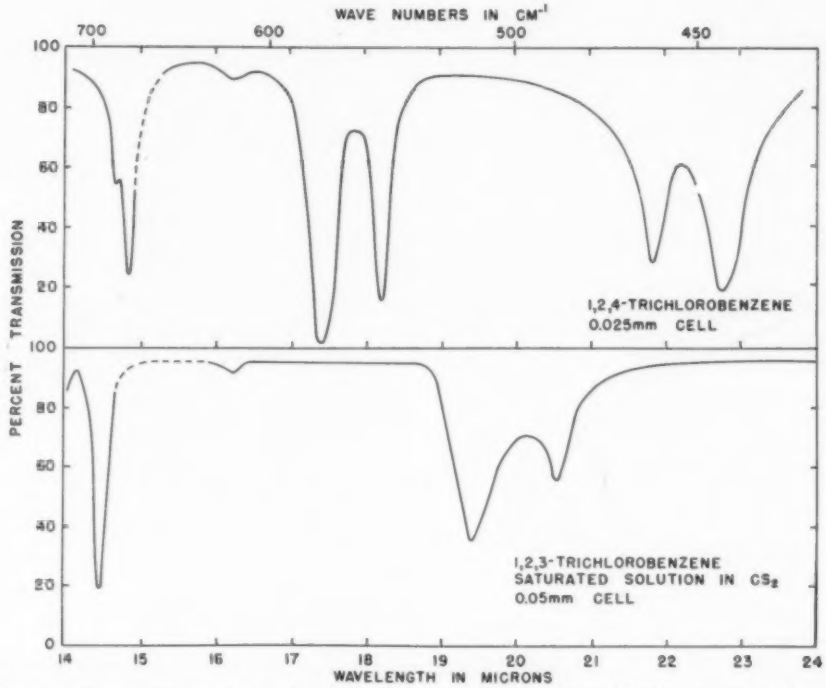

FIGURE 6. *Infrared spectra from 14 to 24 μ of highly purified samples of 1,2,4-trichlorobenzene and 1,2,3-trichlorobenzene.*

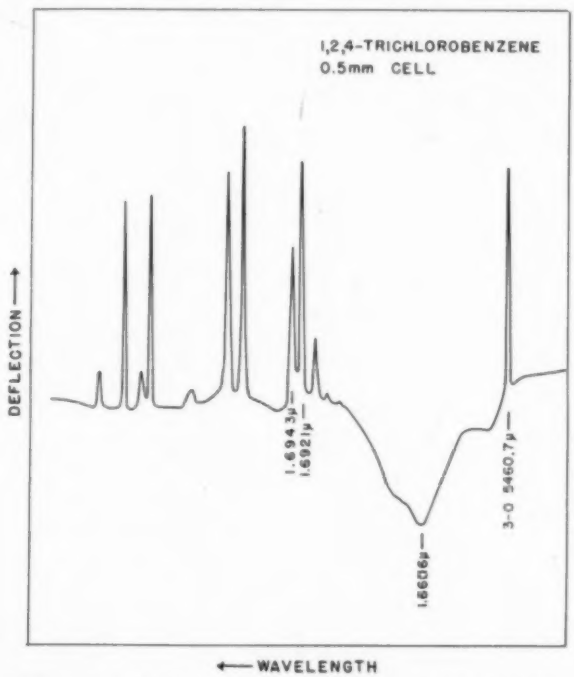

FIGURE 7. *Absorption band at 1.6606 μ of 1,2,4-trichlorobenzene with mercury emission lines superimposed on the spectrum as obtained from the 15,000 lines-per-inch grating instrument.*

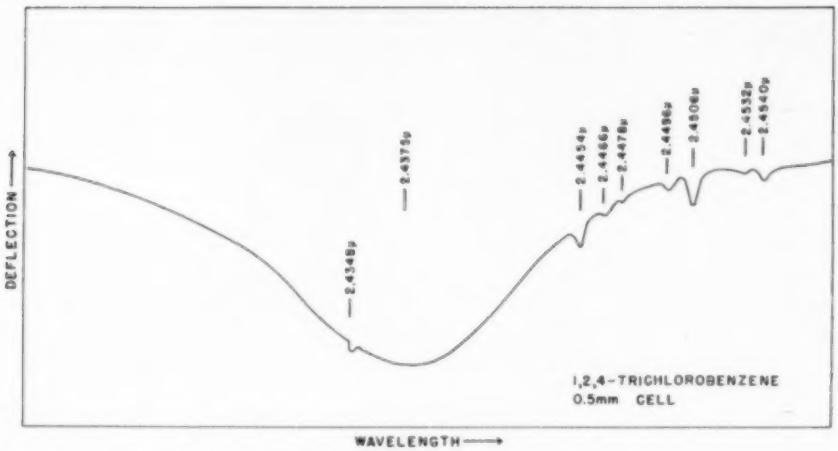

FIGURE 8. *Absorption band at 2.4375 μ of 1,2,4-trichlorobenzene with water vapor lines superimposed on the spectrum, as measured with the 15,000 lines-per-inch grating instrument.*

WASHINGTON, August 29, 1950

Journal of Research of the National Bureau of Standards Vol. 45, No. 6, December 1950 Research Paper 2160

High-Pressure Apparatus for Compressibility Studies and its Application to Measurements on Leather and Collagen

By Charles E. Weir

The design and construction of apparatus to be used to measure volume changes of solids (or liquids) between 1,000- and 10,000-atmosphere pressure is described in detail. Calibration of the equipment and its use in determining the compression ($-\Delta V/V_0$) of leather are discussed. The compression of leather between 1,000 and 10,000 atmospheres is reported. The compression between 2,000- and 10,000-atmosphere pressure is approximately 7 percent and appears to be relatively unaffected by moisture content, type of tannage, or sample variation. The compression of all leathers tested is described by the equation $-\Delta V/V_0 = 1.23\times10^{-5}\ (P-2000) - 5.60\times10^{-10}\ (P-2000)^2 + 1.35\times10^{-14}\ (P-2000)^3$.

I. Introduction

A Bureau program of measurement of physical constants of leather and collagen has resulted in a determination of the expansivity of leather and collagen [1].[1] These experiments also demonstrated that the shrinkage of leather, heretofore considered as analogous to a melting, was in reality a phenomenon occurring over a range of temperatures and resulted in an increase in real volume of the leather-water system studied. Subsequent studies on the rate of shrinkage as a function of temperature, tannage, liquid medium, etc., have been reported [2,3]. In view of the results an investigation of the effect of pressure on leather and the shrinkage process was indicated, including a determination of the compressibility of leather for which only estimates have been available [4].

Experiments involving appreciable pressures are extremely exacting mechanically and have been performed in few laboratories. To obtain information on the apparatus and techniques involved in such measurements, preliminary experiments were conducted on equipment that has been used for many years in the Geophysical Laboratory of the Carnegie Institution of Washington, for measurements at pressures as high as 12,000 bars. Subsequently similar equipment has been constructed at this Bureau and used in conjunction with a hydraulic press in the Geophysical Laboratory. This report deals with a description of the apparatus and a part of the data obtained.

[1] Figures in brackets indicate the literature references at the end of this paper.

II. Apparatus

In theory the apparatus required is simple; in practice, however, limitations imposed by the strength of materials require exacting machine work and the best of materials. An experiment consists essentially of forcing a piston into a vessel containing the sample under study immersed in a suitable liquid, and record-

ing the depth of penetration of the piston at known *internal* pressures.

The apparatus required consists of—

1. A thick-walled pressure vessel having a smooth bore and a second opening provided to permit measurement of the internal hydrostatic pressure.
2. A leak-proof piston, or plug, which is forced into the bore.
3. A ram designed to drive the plug into the vessel.
4. A leak-proof plug carrying an electrically insulated lead from the internal pressure-gage to the external pressure-measuring equipment.
5. The pressure-measuring equipment.
6. A hydraulic press to actuate the ram.
7. Assorted extractors to remove washers, etc.

The pressure vessel and accessories to be described are made in accordance with designs perfected by workers at the Geophysical Laboratory and are the result of wholehearted cooperation by these workers. The equipment is very similar to that described in considerable detail in 1919 by Adams, Williamson, and Johnston [5], but it is believed that a more recent highly detailed description of the apparatus, its fabrication, and use may be of interest and value to potential workers in this field.

The pressure vessel consists of a cylinder of SAE 4340 steel—a carbon, nickel, chrome, manganese, molybdenum, alloyed steel having "deep-hardening" properties—5 in. in diameter and 12 in. long. The cylinder, partly shown in figure 1, contains an axial hole ⅝ in. in diameter and 7 in. long. At the bottom of this bore a 2-in.-long hole is drilled, which decreases from ⅛ to $\frac{1}{16}$ in. in diameter and serves to connect the pressure gage with the contents of the vessel. An opening for the pressure gage and its plug is made into the side of the vessel to connect with the bottom of the $\frac{1}{16}$-in. diameter axial hole. The gage opening consists of an outer hole 1¼ in. deep designed to fit a bolt 1¼ in. in diameter having 12 threads per inch; a central portion ¾ in. in diameter, 1 in. deep having a flat bottom that meets the wall at right angles; and an innermost portion $\frac{5}{16}$ in. in diameter extending slightly beyond and connecting with the axial $\frac{1}{16}$-in. diameter hole. After initial machining, this vessel was heat-treated to procure a hardness of Rockwell C–40. The scale produced in the heat treatment was removed, and the ⅝-in. axial bore that was distorted was ground and lapped to produce a fine finish.

Before the pressure vessel could be used for high-pressure work it had to be subjected to a pressure seasoning followed by a refinishing operation. After the initial machining, the bore of this vessel was observed to increase in diameter by several mils on application of pressure of approximately 10,000 atm. The vessel, however, can be rendered stable, at least in this pressure range, by a seasoning process consisting of subjecting the vessel to an internal pressure far in excess of any subsequently contemplated pressure [6]. For this seasoning, special plugs, which will be described later, were used to fill the openings in the vessel. In seasoning, pressure was applied in increments of 2,000 atm, pressure being maintained for 30 min after each increment, until a maximum calculated internal pressure of 23,000 atm was attained. At the conclusion of this operation all fittings were found to be damaged, while the vessel had increased noticeably in diameter, externally as well as internally. In the refinishing operation it was necessary to enlarge the bore to 0.696 in. compared to the initial value of 0.630 in. The effectiveness of the seasoning treatment is shown by the fact that the vessel has been in use for several months, withstanding approximately 100 applications of pressures as high as 10,200 atm, with no measurable increase in diameter of the bore.

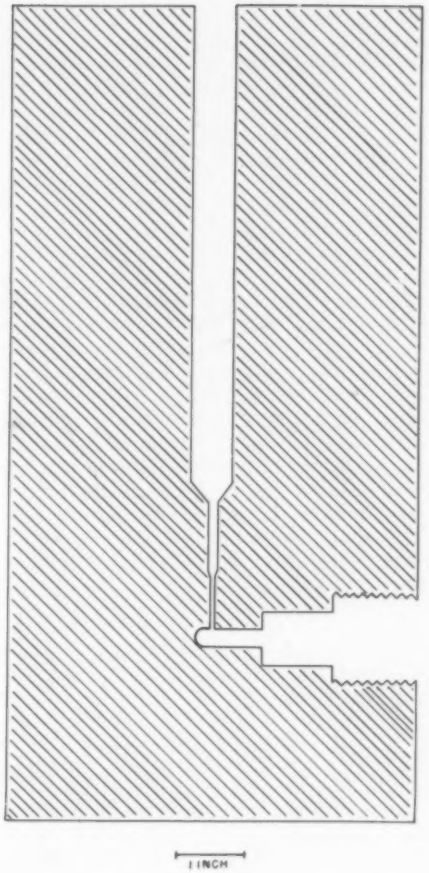

FIGURE 1. *Section of pressure vessel.*

The movable leak-proof plugs [6] and associated washers are shown in figure 2. Plug A is the type used during seasoning and is designed so that the washers may undergo large lateral expansions to follow the considerable distortion occurring in seasoning. Plug B is used in compressibility measurements. Both plugs are made of Sfentor steel, an oil-quenching manganese steel, and consist essentially of a body and stem each ¾ in. in length when finished. The stem is $\frac{5}{16}$ in. in diameter, and is threaded for the upper ⅜ in. of its length with 24 threads per inch to

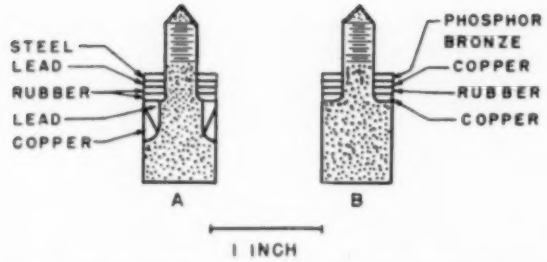

FIGURE 2. *Sections of leak-proof plugs and washers.*

permit extraction. It is very important that the junction of stem and body be filletted to prevent "pinching off" of the stem by the washers. In fabrication, the plug is machined to within 25 mils of the desired size, and heat-treated to procure extreme hardness (at least Rockwell C-60). The hardened piece is ground to size and polished to produce a fine finish, which is designed to minimize high stresses set up in grooves existing in the ground surface. The body of the plug is finished to be ½ to 1 mil smaller than the bore of the vessel. Best results have been obtained with the smaller clearance of ½ mil.

After compression measurements, the frictional force between the washers and the bore is of the order of 800 atms, and the plug must be extracted forcibly. In extraction, large stresses are set up in the stem of the plug, and difficulties have been encountered through breaking of the hardened stem. The failures appeared principally when the stem had been threaded prior to hardening, and were probably the result of small cracks in the threads formed in quenching. The best procedure has been found to grind the threads on the hardened stem. No failures to date have occurred in plugs made in this manner. It might be advantageous to draw the stem somewhat after finishing, but the necessity of resorting to this treatment has not been demonstrated.

The ram, used to drive the movable plug is shown in figure 3, and consists of a cold-rolled steel head shrunk onto a glass-hard Stentor steel shaft. The head serves to center the ram in the press and is relatively unimportant, since all stresses are borne by the shaft. The rod contains a recess at its lower end, which is finished to provide ample clearance of the stem of the plug that fits into it. Considerable clearance is advisable to prevent snapping the stem if moderate tilting occurs. The diameter of the shaft must be such that lateral swelling under compression will not cause binding in the bore of the vessel. In this instance the shaft is 5 mils smaller than the bore. Barring explosions, the ram travel is seldom greater than 2 in., and the length of the shaft should be kept to a minimum to prevent failure from buckling.

The pressure-gage plug, the insulated electrical lead, and its associated washers are shown in figure 4. This is the most complex fitting required and has caused more failures (including explosions) than all

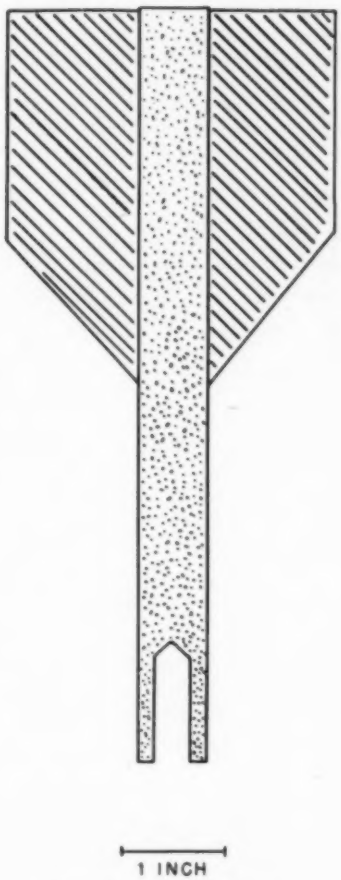

FIGURE 3. *Section of ram.*

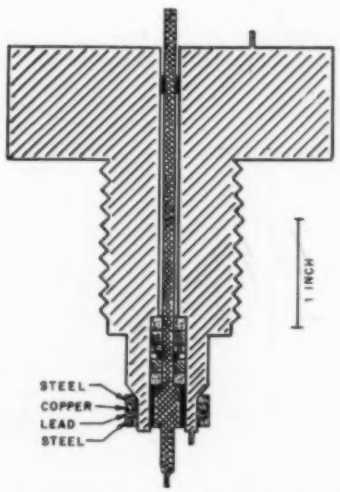

FIGURE 4. *Section of gage plug and insulated lead.*

others combined. The plug and lead are both made of SAE 3440 steel hardened to Rockwell C–40.

The electrical lead consists of a rod 4¾ in. long, being 5/32 in. in diameter for 3½ in. of its length, having a shoulder 0.262 in. in diameter and ⅜ in. long, and ending in another section 5/32 in. in diameter and ½ in. long. The tip of this latter section is approximately 1/32 in. in diameter to facilitate silver-soldering to the gage coil.

The gage plug is 1¼ in. in diameter and is threaded for 1½ in. with 12 threads per inch. The end of the bolt is machined to two concentric cylindrical surfaces, respectively, ¾ in. in diameter and ½ in. long, and 0.615 in. in diameter and ¼ in. long. These surfaces are connected with a conical frustum ⅛ in. long, which produces a seal with the packing washers. A recess 1 in. deep and 5/16 in. in diameter, having a flat bottom with no fillet at its wall, is machined in the end of the bolt, and a 7/32-in. diameter hole penetrates the remaining portion of the bolt. A ¼-in.-deep hole 1/32 in. in diameter is drilled in each face of the bolt, and an oversized pin is driven into each hole to serve as a convenient point for securing electric contact.

The insulating washers shown around the electrical lead are in order from the bottom of the cavity: ⅛-in. limestone, 5/16-in. outside diameter, 5/32-in. inside diameter; ⅛-in. soapstone, 5/16-in outside diameter, 5/32-in. inside diameter; ⅛-in. Neoprene rubber, 0.317-in. outside diameter, 5/32-in. inside diameter; 1/32-in. steel, ¼-in. outside diameter, 5/32-in. inside diameter; ⅛-in. soapstone and ⅛-in. limestone as before. This assembly is seated by using a small jig and an arbor press.

Two Bakelite washers not associated with the pressure seal are useful in preventing short circuits of the electrical lead, which may arise from tilting of this lead under pressure. One washer, 7/32-in. outside diameter and 5/32-in. inside diameter, serves to center the shaft on the low-pressure side, while the other, a thin shell 0.312-in. outside diameter and 0.262-in. inside diameter, protects the shoulder from the plug on the high-pressure side.

In seasoning, a two-piece fitting was used, one being a solid hardened Stentor steel plug having the shape of the end of the plug, the other a 1¼-in. bolt to hold the plug in place.

In operation the worker is protected by placing shields around the plug. Although no tendency has appeared toward failure of the threads, even at seasoning pressures, several failures have occurred in which the electrical lead was ejected with high velocity. These failures were all traced to errors in construction or to failure of steel parts. No difficulties, aside from electric short circuits, have been experienced with the arrangement described. The short circuits have resulted from slow extrusion of the limestone insulating washers into the pressure vessel, and use of a fine-grained lithographic limestone apparently has eliminated this difficulty.

The pressure gage consists of a coil of No. 38DSC manganin wire having a resistance of approximately 100 ohms. It is wound in two layers on thin paper, shellacked, and baked for 15 hrs at 125° C. Half-inch lengths of platinum wire are silver-soldered to the ends of the coil and in turn to the insulated electrical lead and the pin in the face of the plug. The gage coil is mounted on the end of the electrical lead, which fits through the coil and provides support.

The properties and seasoning of manganin pressure gages are discussed in detail by Adams, Goranson, and Gibson [7]. Gages used in these experiments were calibrated by using the water-ice VI transition, which occurs at 8,710 atm at 20° C [8]. As the pressure coefficient of manganin is essentially linear [9], this one point plus the known resistance at 1 atm provides a calibration sufficiently accurate for the present purpose.

The freezing-point apparatus consists of a tube containing distilled water and a few particles of ground glass to facilitate crystallization. The neck of the tube is drawn to a fine capillary, and the tube is inverted and slipped into a steel tube containing several milliliters of mercury. The mercury serves to seal the tube and permit transfer of pressure to the enclosed water. Calibration is performed by subjecting the freezing-point apparatus to pressure in excess of the expected freezing pressure, freezing being noted as a rapid and sudden decrease in resistance of the gage coil. The pressure is then lowered until a moderate rate of rise of resistance corresponding to melting of ice VI is noted. After a period of approximately 1 hr, an equilibrium pressure is attained, but extreme care must be exercised to insure coexistence of water and ice VI at this point. Generally, several equilibrium measurements are required on freezing as well as melting, and such measurements should be in good agreement.

The electric equipment used for measuring the resistance of the gage coil was a G–1 Mueller Bridge. This is an unthermostatted Wheatstone bridge of the shunted-decade type, having a range 0 to 51.111 ohms available in steps of 0.0001 ohm. The method of measurement differs from that used by other principal workers in this field [5, 7] and was suggested by E. F. Mueller of this Bureau.

As the pressure gage is approximately a 100-ohm coil, the bridge cannot be used directly to measure the resistance of the coil. Two similar gage coils are used, with one coil—preferably the smaller of the two—being connected directly into one of the arms of the bridge where it serves essentially as a comparison resistor. This coil is immersed in the same liquid as is used for pressure transmission, and is mounted in a well in a large metal block attached to the side of the pressure vessel. The second coil is the pressure coil and is mounted inside the vessel, as described previously. One battery lead to the bridge is made at the junction of the two coils, as shown in the circuit diagram of the electric set-up in figure 5. In operation the bridge measures the difference in resistance of the two gage coils, one of which is subjected to changes in pressure and temperature—ambient temperature—whereas the other is subjected only to similar temperature changes. As the resistance of manganin increases with pres-

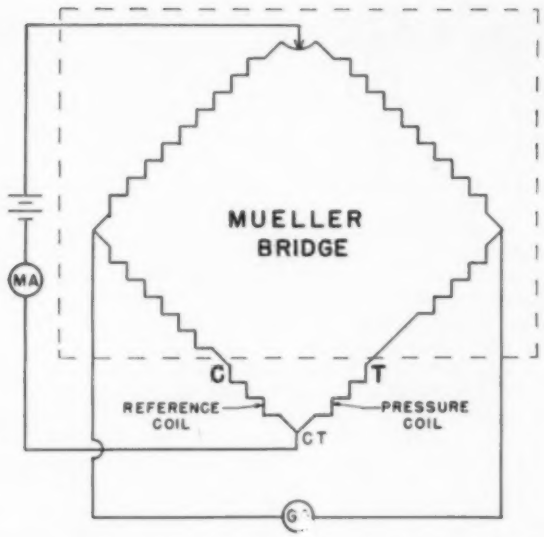

FIGURE 5. *Schematic diagram of pressure-measuring equipment.*

sure, the pressure coil should have the slightly larger resistance to eliminate the necessity for passing through a zero resistance reading. A commutator and mercury contact switch were included in the circuit but were not used in these experiments.

When two 1½-v dry cells were used, the total bridge current was 12 ma, and the gage coil current was 6 ma. With this current a deflection of ½ mm for each 0.0001-ohm step was obtained on the galvanometer scale set up at a distance of 2 m. An atmosphere was found to be equivalent to approximately 0.00026 ohm, and the sensitivity was therefore such that a pressure of less than 1 atm could be read directly.

The maximum variation in resistance of the gage coils noted at 1 atm was equivalent to ±3 atm, and might be caused by the effect of temperature—a maximum temperature variation of ±2° C occurred during all measurements—on the bridge or on the coils or by the effect of pressure on the gage coil resistance. In the absence of precise temperature control this variation was ignored, as it represented a negligible source of error. No difficulties due to contact resistances in the switches were ever experienced.

No description of the accessories required will be given. A complete set of extractors for every part is required, but the design of such instruments is arbitrary. The extractor generally takes the form of a shaft threaded externally at one end and either externally or internally at the other. A large nut fitting the former end is screwed down against a convenient bearing surface and serves to extract the desired part, which is screwed into the latter end of the shaft. It is of the utmost importance that suitable provision be made for extracting every piece before pressure is imposed, for even though parts may have large clearances they are often found to be solidly joined after a single application of pressure.

The dial gage used to measure piston travel was attached to the top platen of the hydraulic press. This gage had a useful range of 0.400 in. and was graduated in 0.0001 in. Suitable gage blocks were used to extend the range of the gage. Calibration showed a maximum error of ±0.0001 in., and no corrections were applied to the readings.

A press suitable for the measurements was not available at this Bureau, and through the cooperation of the Geophysical Laboratory of the Carnegie Institution of Washington the equipment was set up for use with the 500-ton, hand-operated hydraulic press previously described [5].

III. Experimental Method and Calculations

Measurements consist of readings of the depth of the plug in the vessel—as denoted by the dial gage—and the corresponding pressure [5]. Observations are made in order from the maximum pressure at every 1,000 atm. To insure uniform behavior of the packing washers, all measurements are made with the plug moving into the vessel. This situation is obtained by decreasing the pressure to 50 atm below the desired value, and, after a pause to permit attainment of thermal equilibrium, pumping back as closely as possible to the desired pressure. The dial gage readings obtained are interpolated to even thousands of atmospheres to simplify the calculation. This procedure is repeated until the "reference pressure," here 2,000 atm, is reached. Occasionally observations are made at 1,000 atm also, but frictional forces often render these values unreliable. A similar measurement is performed with the specimen replaced by a steel bar having similar volume. The two sets of data are used to calculate the compression of the specimen in terms of that of the steel bar, which is known [10].

The equation required for the calculation was given by Adams et al. [5], but the terminology used here is that given by Adams [13]. The equation is as follows

$$k-k'=S/V_0\Big\{\Delta L(1+\alpha P)+\Delta l'\alpha(P-P')+\Big[\Delta l'(1+\alpha P_0)+\frac{V'-V_r'}{S}\Big]\Big(\frac{k_l-k_l'}{1-k_l'}\Big)\Big\}+(k_r-k_r')\frac{(V_r)_0}{V_0}. \quad (1)$$

In this equation P refers to pressure in atmospheres and V volume; subscripts zero denote 1 atm, subscripts r and l refer to steel reference bar and confining liquid, respectively, and primes denote the experimental reference pressure of 2,000 atm; k is the compression $(V-V_0)/V_0=-\Delta V/V_0$ at pressure P; k' is the compression at 2,000 atm $(V'-V_0)/V_0$;

TABLE 1. *Correction terms used in calculations of compressibility*

Pressure	(k_r-k_r')	$\frac{k_l-k_l'}{1-k_l}$ (Varsol)	αP	$\alpha(P-P')$
atm				
10,000	0.00472	0.1383	0.0130	0.0104
9,000	.00414	.1279	.0117	.0091
8,000	.00352	.1169	.0104	.0078
7,000	.00286	.1037	.0091	.0065
6,000	.00237	.0893	.0078	.0052
5,000	.00178	.0730	.0065	.0039
4,000	.00119	.0536	.0052	.0026
3,000	.00060	.0295	.0039	.0013
2,000	.00000	.0000	.0026	.0000
1,000	−.00060	−.0418	.0013	−.0013

S is the cross-sectional area of the bore at 1 atm (245.88 mm²); α is the pressure coefficient of this area $(1/A_0)\ (dA/dP)=1.3\times10^{-6}$/atm; ΔL is the difference in travel of the piston at pressure P reckoned from the reference pressure of 2,000 atm in the measurements on steel bar and specimen; and $\Delta l'$ is the absolute difference in the position of the piston at the reference pressure in the runs on reference steel and specimen.

It is clear that if $V'=V_r'$ and if $\Delta l'=0$, three terms on the right side of eq 1 disappear. These terms then may be considered as correction terms arising from inequality of volumes of reference steel and specimen and differences in volume of confining liquid. The contribution of these terms may be made negligible if suitable care is exercised in selecting the volume of the reference steel and in filling the pressure vessel.

The values of the correction terms of the right side of eq 1 are given in table 1. The value of α was obtained from application of the equations given by the theory of elasticity for deformation of a cylinder under internal pressure [11]. The compression of the steel reference bar follows from the compressibility of steel given by Bridgman [10] converted into atmospheres. Compression values for Varsol were determined experimentally on the Varsol actually used, and were calculated by setting $V_0=V'=0$ in eq 1.

The volumes of the specimens studied are measured by the method of hydrostatic weighing at atmospheric pressure. The materials of interest have large compressibilities, which are functions of pressure, and the values of the volumes at 2,000 atm required in eq 1 are not easily obtained by successive approximations involving successive calculations and extrapolation to the known values at 1 atm. To place the determination of values of V' on a mathematical basis, eq 1 was rearranged in the form

$$-\frac{\Delta V}{V_0}=\frac{V'}{V_0}\left[\left(\frac{k_l-k_l'}{1-k_l'}\right)-1\right]+S/V_0\left[(1+\alpha P)\Delta L+\alpha(P-P')\Delta l'+\left(\Delta l'-\frac{V_r'}{S}\right)\left(\frac{k_l-k_l'}{1-k_l'}\right)\right]+1+(k_r-k_r')\frac{(V_r)_0}{V_0}. \quad (2)$$

All quantities on the right side of eq 2 are known explicitly except V'.

The compression, $-(\Delta V/V_0)$, has been found to be well represented by a cubic in pressure, as given by

$$-\frac{\Delta V}{V_0}=aP+bP^2+cP^3. \quad (3)$$

The right side of eq 2 and 3 are equated, and the value of V'/V_0 was obtained from the data by the method of least squares. The value of V' so obtained was used in equation 1 to calculate experimental values of $k-k'$.

IV. Preparation and Treatment of Specimens

Measurements were made on three types of commercial leather: chrome, retan, and vegetable tanned, as well as two types of collagen: hide collagen and kangaroo tail tendon.

Test samples of leather and hide collagen consisted of a stack of disks ⅝ in. in diameter and 4 in. long, held together by means of fine wire. The sample of tendon was a bundle of tendons of similar dimensions. The disks comprising the sample were subjected to the following treatments prior to test.

Two samples of chrome tanned hydraulic packing leather denoted as A and B, cut from different areas of the same hide were tested. The specimens were degreased for 24 hr with chloroform, washed in running water for 24 hr, and conditioned at 72° F and 50-percent relative humidity for 2 mo prior to use.

After measurements on these conditioned samples, the Varsol was removed by evaporation at room temperature for 1 week, and exposure to a temperature of 60° C for 24 hr. The samples were then dried at 100° C for 18 hr. Sample A was then tested and the Varsol removed again, as described previously. Both samples were then redried at 100° C for 24 hr in vacuum (<2mmHg) and retested.

One sample of retan upper leather was degreased, washed, and conditioned as described previously. Tests were made only on the conditioned sample.

Two dried samples of vegetable tanned leather obtained from neighboring areas of the same hide were tested. One sample, denoted as A, was prepared by degreasing, washing, and drying at 100° C, as described. The second sample, B, was washed, dried in vacuum for 16 hr, degreased, and then dried at 100° C.

Partially purified hide collagen was obtained by dehydration of a freshly flayed cowhide with acetone. The dehydrated material was split to remove the grain and flesh layers, and the resulting corium was conditioned and used for test.

Tendons were conditioned prior to test and received no chemical treatment.

All samples were weighed prior to test and were then subjected to impregnation with Varsol under a vacuum of approximately 20 mm Hg. Following compression determinations the samples were reweighed in Varsol. From the loss in weight in

910302—50——3

TABLE 2. *Compressibility of conditioned chrome-tanned leather*

Pressure	Sample A V_0=9.595 ml; V''=9.333 ml $\rho_{22°C}$=1.367$_6$ g/cm³					Sample B V_0=9.520 ml; V''=9.281ml $\rho_{22°C}$=1.362$_7$ g/cm³		
	Run—					Run—		
	1	2	3	4	Average	1	2	Average
	*$k-k'$	$k-k'$	$k-k'$	$k-k'$	$k-k'$	$k-k'$	$k-k'$	$k-k'$
atm								
10,000	0.0693	0.0701	0.0674	0.0699	0.0692	0.0697	0.0702	0.0700
9,000	.0630	.0641	.0618	.0643	.0633	.0644	.0642	.0643
8,000	.0558	.0574	.0553	.0577	.0565	.0578	.0573	.0576
7,000	.0481	.0495	.0487	.0493	.0492	.0510	.0500	.0505
6,000	.0398	.0419	.0399	.0413	.0407	.0424	.0418	.0421
5,000	.0319	.0329	.0310	.0327	.0321	.0336	.0345	.0340
4,000	.0221	.0222	.0232	.0226	.0225	.0236	.0230	.0233
3,000	.0121	.0120	.0120	.0121	.0120	.0121	.0125	.0123
2,000	.0000	.0000	.0000	.0000	.0000	.0000	.0000	.0000
Alternate values						Alternate values		
10,000	0.0688	0.0693	0.0703	0.0682	0.0692	0.0713	0.0683	0.0698
9,000	.0632	.0630	.0632	.0628	.0630	.0658	.0628	.0643
8,000	.0565	.0564	.0565	.0559	.0563	.0590	.0563	.0577
7,000	.0492	.0482	.0492	.0488	.0489	.0513	.0496	.0504
6,000	.0406	.0403	.0406	.0405	.0405	.0432	.0410	.0421
5,000	.0321	.0317	.0321	.0315	.0318	.0347	.0322	.0334
4,000	.0225	.0218	.0225	.0223	.0223	.0239	.0227	.0233
3,000	.0121	.0120	.0121	.0120	.0120	.0122	.0124	.0123
2,000	.0000	.0000	.0000	.0000	.0000	.0000	.0000	.0000

* $k-k'$ is equivalent to the relative volume change, $-\Delta V/V_0$, reckoned from 2,000 atm.

Varsol and the density of the Varsol, the volume of the samples was obtained. The density of Varsol was obtained by successive weighings of a steel bar in air, water, and Varsol, respectively, and was found to be 0.7811 g/ml.

V. Results and Discussion

1. Reproducibility

In order to evaluate the reproducibility of the measurements, duplicate experiments were made in many instances. A particular set of measurements was obtained in the following way.

An initial measurement was made on the steel reference bar, and was followed by a measurement on sample A and then on sample B. The second determinations were made by measuring sample A, then sample B, and finally the reference bar. As only two measurements were made in 1 day these determinations required 3 days for completion. The values of compression could be calculated on the basis of either of the two measurements on the steel bar, and both calculations were performed. It is considered that the best calculation is that based on the run nearest in time to the reference run. Values based on the farthest removed reference run are given as alternate values. The results of this experiment are given in table 2.

Runs 1 and 2 of the table refer to the experiment described, and two other runs performed at a different time on sample A are included for comparison. The agreement is good between runs, and within experimental error the compressions of samples A and B are not significantly different.

2. Effect of Moisture on Compression

Measurements were made on sample A after drying it at 100° C, and on both samples A and B after drying them at 100° C in vacuum, as described. The results are given in table 3.

TABLE 3. *Effect of moisture content on compressibility of chrome-tanned leather*

Pressure	Sample A′ Sample A dried at 100° C V_0=7.882 ml; V''=7.608 ml $\rho_{22°C}$=1.389$_8$ g/cm³		Sample A″ Sample A′ dried at 100° C in vacuum V_0=7.691 ml; V''=7.481 ml $\rho_{22°C}$=1.387$_8$ g/cm³	Sample B″ Sample B dried at 100° C and redried at 100° C in vacuum V_0=7.617 ml; V''=7.409 ml $\rho_{22°C}$=1.386$_8$ g/cm³
	Run—			
	1	2		
	*$k-k'$	$k-k'$	$k-k'$	$k-k'$
atm				
10,000	0.0683	0.0687	0.0706	0.0710
9,000	.0627	.0625	.0642	.0646
8,000	.0570	.0568	.0572	.0571
7,000	.0502	.0477	.0494	.0503
6,000	.0414	.0413	.0417	.0414
5,000	.0329	.0329	.0315	.0320
4,000	.0240	.0235	.0229	.0231
3,000	.0128	.0124	.0122	.0123
2,000	.0000	.0000	.0000	.0000
1,000	−.0119	−.0118	−.0134	----------

* $k-k'$ is equivalent to the relative volume change, $-\Delta V/V_0$, reckoned from 2,000 atm.

It is surprising that the removal of moisture causes little or no change in compression of the leather. A total loss in weight of 18.6 percent is involved between conditioned samples of table 2 and the dry samples of table 3. If it is assumed that this total loss in weight represents moisture [12], and the compression of a composite sample containing 18.6 percent of water and 81.4 percent of leather is calculated from the compressions of table 3 and known values for water [13], values are obtained that are of the order of 10 percent higher than the measured values of table 2. Even if the moisture present in the leather is considered to be "bound water" under high pressure, it would appear that the compression of the leather should change upon removal of the water, except in the one case in which the compressibility of the combined water and the leather are nearly identical over the whole pressure range. The probability of such coincidence seems small. This finding deserves further experimental study on this and other hygroscopic materials containing varying amounts of moisture.

3. Compressions of Other Types of Leather and Collagen

The results of measurements of compressions of two types of collagen and retanned and vegetable-tanned leather are given in table 4.

It is to be noted that the compression values of the vegetable-tanned samples agree but appear to be slightly lower than values obtained for chrome-tanned samples. Values for the retan leather, on the other hand, appear somewhat higher than values for chrome leather, while the values obtained for the collagens agree well both with each other and with the chrome leather. The divergences observed with vegetable and retanned leather may be real, but conclusions in this respect will not be made until further more extensive measurements are conducted.

4. Compressibility of Leather

To obtain an explicit expression for compression, a power series in pressure may be fitted to the experimental data. Terms of higher degree than the third in pressure have been found to contribute little to the efficacy of the fit, and a cubic equation in pressure appears to describe the data satisfactorily. Data obtained for different samples, tannages, and moisture contents might all be fitted with such equations, but since there are only slight differences in compressions of these materials the equations evolved would be expected to agree fairly well and to exhibit small variations in coefficients. Therefore, an equation of third degree in pressure was fitted only to the best data—the average values for sample A in table 2—which are considered as representative. Values obtained by use of this equation will closely approximate the experimental values obtained on all leathers tested. The equation obtained by use of the method of least squares is as follows

$$-\Delta V/V_0 = 1.23\times10^{-5}\ (P\text{-}2000) - 5.60\times10^{-10}\ (P\text{-}2000)^2 + 1.35\times10^{-14}\ (P\text{-}2000)^3. \quad (4)$$

The compressibility obtained by differentiating the above equation is found to be

$$-\frac{1}{V_0}\frac{dV}{dP} = 1.23\times10^{-5} - 1.12\times10^{-9}(P-2000) + 4.05\times10^{-14}(P-2000)^2. \quad (5)$$

A previous estimate of the compressibility [4], 33×10^{-6}/bar, is considerably larger than that given by the equation above. However, equation 2 shows the compressibility to be a function of pressure and the value of 33×10^{-6}/bar was obtained at an undetermined pressure much lower than the minimum pressure of 2,000 atm at which eq 2 applies. Extrapolation of eq 4 to atmospheric pressure yields a compressibility considerably smaller than 33×10^{-6}/bar.

VI. Conclusions

The design and construction of apparatus for measuring compression of solids (or liquids) in the pressure range 2,000 to 12,000 atm has been described. The results of measurements made on a natural high polymer, leather, show that the apparatus is capable of yielding data of good reproducibility.

TABLE 4. *Compressibilities of collagen and leather*

Pressure	Dry vegetable-tanned crust leather		Retan (conditioned)	Hide collagen	Kangaroo tendon
	Sample 1 V_0=9.536 ml V'=9.297 ml $\rho_{22°C}$=1.406$_6$ g/cm^3	Sample 2 V_0=9.071 ml V'=8.840 ml $\rho_{22°C}$=1.399$_8$ g/cm^3	V_0=9.380 ml V'=9.033 ml $\rho_{22°C}$=1.310$_3$ g/cm^3	V_0=8.796 ml V'=8.556 ml $\rho_{22°C}$=1.326$_6$ g/cm^3	V_0=6.311 ml V'=6.139 ml $\rho_{22°C}$=1.328$_6$ g/cm^3
	[a] $k-k'$	$k-k'$	$k-k'$	$k-k'$	$k-k'$
atm					
10,000	0.0667	0.0660	0.0748	0.0701	0.0706
9,000	.0606	.0576	.0684	.0629	.0645
8,000	.0538	.0530	.0610	.0566	.0570
7,000	.0465	.0467	.0524	.0494	.0491
6,000	.0387	.0390	.0449	.0414	.0407
5,000	.0299	.0300	.0354	.0316	.0317
4,000	.0219	.0216	.0257	.0236	.0234
3,000	.0114	.0117	.0142	.0122	.0126
2,000	.0000	.0000	.0000	.0000	.0000

[a] $k-k'$ is equivalent to the relative volume change, $-\Delta V/V_0$, reckoned from 2,000 atm.

The data obtained on leather are indicative of a compressibility that is intermediate between the compressibilities exhibited by most solids and those of liquids. The compression is not materially affected by moisture content. Values obtained for chrome-tanned leather and two types of collagen are in good agreement, but the compressions of vegetable and retanned leathers appear to be slightly different. Compressions of samples taken from different areas of the hide are in substantial agreement.

This investigation was made possible by the wholehearted cooperation of members of the Geophysical Laboratory of the Carnegie Institution of Washington and of the Bureau of Standards. The author is particularly indebted to L. H. Adams, H. S. Yoder, and J. Van den Huerk, of the Geophysical Laboratory, for encouragement, invaluable technical advice, and use of the facilities of their laboratory; and to E. F. Mueller and R. E. Wilson, of this Bureau, for advice and assistance in connection with the resistance measurements.

VII. References

[1] C. E. Weir, J. Research NBS **41,** 279 (1948) RP1921.
[2] C. E. Weir, J. Research NBS **42,** 17 (1949) RP1947.
[3] C. E. Weir, J. Research NBS **44,** 599 (1950) RP2106.
[4] C. E. Weir, J. Research NBS **35,** 257 (1945) RP1672.
[5] L. H. Adams, E. D. Williamson, and J. Johnston, J. Am. Chem. Soc. **41,** 12 (1919).
[6] P. W. Bridgman, Pro. Am. Acad. Arts & Sci. **49,** 627 (1914).
[7] L. H. Adams, R. W. Goranson, and R. E. Gibson, Rev. Sci. Instr. **8,** 230 (1937).
[8] P. W. Bridgman, Pro. Am. Acad. Arts & Sci. **47,** 441 (1911).
[9] P. W. Bridgman, Pro. Am. Acad. Arts & Sci. **47,** 321 (1911).
[10] P. W. Bridgman, Pro. Am. Acad. Arts & Sci. **74,** 11 (1940).
[11] S. Timoshenko, Theory of elasticity (McGraw Hill Book Co., Inc., New York, N. Y. 1934).
[12] J. R. Kanagy, J. Am. Leather Chem. Assoc. **36,** 609 (1941).
[13] L. H. Adams, J. Am. Chem. Soc. **53,** 3769 (1931).

WASHINGTON, August 3, 1950.

Journal of Research of the National Bureau of Standards Vol. 45, No. 6, December 1950 Research Paper 2161

Arc and Spark Spectra of Technetium

By William F. Meggers and Bourdon F. Scribner

Four milligrams of highly purified technetium, loaned by the United States Atomic Energy Commission, were used to obtain a description of the arc and spark spectra characteristic of this fission product. Solutions containing 50 to 200 micrograms of technetium were dried on copper electrodes and excited by electric arcs or sparks. A stigmatic concave grating of 22-feet radius was employed to photograph the spectra from 2200 to 9000 angstroms, within which limits more than 2,300 lines characteristic of Tc atoms or ions were recorded. Wavelengths were measured relative to iron standards, relative intensities were estimated on a scale of 1 to 1000, and almost every line was definitely assigned either to neutral Tc atoms or to singly charged (Tc^+) ions. The measured wavelengths range from 2261.30 to 8829.80 angstroms with average probable errors rarely exceeding ± 0.01 angstrom. The average results of wavelength measurements and of intensity estimates for 2,121 lines in Tc I and Tc II spectra are presented. The strongest Tc I lines have wavelengths 4297.06, 4262.26, 4238.19, 4031.63, and 3636.10 angstroms. The strongest Tc II lines have wavelengths 2543.24, 2610.00, and 2647.02 angstroms. This description of Tc I and Tc II spectra will serve for spectro-chemical identification and for structural analyses of these spectra.

I. Introduction

In 1869, when the periodic chart of the atoms was first proposed, Mendeléeff [1][1] saw that the chemical elements homologous to manganese were missing in the two succeeding periods; he called these eka-manganese and dwi-manganese. This was the first hint of the possible existence of the element under discussion. In the following half century many attempts, both chemical and spectroscopic, were made to detect these homologs of manganese, but without success. Moseley's [2] discovery in 1913 of a quantitative relationship between Roentgen frequencies and atomic numbers proved that atomic numbers 43, 61, 72, 75, 85, and 87 were still unknown, and provided a new method of detection by means of Roentgen spectra. This method was applied in 1925 by Noddack, Tacke, and Berg [3], who reported finding, in material extracted from columbite, three K spectrum lines for atomic number 43 and five L spectrum lines for atomic number 75. These two atomic numbers are identical with the homologs of manganese, and the names masurium and rhenium were proposed for them. The discovery of rhenium was abundantly confirmed, and within a few years this new element became a commercial metal. In 1931 the arc spectrum of rhenium was described and interpreted by Meggers [4], who then inquired of the discoverers if a sample of masurium was available for spectroscopic investigation. The Noddacks[2] replied that they had succeeded in concentrating some masurium, and that they would send the first milligram that could be spared. Unfortunately that milligram never materialized, and it later appeared that the extraction of element 43 from natural sources would be unlikely or even impossible [5].

[1] Figures in brackets indicate the literature references at the end of this paper.

[2] In a letter dated Dec. 22, 1931, from W. and I. Noddak to W. F. Meggers.

After the discovery of artificial radioactivity in 1934, it became theoretically possible to manufacture any desired element by artificial nuclear transmutation. Thus element 43 was first prepared in 1937 in the Berkeley cyclotron by bombarding molybdenum with neutrons or deuterons. It was identified, and its radiochemical properties were investigated by Perrier and Segré [6], who named the element technetium [7] because it was the first new element to be produced artificially. The amount of technetium produced in this manner was so small that it could only be detected by means of its characteristic radioactivity, which is enormously more sensitive than either roentgen or optical spectra. However, soon after the discovery of uranium fission in 1939, it was found that element 43 occurs among fission products to the extent of 6.2 percent [8]. In 1948 the isolation of milligram amounts of element 43 from uranium fission was described by Parker, Reed, and Ruch [9]. With these samples the whole-number atomic mass was determined by Inghram [10] to be 99, the first optical spectrogram was made by Timma [11], and the Roentgen emission spectrum was photographed by Burkhart, Peed, and Saunders [12]. Thus far the published information on the optical spectra of Tc consists of estimated relative intensities and approximate wavelengths of 102 lines (4297.2 to 2461.7 A) attributed [11] to element 43. In the light of present information critical examination of those data discloses that possibly 46 of the 102 lines are identifiable as Tc I, and 32 as Tc II, but the remaining 24 do not belong to Tc.

In September 1948, the National Bureau of Standards applied to the United States Atomic Energy Commission for the loan of 5 mg of $^{99}_{43}$Tc with which to make descriptions and analyses of the atomic and ionic emission spectra of technetium. A 3-mg sample was delivered in January 1949. With this sample preliminary results were obtained for wavelengths and relative intensities of about 2,000 Tc lines. These results were reported at the Oak Ridge Spectroscopy Symposium on March 25, 1949 [13] and at the Buffalo meeting of the Optical Society of America on October 29, 1949 [14]. In July 1950 three additional milligrams of $^{99}_{43}$Tc were borrowed for the purpose of completing this description of arc and spark spectra and for the investigation of hyperfine structure of certain spectral lines. The purpose of this paper is to present the wavelengths and relative intensities of 2,121 lines that are characteristic of Tc atoms and ions. These data are suitable for spectrochemical identification and for structural analyses of the first two spectra of Tc. Details of the structural analyses of Tc I and Tc II spectra, and of the investigation of hyperfine structure in Tc spectral lines will be given in subsequent papers.

II. Technetium Spectrograms

The technetium samples came in the form of oxide. These samples were dissolved in dilute ammonium hydroxide to make solutions of known concentration, portions of which could then be added to spectroscopic electrodes so that a definite amount of Tc was deposited on each. Fifty or one hundred micrograms of Tc were dried on the flat-machined end of a copper rod ¼ in. in diameter and 1 in. long. Electrodes with approximately rectangular ends, 6 by 2 mm, were later employed to concentrate more of the light along the optical axis. Two such loaded electrodes were used when oscillatory discharges were employed for exciting the spectra, but when the direct-current arc was employed the best results were obtained by placing 200 μg on the anode. With a desire to economize material, the first spectrograms were made in the blue and ultraviolet with 50 μg on each electrode, but to obtain stronger spectrograms it was necessary to use 100 on each. Also it was desirable to choose light sources that would burn the entire added sample off the ends of the copper electrodes without predominant excitation of the copper spectra. Furthermore, it was necessary to choose two sources with sufficiently different excitation characteristics so that comparisons of spectral line intensities would permit positive assignment of the lines either to neutral atoms or to ionized atoms. These considerations led to the choice of two sets of excitation conditions available in the Applied Research Laboratory Multisource unit.

The spark spectrum was obtained from an oscillatory condenser discharge with the following circuit constants: capacitance 5 μf, charging voltage 940 v, inductance 100 μh, and resistance 0.4 ohm. The arc spectrum was obtained from an overdamped condenser discharge with circuit constants: capacitance 50 μf, charging voltage 940 v, inductance 400 μh and resistance 25 ohms. The gap between the electrodes was set at 4 mm.

Before any Tc spectrograms were attempted, experiments were made with Mo spectrograms, and source conditions were determined that gave a fivefold enhancement of Mo II lines over Mo I lines when the spark spectrum was compared with the arc. These source conditions described above were found to be suitable for an unambiguous separation of Tc I and Tc II lines.

It was immediately seen that the distribution of Tc I and Tc II lines resembled the distribution of first and second spectral lines of other metals; the second spectrum predominates in the ultraviolet and weakens in the visible, whereas the first spectrum is weak in the ultraviolet but predominates in longer waves. Because few Tc II lines are seen in the blue, the Tc spark spectrograms were not extended beyond 4700 A.

Although the arc-like excitation provided by the ARL Multisource unit was satisfactory for the short wave region, it was disappointing for the visible and infrared, partly because it gave weak spectra and partly because it excited the spectra of atmospheric nitrogen and oxygen with such intensity that many portions of the Tc spectra were masked. Consequently, the spectral range 4500 to 9000 A was reobserved with a direct-current arc between ⅛-in. diameter Cu electrodes, the anode being charged with 200 μg of Tc. These direct-current arc spectro-

grams were made with an applied potential of 220v and a current of 7 amps.

The spectrograms were made with a concave grating of 22-ft radius, ruled with 15,000 lines per inch on an aluminized pyrex disk of 6-in. diameter. This grating was placed in a Jarrell-Ash instrument provided with a concave mirror of similar form, so that the spectrograph gave stigmatic slit images. A fixed slit of 20-μ width was used, and the maximum resolving power for sharp lines in the first order spectrum was about 50,000, the reciprocal linear dispersion being about 5 A/mm.

Three positions of the grating and 20-in. plate holder recorded the spectrum between 2100 and 9000 A with successive exposures on three types of photographic plates. The region 2200 to 4700 A was photographed on Eastman 103-uv sensitized plates, the region 4400 to 6900 A on II-F sensitized plates, and 6500 to 9000 A on I-N hypersensitized plates.

By sliding a slotted diaphragm in front of the slit, a series of adjacent spectrograms were made as follows: Iron arc, copper arc, technetium arc on copper, technetium spark on copper, copper spark, iron arc. Spark spectra were omitted in the visible and near infrared regions. The exposure durations were usually 1 sec for the iron arc, 45 sec for the copper blanks, and 30 sec for copper with technetium added. Preliminary tests with Mo added to copper showed that the sample was almost completely burned off in 30 sec. All exposures with Tc deposited on Cu were made with the electrodes mounted in a cylindrical brass cell provided with a quartz window and with an air exhaust through a glass-wool filter designed to trap, and thus conserve, most of the vaporized Tc for future recovery.

At least three satisfactory spectrograms were made for each of the three spectral ranges mentioned. This gave at least six independent determinations for lines appearing in the overlapping portions of these ranges. The positions of Tc spectral lines relative to iron standards were measured to 0.001 mm with an excellent 50-cm comparator constructed by the Gaertner Scientific Corp. In all, approximately 20,000 spectral line images were bisected to obtain the wavelengths of about 2,500 Tc and impurity lines. All lines appearing in the spectra of Cu plus Tc that were not duplicated or masked in the Cu comparison spectra were measured, even though some were easily recognized as impurities. The final values of all the impurity lines served as checks on the scale of wavelengths and on the amazingly high purity of the Tc samples. The principal impurities detected spectroscopically were calcium, magnesium, and silicon, which are common contaminants in chemical operations. Only the stronger lines of lithium, sodium, and potassium were present, and the same is true of iron, nickel, chromium, molybdenum, aluminum, bismuth, and platinum. No trace of ruthenium, rhenium, or any other metals was found. In the identification and elimination of impurity lines, consideration was given to relative intensities as well as to wavelengths. Thus, the line 2496.77 A, with intensity 200 in Tc II, cannot be confused with boron, 2496.778 A, because the stronger line of boron, 2497.733 A, had only intensity 10. A few doubtful coincidences of Tc and impurity lines are retained in table 1, and it is not likely that many Tc lines have been masked by impurities. The chief omissions may be real Tc lines hidden behind the principal lines of copper, 3248, 3274, 5106, 5153, 5218, 5700, 5782, 7933, and 8093 A.

TABLE 1. *Arc and spark spectra of technetium*

λ=wavelength; *c*=complex; *d*=double; *h*=hazy; *H*=very hazy; *w*=wide; *W*=very wide; *s*=shaded to shorter waves; *l*=shaded to longer waves.

λ	Intensity		λ	Intensity		λ	Intensity		λ	Intensity	
A	Arc	Spark	*A*	Arc	Spark	*A*	Arc	Spark	*A*	Arc	Spark
8829. 80	10*c*		8308. 14	10		7981. 86	1		7779. 53	1	
8751. 80	1		8254. 48	2		7968. 27	2		7777. 17	3	
8737. 95	5*cW*		8248. 95	3		7965. 41	5		7746. 60	2	
8722. 70	2		8237. 08	15*c*		7963. 86	1		7737. 36	3	
8719. 97	2		8228. 65	1		7949. 64	2		7705. 70	1	
8716. 77	1		8225. 09	3*c*		7885. 96	2*c*		7697. 36	80*c*	
8707. 21	9		8211. 29	10		7874. 72	5		7684. 43	8	
8652. 76	3*c*		8206. 49	4		7871. 16	50		7681. 73	3	
8543. 63	8		8205. 24	10		7863. 11	1		7675. 32	1	
8537. 66	2		8170. 51	10		7861. 36	30		7658. 31	2	
8531. 07	7		8160. 89	2		7858. 24	2		7624. 49	7	
8522. 56	2		8153. 52	1		7856. 32	7		7618. 39	3	
8514. 70	2		8146. 52	1		7854. 35	1		7579. 20	40	
8481. 37	1		8142. 60	2		7848. 35	1*c*		7573. 99	15	
8404. 00	1		8127. 78	1		7817. 67	150*c*		7550. 98	1	
8383. 68	3		8119. 87	3		7816. 72	5		7548. 40	4	
8346. 59	4*c*		8068. 80	2*c*		7807. 11	1		7545. 45	3	
8319. 09	2*c*		8045. 30	2		7798. 18	4		7543. 32	7	
8315. 49	4		8042. 45	2		7792. 96	100*cW*		7540. 19	100*c*	
8309. 17	10*cw*		7999. 68	10		7782. 92	2		7534. 87	6	

TABLE 1. *Arc and spark spectra of technetium*—Continued

λ	Intensity		λ	Intensity		λ	Intensity		λ	Intensity	
A	Arc	Spark	*A*	Arc	Spark	*A*	Arc	Spark	*A*	Arc	Spark
7471. 75	1*c*		6754. 49	1*c*		6184. 68	5		5915. 74	1	
7470. 10	5		6753. 28	1		6183. 75	2		5908. 57	2*c*	
7461. 54	6		6747. 45	1		6182. 65	3		5905. 85	1	
7452. 45	50*c*		6733. 76	1		6163. 55	2		5905. 46	2	
7434. 08	10		6731. 18	2*cw*		6145. 91	1		5903. 82	1	
7405. 33	15		6687. 03	3		6132. 21	8*c*		5893. 57	2	
7402. 57	4*cd*		6673. 64	9		6130. 81	60		5885. 37	2*cw*	
7396. 79	8*c*		6661. 95	1		6127. 14	1		5879. 26	1	
7395. 05	4*c*		6661. 36	1		6124. 28	1		5874. 74	2	
7366. 28	2*c*		6648. 35	2		6120. 67	150		5873. 60	1	
7360. 02	1		6627. 87	3		6115. 44	1		5871. 22	2	
7338. 18	3		6625. 54	40*cWs*		6111. 98	2		5867. 47	1	
7329. 11	8*c*		6602. 01	1		6111. 06	2		5865. 32	1	
7322. 34	10*c*		6598. 00	1*c*		6102. 95	60*c*		5863. 79	2*c*	
7316. 42	1		6595. 16	1*c*		6099. 38	20		5853. 29	2*c*	
7283. 18	1*c*		6589. 96	1		6093. 71	2		5838. 28	1	
7256. 05	4		6579. 23	9		6085. 22	100*cws*		5836. 28	10	
7251. 53	1*c*		6576. 79	4		6069. 77	4		5831. 45	30	
7157. 59	10*c*		6563. 99	3		6066. 15	1		5827. 14	2	
7156. 78	1		6534. 57	1		6065. 08	20		5826. 49	4*c*	
7141. 23	8		6533. 98	1		6063. 91	3*c*		5823. 09	1	
7093. 08	4*c*		6526. 79	15		6063. 45	4		5821. 24	1	
7086. 11	20*c*		6515. 11	1		6057. 24	2		5819. 11	1*c*	
7071. 38	3		6496. 58	1*c*		6047. 98	4		5814. 20	3	
7048. 49	2*c*		6491. 65	15*c*		6032. 34	6		5805. 19	2	
7029. 51	1		6470. 25	7		6030. 24	1		5802. 39	1	
7019. 95	1		6469. 49	1		6028. 50	1		5799. 83	8*c*	
7016. 50	4		6461. 91	40		6024. 41	2		5794. 62	9*c*	
7006. 22	1*c*		6455. 88	100		6023. 49	4		5777. 92	1	
7002. 33	7*c*		6445. 05	3*c*		6020. 68	1		5775. 02	1	
6998. 60	1		6412. 90	1*c*		6018. 59	1		5773. 61	2	
6990. 22	1		6408. 81	5		6013. 17	1		5771. 45	40*cw*	
6985. 35	1		6392. 38	4		6012. 07	2*c*		5754. 74	2	
6934. 02	1		6389. 85	6		6010. 17	2		5749. 50	1	
6933. 04	1		6388. 38	3*c*		5997. 12	1		5741. 92	1*c*	
6931. 72	2*c*		6356. 71	10		5996. 67	2		5737. 52	1	
6907. 50	2		6354. 83	15		5993. 19	1*cw*		5725. 32	40	
6876. 69	2*c*		6312. 15	10		5986. 76	1		5721. 08	1	
6874. 59	1		6310. 40	4		5980. 57	4*cw*		5719. 52	1	
6871. 65	1		6306. 16	1		5974. 79	1		5696. 61	1*c*	
6866. 64	1		6305. 00	3		5968. 98	1*c*		5696. 03	2	
6862. 30	1		6303. 98	1		5951. 46	4		5694. 30	1*c*	
6860. 67	2		6296. 72	1*c*		5946. 48	1		5692. 22	1	
6856. 85	3		6275. 38	1		5942. 24	2*cw*		5689. 05	15	
6829. 92	1		6255. 74	1		5938. 38	3		5688. 74	2	
6826. 06	1		6248. 94	2		5937. 07	1		5687. 31	15	
6818. 01	1		6244. 17	50*c*		5931. 93	60		5685. 52	1	
6813. 50	1		6239. 67	2		5930. 32	2		5680. 93	1	
6805. 89	1		6236. 77	1*c*		5926. 29	15		5678. 46	2	
6804. 93	1		6214. 02	3		5925. 69	2		5675. 14	1	
6798. 58	3		6204. 40	1		5925. 38	3*c*		5672. 15		
6785. 95	3		6202. 68	2*cw*		5924. 47	100*cW*		5667. 59	*c*	
6776. 50	1		6198. 76	1		5923. 35	10		5667. 03	1*c*	
6761. 40	2		6195. 36	3		5921. 34	1		5664. 89		
6758. 26	2		6192. 65	100*c*		5919. 42	1		5662. 09		

TABLE 1. *Arc and spark spectra of technetium*—Continued

λ	Intensity		λ	Intensity		λ	Intensity		λ	Intensity	
A	Arc	Spark	*A*	Arc	Spark	*A*	Arc	Spark	*A*	Arc	Spark
5661. 52	2		5468. 66	1		5240. 92	1		4980. 41	2	
5658. 05	1		5467. 36	1		5236. 10	1		4978. 52	1	
5655. 99	5		5458. 07	1*c*		5231. 22	1		4976. 34	150	
5644. 93	50		5455. 94	3		5230. 28	1		4967. 18	2	
5644. 32	1		5455. 08	2*c*		5228. 67	2*c*		4956. 32	1	
5642. 12	100		5451. 89	40		5227. 53	4		4954. 94	1	
5640. 76	2		5450. 41	1		5214. 08	1		4948. 79	1	
5637. 77	1		5448. 35	2		5208. 52	2*c*		4948. 06	8	
5636. 83	3*c*		5447. 76	1		5206. 53	4		4947. 04	2	
5636. 24	2		5447. 39	9		5202. 10	1		4944. 20	1	
5629. 92	20		5444. 25	2		5193. 10	3		4938. 79	2	
5625. 20	1		5439. 48	1*c*		5189. 67	2		4936. 10	1	
5620. 45	200*c*		5425. 93	1		5184. 95	1		4933. 79	1*c*	
5617. 63	1		5423. 05	5		5183. 97	2		4929. 71	1	
5616. 76	1		5412. 89	2		5178. 05	1		4923. 58	4	
5615. 23	1		5411. 92	2		5177. 69	1		4920. 65	3	
5611. 46	2		5407. 90	4		5174. 79	100		4915. 79	1	
5606. 37	1*c*		5400. 45	1		5167. 75	1		4914. 68	2	
5603. 52	1		5389. 30	2*c*		5161. 77	80*c*		4913. 01	15	
5602. 22	10		5387. 62	1		5150. 58	10		4909. 55	100	
5596. 53	1*c*		5386. 86	1		5139. 25	10		4908. 50	40	
5589. 01	300*cd*		5383. 45	1*c*		5136. 12	2		4906. 39	1	
5584. 00	2		5382. 64	1		5135. 78	1		4900. 01	1	
5580. 19	1*c*		5377. 39	1		5134. 28	2*c*		4892. 47	3	
5577. 57	1*c*		5376. 27	1		5122. 14	1		4891. 89	150	
5576. 77	2		5375. 19	30*c*		5120. 59	3		4890. 89	3	
5576. 25	2		5366. 02	1		5113. 64	2		4889. 41	1	
5575. 41	1*c*		5364. 01	1		5109. 79	8		4888. 69	2	
5572. 85	2		5360. 65	1		5104. 33	30		4885. 87	1	
5570. 74	1*c*		5359. 21	2		5103. 23	10*c*				
5568. 62	1*c*		5358. 63	15		5102. 51	2		4885. 00	1	
5562. 93	1		5356. 63	6		5100. 69	1		4876. 96	2*d*	
5550. 51	3		5353. 48	50		5099. 97	1		4874. 76	1	
5545. 79	1*c*		5350. 85	1		5096. 27	200		4870. 76	3	
5543. 60	2		5334. 79	15		5090. 74	3		4866. 71	250	
5541. 92	7		5328. 42	1		5086. 91	3		4863. 29	1	
5540. 55	1		5320. 20	30		5083. 94	2		4862. 91	1	
5538. 84	2*c*		5318. 16	1		5069. 54	2		4862. 19	2	
5528. 22	4		5317. 51	2		5060. 69	30		4861. 19	1	
5524. 08	6		5314. 97	10		5058. 32	2		4859. 19	1	
5518. 02	2		5311. 13	1		5055. 27	9		4857. 19	2	
5514. 16	1*c*		5305. 31	4		5051. 27	2		4853. 57	400	
5513. 58	1		5285. 06	30		5032. 44	3		4841. 36	2	
5510. 81	1		5279. 31	1		5027. 88	3		4835. 40	30	
5506. 85	9*cw*		5275. 51	50		5026. 79	5		4834. 36	30	
5505. 25	2		5274. 82	2		5026. 23	15		4831. 33	3	
5502. 93	2		5273. 91	2		5024. 68	1		4820. 75	150	
5500. 04	2		5273. 20	1		5014. 51	4		4816. 79	9	
5495. 96	1		5267. 21	1		5010. 72	1		4813. 26	1	
5490. 32	2		5266. 30	1*c*		5005. 73	2		4811. 79	1	
5485. 32	2		5261. 44	6*c*		5002. 67	3		4809. 37	1	
5484. 99	2		5254. 74	2*c*		5000. 82	1		4805. 63	1	
5482. 97	5		5251. 39	2		4999. 07	1		4800. 62	1	
5482. 83	3		5249. 37	1		4995. 00	15		4799. 96	3	
5471. 92	10		5246. 97	2		4993. 97	1		4791. 62	4	

TABLE 1. *Arc and spark spectra of technetium*—Continued

λ	Intensity		λ	Intensity		λ	Intensity		λ	Intensity	
A	Arc	Spark	*A*	Arc	Spark	*A*	Arc	Spark	*A*	Arc	Spark
4790. 47	3		4616. 86	9	5	4328. 77	3	2	4146. 21	1	
4789. 48	2		4609. 17	4*c*	3*h*	4324. 85	1		4145. 02	80*c*	50*c*
4787. 69	2*c*		4608. 00	2	1	4323. 94	1		4141. 28	3	2
4785. 59	4		4602. 72	2	1	4323. 35	3	2	4139. 85	5	4
4784. 69	1		4594. 06	2	1	4319. 94	1*h*		4139. 10	3	2
4783. 92	2		4593. 36	20	10	4318. 65	2	2	4134. 80	3	2
4780. 56	1		4584. 86	2	1	4314. 03	1		4130. 44	2	1
4779. 84	1		4579. 09	1		4312. 48	1		4128. 27	10	6
4776. 33	2		4578. 46	10	6	4310. 21	3	2	4124. 22	80	50
4773. 86	2		4570. 85	2	1	4308. 59	2	1	4119. 28	4	3
4771. 53	150		4564. 57	30	20	4307. 78	1	1	4115. 08	100	60
4762. 35	2		4563. 80	1	1	4305. 82	4	3	4113. 26	1	
4758. 06	1		4562. 94	1		4305. 52	1		4111. 37	2	1
4756. 09	1		4558. 73	1		4297. 06	500	300	4110. 21	10	6
4752. 71	4		4557. 06	6	4	4294. 35	5	3	4106. 69	2	1
4749. 60	3		4552. 85	5	4	4289. 54	2	1	4106. 21	1	
4746. 02	1		4552. 41	1		4286. 31	1		4105. 08	2	1
4741. 24	1		4552. 21	3	2	4278. 91	40	20	4101. 24	2	1
4740. 59	200		4545. 56	1		4277. 53	1		4100. 08	2	1
4739. 53	1		4542. 10	4	3	4274. 95	3?	2?	4098. 77	1	
4736. 48	2*c*		4539. 54	100	50	4266. 16	1	1	4095. 68	200	100
4719. 28	100		4537. 36	2	1	4262. 67	100	50	4094. 17	2	1
4717. 76	10		4522. 85	200	100	4262. 26	400	200	4093. 68	3	2
4716. 76	1		4515. 98	10	6	4258. 61	1		4091. 54	2	1
4714. 20	2		4501. 74	1		4257. 33	1		4090. 13	2	1
4706. 90	6		4498. 54	1*h*		4243. 00	2	2	4089. 23	1	
4702. 83	1		4495. 03	10	5	4239. 55	2	1	4088. 70	150	80
4694. 28	3		4487. 05	40	20	4238. 19	300	150	4083. 54	3	2
4689. 77	1		4481. 52	10	5	4232. 09	2	1	4083. 20	1	
4689. 34	4		4473. 65	1		4230. 84	6	4	4079. 81	1*h*	1*h*
4687. 97	2		4465. 61	2	1	4230. 22	1		4077. 71	2	1
4686. 37	1		4463. 82	2	1	4229. 96	1		4069. 01	2	1
4683. 58	1		4454. 81	5Ca?	4	4220. 32	2	1	4060. 84	1	
4678. 88	2		4452. 24	2	1	4218. 61	30	15	4057. 81	2	1
4673. 05	2		4434. 98	2	3	4215. 51	1	1	4057. 24	2*h*	1*h*
4672. 82	2		4432. 54	1		4214. 22	1		4056. 08	4*h*	3*h*
4672. 17	5		4429. 60	30	15	4212. 42	1	2	4054. 42	2*h*	1*h*
4669. 30	100	40	4425. 47	1*h*	2*h*	4211. 43	2	1	4053. 18	5	3
4664. 32	2	1	4420. 32	1		4206. 58	9	6	4051. 94	5	3
4660. 21	30	10	4412. 02	2	1	4201. 86	2	1	4049. 10	150	80
4656. 99	1		4383. 10	2	1	4199. 46	2	1	4041. 76	2	1
4654. 64	2	1	4373. 97	2	1	4198. 31	1	4*h*	4041. 52	2	1
4653. 59	1		4370. 73	2	1	4189. 61	3	2	4039. 23	10	6
4648. 34	70	20	4370. 10	2	1	4186. 52	50	30	4037. 09		3*h*
4647. 57	2	1	4369. 26	1		4176. 28	100	60	4037. 01	4*h*+*g*	
4646. 61	1		4368. 92	1		4174. 46	1		4032. 91	1	
4645. 47	2	1	4363. 03	2	1	4172. 53	80	50	4031. 63	300	200
4643. 29	4		4361. 95	1		4170. 28	50	30	4029. 08	1	1
4637. 51	90	40	4359. 25	4	3	4169. 67	10	6	4026. 19	3*h*+*g*	2*h*
4635. 74	2	1	4358. 49	3	2	4167. 43	6	4	4025. 42	1	
4633. 13	2	1	4344. 58	2	1	4165. 62	80	50	4020. 77	10	7
4631. 33	1		4342. 22	1		4161. 53	1		4017. 23	4	3
4630. 57	20	10	4336. 87	10	5	4160. 02	1		4016. 68	3	1
4624. 97	2	1	4332. 46	3	2	4153. 64	1		4012. 01	6	4
4622. 71	3	2	4331. 81		1	4147. 61	2	1	4010. 08	1	

TABLE 1. *Arc and spark spectra of technetium*—Continued

λ	Intensity		λ	Intensity		λ	Intensity		λ	Intensity	
A	Arc	Spark	*A*	Arc	Spark	*A*	Arc	Spark	*A*	Arc	Spark
4007. 13	4	3	3854. 05	1		3768. 80	100	60	3696. 74		1*h*
4004. 69	3	2	3852. 37	2	1	3768. 35	1		3696. 32	4	2
3996. 95	2	1	3851. 23	4	2	3763. 98	2	1	3695. 99	1	
3994. 51	40	30	3847. 59	7	4	3761. 84	20	15	3694. 34	1	
3994. 03	2	1	3847. 35	3	1	3759. 19	1*h*	2*h*	3692. 78	6	4
3992. 06	1		3845. 99	15	10	3758. 56	15	10	3691. 64	2*h*	2*h*
3987. 77	3	2	3844. 28	2*h*	1	3756. 28	1	1*h*	3690. 88	1*h*	
3984. 97	200	100	3843. 98	3	2	3755. 24	5	3	3684. 78	100	60
3982. 18	2	1	3841. 33	10	7	3754. 41	60	40	3683. 50	2	1
3980. 36	4	2	3838. 30	15Ca?	10	3754. 09	3	2	3682. 61	3	2
3979. 63	4	2	3837. 58	20	15	3752. 93	1		3681. 71	1	
3979. 05	1		3832. 82	5	3	3752. 16	30	20	3680. 55	1	2*h*
3975. 02	5	10	3832. 34	15*c*	10*c*	3749. 96	8	5	3680. 34	10	6
3971. 48	1		3830. 34	2	1	3746. 87	200	100	3679. 18	30	20
3970. 21		2*h*	3829. 28	4*d*	4*d*	3746. 18	15	10	3678. 41	2	1
3959. 93		2*h*	3828. 54	9	6	3745. 04	6	4	3678. 10	3	2
3959. 52	3	2	3827. 57	1		3744. 82		2	3675. 88	1	2*h*
3959. 07	2	1	3824. 46	6	4	3744. 04	3	2	3675. 57		2*h*
3955. 74	4	3	3819. 12	2*h*	4*h*	3742. 81	4	3	3675. 44	1	
3953. 69	3	2	3818. 09	3	2	3741. 82	1		3673. 27		1*h*
3951. 83	3	2	3817. 96	4	3	3737. 71	2*h*	5*h*	3669. 96	2	1
3950. 38	2	1	3816. 90	6	4	3737. 44	4	3	3669. 15	1	1
3947. 11	20	15	3815. 50	2	1	3736. 93	4	5+Ca	3668. 96	1	
3946. 58	30	20	3814. 64	5	3	3731. 76	6	4	3667. 51	2	1
3940. 51		1*h*	3811. 28	3	2	3730. 85	1		3664. 94	4	2
3940. 04	1		3810. 57	1		3729. 19	4	3	3664. 58		2*h*
3936. 63	1	1*h*	3809. 78	1	3	3727. 37	3	3	3662. 85	1	
3934. 82	1		3808. 62	1		3726. 36	100*d*	70	3661. 47	30	20
3929. 37	1		3808. 13	1		3726. 19	2	1	3658. 62	80	60
3928. 85	1		3806. 13	1		3724. 41	50	30	3654. 07	2*h*	1*h*
3927. 57	2	2	3804. 00	2	1	3723. 71	30	20	3651. 50	10	8
3923. 67	4	3	3801. 63	1	2*h*	3723. 13	1	1	3650. 37	1	
3922. 13	2	1	3799. 66	3	2	3718. 88	300	150	3648. 06	70	40
3919. 38	6	4	3797. 79	30	20	3717. 32		2	3644. 15	2	1
3917. 73		1*h*	3797. 45	7	4	3717. 04	1		3643. 01	1	
3916. 52	1		3794. 80	2	1	3716. 80	2	1	3641. 16	1*h*	1*h*
3905. 76	1		3792. 10	1		3715. 96	9	6	3640. 23	10	8
3905. 51	2	1	3791. 75	8	6	3714. 52	2	1	3639. 41	30	20
3899. 86	7	4	3791. 30	10	7	3713. 87	2*g*?	1	3638. 88	4	3
3899. 11	1		3786. 56	1*h*	2*h*	3712. 84	5	3	3638. 24	40	30
3893. 23	2	1	3786. 08	5	3	3712. 28	20	15	3636. 10	400	200
3892. 14	20*c*	40*c*	3784. 08	9	6	3711. 40	1		3635. 18	80*c*	60*c*
3889. 14	2	1	3780. 70	70	50	3710. 13	2	1	3634. 27		2*h*
3880. 74	15	10	3779. 72	2	1	3709. 82	2	1	3633. 28	3	2
3879. 19	10	7	3779. 40	50	30	3708. 27	3	2	3630. 42	3	2
3875. 64	3	2	3777. 30	15	10	3707. 65	3	2	3628. 90	1	
3869. 32	1		3776. 04	1		3706. 72	3	2	3627. 86	2	1
3868. 26	15	10	3775. 34	2	1	3706. 05	2	3*h*	3627. 38	30	15
3866. 16	1*h*	3*h*	3773. 43	3	2	3705. 70	1		3625. 58	4	3
3865. 09	1		3772. 78	1		3705. 51	3	2	3619. 79	1	3*h*
3864. 12	10+Mo	7	3772. 38	2	1	3704. 83	6	5	3619. 40	1	
3863. 84	1		3772. 08	3	2	3703. 86	15	10	3618. 96	4	2
3863. 07	4	3	3771. 44	1		3703. 19	2	1	3616. 36		2*h*
3856. 74	10	7	3771. 06	60	40	3697. 76	1		3615. 82	2	1
3854. 34	1		3770. 51	2	1	3697. 43	2	1	3612. 85		1

TABLE 1. *Arc and spark spectra of technetium*—Continued

λ	Intensity		λ	Intensity		λ	Intensity		λ	Intensity	
A	Arc	Spark	*A*	Arc	Spark	*A*	Arc	Spark	*A*	Arc	Spark
3612. 14	1	1	3525. 84	30	20	3437. 45	4	2	3330. 79	3	2
3611. 14	4	5	3522. 11	1		3435. 70	1		3327. 12	3	2
3609. 90	2*h*	4*h*	3521. 29	1		3434. 71	6	3	3325. 56	7	4
3609. 06	1		3519. 43	1	2	3431. 76	2	1	3323. 90		1*h*
3608. 30	100	60	3517. 18	2	1	3427. 87	1		3322. 30	2	1
3607. 66	5	3	3515. 18		1	3426. 66		2	3319. 27		1
3607. 35	50	30	3514. 29	1		3425. 40	1		3318. 77		2*h*
3604. 77		1*h*	3510. 92	5	3	3424. 33	2	6	3317. 66		1
3599. 74	2	1	3508. 27	3	2	3422. 97	1	2	3315. 81	2	7
3597. 43	1		3507. 19	2	1	3421. 47		1	3313. 67	5	3
3595. 70	50	30	3506. 13	2	1	3419. 12	6	3	3312. 53	2	8
3594. 93	2	1	3505. 39	4	8	3418. 58	1	1	3311. 04	2	1
3594. 60	8	5	3503. 80	1		3418. 17	2	1	3310. 65	8	5
3593. 49	9	5	3503. 58	1		3418. 07	2	1	3309. 41	1*h*	2*h*
3591. 51	1	2	3503. 35	1	3*h*	3417. 74	1		3305. 91	6	3
3591. 20	1		3502. 73	50	30	3411. 74	1	1	3305. 61	1	2*h*
3589. 89		2*h*	3502. 49	2	1	3411. 63	3	9	3302. 39	2	1
3587. 96	80	50	3501. 55	1	2*h*	3408. 31	2	1	3301. 98	4	15
3585. 72	2*h*	1	3501. 26	4	2	3407. 27	3	2	3300. 78	3	2
3583. 45	1		3500. 72	20	10	3405. 83	1		3298. 85	15	60
3582. 66	50	30	3499. 15	2	1	3405. 34	3	2	3298. 29		2
3582. 10	15	10	3495. 84	1		3403. 91	2	1	3297. 36	2	5
3581. 27	20	10	3494. 64	8	5	3398. 33	2	1	3296. 27	1	3
3580. 08	20	15	3494. 15	1		3394. 20	8	5	3293. 63		1
3579. 00	1		3493. 41	8	5	3392. 23	1		3291. 96	1	
3576. 50		2*h*	3490. 31	2	1	3391. 37	1	2	3288. 30		1
3576. 33	1		3486. 25	50c	30	3390. 81	1	3	3287. 18	5	10
3575. 45	2	1	3484. 61	1		3388. 18	1	3	3285. 83	1	3
3574. 61	2	1	3482. 69	1	2	3386. 68	2	1	3284. 77	1	
3574. 43	1		3481. 40	1	3*h*	3386. 35	1		3282. 41	20	50
3573. 32	1	2	3475. 60	20	10	3385. 47		1	3276. 30	2	1
3573. 07	1		3475. 18	2	1	3382. 65		1*h*	3272. 55	1	2*h*
3572. 65	1	3	3473. 72	1		3380. 39	2	1	3272. 12	3	2
3570. 67	2	1	3472. 88	1		3378. 07		2*h*	3271. 19	2	1
3568. 87	20	10	3470. 53	6	4	3373. 56	1		3270. 62	2	1
3565. 43	3*d*	1	3467. 95	1*h*	3*h*	3373. 43	2	1	3270. 07	1*h*	2*h*
3565. 23	1		3467. 21		2*h*	3372. 80	1		3269. 81	1	4
3565. 02		1*h*	3466. 29	250c	150	3371. 90	1		3269. 68	2	6
3561. 23	1		3462. 41		2*h*	3371. 59	1		3269. 43	1	2*h*
3560. 90	1		3461. 68	3+Ni	1	3366. 76	10	6	3266. 92	15	80
3560. 34	10	6	3458. 00	1	1	3363. 04	3	10	3266. 31	2	6
3559. 77	5	3	3457. 59	2	1	3362. 62		1	3264. 67	2	4
3556. 07	1	2*h*	3457. 25	15	8	3361. 20	1		3262. 91	1	
3553. 53	2	1	3456. 86	6	3	3359. 20	1*h*	1*h*	3262. 12	1	3
3550. 66	100c	70	3456. 48		1	3350. 86	2	1	3261. 94	8	5
3549. 74	150c	100	3456. 11		2	3350. 56	2	1	3261. 39	3	2
3541. 78	50	30	3454. 08	1		3348. 47	1	2	3259. 93	2	1
3538. 70	10	5	3453. 01	1		3345. 60	8	20	3259. 28	1*h*	
3538. 13	4	2	3451. 05	6	4	3339. 23		1	3256. 34	10	50
3535. 52	10	8	3444. 00		1*h*	3338. 88		2*h*	3256. 12	4	3
3534. 87	3	2	3443. 49	3	2	3338. 27		1*h*	3254. 96	1	4
3531. 34	1		3442. 25		2*h*	3337. 55	2	1	3254. 70	1	
3529. 85	2	1	3441. 09	1*h*	3*h*	3334. 53		1	3252. 06	10	8
3527. 96	1		3438. 74	2	1	3332. 48	2	1	3250. 39		1
3526. 19	7	4	3438. 24		2*h*	3331. 75		1*h*	3249. 31		1

TABLE 1. *Arc and spark spectra of technetium*—Continued

λ	Intensity		λ	Intensity		λ	Intensity		λ	Intensity	
A	Arc	Spark	*A*	Arc	Spark	*A*	Arc	Spark	*A*	Arc	Spark
3244. 19	10	8	3156. 81	1	2	3062. 39	3	2	2988. 61		2Ca?
3242. 29	1	1	3153. 35	1		3062. 13	2	1	2988. 20	1	
3241. 85	3	2	3153. 17	1	2	3061. 78		2*h*	2987. 23		1*h*
3240. 68		1	3150. 26	2	1	3060. 91		2*h*	2985. 38	3	3
3239. 79	1	1	3146. 24	1	1	3060. 69	2	1	2985. 05	1	
3239. 51	1	1	3146. 00		1	3058. 52	1	4	2984. 40	5	15
3238. 50		1	3145. 62	1	3*h*	3057. 52		2	2984. 15	2	1
3237. 02	200*c*	400*c*	3144. 58		2	3057. 34	2	1	2983. 73	1	2*h*
3235. 00		1	3144. 17	1	2	3057. 04	2	1	2982. 55	10	40
3230. 95	5	15	3143. 63	1	2*h*	3055. 47		1*h*	2980. 84		1*h*
3230. 02	3	2	3141. 00	1*h*	3*h*	3053. 10		1*h*	2979. 76	2	3
3226. 05	2	1	3140. 67	1*h*	2*h*	3052. 50	2	3	2976. 57	15	40
3223. 59	1	3	3139. 99	1	1*h*	3051. 57	3	2	2976. 19	2	5
3220. 73	3	2	3138. 33	1	1	3049. 05		1*h*	2973. 67	4	3
3219. 73	2	5	3136. 61	2	10	3047. 55	2	3	2970. 76	1*h*	6*Hl*
3218. 58	1		3133. 35		1	3046. 53	1	4	2968. 79	1	
3218. 25	1	3	3133. 15	1	4	3045. 30		2*h*	2967. 13	3*hl*	10*Hl*
3217. 48	2	1	3131. 26	15	8	3044. 71	1	3	2966. 57	1	3
3217. 12	1	2	3127. 87	1		3043. 78	1		2966. 19	3	8
3216. 53	1		3122. 66	6	3	3043. 08	1		2965. 49		1
3215. 80	1	1	3121. 97	3	6	3042. 66	2+Fe	1	2964. 50	20	60
3214. 90	1	1	3119. 90	2	5	3040. 90	1	1	2962. 58		1
3213. 29	1	1	3119. 68	2	1	3040. 63	1	1	2962. 09	3	9
3212. 01	80*c*	300*c*	3119. 18	3	2	3038. 24	3	2	2961. 63	2	6
3208. 87	1*h*	1*h*	3116. 90	1		3037. 91	15	50	2958. 88	1*h*	2*h*
3202. 84	8	5	3116. 01	2	1	3036. 90	2	1	2958. 48		1
3200. 98	1		3115. 31		1	3034. 61	2	1	2958. 38	1	2
3198. 49	2	1	3110. 59	1	4	3033. 64		1	2957. 83	2	1
3197. 72	2	1	3109. 14	2	5	3033. 18	2	1	2956. 25		1
3197. 53	3	2	3106. 95	2	1	3032. 07	1	2	2955. 94	4	2
3195. 68		2	3105. 39	1	2	3029. 22		1	2953. 18	1	2
3195. 21	50	200	3105. 13	2	8	3026. 89	10	20	2952. 55	2	6
3192. 35		1	3104. 29	1		3026. 44		1	2952. 07	1	3
3192. 07	2	1	3100. 89	2	5	3025. 28	3	2	2951. 05	1	2
3191. 63	1		3099. 54	4	2	3023. 71	4	3	2950. 81	3	6
3190. 36	6	20	3099. 12	6	3	3022. 22	1	3	2950. 40	4	10
3189. 71		1*h*	3098. 58	2	5	3022. 06	1		2950. 26	1	3
3188. 00		1*h*	3097. 28	1	4	3019. 19	2	4	2949. 58	1	
3183. 12	30	15	3095. 77	2	2*d*	3017. 25	6	4	2949. 48	1	2*h*
3182. 80	1	1	3093. 64		2	3016. 31	1		2949. 25	2	1
3182. 38	30	15	3090. 26	2	1	3015. 16	2	5	2948. 64	20	60
3181. 31	1	2*h*	3089. 36	3	2	3009. 76		1	2948. 48	10	20
3180. 31	5	3	3084. 51		1*h*	3008. 78		1	2948. 10	1	2
3178. 34		1	3083. 31	2*d*	4*d*	3007. 00	4	15	2947. 12	2	1
3177. 91	1	2	3081. 10	1	1	3005. 51	1	2	2946. 58	1	2
3174. 75	1	3	3079. 92	1	3	3004. 62		1	2946. 21		1
3173. 30	40	2C	3077. 70	3	10	3004. 40	1	3	2945. 53	1	3
3171. 94	2*d*	2*d*	3076. 27	3	2	3003. 71	2	1	2942. 92	10	30
3171. 47	1	2*Hl*	3074. 31	2	1	3003. 03		2	2941. 84		2
3170. 38	2	6	3072. 92	1	2	3001. 05	5	15	2940. 92		2
3169. 27		1	3070. 28	2	1	2996. 88		1	2940. 49		1
3165. 15	1	4	3069. 97	5	20	2994. 12	1	2	2940. 01	2	1
3161. 70	5	3	3068. 34	2	1	2993. 94	1	1	2939. 25		1
3158. 07	1	2	3066. 61	1		2993. 77	1	3	2938. 98	10	20
3157. 66		1	3066. 40		1	2992. 87	1*h*		2936. 93	4	15

TABLE 1. *Arc and spark spectra of technetium*—Continued

λ	Intensity		λ	Intensity		λ	Intensity		λ	Intensity	
A	Arc	Spark	*A*	Arc	Spark	*A*	Arc	Spark	*A*	Arc	Spark
2934.65		1	2890.47	2	6	2845.06	5	3	2800.79	2	6
2933.94	15	30	2889.23	30	80	2843.78	1	1	2800.46	1	3
2932.94	1	2	2888.48	10	10	2843.35	1	3	2797.75	3	6
2932.12	1	3	2887.76	20	10	2842.30		2	2796.72	15	30
2931.56	1	2	2887.43		1	2840.38	30	100	2795.78	100	200
2931.14	3	8	2886.10	2	5	2839.87	2	10	2795.08	2	4
2930.50	3	2	2885.55	2*h*	6*h*	2838.88	1	3	2794.55	4	2
2930.05	2	5	2884.76	1	2	2838.56	8	15	2794.24	15	30
2929.53	2	8	2883.51		1	2836.91		1*h*	2793.67		1
2928.45	4	10	2882.39	5	10	2836.13	10	30	2792.98		2
2928.20	10	5	2881.32		2*h*	2835.63	2	1	2792.09	1*h*	2*h*
2927.32	1	3	2881.15	2	2	2834.75	1	2	2790.46	2	2
2925.10	1	3	2880.43	20	60	2834.32		2	2790.28	1	1
2924.87	1	1	2879.15	4	10	2833.60	15	40	2789.27	20	40
2924.27	3	10	2878.70	3	8	2831.19	30	100	2788.90	2	3
2923.35	20	40	2877.18		1	2830.87	1	3	2788.81	1	2
2922.75	10	20	2874.12	2	4	2829.62	1*h*	2*h*	2787.95	2	6
2921.94	8	4	2873.93		1	2829.09	1	2	2787.65		1
2921.52	4	15	2873.68	2	1	2828.07	15	8	2787.26	2	1
2921.07	15	60	2872.24	5*cw*	15*cw*	2826.18	10	30	2785.60	15	7
2919.66		1	2871.98	1	2	2825.98	2	1	2785.30	2	5
2915.86		1	2871.45	1	2*h*Cr?	2825.35	15	40	2785.15	1	2
2914.24		1*h*	2870.43	2	6Cr?	2825.06	10	30	2784.74		1
2913.81	1	1	2870.31		2	2822.92	1*h*	2*h*	2784.39	1	3
2913.17	15	10	2869.51	2	1	2821.62	10	20	2782.08	30	15
2912.01	2	4	2869.30	6	10	2821.37	30	100	2781.24	2	1
2911.71	1	2	2868.81	1	1	2820.19	2	6	2779.81	10Mg?	15
2910.70	1	2	2868.11	5	3	2819.48	2	1	2778.93	5	6
2910.23	20	40	2867.22	1		2819.06	1	2	2778.13	2	4
2909.09	3	10	2866.09	20*c*	60*c*	2818.65	2	6	2777.65		1
2907.99	2		2864.91		2	2817.62	3	7	2777.33	40	100
2907.63	2*h*	4*h*	2864.51	10	5	2817.29	1	2	2776.57	1	2
2906.90	1*h*	2*h*	2863.54		1	2817.01	5	10	2776.06	2	4
2906.63	6	20	2863.35	2		2816.51	2	6	2775.61	10	30
2906.26	1	2	2862.77		1	2815.97	2	4	2775.08	1	2
2904.96	1		2861.70	2	8	2814.99	2	4	2774.29	1	2
2903.84	3	2	2861.35		1	2814.88	20	10	2773.79	15	50
2902.93	1	2	2860.98	2	1	2814.64	2	4	2773.32	2	6
2902.54	1	2	2860.78	30	60	2814.20	15	30	2772.06	1	2
2902.15	15	40	2859.13	40	40	2813.80	10	20	2771.80	1	3
2900.69	5	15	2857.15	15	10	2813.50	2*d*	3*d*	2771.22	10*c*	30*c*
2899.37		1	2855.66	2	2	2813.00	1	3	2769.07	1	2
2896.58	1	2	2853.64		1*h*	2811.62	80	200	2768.40	1	2
2896.36	15	10	2853.28		1	2811.15		1*h*	2768.10		1
2895.48	2	5	2851.23		1	2810.24	4	8	2767.34	1*h*	3*h*
2894.83	2	5	2850.97	8	8	2810.06	1		2766.90	10	5
2894.34	6	3	2850.18		1	2809.66	20*c*	60*c*	2765.98	3	1
2893.90	1	3	2849.21	4	3	2808.38	15	8	2765.73	3	7
2893.47	5	2	2847.88		1	2807.93	3*d*	6*d*	2765.52		1
2893.18	5	2	2847.68		1	2807.43		1*h*	2764.51		1
2892.78	10	30	2846.74	5	15	2807.09		1*h*	2763.25	2	8
2892.35	5	20	2846.62	1	3	2806.65	2	5	2762.36	10	5
2891.34	2	5	2846.40	15	50	2805.19	1	3	2762.16	7	3
2891.20	1	3	2845.78		1	2803.35		1	2761.29	1	3
2890.81	20*c*	60*c*	2845.46	1	2	2803.03	5	10?	2760.40	1	

TABLE 1. *Arc and spark spectra of technetium*—Continued

λ	Intensity		λ	Intensity		λ	Intensity		λ	Intensity	
A	Arc	Spark	*A*	Arc	Spark	*A*	Arc	Spark	*A*	Arc	Spark
2760.13	1*h*	3*h*	2714.67	2	4	2671.02	2	6	2635.77	1	3
2758.72		2	2714.58	3	6	2670.84	1	2	2634.92	150	300
2757.58	1	3	2712.62	10	30	2670.12	4	7	2630.30		1*h*
2757.25	2	4	2711.94	1*h*	2*h*	2669.85	1	2*h*	2629.52		1*h*
2757.01	1	2	2711.50	2	6	2669.67	1	2*h*	2627.97	5*c*	15*c*
2756.50		1	2710.76	5	15	2668.95	5*d*	15*d*	2626.66		1
2755.77	10	5	2710.54	3	8	2668.30		1	2626.42	1	3
2753.06	1	3	2708.81	10	5	2667.80	1	2	2625.99	5	15
2752.30	1	3	2707.89	30	100	2667.18	1	2	2625.51	20	60
2751.49	15	40	2707.34	2	3	2665.76	8	20	2624.38	2	6
2749.30	3	8	2706.94	1	3	2665.10	2	6	2622.83	2	4
2749.21	3	8	2702.96	30	100	2664.69	4*h*	10*h*	2620.80	2	5
2747.40	2	5	2702.47	2	5	2663.95	2	4	2620.30	1	2
2744.35		1	2702.30	2	1	2663.17		1	2619.94	3	10
2743.84	10	30	2701.65	2	4	2662.66	7	20	2619.30	3	10
2742.76	1	2	2700.67	2	4	2662.32	5	3	2618.77	1	2
2742.54		2*h*	2699.80	2	6	2661.66	10	30	2617.58	2	6Fe?
2741.17	3	8	2699.42		1	2661.17	1	3	2616.07	7	20
2740.02	3*h*	10*hl*	2697.60	1	2	2660.91	15	30	2615.88	30	15
2739.28	1	2	2697.39	2	5	2658.59		2	2615.15	1	3
2738.83	40	150	2696.56	15	30	2658.19		2	2614.63	1	3
2737.99	4	2	2694.79	2	5	2657.98		1	2614.24	50	30
2737.69	4	10	2694.56		1	2657.59		1	2613.28	3	10
2737.14	2	6	2693.76	4	10	2657.34	2	1	2610.90	1	3
2736.85	30	100	2693.13	4	2	2657.04		1	2610.66		2
2736.52	3	10	2691.82	8	30	2654.90	1	1	2610.00	400	800
2736.23	8	7	2691.32	6	20	2654.32	7	3	2609.04		1
2735.94	2	4	2690.69	1		2653.75	2	6	2608.88	30	10
2735.16	3	8	2690.46	1	2	2653.58	2	1	2608.15	3	9
2733.80	1	2	2688.27	6	15	2653.39		1	2607.26	3	9
2733.24	1	2	2688.07	1	2	2652.90	3	8	2605.83	1	2
2732.89	10	5	2687.34	2	7	2652.36	50	150	2605.41	10	30
2730.53	20	10	2686.04	1	3	2652.10	1	1	2604.88	5	15
2730.19	1	2	2685.41	10*c*	30*c*	2651.81		1	2603.74	2	6
2729.73	1*h*	2*h*	2684.97		1	2650.60	5+*g*?	10	2602.55	3	7
2728.48	4	2	2684.51	5	15	2650.42	1		2602.11	10	20
2728.33		1	2684.22	1	2	2650.21		1	2600.92	1	3
2727.62	2	6	2683.90	3	1	2649.19	10	20	2599.41	1	3
2727.08	3	8	2683.73	1	2	2648.32	20	60	2598.63	2	5
2726.70	30	15	2683.14	5	4	2647.02	300	600	2597.21	15	30
2726.18	2	4	2682.77	10	20	2646.26	10	20	2596.78	5	10
2725.66	15	40	2682.67	10	20	2645.60	2	4	2595.75	2	1
2724.20	10	30	2682.33	3	8	2645.38	2*d*	2	2593.68	2	1
2723.75	2	6	2681.60	1	2	2644.51	40	150	2593.61	2	5
2723.40	5	15	2681.21	30	100	2643.02	15	40	2593.26	2	1
2723.02		1	2680.96	2	6	2642.54	1	2	2593.06	6	20
2721.56		1	2680.67	3	8	2642.38	3	1	2592.82	6	4
2719.80	1	3	2679.43	1	2	2642.13	1	2	2591.15	1	2
2719.31	10	20	2679.03	1	3	2641.28	2	1	2589.88	6	3
2718.19	1	2	2678.58	5	10	2640.49	1	2	2588.93	3	8
2716.69	4	10	2675.64	2	7	2640.17	10*c*	20*c*	2587.77	1	4
2716.55	4	10	2675.24	20	50	2639.33	1	3	2586.89	1*h*	4*h*
2715.84	4	10	2674.61	1	2	2639.07	2	4	2586.71	2	3
2715.47	3	8	2673.85		1	2638.80	2	6	2586.27		1
2715.21	2	1	2673.43	20	50	2636.35	6	6	2585.91	3	4Fe?

TABLE 1. *Arc and spark spectra of technetium*—Continued

λ	Intensity		λ	Intensity		λ	Intensity		λ	Intensity	
A	Arc	Spark	*A*	Arc	Spark	*A*	Arc	Spark	*A*	Arc	Spark
2585. 49		1*h*	2550. 05	3	10	2503. 56	1		2461. 86	1	
2585. 06	1*d*	4*d*	2549. 74		1	2503. 29	1	4	2461. 67	1	4
2584. 59	1*h*	2*h*	2549. 35		1	2502. 36	2	1	2461. 52	2	
2583. 09		2	2547. 94	20	50	2501. 86		1	2459. 67	1	
2582. 22	3*h*	10*hl*	2547. 01	1	4	2501. 38		2	2458. 99	2	1
2581. 00	3	7	2545. 75	1	2	2501. 00	3	1	2456. 47	2*d*	
2580. 86	2	4	2545. 55	3	2	2500. 65		1	2456. 17		1
2578. 78	15*h*	40*hl*	2544. 42	4	8	2500. 10	1	1	2455. 95		3*h*
2578. 31	15	40	2543. 24	500	1000	2499. 60	1	4	2454. 48		1
2577. 87	10	20	2541. 38	2	6	2497. 24	10	20	2453. 97	1	3
2577. 02	1	2	2540. 60	2	5	2496. 77	100	200	2453. 70	2	1
2576. 30	10	30	2540. 46	1*h*	3*h*	2495. 04		1	2452. 42	3	7
2576. 12	1		2538. 99	2	1	2494. 14	2	1	2451. 76	1	3
2575. 59	2	1	2538. 70	1	4	2493. 44	4	5	2450. 63	2	4
2575. 24	5	10	2538. 03	1*h*	2*h*	2492. 73	6	3	2450. 10	2	4
2575. 08	5	10	2537. 52	1	2	2491. 26	2	1	2449. 12	2	6
2574. 45	6	10	2537. 39	1	2	2491. 06	3	6	2448. 62	1	4
2573. 88	1*h*	2*h*	2534. 59	5	15	2490. 85	1		2447. 89	4	7
2573. 49	1	2	2533. 48	2	1	2490. 71		2*h*	2447. 45	1	3
2573. 38	1	2	2532. 97	4	10	2490. 11		3*h*	2446. 86	1	
2573. 17	1	2	2532. 04	2	8	2489. 47	4	6	2445. 78	1	
2572. 92	1	2	2531. 38	3	10	2489. 06		3	2445. 57	1	3
2571. 57	2	3	2530. 35	15	40	2488. 03		3*h*	2444. 01		2*h*
2571. 18	2	4	2528. 10	1	2	2487. 98	2	3	2442. 52		1
2569. 89	5	15	2527. 63	3	10	2487. 74		1	2441. 51		1
2569. 64		1	2525. 77		1	2487. 24	2	5	2441. 32		1
2568. 67	1	2	2525. 27	1	3	2487. 04	2	3	2439. 09	1	
2568. 39	1	2	2525. 05	1		2486. 48	2	1	2438. 76	1	3
2567. 74	3*d*	8*d*	2523. 88	2	5	2485. 59	3	8	2437. 00	3	2
2567. 52	1	2	2523. 41	5*c*	15*c*	2484. 58	2	5	2436. 81		2
2567. 04	30	100	2522. 50	4*d*	10*d*	2482. 60		1	2435. 84	4	2
2566. 33	2*h*	5*h*	2521. 86	2	3	2481. 17		1	2435. 63		2
2566. 03	3	10	2521. 64		1	2481. 00		1	2434. 85		1
2565. 67		1	2521. 07		1	2480. 70	5	2	2434. 38		2
2565. 17	1	3	2520. 65	1	3*h*	2479. 24		2	2433. 75	1	
2564. 67	3	5	2520. 04	2	4	2478. 83		2	2432. 62		2
2563. 32	1		2519. 83	1	2	2477. 80	1	2	2431. 39		1
2563. 12	1	1	2519. 42	1	3	2477. 52		1	2431. 11		1
2562. 82	2	1	2519. 17	10+Si	15*d*	2476. 90		1	2429. 55	1	3
2562. 55	1	2	2517. 15	5	20	2476. 29	1	5	2423. 25	15	7
2562. 01	2	6	2516. 85	5	15*h*	2475. 15	3	5	2421. 29	1	3
2561. 15	1	3	2516. 26	2	4	2474. 11	3	10	2420. 79	1	3
2560. 63	4	2	2515. 92	1	3	2473. 15		2	2418. 69	1	2*h*
2560. 17		1	2513. 60	1		2472. 13		2	2418. 05	2	1
2559. 43		1	2512. 96		1	2471. 29	1	3	2417. 82		1
2559. 21	1		2512. 27	1	2	2467. 53	1*h*	4*h*	2417. 53	1	4
2559. 00	1	3	2511. 28	1	3	2467. 07		2	2417. 10		1
2558. 62	40	150	2510. 17	5	3	2466. 88	4	2	2416. 70		1
2558. 22	10	30	2509. 45		1	2465. 75	2	1	2416. 23	4	2
2557. 40	2	5*h*	2508. 83	2	2	2465. 10	5	3	2414. 47	2	6
2556. 84	1	2*d*	2508. 39		1	2464. 82		1	2412. 62	1	
2556. 10	3	8	2507. 99	3*h*	8*h*	2464. 48	3	7	2411. 30	1	3
2554. 78	1	3	2507. 14	15	30	2463. 70	15	8	2410. 20		1
2554. 36	1*h*	2	2505. 04	2	7	2463. 53		2*h*	2408. 82	1	
2550. 78		1	2503. 98	5	20	2462. 11	1	2	2408. 16	2	6

TABLE 1. *Arc and spark spectra of technetium*—Continued

λ	Intensity		λ	Intensity		λ	Intensity		λ	Intensity	
A	Arc	Spark	*A*	Arc	Spark	*A*	Arc	Spark	*A*	Arc	Spark
2407. 87	1		2384. 66	4	10	2360. 44		1	2316. 72		1
2407. 11	1	3	2382. 98	1		2354. 08		1	2315. 32		2
2405. 13	1		2382. 39		2	2353. 16		1	2313. 91		1
2404. 10	5	15	2382. 05	6	3	2349. 17		1	2300. 97		1
2400. 90	1	3	2376. 05	7	15	2346. 59		2	2300. 44		1
2398. 67	7	20	2373. 77		1	2345. 17	1	3	2299. 96		1
2396. 64		1	2369. 05		2	2344. 84	1	3	2298. 14	4	10
2394. 97	2	1	2368. 35		1	2344. 71		1	2292. 14		1
2394. 49		1	2368. 01		1	2341. 67		2*h*	2291. 64		1
2393. 42		1	2367. 67		1	2331. 78		2	2285. 47	1	3
2392. 02	2	1	2366. 55	2	4	2329. 49		1	2282. 41		1
2390. 93		1	2365. 91		2	2328. 41	1	3	2280. 33		2
2389. 36		1	2365. 53		1	2327. 69		1	2272. 45		1
2386. 03		1	2361. 80	2	2	2324. 57	1		2271. 14	1*d*	4*d*
2385. 32		1	2360. 78		2	2318. 74		1	2266. 24		2
									2261. 30		1

III. Results

The results of this investigation are presented in table 1, where wavelengths and relative intensities of 2,121 spectral lines characteristic of technetium atoms and ions are given. In this table the wavelengths represent the averages of two to six independent determinations. Several hundred faint lines that were measured only once on the strongest spectrograms have been omitted from table 1, but some of these may be reported later if any confirm predictions from atomic energy levels.

The average probable error in these wavelengths is believed to be less than ± 0.01 A. There are three reasons for this belief, namely, computed probable errors of lines measured on six spectrograms, agreement of the wavelengths of impurity lines with their accepted values, and the average difference between the measured values of classified lines and their values computed from atomic energy levels derived from these observations [14].

In addition to six-figure wavelengths, estimated relative intensities of arc and spark lines of Tc are given in table 1. These intensities range from 1,000 for the strongest line to 1, which represents the weak lines whose reality is unequivocal because they were observed two or more times. In the spectral range in which arc and spark intensities were compared (4700 to 2200 A) Tc I lines have nearly double intensity in the arc, whereas Tc II lines have about treble intensity in the spark. Most of the Tc II and Tc I line-intensities thus differ by a factor of 5 or 6, and their assignment is unambiguous. A few lines, mostly faint ones, appear to have about the same intensity in arc and spark, but naturally a few approximate coincidences of Tc I and Tc II lines may be expected.

Occasionally the intensity numbers are accompanied by literal symbols having the meanings given in the table. Some of these symbols are especially significant for Tc spectra because they suggest hyperfine structure due to interaction of valence electrons with atomic nuclei. This hyperfine structure was observed in manganese spectra and in rhenium spectra, unresolved by gratings in the former case but easily resolved in the latter. The hyperfine structure of Tc lines appears to be intermediate between Mn and Re. Many Tc lines, especially among longer waves, appear as flat-topped images, four or five times as wide as the slit. These lines are under investigation with interferometers.

Besides a general resemblance of Tc spectra with those of Mn and Re, we can now define in detail the analogous spectral lines of the three elements or their ions. For neutral atoms of Mn, Tc, or Re the resonance lines are known as $d^5\,s^2\,{}^6S_{2½} - d^5 s^1\,p^1\,{}^8P_{3½,\,2½,\,1½}$, and the respective wavelengths are 4030.76, 4033.07, 4034.49 A in Mn; 4297.06, 4262.26, 4238.19 A in Tc; and 3460.47, 3464.72, 3451.88 A in Re. For singly ionized atoms of Mn, Tc, or Re the resonance lines are known as $d^5\,s^1\,{}^7S_3 - d^5\,p^1\,{}^7P_{4,3,2}$, and the respective wavelengths are 2576.10, 2593.73, 2605.69 A for Mn^+; 2543.24, 2610.00, 2647.02 A for Tc^+; but not yet revealed for Re^+. Full details concerning the interpretations of lines in the first two spectra of Tc will be divulged in another paper. The above-mentioned resonance lines of Tc and Tc^+ are probably useful for detecting this element in concentrations of 10^{-7}; the fact that they cannot be found in any spectral tables excluding fission products may be regarded as proof that technetium is not spectroscopically detectable in nature.

The authors acknowledge the generous cooperation of the United States Atomic Energy Commission in lending samples of technetium for this investigation, and compliment G. W. Parker of the

Oak Ridge National Laboratory on the high purity of these samples. Assistance with wavelength calculations was given by W. Lyle, R. Cross, and R. Murphy, and the direct-current arc spectrograms were made by W. Bozman.

IV. References

[1] D. I. Mendeléeff, J. Russ. Chem. Soc. **1,** 60 (1869).
[2] H. J. G. Moseley, Phil. Mag. **26,** 1024 (1913); **27,** 703 (1914).
[3] W. Noddack, I. Tacke, und O. Berg, Naturwissenschaften **13,** 567 (1925).
[4] W. F. Meggers, J. Research NBS **6,** 1027 (1931) RP322.
[5] E. Segré, Sci. Monthly **57,** 12 (1943).
[6] C. Perrier and E. Segré, J. Chem. Phys. **5,** 712 (1937); **7,** 155 (1939).
[7] C. Perrier and E. Segré, Nature **159,** 24 (1947).
[8] Plutonium Project, J. Am. Chem. Soc. **68,** 2411 (1946).
[9] G. W. Parker, J. Reed, and J. W. Ruch, CNL–1, Clinton National Laboratory, Contract No. W–35–058–ing–71, (Jan. 9, 1948).
[10] M. G. Inghram, Phys. Rev. **72,** 1269 (1947).
[11] D. L. Timma, J. Optical Soc. Am. **39,** 898 (1949).
[12] L. E. Burkhart, W. F. Peed and B. G. Saunders, Phys. Rev. **73,** 347 (1948).
[13] W. F. Meggers and B. F. Scribner, Y–476, Oak Ridge Spectroscopy Symposium, Abstracts of Papers (March 24 to 25, 1949).
[14] W. F. Meggers and B. F. Scribner, J. Opt. Soc. Am. **39,** 1059 (Abstract) (1949).

Washington, August 21, 1950.

Journal of Research of the National Bureau of Standards Vol. 45, No. 6, December 1950 Research Paper 2162

Dissociation Constants of 4-Aminobenzophenone Calculated From Ultraviolet Spectra at Several Temperatures

By Elizabeth E. Sager and Iris J. Siewers

Many of the physical-chemical properties of compounds of low solubility are difficult to determine because of the necessarily small concentrations of material. In many cases advantage may be taken of measurements of the absorption spectra if the bands occur in favorable ranges of the spectrum. The diphenyl ketones fall in this category and have been the subject of recent studies.

The ultraviolet absorption spectra of several concentrations of benzophenone, 4-aminobenzophenone, and 4,4′-diaminobenzophenone have been measured and their molar absorbencies determined. The dissociation of 4-aminobenzophenone, a weak base, has been carefully studied at temperatures from 10° to 40° C in 5-degree steps. Dissociation constants for each temperature, as well as activity coefficient terms, have been calculated. The heat of dissociation has also been determined.

I. Introduction

The acidic or basic properties of many slightly soluble compounds have not been determined because of experimental difficulties in applying the usual titration or electromotive-force methods to very low concentrations. Diphenylketones, such as benzophenone, 4-aminobenzophenone and 4,4′-diaminobenzophenone, are practically insoluble in water and fall in this category. They are colorless in aqueous solution, but their aromatic structure suggests that their ultraviolet spectra may be used to study some of their chemical properties. Accurate spectrophotometric measurements of concentrations as low as 10^{-4} or 10^{-5} molar can now be made at many temperatures. The observed changes in spectral absorbancy with changes in hydrogen-ion concentrations can be used to calculate dissociation constants and other related thermodynamic quantities.

The molar absorbancies of the molecular and ionic states of benzophenone, 4-aminobenzophenone, and 4,4′-diaminobenzophenone were first determined and compared. The parent compound, benzophenone, has no group to ionize, and its spectral curves are identical whether the material is in aqueous, acid, or basic medium. 4-Aminobenzophenone is a weak base and does not dissociate appreciably in aqueous solution, as demonstrated by identical curves of the free base in water and in various concentrations of alkali. Moderately strong acid is required to effect complete dissociation, as evidenced by the entirely different absorbancy curve in the near ultraviolet. 4,4′-Diaminobenzophenone has two groups whose dissociation ranges overlap, and extensive experimental data will be required to determine the constants.

A comprehensive study of the dissociation of 4-aminobenzophenone has been made at several temperatures, and the constants at 10°, 15°, 20°, 25°, 30°, 35°, and 40° C have been calculated and are reported in this paper. Hydrochloric acid was used to control the hydrogen-ion concentrations at various stages during the dissociation. The contribution of the 10^{-5}-M base to ionic strengths of 10^{-3} and 10^{-2}-M hydrochloric acid is so small that it can be neglected—thus the hydrogen-ion concentration may be taken as that of the known amount of hydrochloric acid.

The limiting spectral absorbancy curves of the free base and of the ionized compound do not change with change in temperature in the range studied, which is very fortunate. At a given temperature, then, all changes in absorbancy for one dissociation series may be attributed solely to the dissociation reaction. Another favorable factor is that 4-aminobenzophenone dissociates over a pH range of 1 to 3, where the temperature has little influence upon pH values.

For instance, the pH of 0.005-M hydrochloric acid on a comparative scale at 10° C is 2.332, and at 40° C it is 2.334, a negligible difference.

The concentration constants for the dissociation are determined in the following manner. The degree of dissociation and resulting ratios of free base to ions are calculated from the absorbancy data. The hydrogen-ion concentrations are known from the amounts of hydrochloric acid in the solutions. The products of the hydrogen-ion concentration and the ratios of free base to ions give the concentration constants, K_c. By plotting $-\log_{10}K_c$ as a function of ionic strength, practically straight lines with slight slopes are obtained that may be extrapolated to infinite dilution for estimated $-\log_{10}K_a$, or pK_a values for each temperature. The activity coefficient terms for the weak base can also be expressed as a function of ionic strength. Employing the usual thermodynamic equations, the heat of dissociation, ΔH, may also be calculated.

II. Experimental Procedure

1. Materials

Benzophenone was obtained from Eastman Kodak Co., and 4-aminobenzophenone and 4,4′-diaminobenzophenone were obtained from Dow Chemical Co. The benzophenone, a white crystalline compound, melted at 48.6° to 49.2° C. The 4-aminobenzophenone, a pale yellow crystalline compound, melted at 123.0° to 123.4° C. The 4,4′-diaminobenzophenone, a yellow crystalline material, melted at 244.1° to 244.4° C.

Hydrochloric acid of reagent grade was used to make stock solutions, 10^{-1}-M, for the majority of the dilutions. Stronger acid was required in some cases for determining limiting absorbancy curves. Sodium hydroxide, approximately 10^{-1}-M, was prepared free from carbonate, from which weaker concentrations of alkali were made. Conductivity water was used to dissolve the compounds under investigation and in making all stock solutions and subsequent dilutions.

2. Equipment

A model DU Beckman spectrophotometer was modified with a constant-temperature cell compartment of our own design.[1] The cell compartment is essentially a metal-box air bath, jacketed on all sides, top, and bottom, through which water circulates from a constant-temperature bath.[2] It was designed especially to accommodate large cylindrical absorption cells of 38-mm inside diameter, described in previous publications [1, 2, 3].[3] The cells are Pyrex cylinders of 1-, 2-, and 5-cm length with openings for filling and emptying and are fitted with removable end-plates of crystalline quartz. The cell assemblies are held together with metal containers and screw caps, using Bakelite and rubber gaskets. All cells, end-plates, and metal parts were made at this Bureau. One complete cell assembly measures about 44 mm in over-all diameter and 60 mm in over-all length. To allow passage of the radiant energy from the exit slit through the cells and solutions to the photocell compartment, two round openings about 22 mm in diameter were made in opposite sides of the water-jacketed box. Only two cells can be accommodated. Each cell is held in a metal cradle attached to a sliding rod, by which mechanism they can be placed alternately in the path of radiant energy. The metal housing with the source of energy was moved back about 1 in. so that it is not in contact with the metal walls of the cell compartment.

[1] The constant-temperature cell compartment was designed with the aid of W. S. Hertstein, draftsman, of the Instrument Shop of this Bureau, who made many helpful suggestions. I. W. Lund, also of the Instrument Shop, constructed the metal box, metal holders, and other parts necessary to modify the instrument.

[2] A 16-gallon constant-temperature bath of American Instrument Co. design was used.

[3] Figures in brackets indicate the literature references at the end of this paper.

3. Temperature Control

The water bath was maintained at the desired temperature, between 10° and 40° C within ±0.1 deg C. Water, initially at the bath temperature, circulates through four lengths of hose attached to the two inlets and outlets of the cell compartment and cover in the room at 25° C. Consequently, the temperature within the cell compartment is not exactly that of the water bath when it is above or below 25° C. The temperatures reported are readings taken from a thermometer with only the mercury-bulb tip inserted in a rubber stopper in the removable top. Care was taken not to allow more than the tip of the thermometer inside the box during spectrophotometric observations, so that extraneous light could not be introduced. In order to shorten the time for the solutions in the cells to attain the desired equilibrium temperature, several volumetric flasks containing the solutions for a series were placed in wire baskets that were suspended in the water bath. The cells were emptied, washed, and filled in the room at 25° C, and 30 min or more was allowed for the solutions in the cells to attain constant temperature.

4. Spectrophotometric Observations

The transmittancy readings were made at wavelength settings 2 mμ apart over the ultraviolet range of 210 to 400 mμ, inclusive. Usually the maxima and minima of the bands were first read, then the series of observations recorded at even wavelengths from 210 through 400 mμ. A check of the values at selected wavelengths was then made in reverse order. In this manner any change or trend in the transmittancy readings could usually be detected. A period of 30 to 40 min was required to make 160 or more observations. The reproducibility of transmittancy observations was usually within ±0.1 percent.

5. pH Measurements

In this study pH measurements were used only as a check on the prepared solutions, as hydrogen-ion

concentrations were the known hydrochloric acid concentrations. All solutions were measured with commercial glass-electrode assemblies at 25° C. A Cambridge pH meter was used for most of the measurements, but Beckman and Leeds and Northrup instruments were also employed.

III. Molar Absorbancies of Benzophenone, 4-Aminobenzophenone, 4,4′-Diaminobenzophenone

Spectrophotometric measurements of various concentrations of benzophenone, 4-aminobenzophenone, and 4,4′-diaminobenzophenone were made using 1-, 2-, and 5-cm absorption cells. This was done first to check the validity of the Beer-Lambert law of absorption, which states that at any given wavelength or wave number

$$a_M = A_s/bM \qquad (1)$$

in which a_M is the molar absorbancy index, A_s is the specific absorbancy of the sample ($-\log_{10}$ transmittancy), b is the depth of solution in centimeters through which the radiant energy passes, and M is the molar concentration of the absorbing compound. One may vary the concentration of the compound or change the depth of solution by using different cell lengths, and if the same curves of molar absorbancy index are obtained over the spectral range of observed wavelengths, then A_s/bM is a constant and there is conformation to the absorption law.

The three curves in figure 1 represent the molecular, or undissociated, states of benzophenone, R; 4-aminobenzophenone, RNH_2; and 4,4′-diaminobenzophenone, $R(NH_2)_2$ in aqueous or alkaline solution at 25° C. Molar absorbancy index is plotted as a function of wave number with the corresponding wavelengths shown at the top of the figure. Benzophenone has a maximum molar absorbancy index of 17,300 at 38,760 cm^{-1} (258 mμ). 4-Aminobenzophenone shows a maximum absorbancy index of 15,900 at 30,100 cm^{-1} (332 mμ) with a secondary band of 11,900 index at 40,800 cm^{-1} (245 mμ). 4,4′-Diaminobenzophenone shows greatly increased absorbancy with a main band of 23,500 index at 29,600 cm^{-1} (338 mμ) and a secondary band of 13,000 index at 42,400 cm^{-1} (236 mμ).

The same curve is obtained for benzophenone whether in aqueous solution, or acid or alkaline medium, as it has no group to dissociate. Also the curves are the same for the two amino compounds whether in aqueous solution or in alkali, demonstrating the fact that in water they do not dissociate appreciably but remain as free bases in the molecular state. To avoid confusion, the curves for the ionic states or the dissociated states of the aminobenzophenones are not given in this graph. However, they are similar to the curve for benzophenone with slightly increased absorbancy and slight shift of their bands of maximum absorbancy to higher wave numbers.

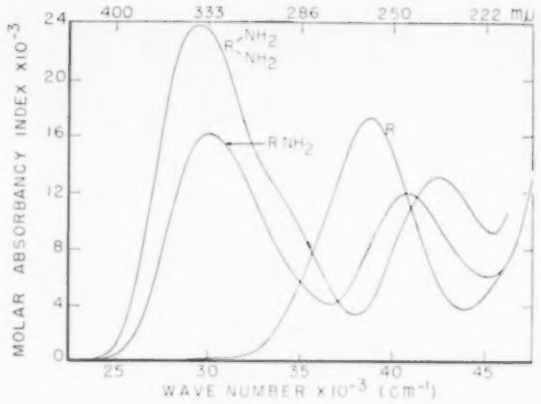

FIGURE 1. *Comparison of the ultraviolet absorption spectra of benzophenone,* R, *4-aminobenzophenone,* RNH_2, *and 4,4′-diaminobenzophenone,* $R(NH_2)_2$.

IV. Calculation of Dissociation Constants of 4-Aminobenzophenone from Spectral Data

1. Spectral Absorbancy Data

A typical set of transmittancy measurements over the ultraviolet range of the spectrum for a dissociation series is shown in figure 2. They are of 4-aminobenzophenone, 5×10^{-5}-M in 1-cm cells at various hydrogen-ion concentrations at 25° C given in table 1. The observed transmittancies in percentage are plotted as a function of wavelength. The free base, or undissociated 4-aminobenzophenone, is represented by curve 17. The completely dissociated compound is plotted as curve 1, and the 15 intermediate curves represent the partially dissociated base at various stages at known hydrogen-ion concentrations. It is readily seen that the two limiting curves, 1 and 17, intersect each other at three points, giving at least two well-defined isosbestic points at 242 mμ and at 283.5 mμ, which hold

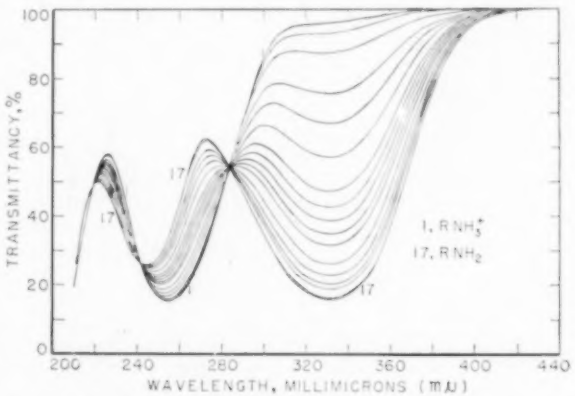

FIGURE 2. *Transmittancy curves of 4-aminobenzophenone as the free base (curve 17), the dissociated compound (curve 1), and 15 intermediate stages during the dissociation.*

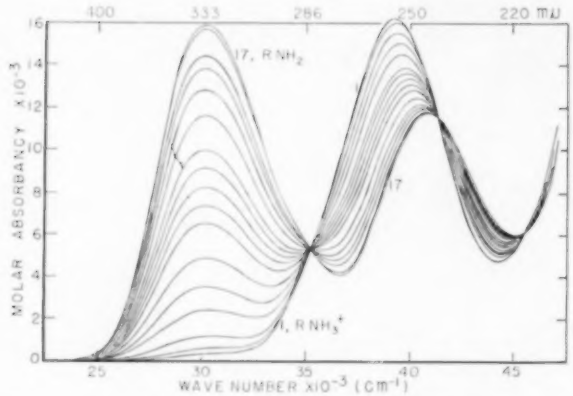

FIGURE 3. *Molar absorbancy curves of 4-aminobenzophenone as the free base (curve 17), the dissociated compound (curve 1), and 15 intermediate stages during the dissociation.*

for the entire series. The constancy of these points of equal transmittancy or absorbancy is very important in that it indicates purity and stability of the compound, and also that only one reaction is taking place, in this case, that of dissociation.

The same data are presented in figure 3, with molar absorbancy index $\times 10^{-3}$ plotted as a function of wave number with the corresponding wavelengths given at the top of the figure. Curves 1 and 17 represent the dissociated and free base, respectively. As the concentration of hydrogen-ion is increased the broad band of the free base at 30,100 cm^{-1} decreases, until upon complete dissociation there is almost negligible absorbancy. One might assume that sufficient acid would suppress this band completely, but high concentrations of acid were found to cause other chemical changes, indicated by some changes in absorbancy at higher wave numbers and a slight shift in the isosbestic points. The limiting curve for the dissociated state was very carefully determined using 0.3-, 0.4-, 0.5-, 0.6-, 0.81-, 1.0-, and 2.0-*M* hydrochloric acid. At 0.6-*M* acid, the absorbancy at wave number 30,100 was lowest and there was no evidence of displacement of the isosbestic points.

The secondary band of the free base, curve 17, with maximum absorbancy at 40,800 cm^{-1}, increases with increase in hydrogen-ion concentration and shifts toward the lower wave numbers as it approaches the absorbancy of the dissociated compound, curve 1. Practically all measurements in this portion of the ultraviolet range are on steep sides of the bands, as evidenced in figure 2, and do not have the accuracy of the measurements at lower wave numbers.

2. Method of Calculation of Concentration Constants

The acidic dissociation of the ammonium ion of 4-aminobenzophenone may be expressed as follows

$$RNH_3^+ \rightleftarrows RNH_2 + H^+.$$

The concentration constant, K_c, may first be calculated, neglecting for the present the activity coefficient terms for the free base and ions, according to the equation

$$K_c = \frac{[RNH_2][H^+]}{[RNH_3^+]}, \tag{2}$$

in which $[RNH_2]$, $[H^+]$, and $[RNH_3^+]$ are the concentrations of free base, hydrogen-ion, and dissociated compound, respectively. A familiar way of expressing this relation is

$$K_c = \frac{(1-\alpha)[H^+]}{\alpha}, \tag{3}$$

in which α represents the degree of dissociation into ions and $1-\alpha$ the remaining free base.

The amounts of either base or ions are proportional to their molar absorbancy indices as in eq 1. For brevity let $a_M(R)$, $a_M(R^+)$, and a_M', represent, respectively, the molar absorbancy index at any wavelength of the free base, the ions, and mixtures of the two during the dissociation.

As differences in absorbancies are used to calculate α or the amount of RNH_3^+ formed at any stage in the dissociation, a graphical illustration of the differences is given in figure 4. The total change in absorbancy from free base to ions is given as the outer curve labeled $a_M(RNH_2) - a_M(RNH_3^+)$. The differences for intermediate stages are represented by the 12 remaining curves, one of which is labeled $a_M(RNH_2) - a_M'$. One can readily see that the differences are positive for the large band nearest the visible, zero for the isosbestic point at 283 mμ, all negative between 283 and 242 mμ, and positive again for the data at the lower wavelengths. The degree of dissociation, or α, is calculated according to eq 4, and the amount of free base remaining, $1-\alpha$, according to eq 5 as follows:

$$\alpha = \frac{a_M(R) - a_M'}{a_M(R) - a_M(R^+)}, \tag{4}$$

$$1-\alpha = \frac{a_M' - a_M(R^+)}{a_M(R) - a_M(R^+)}, \tag{5}$$

Theoretically, the values of α should be the same across the spectral range regardless of wavelength selected. It is obvious that the best estimates will be obtained where the differences in absorbancies are greatest. Data too near the isosbestic points are worthless in such calculations. It is wise to examine the α values across reasonable wavelength ranges in more than one band, to detect a possible trend. Such trends have often been noted [1, 2], particularly where impurities may be involved, or where another reaction can conceivably take place simultaneously. Dissociation constants calculated from absorbancies at one or two wavelengths are not necessarily reliable. In this case the authors selected the wavelength range of 314 to 350 mμ, inclusive, to calculate an average α from 19 wavelengths. A comparison was made with values calculated from 256 to 264 mμ in which greater variations occurred because

observations were made on steep slopes of bands, and there was satisfactory agreement.

The ratios of free base to ions may be calculated directly by combining eq 4 and 5, thus

$$\frac{1-\alpha}{\alpha}=\frac{a_{M'}-a_M(\mathrm{R}^+)}{a_M(\mathrm{R})-a_{M'}} \qquad (6)$$

This ratio multiplied by the hydrogen-ion concentration gives the concentration constant K_c, as in eq 2 or 3. pK_c, the negative of the common logarithm of K_c, can then be calculated.

3. Presentation of Data

Typical absorbancy data and calculated values for the dissociation of 4-aminobenzophenone at 25° C are given in table 1. Two series show reproducibility of results from two different runs, using freshly prepared solutions throughout. The molar concentration of hydrochloric acid is given in column 1. Molar absorbancy index at 332 mμ is listed in column 2. Column 3 shows α calculated from absorbancies at one wavelength (332 mμ), and column 4 gives an average α calculated from absorbancies at 19 wavelengths from 314 to 350 mμ, inclusive. Inasmuch as the transmittancy observations are subject to error in the third figure, this error is carried in the subsequent calculations. An average α, however, should minimize the error. Values of α below 0.1 and above 0.9 yield unusually large or small ratios of free base to ions and were not included in the calculations of the constants.

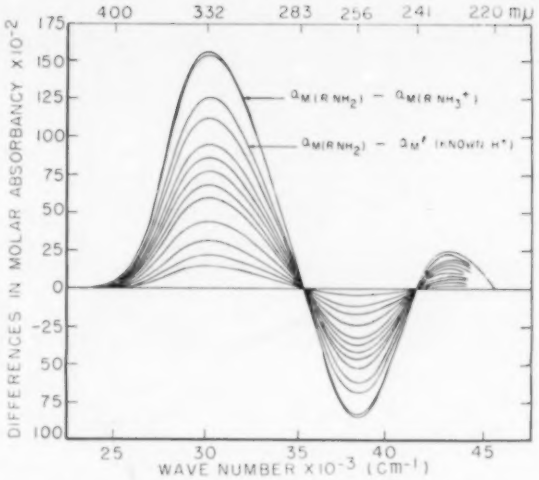

FIGURE 4. *Differences in absorbancy of undissociated 4-aminobenzophenone and the partially and completely dissociated compound.*

TABLE 1. *Dissociation of 4-aminobenzophenone at 25° C.*

Molar concentration of HCl $[H^+]$	Molar absorbancy index, λ332 a_M	Amount dissociated into ions, λ332, 1 wavelength α	Amount dissociated into ions, λ314 to 350, incl. Average of 19λ	Ratio of free base to ions, $(1-\alpha)/\alpha$	Concentration constant, $K_c\times10^5$ $[H^+]\frac{(1-\alpha)}{\alpha}$	$-\mathrm{Log}_{10}K_c$, pK_c
SERIES A						
0.0000	15,900	0.000	0.000	.....	.....	.....
.0001	15,700	.013	.014	.....	.....	.....
.0065	14,500	.090	.092	.....	.....	.....
.0010	13,800	.135	.133	6.518	6.518	2.186
.0016	12,800	.199	.195	4.102	6.563	2.183
.0026	11,600	.276	.277	2.610	6.786	2.168
.0041	9,980	.381	.380	1.632	6.691	2.175
.0052	9,150	.434	.433	1.309	6.807	2.167
.0065	8,250	.492	.492	1.032	6.708	2.174
.0102	6,500	.604	.606	0.828	6,707	2.174
.0161	4,870	.709	.711	.406	6.537	2.185
.0256	3,470	.799	.799	.252	6.451	2.190
.0405	2,410	.868	.868	.152	6.156	2.208
.1020	1,180	.947	.948	.....	.....	.....
.6440	350	1.000	1.000	.....	.....	.....
SERIES B						
0.0000	15,900	0.000	0.000	.....	.....	.....
.0016	12,800	.199	.195	4.128	6.605	2.180
.0041	10,000	.379	.378	1.646	6.749	2.171
.0051	9,150	.434	.434	1.304	6.650	2.177
.0064	8,270	.491	.491	1.037	6.637	2.178
.0081	7,370	.549	.547	.828	6.707	2.173
.0102	6,500	.604	.606	.650	6.630	2.178
.0130	5,550	.666	.665	.504	6.552	2.183
.0160	4,870	.709	.709	.410	6.560	2.183
.0200	4,150	.756	.756	.323	6.460	2.190
.0256	3,470	.799	.800	.250	6.400	2.193
.1020	1,160	.948	.949	.....	.....	.....
.6440	350	1.000	1.000	.....	.....	.....

The concentration constant, $K_c \times 10^3$, is given in column 6, and $-\log_{10} K_c$, or pK_c, in column 7. The increase in pK_c with increase in ionic strength is slight, but nevertheless there is a trend. The arithmetic mean of the values of pK_c for each series is 2.18, corresponding to 0.0066 moles/liter for K_c.

A summary of calculations from spectrophotometric data that was taken of the dissociation of 4-aminobenzophenone at 10°, 15°, 20°, 30°, 35°, and 40° C is given in table 2. Each series of solutions for the dissociation at one temperature was completed before changing the temperature of the water bath for the next series. Practically the same amounts of hydrochloric acid were used for each series to facilitate direct comparison of the amount of free base dissociated into ions at a particular hydrogen-ion concentration at different temperatures. The spectrophotometric observations were made as usual over the ultraviolet spectral range of 210 to 400 mμ, to assure accuracy of data and adherence to isosbestic points, but the degree of dissociation is the average calculated from the 19 wavelengths between 314 and 350 mμ. It was feared that erratic results might be obtained from the measurements at 10° C, as a slight film formed on the outer faces of the quartz end-plates as they were removed from the cell compartment at 10° to the room at 25° C for filling and emptying. However, the results do not seem to be out of line. At 15° C the film was not visible to the naked eye.

TABLE 2. *Dissociation of 4-aminobenzophenone at 10°, 15°, 20°, 30°, 35°, and 40° C*

Molar concentration of HCl [H⁺]	Degree of dissociation, α	$K_c \times 10^3$	$-\text{Log}_{10} K_c$, pK_c	Degree of dissociation, α	$K_c \times 10^3$	$-\text{Log}_{10} K_c$, pK_c	Degree of dissociation, α	$K_c \times 10^3$	$-\text{Log}_{10} K_c$, pK_c
	10° C			15° C			20° C		
0.0000	0.000			0.000			0.000		
.0016	.271	4.304	2.366	.240	5.067	2.295	.216	5.808	2.236
.0041	.482	4.407	2.356	.440	5.219	2.282	.413	5.826	2.234
.0051	.537	4.397	2.357	.502	5.059	2.296	.468	5.799	2.237
.0064	.601	4.250	2.371	.558	5.069	2.295	.534	5.587	2.252
.0081	.653	4.301	2.366	.613	5.119	2.292	.588	5.678	2.246
.0102	.707	4.223	2.374	.670	5.018	2.299	.643	5.661	2.247
.0130	.753	4.264	2.370	.721	5.031	2.298	.699	5.603	2.251
.0160	.794	4.144	2.382	.763	4.976	2.303	.741	5.600	2.252
.0200	.828	4.160	2.381	.802	4.940	2.304	.784	5.520	2.258
.0256	.864	4.019	2.396	.840	4.864	2.313	.826	5.402	2.267
.1020	.969			.961			.960		
.6440	1.000			1.000			1.000		
	30° C			35° C			40° C		
0.0000	0.000			0.000			0.000		
.0016	.175	7.542	2.122	.159	8.462	2.072	.145	9.434	2.025
.0041	.348	7.683	2.114	.318	8.794	2.055	.295	9.799	2.008
.0051	.404	7.522	2.123	.371	8.644	2.063	.350	9.471	2.023
.0064	.458	7.571	2.121	.426	8.621	2.064	.405	9.402	2.026
.0081	.521	7.444	2.128	.488	8.497	2.070	.464	9.356	2.029
.0102	.578	7.446	2.128	.545	8.517	2.069	.520	9.415	2.026
.0130	.637	7.410	2.130	.603	8.554	2.067	.581	9.373	2.028
.0160	.686	7.328	2.135	.654	8.464	2.072	.633	9.280	2.032
.0200	.733	7.280	2.137	.702	8.482	2.072	.683	9.280	2.032
.0256	.784	7.066	2.151	.756	8.269	2.082	.738	9.088	2.041
.1020	.945			.930			.931		
.6440	1.000			1.000			1.000		

It is readily seen from the table that for any given hydrogen-ion concentration the degree of dissociation decreases with increase in temperature. The concentration constant thereby increases, and pK_c correspondingly decreases.

Of interest is the magnitude of error that any variation in temperature may have upon the absorbancy of a given solution. As the limiting curves, all free base or all ions, were found to be substantially unchanged over the temperature range studied, any change in absorbancy can be attributed solely to the change in constant of the dissociation reaction with change in temperature. A solution of 4-aminobenzophenone in 0.0064-*M* hydrochloric acid, which at 25° C is practically half base and half ions, was placed in the cells, and the temperature of the bath was changed in the following manner. An equilibrium temperature of 25° C was first attained, and observations were made at 2-mμ wavelength settings from 314 to 350 mμ, inclusive. The bath was then changed to give equilibrium temperatures in 5-deg steps, first up to 40° C, then in reverse order down to 10° C, and again up to 25° C as a check. The cells were not removed from the cell compartment, and about 3 days was required for the experiment. The changes in absorbancy were determined and the stability of the solution also proved. The results are shown in figure 5, in which specific absorbancy of the solution is plotted as a function of wavelength. In this particular case there is roughly an 8-percent increase in absorbancy with a 5-deg increase in temperature. It is evident that for accurate results close temperature control is necessary for all intermediate stages in the dissociation.

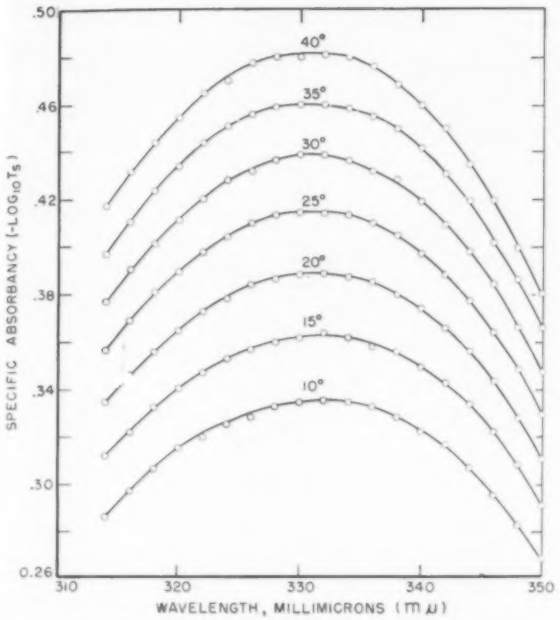

FIGURE 5. *Effect of temperature upon the absorbancy of 4-aminobenzophenone, partially dissociated in 0.0064-M hydrochloric acid* (pH *2.23*).

V. Other Related Thermodynamic Quantities

1. Estimation of pK_a and K_a from 10° to 40° C

True thermodynamic constants, K_a, may be calculated at each temperature studied by eq 7

$$K_a = K_c \frac{f_{H^+} f_{RNH_2}}{f_{RNH_3^+}}, \qquad (7)$$

in which the activity coefficients, f, are expressed with the appropriate subscripts.

When pK_c is plotted as a function of ionic strength at each temperature, it is found that straight lines may be drawn through the values, giving slight slopes. Extrapolation to infinite dilution should give the pK_a values, and the activity coefficient terms may then be expressed as a linear function of ionic strength. The results are shown in figure 6. The experimental error is at least ± 0.01 pK unit, and the lines were drawn as visual estimates. pK_a was found to be 2.36, 2.28, 2.24, 2.17, 2.12, 2.06, and 2.02 for 10°, 15°, 20°, 25°, 30°, 35°, and 40° C. K_a is then 0.0044, 0.0052, 0.0058, 0.0068, 0.0076, 0.0087, and 0.0096 in the same order.

2. Activity Coefficient Terms

The straight lines in figure 6 may be used to select pK_c values at any ionic strength between 0 and 0.03. Corresponding K_c values may then be derived. As the ratio of K_a to K_c is equal to the activity coefficient term $f_{H^+} f_{RNH_2} / f_{RNH_3^+}$, this term, called f_R, may now be calculated. Some terms are shown in table 3 for a

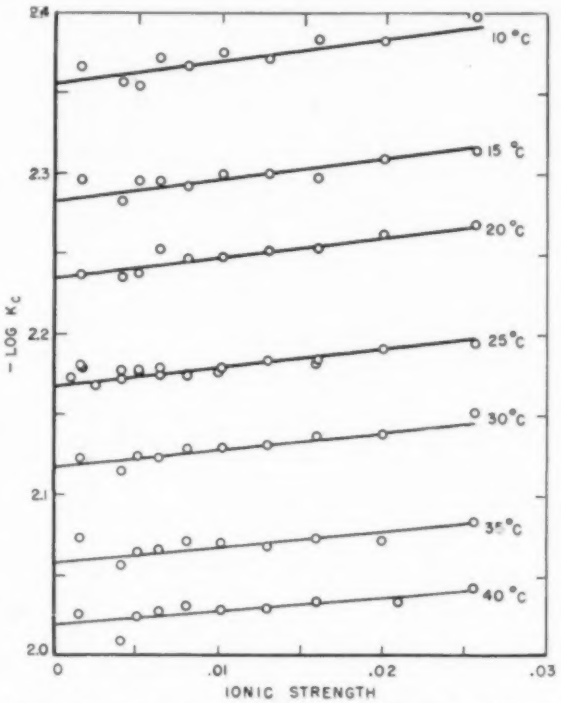

FIGURE 6. pK_c *values of 4-aminobenzophenone at different stages in the dissociation in hydrochloric acid.*

TABLE 3. *Activity coefficient terms,* $f_{H^+} f_{RNH_2} / f_{RNH_3^+}$ *or* f_H, *calculated for several temperatures*

Ionic strength	Degrees Celsius—													
	10		15		20		25		30		35		40	
	$K_c \times 10^3$	f_R	$K_c \times 10^3$	f_R	$K_c \times 10^3$	f_R	$K_c \times 10^3$	f_R	$K_c \times 10^3$	f_R	$K_c \times 10^3$	f_R	$K_c \times 10^3$	f_R
0.000 (K_a)	4.41	....	5.21	....	5.83	....	6.81	....	7.64	....	8.77	....	9.57	....
.005	4.34	1.02	5.14	1.01	5.74	1.02	6.71	1.01	7.53	1.01	8.67	1.01	9.48	1.01
.010	4.27	1.03	5.06	1.03	5.66	1.03	6.62	1.03	7.46	1.03	8.57	1.02	9.40	1.02
.015	4.21	1.05	4.98	1.04	5.58	1.04	6.53	1.04	7.38	1.04	8.47	1.04	9.31	1.03
.020	4.15	1.06	4.92	1.06	5.52	1.06	6.46	1.05	7.30	1.05	8.38	1.05	9.20	1.04
.025	4.09	1.08	4.84	1.08	5.43	1.07	6.37	1.07	7.19	1.06	8.30	1.06	9.14	1.05
.030	4.02	1.10	4.78	1.09	5.35	1.09	6.28	1.09	7.10	1.08	8.20	1.07	9.06	1.06

few ionic strengths at the seven temperatures at which measurements were made.

There are little data in the literature on activity coefficient terms of weak bases at low ionic strengths. However, if the terms at high ionic strengths are extrapolated to lower strengths, the results of Randall and Failey [4], Harned and Robinson [5], and Harned and Mannweiler [6] obtained by electromotive-force methods and Weil and Morris [7], who used spectrophotometric methods, are in agreement with our results.

3. Heat of Dissociation

If one now plots the $-\log K_a$ values for each temperature as a function of $1/T$, a practically straight line is obtained as shown in figure 7. Thus the heat of dissociation can be assumed to be practically constant, and ΔH may be calculated according to eq 8

$$d \log K/dT = \Delta H/2.3\ RT^2, \qquad (8)$$

in which ΔH represents the molar changes of heat content for the dissociation, R is the gas constant 8.3144 joules deg^{-1} $mole^{-1}$, and T is the temperature in degrees Kelvin (degrees Celsius + 273.16). ΔH is found to be 19,000 joules deg^{-1} $mole^{-1}$.

4. Basic Ionization Constant, K_b

One may derive the basic ionization constant, K_b, from the usual relationship

$$K_b = K_w/K_a,$$

in which K_w is the activity product for water. For example, at 25° C K_b is equal to $10^{-14}/(6.6\times10^{-3})$, which yields a value of 1.6×10^{-11}. pK_b is then approximately 11.8.

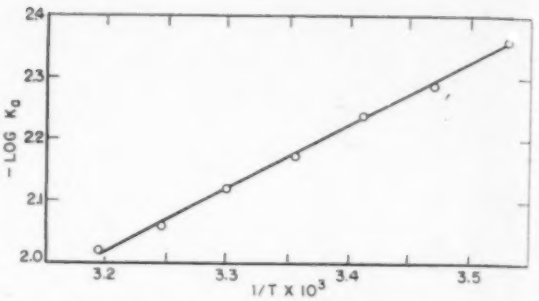

FIGURE 7. pK_a *values at temperatures from 10° to 40° C plotted as a function of* $1/T$.

VI. References

[1] Elizabeth E. Sager, Harry J. Keegan, and S. F. Acree, J. Research NBS **31,** 323 (1943) RP1569.

[2] Elizabeth E. Sager, Marjorie R. Schooley, and S. F. Acree, J. Research NBS **31,** 197 (1943) RP1558.

[3] Elizabeth E. Sager, Marjorie R. Schooley, Alice S. Carr, and S. F. Acree, J. Research NBS **35,** 521 (1945) RP1686.

[4] M. Randall and C. F. Failey, Chem. Rev. **4,** 27k (1927).

[5] H. H. Harned and R. A. Robinson, J. Am. Chem. Soc. **50,** 3157 (1928).

[6] H. H. Harned and G. E. Mannweiler, J. Am. Chem. Soc. **57,** 1873 (1935).

[7] I. Weil and J. C. Morris, J. Am. Chem. Soc. **71,** 3123 (1949).

WASHINGTON, August 14, 1950

Journal of Research of the National Bureau of Standards Vol. 45, No. 6, December 1950 Research Paper 2163

A New Method of Radioactive Standard Calibration

By Howard H. Seliger

By proper arrangement of experimental observations and statistical analysis it has been possible to make Geiger-counter measurements of different activity samples independent of intermittent disturbing effects. The results of 5,328 individual measurements, involving more than 1.4×10^8 counts made by using a Latin square arrangement, are shown to have an error distribution identical with that expected from the statistical nature of the disintegration process. A completely worked out example of a calibration procedure is given, in which it has been possible to achieve a higher degree of accuracy in only 30 percent of the original counting time.

I. Introduction

Anyone who has had occasion to make Geiger-counter measurements on radioactive isotopes has found at times that his results were not self-consistent; or more precisely, that readings taken at time A could not be duplicated within the expected Poisson deviation at time B. Sometimes upon further investigation it was found that these variations were due to fluctuations in the electronic voltage supply, slight changes in sensitivity of the Geiger counter itself, or other transient effects. Most often, if it were not too time-consuming, the original data were discarded and the measurements repeated, this time with the fingers crossed. In this paper a procedure for arranging and analyzing a series of measurements is described that eliminates intermittent disturbing effects and that permits a determination to be made as to whether the variance of the set of readings is a reasonable one to expect on the basis of a Poisson distribution of counts. The end result is that all readings of a set are treated

as though they were taken at the same time with the same equipment.

II. Part 1 of the Solution—the Chi Square Test

If we know that radioactive disintegrations follow a Poisson law, we can predict the variation within which individual values should lie. Our problem is to determine the probability that the variation of an observed set of readings is a reasonable one to expect if the variations are due only to the randomness of the disintegration process. This probability distribution of the ratio of the observed variation to the expected variation has been calculated and is known as the Chi square distribution.[1] The Chi square statistic is defined as the sum of squares of the deviations divided by the mean, or

$$\chi^2=\frac{\sum_i (X_i-\overline{X})^2}{\overline{X}} \qquad (1)$$

where X_i is the observed counts per reading, $\overline{X}$ is the expected, or average, counts per reading and $\sum_i$ denotes the summation over all the readings. Then $\sum_i (X_i-\overline{X})^2$ is the sum of the squares of the deviations from the mean count, and therefore an estimate of $n\sigma^2$ calculated from the individual counts. When the measurements do follow a Poisson law, the average count is known to be an estimate of σ^2 for the measurements. Thus the expected value of this ratio (eq 1) when the data follow Poisson's law is n. This is, however, subject to statistical variations. Tables are available showing for various n the probability limits for this ratio (see footnote 1).

Let us now apply this simple test to a set of consecutive readings taken with a Geiger counter and scaler, with a constant activity source. All readings are taken for a constant time interval, which does not enter into the calculations.

Reading number	Total counts	Reading number	Total counts
1	14, 805	6	15, 292
2	15, 378	7	15, 287
3	15, 021	8	15, 398
4	15, 040	9	15, 384
5	15, 335	10	14, 908

$$\sum_1^{10}(X_i-\overline{X})^2=435{,}622,$$

$$\overline{X}=15{,}185,$$

$$\chi^2=28.7.$$

As we have 10 readings, there are 9 degrees of freedom. If we look up a table of χ^2 for $n=9$, we find that the probability of getting a ratio of 28.7 is less than one chance in a thousand.[2] Therefore, we conclude that the above set of readings do not follow a Poisson distribution, and that data taken with the counter and scaler are not reliable. Conversely, if this ratio came out within the values 14.68 and 4.17, which are the 10-percent and 90-percent probability limits, respectively, we could conclude satisfactory operation on the part of our equipment and continue with our measurements. Thus even this simple application of the Chi square test is an extremely useful one for checking equipment, and in the following sections we shall show how it and the method of Latin squares are used together for more complicated data analysis.

III. Part 2 of the Solution—the Latin Square

The Latin square was originally developed for agricultural field trials. If K different strains of corn are to be compared, the experimental area is subdivided into a checkerboard of K rows and K columns, making available K^2 plots. The plantings are applied so that each strain appears once in each row and in each column of the K^2 plots. This requires that there be K plots assigned to each strain of corn. Every row and every column of the area contains a complete set of the K strains under test. Intuitively it may be seen that such an arrangement will be effective in reducing the error of comparisons among the strains since if any one of the columns or rows is more fertile than the others, all K strains obtain this advantage and the relative performance of the several strains is unaffected. If there exist fertility gradients in the area that would ordinarily interfere with the accuracy of the comparisons, the Latin square method of allocating the plantings to the plots has ensured a more nearly equal opportunity for all strains.

A typical 4 by 4 Latin square arrangement is shown in figure 1, a. The four plants of any given strain appear in the four rows and four columns. The four plots of any one strain may in consequence show considerable variation among themselves, and should not be used directly as an estimate of the error in the comparison of the different strains. However, the comparison of the averages for the strains has been made more accurate by insuring that all strains sample the various strips of fertility. Thus differences among rows and columns no longer contribute to the error of the comparison. It is necessary then to find another way of estimating the error of the average for each strain, as the customary method of calculating the dispersion from plots receiving the same strain is no longer applicable. However, before we proceed to outline the new method for calculating the dispersion, let us carry on with the development of the Latin square arrangement. In figure 1, b, is a Latin square arrangement for the Greek letters α, β, γ, δ. Now let us superpose figure 1, b, upon figure 1, a to obtain figure 1, c. If the

[1] Peters and VanVoorhies, Statistical procedures and their mathematical bases, p. 404 (McGraw Hill Book Co., Inc., New York, N. Y., 1940); Fisher, Statistical methods for research workers, p. 58 (Oliver and Boyd, London, 1944); K. A. Brownlee, Industrial experimentation, 3d ed., p. 39 (British Ministry of Supply, Directorate of Royal Ordnance Factories, 1948).

[2] K. A. Brownlee, Industrial experimentation, 3d ed., p. 161 (British Ministry of Supply, Directorate of Royal Ordnance Factories, 1948).

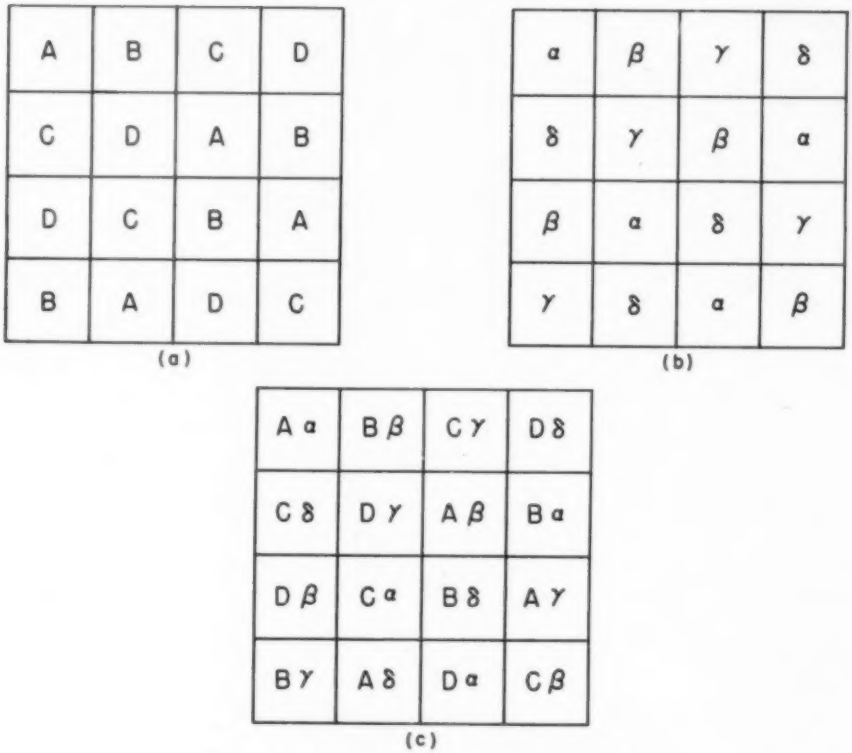

FIGURE 1. *General Latin square arrangement.*

a, Latin square for strains A, B, C, D; b, Latin square with Greek letters; c, superposition of b upon a, subject to the same restricting conditions.

four alpha plots in figure 1, c, are examined, it will be seen that these four plots contain a representative plot from every row and every column and every strain, the strains still being the roman letters A, B, C, D. The same is true for the beta, gamma and delta plots. The averages for these Greek sets therefore should show good agreement, and the variation among these four averages does in fact provide the estimate of error relevant to the comparison of the averages for the four strains. In the same manner, Arabic numerals can be assigned to the plots, so that the four plots marked 1 in figure 2 contain representatives from every row, column, strain, and Greek letter. This is also true for the plots marked 2, 3, and 4. These four sets also should agree and can be used as a further estimate of the experimental error. The Latin square shown in figure 2 is now unique, or completely orthogonal, in that this is the only way in which the individual simple Latin squares composed of Latin letters, Greek letters, and Arabic numerals, as shown in figure 1, can be superposed subject to the restricting conditions above. We would expect, therefore, that there should be associated with these classifications as many degrees of freedom as there would be if only one number or letter appeared in each of the 16 squares.

It is customary to summarize the statistical computations for experimental arrangements of this type in a tabulation of the analysis of variance of the five classifications that have been enumerated. They are

	Degrees of freedom
Variation among the four row averages	3
Variation among the four column averages	3
Variation among the four strain (Latin letter) averages	3
Variation among the four Greek letter averages	3
Variation among the four Arabic number averages	3

As seen with each of these is associated three degrees of freedom (corresponding to the usual $(n-1)$ divisor in computing standard deviations). The total of 15 degrees of freedom is that properly assigned to 16 observations if a standard deviation were computed for the 16 results ignoring all classifications among the plots. Now, not only do the degrees of freedom add up to the correct total, but the sum of the squares of the deviations within each classification, when added up over the 5 classifications will be found equal to one-fourth of the sum of the squares of the deviations of the 16 observations

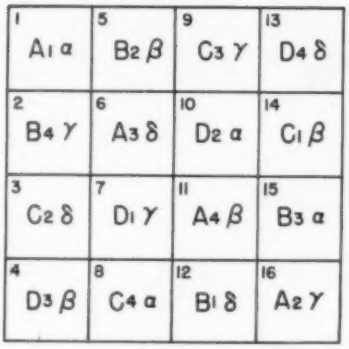

FIGURE 2. *Arrangement of Latin square to indicate sequence of readings.*

about the grand average. (The factor one-fourth arises because the five components have been computed from averages of four, in contrast to the use of individual observations). It is therefore possible to partition the over-all variance into these five portions. Two of these are the rows and the columns, which by experimental arrangement, have been removed from participation in the experimental comparisons. One portion (Latin letters) directly reflects differences among the strains and the remaining two portions (Greek letters and Arabic numbers), yield independent estimates of the experimental error. Completely worked out examples of this form of Latin square will be found in Brownlee (see footnote 1). The net result is that the computation leads to determining the ratio of the mean sum of squares for each classification to the mean sum of squares for error, as defined by Brownlee (see footnote 1). This ratio, called F, has the expected value of unity in all cases where the classification under examination contributes nothing to the variation of the results, as would have been the case for instance if only one strain of corn had been sown in all 16 plots. The computed value of F will in such a case be expected to fall in the neighborhood of unity, the reasonable limits of variation being determined by the number of degrees of freedom attached to the numerator and denominator of the ratio. The theoretical distribution of the F ratio has been tabulated (see footnote 1) and is an indispensable guide in passing judgment on a particular value of F. These tabulations are listed as Tables of Variance Ratio for various significance levels, corresponding to the probability levels in the χ^2 test in section II.

IV. Chi Square Test Modified for the Latin Square

In section II the principle of the Chi square distribution was demonstrated, and in section III the use of the Latin square for the separation of disturbing factors from the error calculations and for the calculation of variance ratios was outlined. The next steps in our sequence are: (1) To apply the Latin square to our particular problem of calibrating unknown sources of different activities against a known standard source; (2) to modify the calculation of the Chi square test to fit the data taken in our Latin square arrangement.

Perhaps the application of the Latin square to our particular problem will be easier to follow if we start with the end result and then discuss the logic of the arrangement as given. Consider again the Latin square in figure 2. The 16 subdivisions of the large square are numbered consecutively from 1 to 16 in columnar order in the upper left-hand corners. These numbers represent the sequence of the readings taken. The Latin letters A, B, C, and D represent a primary standard source and three unknown sources, respectively. We shall consider the standard source and the three unknown sources as our "strains". As the observed counting rates due to the sources A, B, C, and D are in general different, (due to the fact that the absolute disintegration rates of the sources are different) a variance among the four source averages (Latin letters) is to be expected and therefore should not be included in any error calculations. However, the sums of sets of four readings as for instance the sum of the α's, include only one reading each of A, B, C, and D, and therefore the sum of the α's theoretically should be equal to the sum of the β's, γ's, and δ's. This being the case, we can perform our Chi square calculation on the sums of four readings instead of on the individual readings. Again, from section III, we have the following sets of sums of four readings: Rows; columns; like Latin letters (sources); like Greek letters; like Arabic numbers.

The variation among the sources (Latin letters) is immediately ruled out for the reason already given. From the sequence of the measurements as given by the numbers in the upper left-hand corners of the squares in figure 2, it is seen that the sums of the columns will be especially sensitive to short-term intermittent disturbing factors of all kinds. Thus the variance among the four column averages should not be included in any error calculation. Moreover, these intermittent fluctuations, if they occur, are analogous to the fertility differences in our agricultural example, so that the relative performance of our four sources should be unaffected (if we consider sums and not individuals).

Now we have remaining three sets of four sums each for the calculation of error. These are the rows, the Greek letters and the Arabic numbers. The next step is to modify our Chi square calculation to fit these data.

We know that in our particular case of radioactive disintegrations σ^2, the standard deviation squared of our Poisson distribution, is equal to N, where N is the total counts involved. The estimate of $n\sigma^2$ can be calculated from the three sets of four sums. In this case there are 3 degrees of freedom from each set, making a total of 9 degrees of freedom.

Table 1 shows a complete set of data taken in the calibration of three unknown sources B, C, and D against a laboratory standard source, A. In order to indicate clearly the sequence of the readings and

TABLE 1. *Data as taken in an actual calibration of sources.*

READ NO.	SAMPLE	TOTAL COUNTS	TOTAL SEC	COUNTS/SEC GROSS	COUNTS/SEC NET
1	A	34480	1277	27.00	26.46
2	B	27364	973.1	28.12	27.58
3	C	25650	864	29.69	29.15
4	D	25774	856.8	30.08	29.54
5	B	27060	947.1	28.57	28.03
6	A	30540	1109	27.54	27.00
7	D	27478	914	30.06	29.52
8	C	25628	850	30.15	29.61
9	C	25614	858	29.85	29.31
10	D	26404	878.1	30.07	29.53
11	A	26082	965.4	27.02	26.48
12	B	25612	903.2	28.36	27.82
13	D	25650	864	29.69	29.15
14	C	25696	866.2	29.67	29.13
15	B	25654	902.1	28.44	27.90
16	A	26510	980	27.05	26.51

the method of summation, these data have been arranged in the form of a Latin square in table 2.

The analysis is performed in the following manner:

1. Calculate the average row sum of the four sets of row sums. Notice here that in order to do this, all 16 readings are included, and this grand sum is divided by 4. Therefore the average row sum is equal to the average Greek letter sum and also to the average Arabic number sum. Let us call this value

$$\overline{\Sigma(4)}=113.18.$$

2. Calculate the sum of squares of the deviations of the individual row sums from the average sum of four.

$$(0.23^2+0.06^2+0.13^2+0.30^2=0.1634).$$

3. Calculate the sum of squares of the deviations of the individual Greek letter sums from the average sum of four.

$$(0.25^2+0.04^2+0.57^2+0.36^2=0.5186).$$

4. Calculate the sum of squares of the deviations of the individual Arabic numbers sums from the average sum of four.

$$(0.32^2+0^2+0.26^2+0.06^2=0.1736).$$

TABLE 2. *Data from table 1 arranged in a Latin square to make the summation procedure easier to follow.*

					ROW TOTALS
	1 26.46 A1α	5 28.03 B2β	9 29.31 C3γ	13 29.15 D4δ	112.95
	2 27.58 B4γ	6 27.00 A3δ	10 29.53 D2α	14 29.13 C1β	113.24
	3 29.15 C2δ	7 29.52 D1γ	11 26.48 A4β	15 27.90 B3α	113.05
	4 29.54 D3β	8 29.61 C4α	12 27.82 B1δ	16 26.51 A2γ	113.48
COLUMN TOTALS	112.73	114.16	113.14	112.69	
ARABIC	1+7+12+14	3+5+10+16	4+6+9+15	2+8+11+13	
TOTALS	112.93	113.22	113.75	112.82	
GREEK	1+8+10+15	4+5+11+14	2+7+9+16	3+6+12+13	
TOTALS	113.50	113.18	112.92	113.12	
LATIN OR SAMPLE	A	B	C	D	
TOTALS	106.45	111.33	117.20	117.74	

5. Sum these three sums of squares.

$$(0.1634+0.5186+0.1736=0.8556).$$

6. We must digress for a moment and consider now the basis for this calculation. The expected standard deviation squared of a number of events that follow a Poisson law is N, when N is the total number of events. However, as is seen in table 1, our sample deviations are calculated from observed counting rates. In order that our ratio of observed to expected deviations be a unitless quantity, we must express the sum of squares of the deviations as total counts. This can be done in the following manner:

In each individual measurement we observe at least 25,600 counts, which is 200 message register counts on a scale of 128. Therefore, we can, with negligible error, assume that for a set of four readings the total number of counts involved is $4\times25{,}600=102{,}400$. If we divide this value by the average counting rate for a sum of four readings, we get a value with the units of seconds,

corresponding to the average time per reading. This value squared will, when multiplied by the sum of squares of the deviations that has the units of [(counts)/(seconds)]², give units of (counts)², the same as our denominator.

Our calculated ratio is now

$$\chi^2=\frac{0.8556\times\left[\frac{102{,}400}{113.18}\right]^2}{102{,}400}=6.84$$

In our table of χ^2 we find, for 9 degrees of freedom

$$\chi^2_{.70}=6.39,$$

$$\chi^2_{.50}=8.34.$$

Thus our ratio has greater than a 50-percent probability of occurence on the basis of a Poisson law, and we conclude that the resulting calibrations are perfectly acceptable.

As an illustration of the efficiency of this method in eliminating transient disturbances from the measurements, let us perform an F test on the column totals. The mean square column deviations are 1.4046/3, as here we have 3 degrees of freedom. The mean-square-error deviations are 0.8556/9, since there we used 9 degrees of freedom. Thus the ratio 4.92, as we can see from tables of Variance Ratio has reached the 5-percent significance level. Evidently in this case the Latin square arrangement was successful in removing this effect from the variance of the sample averages. It is the elimination of these disturbances that accounts for the increased accuracy over the old direct-comparison method and the subsequent 70 percent shorter counting time. This reduction in counting time is due to two factors. First, the number of runs used was reduced. Where previously a standard source and three unknown sources were run alternately, so that for 4 runs on each of the three unknowns the standard would be run 13 times, making a total of 25 runs for the entire set of readings, we now have only 16 runs in which the standard is measured as many times as the unknowns. Second, as the extraneous (nonPoisson) variation was present in the former method, a much larger counting time was necessary than that based on a Poisson distribution in order to obtain the precision called for. The Latin square arrangement permits the counting time to be cut in half, and the precision of the measurements is still greater than in the old method.

The standard deviation of any of the sums of four is

$$s_\Sigma=\left[\frac{0.8556}{9}\right]^{\frac{1}{2}}=.308.$$

The standard deviation of any individual counting rate is

$$s=\left[\frac{0.8556}{4\times9}\right]^{\frac{1}{2}}=0.154.$$

For example, the average counting rates of sources A, B, C, and D, which are the objectives of this entire procedure, are, respectively, 26.61, 27.83, 29.30, and 29.44 $\pm$ .15 *c/s*. These results can also be calculated as shown in Brownlee (see footnote 1). However, the method as demonstrated is more direct and easier to calculate.

V. Summary

In this paper two things have been accomplished. First, by the arrangement of the experimental data in the form of the orthogonal Latin square, thereby eliminating intermittent effects, the accuracy has been increased to such an extent that only 30 percent of the original counting time is required. Second, it is now possible to determine the actual experimental standard deviation of any particular average reading, and in the process of obtaining this standard deviation it is also possible to determine whether or not the readings follow a Poisson law, which is the case when the equipment is operating satisfactorily.

As can be seen, the use of Latin squares for the statistical arrangement of measurements is an extremely powerful tool, by means of which a number of separate effects may be determined or eliminated. It has proved to be extremely efficient in the laboratory, not only in the actual calibration of standards, but in obtaining useful information relative to the long-range operating characteristics of the Geiger counters and associated electronic equipment. The general method as outlined should be applicable to a large variety of other types of measurements, especially where time effects or other disturbing factors are a source of trouble.

The results of 333 such sets of data as shown in tables 1 and 2 have been tabulated and are presented in figure 3, together with their theoretical distribution. As can be seen from the figure, the experimental distribution closely approximates the theoretical one. There is one more point that can be

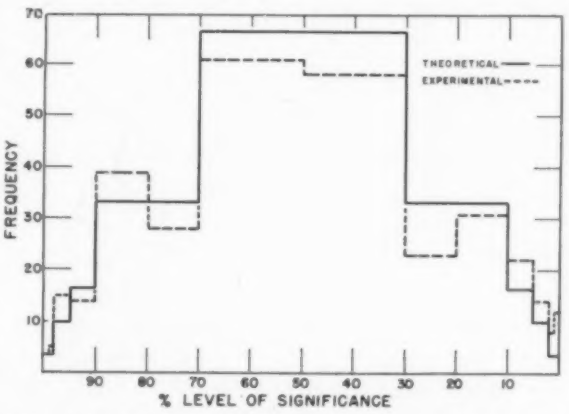

FIGURE 3. *Frequency distribution of 333 sets of Chi square data (broken line) compared with theoretical distribution (solid line).*

made only after the accumulation of such a large amount of data as this. The small peaks at the right of figure 3 indicate a slight tendency for the observed counts to be influenced by effects other than statistical fluctuations. However, it must be remembered that the data include instances where either counters or scaling circuits have gone bad and have evidenced a need for repair or replacement, so that this slight excess is to be expected. It is believed that this is the first time that such a large collection of Chi square values has been obtained from the ratio of the error variance of Latin squares to the expected (Poisson) variance.

It is well known that individual measurements of radioactive disintegrations follow a Poisson law, but the close agreement between the experimental and theoretical curves illustrates one further point: that the Latin square arrangement has been completely successful in eliminating extraneous, non-Poisson fluctuations from the measurements.

The author thanks W. J. Youden and J. M. Cameron, of the Statistical Engineering Section, for their suggestions as to the use of the Latin squares and for many valuable hours of discussion; and Margaret Selgin and Lucy Cavallo, of the Radioactivity Section, who performed the calculations summarized in figure 3.

WASHINGTON, July 26, 1950.

Journal of Research of the National Bureau of Standards Vol. 45, No. 6, December 1950 Research Paper 2164

A Problem in Precision Cam Design

By Joseph Blum

This paper proposes an analytic method for determining the profile of a cam required in a device that demands high precision. The method is applicable whenever the equation for the profile can be obtained by making a less stringent assumption, namely, that the follower makes contact at a fixed point of its extremity. The true profile can then be determined numerically by considering it as the envelope of a family of curves.

The design of an X-ray spectrograph often requires that a constant rate of oscillation be maintained in the crystal holder. The crystal rotates through an angle β (the angle of travel), reverses its direction and then proceeds with the same angular velocity. This type of motion may be obtained from a cam rotating with constant angular velocity, ω. An analytic method for computing the profile of the cam is presented in this paper which extends, in a certain sense, the application of a paper written by J. B. Friauf;[1] the notation therein will be preserved to a considerable extent.

[1] J. B. Friauf, The design of a cam for an X-ray spectrograph, J. Opt. Soc. Am. Rev. Sci. Instr. **11,** 289 to 296 (1925).

In figure 1, a, O represents the axis about which the cam rotates, A the axis about which the crystal holder rotates, and B the center of the ball at the end of the follower. The follower ACB makes contact with the cam and serves to rotate the crystal holder. The distances AO and AB are equal; denote this common length by R. Let r_1 and r_2 be, respectively, the least and greatest radii measured from O to the point B; let r be the variable radius, OB corresponding to the angle α, which r makes with the least radius r_1.

Denote the time by t and let $t=0$ represent the time when the least radius coincides with the line segment extending from O to A. Then the angle

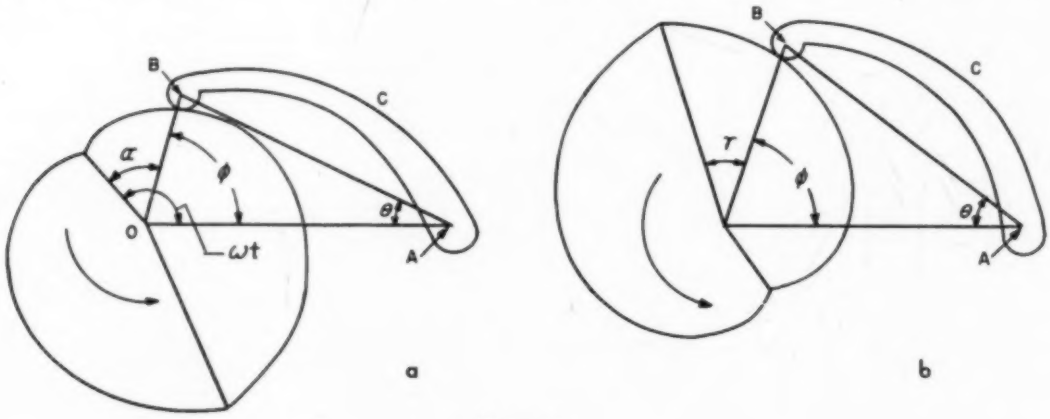

FIGURE 1.

between r_1 and OA is given by ωt. Let θ denote angle OAB and ϕ the angle AOB. Unless otherwise indicated, all angles are in radians.

From figure 1, a, it is clear that

$$\sin \frac{\theta}{2} = \frac{r}{2R}, \tag{1}$$

from which it follows that the smallest angle θ_1 occurs when $r=r_1$ and the largest angle θ_2 when $r=r_2$, or

$$\sin \frac{\theta_1}{2} = \frac{r_1}{2R}, \tag{2}$$

and

$$\sin \frac{\theta_2}{2} = \frac{r_2}{2R}. \tag{3}$$

It is also clear that $\beta=\theta_2-\theta_1$. Differentiating eq 1 yields

$$\cos \frac{\theta}{2} \frac{d\theta}{dt} = \frac{1}{R} \frac{dr}{dt} = \frac{1}{R} \frac{dr}{d\alpha} \frac{d\alpha}{dt}. \tag{4}$$

$$\text{Since } \alpha = \omega t - \phi, \quad \frac{d\alpha}{dt} = \omega - \frac{d\phi}{dt}.$$

Substituting this into eq 4 yields

$$\cos \frac{\theta}{2} \frac{d\theta}{dt} = \frac{1}{R} \frac{dr}{d\alpha} \left(\omega - \frac{d\phi}{dt} \right). \tag{5}$$

Again, since $\phi = \frac{1}{2}(\pi-\theta)$, $(d\phi/dt = -\frac{1}{2}(d\theta/dt)$, and substituting this into eq 5 results in

$$\cos \frac{\theta}{2} \frac{d\theta}{dt} = \frac{1}{R} \frac{dr}{d\alpha} \left(\omega + \frac{1}{2} \frac{d\theta}{dt} \right). \tag{6}$$

The follower rotates through the angle β during the same time interval that it takes the cam to rotate through π radians. Therefore, as the respective angular velocities are constant,

$$\frac{\frac{d\theta}{dt}}{\omega} = \frac{\beta}{\pi}, \text{ or } \frac{d\theta}{dt} = \frac{\beta\omega}{\pi}.$$

Substituting this into eq 6 gives

$$\cos \frac{\theta}{2} = \frac{1}{R} \frac{dr}{d\alpha} \left(\frac{\pi}{\beta} + \frac{1}{2} \right). \tag{7}$$

From eq 1 $\cos(\theta/2) = (1/2R)\sqrt{4R^2-r^2}$. Substituting this into eq 7 and simplifying yields

$$\frac{2\,dr}{\sqrt{4R^2-r^2}} = \frac{d\alpha}{\beta_1}, \tag{8}$$

where $\beta_1 = \pi/\beta + \frac{1}{2}$.

After integrating this equation there is obtained

$$2 \sin^{-1} \frac{r}{2R} = \frac{\alpha}{\beta_1} + C_1 \tag{9}$$

where C_1 is the constant of integration.

When $\alpha=0$, $r=r_1$; solving for C_1 results in $C_1 = 2 \sin^{-1} r_1/2R = \theta_1$. Equation 9 can be expressed in the form

$$r = 2R \sin \frac{1}{2} \left\{ \frac{\alpha}{\beta_1} + \theta_1 \right\}. \tag{10}$$

The greatest radius, r_2, occurs when $\alpha = \pi + \beta/2$, which may be vertified by substituting into eq 10.

If the ball that makes contact with the cam were sufficiently small, then eq 10 would give one part of the cam's contour, and a similar equation would give the remaining part. Frequently, however, this condition is not met, and the method given in the reference in footnote 1 must be extended to secure a high level of precision. Consider then the family of circles of radius ρ, whose centers lie on the curve given by eq 10. The envelope of this family consists of two distinct curves; the one that lies nearer the center of curvature of eq 10 coincides with the contour of the cam. This envelope can be obtained by a numerical determination of the C-discriminant.[2]

Let the curve of eq 10 be given in Cartesian coordinates by

$$y = f(x). \tag{11}$$

Let (x,y) be an arbitrary point on this curve. The equation of the circle with radius ρ and center (x,y) is given by

$$(X-x)^2 + (Y-y)^2 = \rho^2. \tag{12}$$

Substituting $y=f(x)$ into eq 12, there is obtained a one-parameter family of circles

$$\{X-x\}^2 + \{Y-f(x)\}^2 = \rho^2. \tag{13}$$

Differentiating eq 13 with respect to x yields

$$\{X-x\} + f'(x)\{Y-f(x)\} = 0. \tag{14}$$

The C-discriminant is obtained by solving eq 13 and 14 simultaneously for a discrete set of values of the parameter x. The method outlined below yields the numerical solution:

1. For a selected set of values α_i; determine the values of r_i by using eq 10. Denote these points by P_i.

2. Let τ_i be the angle of inclination of the tangent line at P_i; let ψ_i be the angle between the radius r_i and the tangent line. Then, since $\tau_i = \alpha_i + \psi_i$,

$$f'(x) = \tan \tau_i = \frac{\tan \alpha_i + \tan \psi_i}{1 - \tan \alpha_i \tan \psi_i}.$$

Now $\tan \psi_i = r_i/r_i'$, where r_i' is the derivative $dr/d\alpha$ evaluated at P_i. This leads to

$$\tan \psi_i = 2\beta_1 \tan \frac{1}{2} \left(\frac{\alpha_i}{\beta_i} + \theta_1 \right).$$

[2] E. L. Ince, Ordinary differential equations, p. 85 to 86 (Longmans, Green & Co., New York, N. Y., 1944).

These relations enable one to compute the value of $f'(x)$.

3. The solution of eq 13 and 14 is easily obtained in the form

$$\left.\begin{aligned} X_i &= x_i \pm \frac{\rho f'(x_i)}{\sqrt{1+\{f'(x_i)\}^2}} \\ Y_i &= y_i + \frac{\rho}{\sqrt{1+\{f'(x_i)\}^2}} \end{aligned}\right\} \tag{15}$$

The points (X_i, Y_i) are on the envelope, as required.

To obtain the other part of the cam, consider that phase of the motion in which the angle θ decreases (fig. 1, b). For this phase,

$$\frac{d\theta}{dt} = -\frac{\beta\omega}{\pi}.$$

Substituting this into eq 6 results in

$$\cos\frac{\theta}{2} = \frac{1}{R}\frac{dr}{d\gamma}\left(\frac{1}{2}-\frac{\pi}{\beta}\right), \tag{16}$$

where γ denotes the angle that r makes with the greatest radius r_2 (see fig 1,b). Substituting $\cos(\theta/2) = (1/2R)\sqrt{4R^2-r^2}$ into eq (16) and simplifying gives

$$\frac{2dr}{\sqrt{4R^2-r^2}} = \frac{d\gamma}{\beta_2}, \tag{17}$$

where $\beta_2 = 1/2 - \pi/\beta$.

When eq 17 is integrated there results

$$2\sin^{-1}\frac{r}{2R} = \frac{\gamma}{\beta_2} + C_2, \tag{18}$$

where C_2 is the constant of integration. When $\gamma = 0$, $r = r_2$; solving for C_2 yields $C_2 = 2\sin^{-1} r_2/2R = \theta_2$. Equation 18 can be expressed in the form

$$r = 2R\sin\frac{1}{2}\left(\frac{\gamma}{\beta_2}+\theta_2\right). \tag{19}$$

As a check, when $\gamma = \pi - \beta/2$, $r = 2R\sin\frac{1}{2}(\theta_2-\beta) = 2R\sin\frac{1}{2}\theta_1 = r_1$. The envelope of the family of circles with centers on the curve (19) and radius ρ leads to the remainder of the contour of the cam.

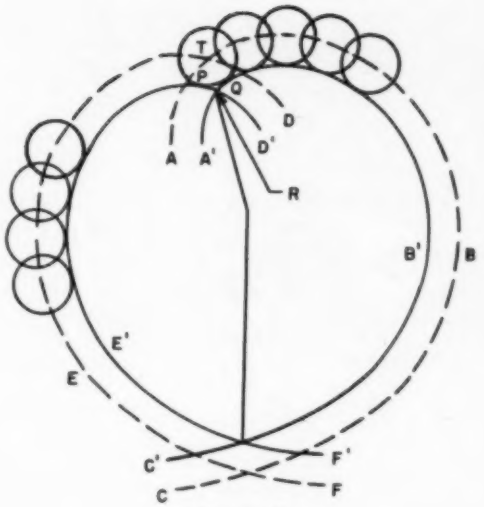

FIGURE 2.

To complete the analysis, consider figure 2. The arc ABC is the locus of eq 10, and arc $A'RB'C'$ is its envelope. Similarly, the arc DEF is the locus of eq 19; arc $D'RE'F'$ is its envelope and may be found numerically by following the procedure outlined above for eq 10. The high point of the cam is located numerically by solving for the intersection of the two envelopes. The low portion of the cam does not coincide with the envelope, as is evident from the figure. Let T be the point of intersection of the curves 10 and 19. The circular arc, PQ, with center at T and radius ρ constitutes the low portion of the cam. These considerations enable one to complete the numerical solution of the cam design.

In summary, it should be noted that the essential idea in this approach is to first find the equation of the contour, assuming that the follower makes contact at a fixed point of its extremity; then, by using the true form of the follower, obtain the actual cam contour by determining the envelope of a family of curves. It is evident that the analytic method applied in this particular case may be used in other problems of precise cam design.

WASHINGTON, August 4, 1950.

Journal of Research of the National Bureau of Standards Vol. 45, No. 6, December 1950 Research Paper 2165

Real Roots of Real Dirichlet L-Series [1]

By J. Barkley Rosser

In the theory of the distribution of primes in arithmetic series, in assigning bounds in the three prime theorem, and in studying the class number of quadratic fields, a knowledge of the location of the real zeros of $L(s, \chi)$ is of value. A long standing conjecture is that there are no positive real zeros for any k. If proved, this result would be of value in each of the fields mentioned above. By a certain computational procedure the conjecture has already been verified for each individual $k \leq 67$. In the present paper, this earlier computational procedure was tried for each $k \leq 227$ and failed for $k = 163$. An improved computational procedure is given in the present paper, but still the case $k = 163$ remained difficult. Finally, a new formula for $L(s, \chi)$ was discovered that made it possible to treat many values of k simultaneously. By means of this formula, the difficult case of $k = 163$ was finally treated adequately.

I. Introduction

Let k be a positive integer. Let χ be a real, non-principal character (mod k) and let

$$L(s, \chi) = \sum_{n=1}^{\infty} \frac{\chi(n)}{n^s}.$$

By a computation using the methods of [1] it was shown that if $2 \leq k \leq 227$ and $k \neq 163$, then $L(s, \chi)$ has no positive real zeros. This computation was laid out by G. Gourrich. Computation on IBM equipment was furnished by Miss L. Cutler and E. Rea under the direction of E. C. Yowell. Computation on desk computers was furnished by Miss. L. Forthal and W. Paine under the direction of G Blanch.

For $k = 163$, the method of [1] definitely failed. It seems likely that by making a careful refinement of the estimates of [1] by means of an extensive computation, one could handle the case $k = 163$. However, this did not seem a very profitable undertaking, and so a further study of $L(s, \chi)$ for positive real s was made, and various alternative methods were devised. Some of these seem clearly superior to the method of [1]. One such superior method is a generalization of the method of Chowla (see [3]). Using this method and a table of characters (mod k) prepared by Miss L. Cutler and E. Rea, it was a fairly quick matter for G. Gourrich to check that if $k \leq 227$ and $k \neq 163$, then $L(s, \chi)$ has no positive real zeros. Even by this method, the case $k = 163$ remained very difficult. Probably the method will handle the case $k = 163$, but it seemed clear that even by this method the case $k = 163$ would require very extensive computations, and it seemed worthwhile to devise still further methods. This was done, and a method was finally found by which the case $k = 163$ can be handled rather easily, with only a minor computation.

In the meantime, Chowla and Selberg (see [7]) have announced still another method for treating the case $k = 163$.

One may conclude that it is now quite firmly established that if $k \leq 227$, then $L(s, \chi)$ has no positive real zeros.

II. Generalization of Chowla's Method

Throughout this section, we lay down the following conventions. χ is a real primitive character. K shall be a positive integer, $\phi(n)$ shall be a function of positive integers which is periodic with period K, $L(s, \phi)$ shall denote the function that is got by analytic continuation from

$$\sum_{n=1}^{\infty} \frac{\phi(n)}{n^s},$$

so that for $R(s) > 1$

$$L(s, \phi) = \sum_{n=1}^{\infty} \frac{\phi(n)}{n^s},$$

and $f(z, \phi)$ shall denote the function that is got by analytic continuation from

$$\sum_{n=1}^{\infty} \phi(n) e^{-nz},$$

so that for $R(z) > 0$,

$$f(z, \phi) = \sum_{n=1}^{\infty} \phi(n) e^{-nz}.$$

We cite without proof various results, the proofs for which can easily be derived from the results of chapter XIII of [5].

Theorem 1. For $s \neq 1$,

$$L(s, \phi) = K^{-s} \sum_{n=1}^{K} \phi(n) \zeta\left(s, \frac{n}{K}\right).$$

Corollary. If

$$\sum_{n=1}^{K} \phi(n) = 0,$$

then $L(s, \phi)$ is analytic for all s.

[1] The preparation of this paper was sponsored (in part) by the Office of Naval Research.

Theorem 2. For all z different from $2\pi mi/K$ (m an integer)

$$f(z,\phi)=\frac{1}{e^{Kz}-1}\sum_{n=1}^{K}\phi(n)e^{(K-n)z}.$$

Corollary. If

$$\sum_{n=1}^{K}\phi(n)=0,$$

then $f(z,\phi)$ is analytic for $|z|<2\pi/K$, and

$$f(0,\phi)=\sum_{n=1}^{K}\phi(n)\left(1-\frac{n}{K}\right).$$

Theorem 3. If $R(s)>1$, then

$$\Gamma(s)L(s,\phi)=\int_0^\infty x^{s-1}f(x,\phi)dx.$$

Corollary. If

$$\sum_{n=1}^{K}\phi(n)=0,$$

then for $R(s)>0$,

$$\Gamma(s)L(s,\phi)=\int_0^\infty x^{s-1}f(x,\phi)dx.$$

Since

$$\sum_{n=1}^{k}\chi(n)=0,$$

the results stated in the three corollaries hold if we replace ϕ by χ and K by k. In particular, if we can prove that $f(x,\chi)\geq 0$ for $x\geq 0$, it will follow from the corollary to theorem 3 that $L(s,\chi)$ has no positive real zeros. This can be readily proved for many values of k. The method of proof is as follows. With Chowla, we define

$$\phi_0(n) \quad =\phi(n)$$

$$\phi_{r+1}(n)=\sum_{m=1}^{n}\phi_r(m).$$

We then have the following known result (see [4]).

Theorem 4. For $x>0$,

$$f(x,\phi)=(1-e^{-x})^r f(x,\phi_r).$$

Then, if there is an r for which $\chi_r(n)$ is nonnegative for $n\geq 1$, we infer that $f(x,\chi)\geq 0$ for $x\geq 0$, and hence that $L(s,\chi)$ has no positive real zeros.

For many k's, we can prove by a brief computation that there is an r such that $\chi_r(n)\geq 0$ for $n\geq 1$. For a typical case, consider $k=53$ and let χ be the real nonprincipal character (mod 53). In this case $\chi(n)$, $\chi_1(n)$, and $\chi_2(n)$ are sometimes negative, but $\chi_3(n)$ is nonnegative for all positive n. The computations on which this statement is based are given in table 1 (at the end of the paper). The method of computation of table 1 is particularly simple, since from the definition of χ_{r+1} we have

$$\chi_{r+1}(n+1)=\chi_{r+1}(n)+\chi_r(n+1).$$

So for $r\geq 1$ and $n\geq 2$, $\chi_r(n)$ is the sum of the numbers immediately above it and immediately to the left of it in table 1.

We have

$$\chi_1(n+53)=\chi_1(53)+\sum_{m=54}^{n+53}\chi(m).$$

However $\chi_1(53)=0$ (see table 1) and χ is periodic with period 53. So

$$\chi_1(n+53)=\sum_{m=1}^{n}\chi(m)=\chi_1(n).$$

So $\chi_1(n)$ is periodic with period 53. Similarly, $\chi_2(n)$ is periodic with period 53. However $\chi_3(53)=742$ (see table 1) so that

$$\chi_3(n+53)=742+\chi_3(n).$$

As $\chi_3(n)\geq 0$ for $1\leq n\leq 53$ (see table 1), it follows that $\chi_3(n)\geq 0$ for $n\geq 1$.

In table 2, we have listed those k's ≤ 227 for which there is a primitive χ and for which we could find an r such that $\chi_r(n)\geq 0$ for $n\geq 1$. Opposite each k is listed the least value of r for which $\chi_r(n)\geq 0$ for $n\geq 1$. Opposite 8 in table 2 is given the r corresponding to the character $\chi(1)=1$, $\chi(3)=-1$, $\chi(5)=-1$, $\chi(7)=1$, and opposite 8* is given the r corresponding to the character $\chi(1)=1$, $\chi(3)=1$, $\chi(5)=-1$, $\chi(7)=-1$. The corresponding χ's (mod 24) are indicated by entries 24 and 24* in table 2. Similarly for 40 and 40*, 56 and 56*, etc.

It will be noted that so far we are using exactly Chowla's method (see [3]), though our justification for the method is different from Chowla's. As noted by Heilbronn in [4], there exist values of k such that no $\chi_r(n)$ is nonnegative for every $n\geq 1$. In fact one can prove that $k=163$ is such a k; for actual computation for $k=163$ discloses that $f(\log(10/7),\chi)$ is negative, so that by theorem 4 there cannot be any completely nonnegative χ_r.

Our efforts to find an r for the cases $k=43$, 67, 88, 123, 148, 173, 187, 188, and 197 were sufficiently unrewarded that we suspect that for these values of k also there is no r. At any rate we devised an improvement of Chowla's method to handle these intractable k's (except perhaps $k=163$).

Theorem 5. If

$$F(s)=\int_0^\infty x^{s-1}f(x)dx,$$

then

$$(1+\alpha r^{-s})F(s)=\int_0^\infty x^{s-1}\{f(x)+\alpha f(rx)\}dx.$$

Theorem 6. If r is a positive integer and $\theta(n)$ is the coefficient of n^{-s} in the Dirichlet series expansion of

$$(1+\alpha r^{-s})L(s,\phi),$$

then

$$f(x,\theta)=f(x,\phi)+\alpha f(rx,\phi).$$

We now illustrate the use of these theorems for the case $k=67$. Note that for $k=67$, $\chi(2)=\chi(3)=\chi(5)=-1$. So

$$L(s,\chi)=\prod_p(1-\chi(p)p^{-s})^{-1}$$

$$=\frac{1}{(1+2^{-s})(1+3^{-s})(1+5^{-s})}\prod_{p\geq 7}(1-\chi(p)p^{-s})^{-1}.$$

So the Dirichlet series expansion of

$$(1+2^{-s})L(s,\chi)$$

consists of the Dirichlet series expansion of $L(s,\chi)$ with all terms n^{-s} removed for which n is divisible by 2. Similarly, to get the Dirichlet series expansion of

$$(1+2^{-s})(1+3^{-s})L(s,\chi),$$

we remove all terms n^{-s} for which n is divisible by either 2 or 3. Similarly for

$$(1+2^{-s})(1+3^{-s})(1+5^{-s})L(s,\chi).$$

We now verify by actual computation that $\chi_2(n)\geq 0$ for $n\geq 25$. Define $\phi(n)$ to be the coefficient of n^{-s} in the Dirichlet series expansion of

$$(1+2^{-s})L(s,\chi).$$

Then

$$(1+2^{-s})\Gamma(s)L(s,\chi)=\int_0^\infty x^{s-1}f(x,\phi)dx$$

and

$$f(x,\phi)=f(x,\chi)+f(2x,\chi).$$

Now

$$(1-e^{-x})^2 f(x,\phi_2)=f(x,\phi)$$

$$=f(x,\chi)+f(2x,\chi)$$

$$=(1-e^{-x})^2 f(x,\chi_2)+(1-e^{-2x})^2 f(2x,\chi_2)$$

$$=(1-e^{-x})^2\{f(x,\chi_2)+(1+e^{-x})^2 f(2x,\chi_2)\}.$$

So

$$f(x,\phi_2)=f(x,\chi_2)+(1+e^{-x})^2 f(2x,\chi_2).$$

As each side of this is a power series in e^{-x}, corresponding coefficients must be equal. So

$$\phi_2(2n)=\chi_2(2n)+\chi_2(n)+\chi_2(n-1)$$

$$\phi_2(2n+1)=\chi_2(2n+1)+2\chi_2(n).$$

Recalling that $\chi_2(n)\geq 0$ for $n\geq 25$, we see that surely $\phi_2(n)\geq 0$ for $n\geq 51$. Actual computation of $\phi_2(n)$ for $1\leq n\leq 50$ discloses that actually $\phi_2(n)\geq 0$ for $n\geq 31$.

If we now define $\theta(n)$ as the coefficient of n^{-s} in the Dirichlet series expansion of

$$(1+2^{-s})(1+3^{-s})L(s,\chi),$$

then

$$(1+2^{-s})(1+3^{-s})\Gamma(s)L(s,\chi)=\int_0^\infty x^{-s}f(x,\theta)dx$$

and

$$f(x,\theta)=f(x,\phi)+f(3x,\phi).$$

This latter equation gives a relation between θ_2 and ϕ_2. Using this relation with the result $\phi_2(n)\geq 0$ for $n\geq 31$ leads to the inference that $\theta_2(n)\geq 0$ for $n\geq 95$. Actual computation of $\theta_2(n)$ for $1\leq n\leq 94$ discloses that actually $\theta_2(n)\geq 0$ for $n\geq 41$.

We proceed one step further, defining $\eta(n)$ as the coefficient of n^{-s} in the Dirichlet series expansion of

$$(1+2^{-s})(1+3^{-s})(1+5^{-s})L(s,\chi).$$

Then

$$(1+2^{-s})(1+3^{-s})(1+5^{-s})\Gamma(s)L(s,\chi)=\int_0^\infty x^{s-1}f(s,\eta)dx.$$

Also we find that $\eta_2(n)\geq 0$ for $n\geq 29$. We now ascertain by actual computation that $\eta_3(n)\geq 0$ for $n\leq 28$, and so conclude that $\eta_3(n)\geq 0$ for $n\geq 1$. Then $f(x,\eta)\geq 0$ for $x\geq 0$. So

$$(1+2^{-s})(1+3^{-s})(1+5^{-s})\Gamma(s)L(s,\chi)>0$$

for $s>0$ and so $L(s,\chi)>0$ for $s>0$.

For other k's we proceeded similarly, except that when $\chi(-1)=1$ it was necessary to work with χ_3, ϕ_3, θ_3, etc., instead of with χ_2, ϕ_2, θ_2, etc., because the latter are periodic when $\chi(-1)=1$.

In table 3 we have listed against k the combination

$$\prod(1+p_i^{-s})L(s,\chi),$$

which was used with that k and also the least value of r which sufficed with this combination.

We note in passing that we can handle the case $k=43$ with the combination

$$(1+2^{-s})L(s,\chi),$$

but we need to take $r=9$, so that it is less laborious to take the combination

$$(1+2^{-s})(1+3^{-s})L(s,\chi)$$

for which $r=2$ suffices.

We suspect that this method will work for $k=163$. However for $k=163$, the combination

$$\prod(1+p_i^{-s})L(s,\chi)$$

will require at least five factors, and likely more than five, and the computations involved appear to be very extensive. So we sought other methods.

III. Another Method

We let χ be a real primitive character. Define

$$\xi(s)=\pi^{-s/2}\Gamma\left(\frac{s}{2}\right)\zeta(s) \tag{1}$$

$$\xi(s,\chi)=\left(\frac{\pi}{k}\right)^{-s/2}\Gamma\left(\frac{s}{2}\right)L(s,\chi) \tag{2}$$

if $\chi(-1)=1$,

$$\xi(s,\chi)=\left(\frac{\pi}{k}\right)^{-(s+1)/2}\Gamma\left(\frac{s+1}{2}\right)L(s,\chi) \tag{3}$$

if $\chi(-1)=-1$.

We have the known results

$$\xi(s)=\xi(1-s), \tag{4}$$

$$\xi(s,\chi)=\xi(1-s,\chi). \tag{5}$$

Also known is:

Theorem 7. If k_1 and k_2 are any real constants, then for $k_1\le\sigma\le k_2$,

$$\xi(s)-\frac{1}{s(s-1)}$$

and $\xi(s,\chi)$ are bounded.

Theorem 8. There is a function $f(x)$ with the following properties:

(I) $f(x)$ is analytic for $R(x)>0$.

(II) $f(x)$ is positive for $x>0$.

(III) $f(x)$ is monotone decreasing for $x>0$.

(IV) For $x\ge 1$,

$$f(x)\le \exp\left(-\frac{2\pi x}{\sqrt{k}}\right)f(1)\exp\left(\frac{2\pi}{\sqrt{k}}\right).$$

(V) There is a positive constant A such that for $x>0$,

$$\frac{A}{\sqrt{4x+1}}\exp\left(-\frac{2\pi x}{\sqrt{k}}\right)\le f(x).$$

(VI) For $\sigma>\sigma_{k_2}$,

$$\xi(s)\xi(s,\chi)=\int_0^\infty x^{s-1}f(x)dx.$$

Proof. Define c_n as the coefficient of n^{-s} in the Dirichlet series expansion of $\zeta(s)L(s,\chi)$, so that for $\sigma>1$,

$$\zeta(s)L(s,\chi)=\sum_{n=1}^{\infty}\frac{c_n}{n^s}.$$

Then $c_1=1$ and $c_n\ge 0$.

Case 1. $\chi(-1)=1$. We have

$$\left(\frac{\pi}{\sqrt{k}}\right)^{-s/2}\Gamma\left(\frac{s}{2}\right)n^{-s/2}=\int_0^\infty v^{s/2}\exp\left(-\frac{\pi nv}{\sqrt{k}}\right)\frac{dv}{v}.$$

So

$$\pi^{-s/2}\Gamma\left(\frac{s}{2}\right)\left(\frac{\pi}{k}\right)^{-s/2}\Gamma\left(\frac{s}{2}\right)n^{-s}$$

$$=\int_0^\infty\int_0^\infty (vw)^{s/2}\exp\left(-\frac{\pi n(v+w)}{\sqrt{k}}\right)\frac{dv}{v}\frac{dw}{w}.$$

Multiplying by c_n and summing gives for $\sigma>\sigma_k$

$$\xi(s)\xi(s,\chi)$$

$$=\int_0^\infty\int_0^\infty (vw)^{s/2}\left\{\sum_{n=1}^{\infty}c_n\exp\left(-\frac{\pi n(v+w)}{\sqrt{k}}\right)\right\}\frac{dv}{v}\frac{dw}{w}.$$

We now treat the integral on the right as a double integral over the first quadrant. Since the integrand is symmetric in v and w, we may replace the integral by twice the integral over the area in the first quadrant below the 45° ray thru the origin. In this, we introduce

$$x=\sqrt{vw}$$

$$y=v+w$$

as new variables of integration, getting

$$\xi(s)\xi(s,\chi)$$

$$=4\int_0^\infty x^{s-1}dx\int_{2x}^\infty\left\{\sum_{n=1}^{\infty}c_n\exp\left(-\frac{\pi ny}{\sqrt{k}}\right)\right\}\frac{dy}{\sqrt{y^2-4x^2}}.$$

We take

$$f(x)=4\int_{2x}^\infty\left\{\sum_{n=1}^{\infty}c_n\exp\left(-\frac{\pi ny}{\sqrt{k}}\right)\right\}\frac{dy}{\sqrt{y^2-4x^2}} \tag{6}$$

and conclude (II) and (VI) of our theorem. We put $y=2x+z$ in eq 6 and get

$$f(x)=4\int_0^\infty\left\{\sum_{n=1}^{\infty}c_n\exp\left(-\frac{\pi n(2x+z)}{\sqrt{k}}\right)\right\}\frac{dz}{\sqrt{z}\sqrt{4x+z}}. \tag{7}$$

Then (I) and (III) of our theorem are evident. Further, for $x\ge 1$, we write

$$f(x)=4\exp\left(-\frac{2\pi x}{\sqrt{k}}\right)\int_0^\infty\left\{\sum_{n=1}^\infty c_n\exp\left(-\frac{\pi n(2x+z)}{\sqrt{k}}+\frac{2\pi x}{\sqrt{k}}\right)\right\}\frac{dz}{\sqrt{z}\,\sqrt{4x+z}}$$

$$\leq 4\exp\left(-\frac{2\pi x}{\sqrt{k}}\right)\int_0^\infty\left\{\sum_{n=1}^\infty c_n\exp\left(-\frac{\pi n(2+z)}{\sqrt{k}}+\frac{2\pi}{\sqrt{k}}\right)\right\}\frac{dz}{\sqrt{z}\,\sqrt{4+z}}$$

$$\leq \exp\left(-\frac{2\pi x}{\sqrt{k}}\right)\left\{f(1)\exp\left(\frac{2\pi}{\sqrt{k}}\right)\right\}.$$

So (IV) holds.

By eq 7, using only the first term of the series, we get

$$f(x)\geq 4\int_0^\infty\exp\left(-\frac{\pi(2x+z)}{\sqrt{k}}\right)\frac{dz}{\sqrt{z}\,\sqrt{4x+z}}$$

$$\geq 4\int_0^1\exp\left(-\frac{\pi(2x+z)}{\sqrt{k}}\right)\frac{dz}{\sqrt{z}\,\sqrt{4x+z}}$$

$$\geq \frac{4}{\sqrt{4x+1}}\exp\left(-\frac{2\pi x}{\sqrt{k}}\right)\int_0^1\exp\left(-\frac{\pi z}{\sqrt{k}}\right)\frac{dz}{\sqrt{z}}.$$

So (V) holds.

In the relation

$$K_0(z)=\int_0^\infty\exp\left(-z\cosh\phi\right)d\phi$$

(see [5], p. 384, Example 40) put $\cosh\phi=1+t$. There results

$$K_0(z)=\int_0^\infty\exp\left(-z(1+t)\right)\frac{dt}{\sqrt{t^2+2t}}.$$

So for $x>0$

$$4K_0\left(\frac{2\pi nx}{\sqrt{k}}\right)=4\int_0^\infty\exp\left(-\frac{2\pi nx(1+t)}{\sqrt{k}}\right)\frac{dt}{\sqrt{t^2+2t}}.$$

Putting $t=z/2x$, we get

$$4K_0\left(\frac{2\pi nx}{\sqrt{k}}\right)=4\int_0^\infty\exp\left(-\frac{\pi n(2x+z)}{\sqrt{k}}\right)\frac{dz}{\sqrt{k}\,\sqrt{4x+z}}.$$

So by eq 7,

$$f(x)=4\sum_{n=1}^\infty c_nK_0\left(\frac{2\pi nx}{\sqrt{k}}\right).$$

Case 2. $\chi(-1)=-1$. By the duplication formula for the gamma function

$$\pi^{-s/2}\Gamma\left(\frac{s}{2}\right)\left(\frac{\pi}{k}\right)^{-(s+1)/2}\Gamma\left(\frac{s+1}{2}\right)n^{-s}$$

$$=2\sqrt{k}\left(\frac{2\pi}{\sqrt{k}}\right)^{-s}\Gamma(s)n^{-s}$$

$$=2\sqrt{k}\int_0^\infty x^{s-1}\exp\left(-\frac{2\pi nx}{\sqrt{k}}\right)dx.$$

Multiplying by c_n and summing gives for $\sigma>\sigma_k$

$$\xi(s)\xi(s,\chi)=2\sqrt{k}\int_0^\infty x^{s-1}\left\{\sum_{n=1}^\infty c_n\exp\left(-\frac{2\pi nx}{\sqrt{k}}\right)\right\}dx.$$

We now take

$$f(x)=2\sqrt{k}\sum_{n=1}^\infty c_n\exp\left(-\frac{2\pi nx}{\sqrt{k}}\right) \tag{8}$$

and conclude (I), (II), (III), and (VI) of our theorem. We can easily show that for $x\geq 1$,

$$f(x)\leq\exp\left(-\frac{2\pi x}{\sqrt{k}}\right)\left\{f(1)\exp\left(\frac{2\pi}{\sqrt{k}}\right)\right\}$$

and so (IV) holds. Using the first term of eq 8 gives

$$f(x)>2\sqrt{k}\exp\left(-\frac{2\pi x}{\sqrt{k}}\right).$$

So we may take $A=2\sqrt{k}$ in (V).

Theorem 9. For all s

$$\xi(s)\xi(s,\chi)=\frac{\xi(1,\chi)}{s(s-1)}+\int_1^\infty(x^{s-1}+x^{-s})f(x)dx.$$

Proof. Use the method of Heilbronn (see [8]).

Theorem 10. For $R(x)>0$,

$$f\left(\frac{1}{x}\right)=xf(x)+(x-1)\xi(1,\chi).$$

Proof. Comparing (VI) of theorem 8 with theorem gives for $\sigma>\sigma_k$

$$\int_0^1 x^{s-1}f(x)dx=\frac{\xi(1,\chi)}{s(s-1)}+\int_1^\infty x^{-s}f(x)dx.$$

We can rewrite this as

$$\int_0^1 x^{s-1}f(x)dx=\xi(1,\chi)\int_0^1 x^{s-2}dx$$

$$-\xi(1,\chi)\int_0^1 x^{s-1}dx+\int_0^1 x^{s-2}f\left(\frac{1}{x}\right)dx$$

$$=\int_0^1 x^{s-1}\left\{\xi(1,\chi)\left(\frac{1}{x}-1\right)+\frac{1}{x}f\left(\frac{1}{x}\right)\right\}dx.$$

Replacing x by e^{-t} in these integrals and using the uniqueness theorem for Laplace transforms, we infer that for $0<x<1$

$$f(x)=\xi(1,\chi)\left(\frac{1}{x}-1\right)+\frac{1}{x}f\left(\frac{1}{x}\right).$$

So our theorem holds for $0<x<1$. Then by analytic continuation, it holds for $R(x)>0$.

If we let $x\to\infty$ in this result, we have $xf(x)\to 0$ and

$$f\left(\frac{1}{x}\right)>f(1)>0.$$

So we have an alternative proof of the known result that $\xi(1,\chi)>0$. If we differentiate both sides and put $x=1$, we infer:

Theorem 11.

$$\xi(1,\chi)=-f(1)-2f'(1).$$

Another consequence of theorem 10 is that

$$f(x)=0\left(\frac{1}{x}\right)$$

as $x\to 0$. Hence in (VI) of theorem 8, we can take $\sigma_k=1$.

Theorem 12. For $0<s<1$,

$$-\xi(s)\xi(s,\chi)=\int_1^\infty (x^{s-2}+x^{-s-1})\{\xi(1,\chi)-xf(x)\}dx.$$

Proof. Use theorem 9.

It is clear from this that if $xf(x)\le\xi(1,\chi)$ for $1\le x$, then $L(s,\chi)>0$ for $s>0$. There are many k's for which $xf(x)\le\xi(1,\chi)$ for $1\le x$. For example, let $\chi(-1)=-1$ and $k\le 39$. Then

$$\frac{2\pi}{\sqrt{k}}>1.$$

Hence by eq 8

$$f(x)=2\sqrt{k}\sum_{n=1}^{\infty}c_n\exp\left(-\frac{2\pi nx}{\sqrt{k}}\right),$$

$$xf(x)=2\sqrt{k}\sum_{n=1}^{\infty}c_n x\exp\left(-\frac{2\pi nx}{\sqrt{k}}\right).$$

However, with $2\pi/\sqrt{k}>1$,

$$x\exp\left(-\frac{2\pi nx}{\sqrt{k}}\right)$$

is decreasing for $x>1$. So $xf(x)$ is a decreasing function for $x\ge 1$. So we have only to prove

$$f(1)<\xi(1,\chi).$$

So, by theorem 11, it suffices to prove

$$-f'(1)>f(1).$$

However

$$-f'(1)=2\sqrt{k}\sum_{n=1}^{\infty}c_n\frac{2\pi n}{\sqrt{k}}\exp\left(-\frac{2\pi n}{\sqrt{k}}\right)$$

$$>2\sqrt{k}\sum_{n=1}^{\infty}c_n\exp\left(-\frac{2\pi n}{\sqrt{k}}\right)$$

$$>f(1).$$

If $\chi(-1)=1$, one can carry out similar reasoning based on eq 7, since

$$\int_0^\infty \exp\left(-\frac{\pi nz}{\sqrt{k}}\right)\frac{dz}{\sqrt{z}\sqrt{4x+z}}$$

is a decreasing function of x.

Thus we conclude by a very simple reasoning, which does not even involve inspection of the values of χ, that for $k\le 39$, $L(s,\chi)$ has no positive real zeros.

For larger k's, we would need to know the values of $\chi(n)$ for some of the smaller values of n. However, usually a knowledge of the values of $\chi(n)$ for $n\le\sqrt{k}$ would be more than ample.

Unfortunately, this method is not general. In particular, it fails for $k=163$. Indeed (as we will show in the next section) for $k=163$,

$$f(1)>\xi(1,\chi)$$

so that it is impossible to have $xf(x)\le\xi(1,\chi)$ for $x\ge 1$. So for $k=163$, more subtle methods are required.

IV. Treatment of $k=163$

Throughout this section, let $k=163$. Then $\chi(-1)=-1$. Also, the class number of $\sqrt{-k}$ is unity, so that

$$\xi(1,\chi)=\sqrt{k}. \tag{9}$$

Temporarily define

$$g(x)=\xi(1,\chi)-xf(x). \tag{10}$$

Lemma 1. For $1\le x\le\sqrt{k}/2\pi$, $g'(x)<0$.

Proof. Using the first term of eq 8, we get

$$g(x)<\xi(1,\chi)-2\sqrt{k}x\exp\left(-\frac{2\pi x}{\sqrt{k}}\right)$$

$$<\sqrt{k}\left(1-2x\exp\left(-\frac{2\pi x}{\sqrt{k}}\right)\right).$$

As

$$x\exp\left(-\frac{2\pi x}{\sqrt{k}}\right)$$

is increasing for $1 \leq x < \sqrt{k}/2\pi$, it suffices to prove

$$\frac{1}{2} < \exp\left(-\frac{2\pi}{\sqrt{k}}\right).$$

However, for $k=163$,

$$\exp\left(-\frac{2\pi}{\sqrt{k}}\right)=0.61,$$

and our lemma is proved.

Lemma 2. For $(\sqrt{k}/2\pi) \leq x$, $g'(x)>0$.

Proof. For $(\sqrt{k}/2\pi) \leq x$,

$$\frac{d}{dx}\left\{x \exp\left(-\frac{2\pi x}{\sqrt{k}}\right)\right\} \leq 0$$

and for $n>1$

$$\frac{d}{dx}\left\{x \exp\left(-\frac{2\pi n x}{\sqrt{k}}\right)\right\}<0.$$

Multiplying by $2c_n\sqrt{k}$ and summing gives

$$\frac{d}{dx}\{x f(x)\}<0$$

for $(\sqrt{k}/2\pi) \leq x$. This establishes our lemma.

Lemma 3. There is a number a such that:
(I) $1<a$.
(II) For $1 \leq x < a$, $g(x)<0$.
(III) For $a<x$, $g(x)>0$.

Proof. Obvious by lemma 1, lemma 2, and the fact that

$$\lim_{x \to \infty} g(x) = \xi(1, \chi) > 0.$$

Indeed, we have $a > \sqrt{k}/2\pi$, but this fact is not needed.

Lemma 4. For $1/2 \leq s < 1$,

$$-\frac{\xi(s)\xi(s,\chi)}{a^{s-1}+a^{-s}}$$

is a monotone, nondecreasing function of s.

Proof. By theorem 12,

$$-\frac{\xi(s)\xi(s,\chi)}{a^{s-1}+a^{-s}} = \int_1^\infty \frac{x^{s-1}+x^{-s}}{a^{s-1}+a^{-s}} \frac{g(x)}{x}\, dx.$$

So

$$\frac{\partial}{\partial s}\left\{-\frac{\xi(s)\xi(s,\chi)}{a^{s-1}+a^{-s}}\right\} = \int_1^\infty \frac{\partial}{\partial s}\left\{\frac{x^{s-1}+x^{-s}}{a^{s-1}+a^{-s}}\right\} \frac{g(x)}{x}\, dx.$$

However,

$$\frac{\partial}{\partial s}\left\{\frac{x^{s-1}+x^{-s}}{a^{s-1}+a^{-s}}\right\} = \frac{((ax)^{2s-1}-1)(\log x - \log a)}{(ax)^s(a^{s-1}+a^{-s})^2} + \frac{(x^{2s-1}-a^{2s-1})(\log x + \log a)}{(ax)^s(a^{s-1}+a^{-s})^2}.$$

So for $1/2<s$, we see that

$$\frac{\partial}{\partial s}\left\{\frac{x^{s-1}+x^{-s}}{a^{s-1}+a^{-s}}\right\}$$

is negative if $1 \leq x < a$ and positive if $a<x$. So by lemma 3, we see that for $1/2 \leq s$

$$\frac{\partial}{\partial s}\left\{\frac{x^{s-1}+x^{-s}}{a^{s-1}+a^{-s}}\right\}\frac{g(x)}{x}$$

is nonnegative for $1 \leq x$. Thus our lemma is proved.

If we can prove that the function

$$-\frac{\xi(s)\xi(s,\chi)}{a^{s-1}+a^s}$$

is positive at $s=1/2$, we can conclude that it is positive for $s \geq 1/2$. As it is unchanged by replacing s by $1-s$, we could conclude that it is positive for $0<s<1$. So we have proved:

Lemma 5. If $L(s, \chi)$ is positive for $s=1/2$, then it is positive for $s>0$.

We have now reduced the problem to that of proving that $L(1/2,\chi)>0$. This result is proved in [7]. Alternatively, one can compute $L(1/2,\chi)$ explicitly by means of the formula

$$L\left(\frac{1}{2},\chi\right) = \frac{2\left(\frac{\pi}{163}\right)^{\frac{3}{4}}}{\Gamma\left(\frac{3}{4}\right)} \sum_{n=1}^{\infty} n\chi(n) \int_1^\infty x^{-1/4} \exp\left(-\frac{n^2\pi x}{163}\right) dx.$$

This is not exactly an agreeable computation, but by using a table of the incomplete gamma function, it is not unduly laborious. The computation was carried out by Miss S. Marks under the direction of G. Blanch, and the value

$$L\left(\frac{1}{2},\chi\right)=0.06910$$

was obtained.

A shorter computation results if we use theorem 9. Putting $s=1/2$ in this, we see that it suffices to prove that

$$-4\xi(1,\chi)+2\int_1^\infty x^{-1/2} f(x)\, dx$$

is negative. That is, using eq 8 and eq 9, it suffices to prove

$$1 > \sum_{n=1}^{\infty} c_n \int_0^\infty x^{-1/2} \exp\left(-\frac{2\pi n x}{\sqrt{k}}\right) dx.$$

That is, it suffices to prove

$$\frac{1}{\sqrt{2}\sqrt{k}} > \sum_{n=1}^{\infty} \frac{c_n}{\sqrt{n}} \operatorname{erfc}\left(2\sqrt{\frac{\pi n}{\sqrt{k}}}\right)$$

where

$$\operatorname{erfc}(y)=\frac{1}{\sqrt{2\pi}}\int_y^\infty \exp\left(-\frac{1}{2}t^2\right)dt.$$

Now for $k=163$, we have $\chi(p)=-1$ for every prime p with $2\leq p\leq 37$. So for $n\leq 40$, $c_n=1$ when n is a perfect square, and zero otherwise. So we need only show

$$\frac{1}{\sqrt{2\sqrt{k}}}>\operatorname{erfc}\left(2\sqrt{\frac{\pi}{\sqrt{k}}}\right)+\frac{1}{2}\operatorname{erfc}\left(4\sqrt{\frac{\pi}{\sqrt{k}}}\right)+\frac{1}{3}\operatorname{erfc}\left(6\sqrt{\frac{\pi}{\sqrt{k}}}\right)+\cdots$$

that is, we need only show

$$0.1979>\operatorname{erfc}(0.9921)+\frac{1}{2}\operatorname{erfc}(2(0.9921))+\frac{1}{3}\operatorname{erfc}(3(0.9921))+\cdots.$$

Using a four-place table of erfc, we get

$$\operatorname{erfc}(0.9921)=0.1606$$
$$\frac{1}{2}\operatorname{erfc}(2(0.9921))=0.0118$$
$$\frac{1}{3}\operatorname{erfc}(3(0.9921))=0.0005$$
$$\frac{1}{4}\operatorname{erfc}(4(0.0021))=0.0000$$

As $0.1979>0.1729$, we conclude that $L(1/2,\chi)>0$.

V. Miscellaneous Results

If $L(s,\chi)$ is to be positive for $0<s$, then from

$$\Gamma(s)L(s,\chi)=\int_0^\infty x^{s-1}f(x,\chi)dx$$

we see that

$$\int_0^\infty x^{s-1}f(x,\chi)dx$$

must be positive even when $f(x,\chi)$ is negative for some x (as when $k=163$). In an effort to prove this for various k's, we undertook to find more about the behavior of $f(x,\chi)$. Nothing particularly useful for our purpose was discovered. However miscellaneous results were found, and we list them without proof.

Theorem 13. For $s\neq 1$,

$$L(s,\phi)=-\frac{\Gamma(1-s)}{2\pi i}\int(-z)^{s-1}f(z,\phi)dz$$

where the contour begins at $+\infty$ on the real axis, encircles the origin counterclockwise once, and returns to $+\infty$ on the real axis, and where the contour does not encircle any of the points $\pm 2\pi mi/K$ (m a positive integer), and where $|\arg(-z)|\leq\pi$.

Theorem 14. If

$$\sum_{n=1}^{K}\phi(n)=0,$$

then

$$f^{(m)}(0,\phi)=(-1)^m L(-m,\phi).$$

Define

$$T_m=T(m,K,\phi)=\sum_{r=1}^{K}\phi(r)\left(1-\frac{r}{K}\right)^m.$$

Theorem 15. For $M\geq 1$,

$$T_M=\frac{(-1)^M}{K^M}\sum_{N=0}^{M}(-1)^N\phi_{N+1}(K)\Delta^N(1^M),$$

where $\Delta^N(1^M)$ denotes the N-th difference of x^M evaluated at $x=1$. That is

$$\Delta^N(1^M)=(-1)^N\sum_{r=0}^{N}(-1)^r\frac{N!}{(N-r)!r!}(1+r)^M.$$

Theorem 16. If

$$\sum_{n=1}^{K}\phi(n)=0,$$

then

$$f^{(m)}(0,\phi)=\frac{(m!)K^m}{(m+1)!}\left\{T_{m+1}-\frac{m+1}{2}T_m+\frac{(m+1)_m}{2!}B_1T_{m-1}-\frac{(m+1)(m)(m-1)(m-2)}{4!}B_2T_{m-3}+\cdots\right\}$$

where B_m is the m-th Bernoulli number as defined on p. 125 of [5].

Theorem 17. For x positive and small

$$f(x,\phi)=e^{-x}\sum_{r=0}^{\infty}A_r(1-e^{-x})^r,$$

where

$$A_r=\frac{1}{r!}\left[\left(\frac{d}{dx}+1\right)\left(\frac{d}{dx}+2\right)\cdots\left(\frac{d}{dx}+r\right)f(x,\phi)\right]_{x=0}.$$

Theorem 18. If χ is a primitive real character and $\chi(-1)=1$, then:

(1) For $|z|<\frac{2\pi}{k}$,

$$f(z,\chi)=\frac{\sqrt{k}}{\pi}\sum_{m=0}^{\infty}(-1)^m\left(\frac{kz}{2\pi}\right)^{2m+1}L(2+2m,\chi).$$

(2) For $|z|<\frac{2\pi R}{k}$, $z\neq\frac{2\pi mi}{k}$,

$$f(z,\chi)=\frac{\sqrt{k}}{\pi}\frac{kz}{2\pi}\sum_{r=1}^{R-1}\frac{\chi(r)}{r^2}\frac{1}{1+\left(\frac{kz}{2\pi r}\right)^2}$$

$$+\frac{\sqrt{k}}{\pi}\sum_{m=0}^{\infty}(-1)^m\left(\frac{kz}{2\pi}\right)^{2m+1}\left\{L(2+2m,\chi)-\sum_{r=1}^{R-1}\frac{\chi(r)}{r^{2+2m}}\right\}.$$

(3) For $z\neq\frac{2\pi mi}{k}$,

$$f(z,\chi)=\frac{\sqrt{k}}{\pi}\frac{kz}{2\pi}\sum_{r=1}^{\infty}\frac{\chi(r)}{r^2}\frac{1}{1+\left(\frac{kz}{2\pi r}\right)^2}.$$

(4) For $z\neq\frac{2\pi mi}{k}$,

$$f(z,\chi)=\frac{\sqrt{k}}{\pi}\sum_{m=0}^{M-1}(-1)^m\left(\frac{kz}{2\pi}\right)^{2m+1}L(2+2m,\chi)$$

$$+(-1)^M\frac{\sqrt{k}}{\pi}\left(\frac{kz}{2\pi}\right)^{2M+1}\sum_{r=1}^{\infty}\frac{\chi(r)}{r^{2+2M}}\frac{1}{1+\left(\frac{kz}{2\pi r}\right)^2}.$$

Theorem 19. If χ is a primitive real character and $\chi(-1)=-1$, then:

(1) For $|z|<\frac{2\pi}{k}$,

$$f(z,\chi)=\frac{\sqrt{k}}{\pi}\sum_{m=0}^{\infty}(-1)^m\left(\frac{kz}{2\pi}\right)^{2m}L(1+2m,\chi).$$

(2) For $|z|<\frac{2\pi R}{k}$, $z\neq\frac{2\pi mi}{k}$,

$$f(z,\chi)=\frac{\sqrt{k}}{\pi}\sum_{r=1}^{R-1}\frac{\chi(r)}{r}\frac{1}{1+\left(\frac{kz}{2\pi r}\right)^2}$$

$$+\frac{\sqrt{k}}{\pi}\sum_{m=0}^{\infty}(-1)^m\left(\frac{kz}{2\pi}\right)^{2m}\left\{L(1+2m,\chi)-\sum_{r=1}^{R-1}\frac{\chi(r)}{r^{1+2m}}\right\}.$$

(3) For $z\neq\frac{2\pi mi}{k}$,

$$f(z,\chi)=\frac{\sqrt{k}}{\pi}\sum_{r=1}^{\infty}\frac{\chi(r)}{r}\frac{1}{1+\left(\frac{kz}{2\pi r}\right)^2}.$$

(4) For $z\neq\frac{2\pi mi}{k}$,

$$f(z,\chi)=\frac{\sqrt{k}}{\pi}\sum_{m=0}^{M}(-1)^m\left(\frac{kz}{2\pi}\right)^{2m+1}L(1+2m,\chi)$$

$$+(-1)^M\frac{\sqrt{k}}{2\pi}\left(\frac{kz}{2\pi}\right)^{2M}\sum_{r=1}^{\infty}\frac{\chi(r)}{r^{1+2M}}\frac{1}{1+\left(\frac{kz}{2\pi r}\right)^2}.$$

TABLE 1. *Characters and sums of characters (mod 53)*

n	$\chi^{(n)}$	$\chi_1^{(n)}$	$\chi_2^{(n)}$	$\chi_3^{(n)}$
1	1	1	1	1
2	−1	0	1	2
3	−1	−1	0	2
4	1	0	0	2
5	−1	−1	−1	1
6	1	0	−1	0
7	1	1	0	0
8	−1	0	0	0
9	1	1	1	1
10	1	2	3	4
11	1	3	6	10
12	−1	2	8	18
13	1	3	11	29
14	−1	2	13	42
15	1	3	16	58
16	1	4	20	78
17	1	5	25	103
18	−1	4	29	132
19	−1	3	32	164
20	−1	2	34	198
21	−1	1	35	233
22	−1	0	35	268
23	−1	−1	34	302
24	1	0	34	336
25	1	1	35	371
26	−1	0	35	406
27	−1	−1	34	440
28	1	0	34	474
29	1	1	35	509
30	−1	0	35	544
31	−1	−1	34	578
32	−1	−2	32	610
33	−1	−3	29	639
34	−1	−4	25	664
35	−1	−5	20	684
36	1	−4	16	700
37	1	−3	13	713
38	1	−2	11	724
39	−1	−3	8	732
40	1	−2	6	738
41	−1	−3	3	741
42	1	−2	1	742
43	1	−1	0	742
44	1	0	0	742
45	−1	−1	−1	741
46	1	0	−1	740
47	1	1	0	740
48	−1	0	0	740
49	1	1	1	741
50	−1	0	1	742
51	−1	−1	0	742
52	1	0	0	742
53	0	0	0	742

TABLE 2. *Values of k and corresponding values of r*

k	r	k	r	k	r	k	r
3	1	55	1	109	2	165	2
4	1	56	1	111	1	167	1
5	2	56*	2	113	2	168	2
7	1	57	2	115	4	168*	2
8	2	59	1	116	1	172	2
8*	1	60	2	119	1	177	2
11	1	61	2	120	1	179	2
12	2	65	2	120*	2	181	2
13	2	68	1	124	2	183	1
15	1	69	2	127	2	184	2
17	2	71	1	129	2	184*	2
19	2	73	2	131	1	185	2
20	1	76	2	132	1	191	1
21	2	77	7	133	2	193	2
23	1	79	1	136	2	195	2
24	1	83	1	136*	1	199	1
24*	2	84	1	137	2	201	2
28	2	85	2	139	2	203	2
29	2	87	1	140	2	204	2
31	1	88*	2	141	2	205	2
33	2	89	2	143	1	209	2
35	1	91	3	145	2	211	3
37	2	92	2	149	2	212	1
39	1	93	2	151	1	213	6
40	2	95	1	152	1	215	1
40*	1	97	2	152*	9	217	2
41	2	101	2	155	2	219	2
44	2	103	1	156	2	220	2
47	1	104	2	157	2	221	2
51	2	104*	1	159	1	223	2
52	2	105	2	161	2	227	2
53	3	107	2	164	1		

TABLE 3. *Values of k and corresponding combinations and values of r*

k	Combination	r
43	$(1+2^{-s})(1+3^{-s})L(s,\chi)$	2
67	$(1+2^{-s})(1+3^{-s})(1+5^{-s})L(s,\chi)$	3
88	$(1+3^{-s})L(s,\chi)$	4
123	$(1+2^{-s})(1+5^{-s})L(s,\chi)$	2
148	$(1+3^{-s})(1+5^{-s})(1+7^{-s})L(s,\chi)$	3
173	$(1+2^{-s})(1+3^{-s})(1+5^{-s})L(s,\chi)$	4
187	$(1+2^{-s})(1+3^{-s})(1+5^{-s})L(s,\chi)$	3
188	$(1+3^{-s})L(s,\chi)$	3
197	$(1+2^{-s})L(s,\chi)$	2

VI. References

[1] J. Barkley Rosser, Real roots of Dirichlet L-series, Bul. Am. Math. Soc. **55**, 906 to 913 (1949).

[2] E. Landau, Handbuch der Lehre von der Verteilung der Primzahlen, **1**, Leipzig, Teubner, 1909.

[3] S. Chowla, Note on Dirichlet's L-functions, Acta Arithmetica, **1**, 113 to 114 (1935).

[4] H. Heilbronn, On real characters, Acta Arithmetica, **2**, 212 to 213 (1937).

[5] E. T. Whittaker and G. N. Watson, A course of modern analysis, American Edition (The Macmillan Co., New York, N. Y., 1947).

[6] E. Landau, Vorlesungen über zahlentheorie, **1**, Leipzig, Hirzel, 1927.

[7] S. Chowla and A. Selberg, On Epstein's Zeta Function (I), Proc. Nat. Acad. of Sciences, **35**, 371 to 374 (1949).

[8] H. Heilbronn, On Dirichlet series which satisfy a certain functional equation, Quart. Jour. of Math., Oxford series, **9**, 194 to 195 (1938).

LOS ANGELES, January 11, 1950.

Journal of Research of the National Bureau of Standards Vol. 45, No. 6, December 1950 Research Paper 2165

Forced Oscillations in Nonlinear Systems[1]

By Mary L. Cartwright

This paper shows how the approximate form of the solutions of a certain nonlinear differential equation occurring in radio work may be obtained from certain general results and gives the proof of the general results in detail. The proof of the general statement depends on a type of method that can be applied with minor modifications to any equation of the type

$$\ddot{x}+k\,f(x)\,\dot{x}+g(x)=k\,p(t),$$

where $p(t)$ has period $2\pi/\lambda$, and $\int_0^t p(t)dt$ is bounded for all t, $f(x)\geq 1$ for $|x|\geq a$, and $g(x)/x\geq 1$ for $|x|\geq a$.

For some years Professor J. E. Littlewood and I have been working on nonlinear differential equations [2] of a type which occur in radio work and elsewhere. One of the most interesting of these equations is

$$\ddot{x}=k(1-x^2)\dot{x}+x-bk\lambda\cos(\lambda t+\alpha), \qquad (1)$$

especially for k large and $0<b<2/3$. Our attention was drawn to it by a remark of van der Pol,[3] which suggested that it corresponded to a physical system investigated by him and van der Mark.[4] For certain values of the parameters the physical system had two possible stable oscillations, one of period $4n\pi/\lambda$ and one of period $(2n+1)2\pi/\lambda$. As a matter of fact in the case of (1), owing to the strictly symmetrical nonlinear function $1-x^2$, the period $4n\pi/\lambda$ does not occur, but for certain values of b there are two stable oscillations of periods $(2n\pm1)2\pi/\lambda$.

It would take too long to give a complete proof of this statement here, but I propose to show how the approximate form of the solutions may be obtained from certain very general results, and give the proof of the general results in detail. The proof

[1] This paper contains material presented in lecture form to the staff of the Institute for Numerical Analysis of the National Bureau of Standards on January 28, 1949. Miss Cartwright was a consultant at the INA at the time this lecture was delivered.

[2] See M. L. Cartwright and J. E. Littlewood, J. London Math. Soc. **20**, 180–189 (1945), and Ann. Math. **48**, 472–494 (1947); also M. L. Cartwright, J. Inst. Elec. Eng. (Radio Section) **93** (III), 88–96 (1948, and Proc. Cambridge Phil. Soc, **45**, 495 (1949).

[3] B. van der Pol, Proc. Inst. Radio Eng. **22**, 1051–1086 (1934).

[4] B. van der Pol and J. van der Mark, Nature **120**, 363–364 (1927)

of the general statement depends on the type of method which we use throughout. It can be applied with minor modifications to any equation of the form

$$\ddot{x}+kf(x)\dot{x}+g(x)=kp(t), \tag{2}$$

where $p(t)$ has period $2\pi/\lambda$, and $\int_0^t p(t)dt$ is bounded for all t, $f(x)\geq 1$ for $|x|\geq a$, and $g(x)/x\geq 1$ for $|x|\geq a$, provided of course that f, g, p satisfy the usual conditions required for the existence and uniqueness of solutions, and are either independent of k or satisfy certain simple inequalities independent of k.

We assume throughout that $k\geq 1$, and usually that it is large. We first observe that the α in (1) is merely inserted for convenience. It enables us to choose the origin of t as we wish. We shall write $x_0,\dot{x}_0$ for the values of x and $\dot{x}$ at $t=0$.

There are two main weapons of attack besides the equation (1) itself. The first is *the integrated equation*

$$\dot{x}-\dot{x}_0+k\left(\frac{x^3}{3}-x-\frac{x_0^3}{3}+x_0\right)+\int_0^t x\,dt$$
$$=bk\,[\sin(\lambda t+\alpha)-\sin\alpha]; \tag{3}$$

the second is *the energy equation* which is obtained by multiplying (1) by $2\dot{x}$ and integrating,

$$\dot{x}^2-\dot{x}_0^2+2k\int_0^t(x^2-1)\dot{x}^2dt+x^2-x_0^2$$
$$=2bk\lambda\int_0^t\dot{x}\cos(\lambda t+\alpha)dt. \tag{4}$$

In some ways the integrated equation is more fundamental than (1), and that is why the λ is inserted on the righthand side of (1). The energy equation may be rewritten with $\dot{x}=y$, $\dot{x}_0=y_0$ in the form

$$x^2+y^2-(x_0^2+y_0^2)$$
$$=2k\left\{\int_0^t b\lambda\dot{x}\cos(\lambda t+\alpha)-(x^2-1)\dot{x}^2\right\}dt. \tag{4'}$$

The righthand side of (4′) will be dominated by the term $x^2\dot{x}^2$ when x is large unless $\dot{x}$ is then very small, and it seems improbable that $\dot{x}$ can be small for most of the time that x is large. This suggests that x^2+y^2 decreases rapidly over any arc for which x is large, and therefore that x is bounded for sufficiently large t. The general result which I propose to prove later is the following:

Theorem 1: *If $x=x(t,x_0,\dot{x}_0)$ is any solution of (1) for which $x=x_0,\dot{x}=\dot{x}_0$ when $t=0$, then*

$$|x|<B,|\dot{x}|<Bk, \tag{5}$$

where B is a constant independent of k and t, for $k\geq 1$, $t>t_0(x_0,\dot{x}_0)$.

Assuming for the moment the result of theorem 1, we may argue as follows: eq 3 can be rearranged in the form

$$\frac{x^3}{3}-x=b\sin(\lambda t+\alpha)+C-\frac{\dot{x}}{k}-\frac{1}{k}\int_0^t x\,dt, \tag{3'}$$

where C is a constant depending on $x_0,\dot{x}_0,b$ and α, and in virtue of (5) the last term is $O(1/k)$ for large values of k and $0\leq t\leq 2\pi/\lambda$. Hence there are two extreme possibilities: *either* $\dot{x}$ is comparable with k in magnitude, *or* x is given approximately by the equation $x=X$, where

$$F(X)=\frac{X^3}{3}-X=b\sin(\lambda t+\alpha)+C. \tag{6}$$

Both these possibilities may occur for arbitrarily large values of t, and also of course there are transitions from one to the other. For fixed t and b and C such that $(-2/3)<b\sin(\lambda t+\alpha)+C<2/3$, eq 6 has three roots,

$$X_1<-1<X_2<1<X_3=X_3(t,C),$$

as may be seen from figure 1. If $b>2/3$, $b\sin(\lambda t+\alpha)+C$ runs outside the interval $[-2/3,\ 2/3]$ for some t in each period; we suppose that $0<b<2/3$ because this is the most interesting range. It may be observed from figure 1 that if X_1 and X_3 increase with t, X_2 decreases and vice-versa, so the solutions over $0\leq t\leq 2\pi/\lambda$ are approximately as shown in figure 2, provided that $|\dot{x}|\leq B$.

If we integrate over a second period $2\pi/\lambda\leq t\leq 4\pi/\lambda$, we have (3′) with C' in place of C where

$$C'=C-\frac{1}{k}\int_{2\pi/\lambda}^{4\pi/\lambda}x\,dt=C-\frac{1}{k}\int_{2\pi/\lambda}^{4\pi/\lambda}X_s(t,C)dt+O\left(\frac{1}{k^2}\right),$$
$$s=1,2,3.$$

Hence if $|\dot{x}|<B$, the solution is given approximately by $X_s(t,C')$ over the next period. The difference $C'-C$ is actually of the same order as $\dot{x}/k$, which occurs in the error term in (3′), but it can be shown that in the circumstances considered $\dot{x}$ is of the form $\dot{x}_s(t,C)+O(k^{-\frac{1}{2}})$. Putting this and $x=X_s(t,C)+O(k^{-1})$ in (3′), and remembering that X_s and $\dot{x}_s$ are periodic, we see than the nonperiodic error is

$$\frac{1}{k}\int_0^t X_s(t,C)dt+O\left(\frac{1}{k^2}\right).$$

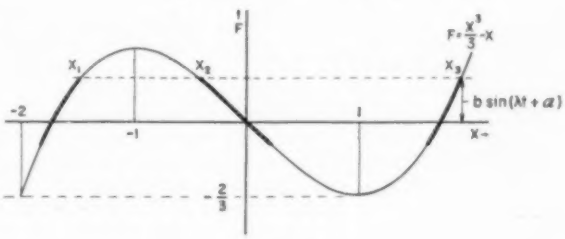

FIGURE 1.

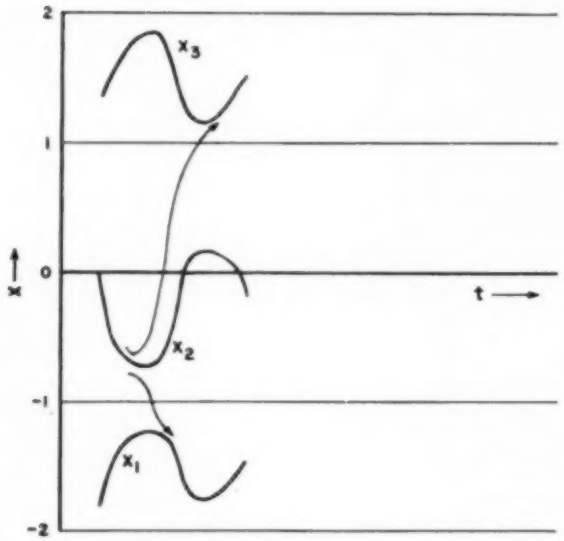

FIGURE 2.

and so the second wave will certainly be lower than the first in the case of X_3 by an amount of order $1/k$, and the solution will perform descending waves as shown in figure 3. The second wave will be higher than the first in the case of X_1, and higher or lower for X_2, unless

$$\int_0^{2\pi/\lambda} X_2(t,C)dt=0$$

(so that $C'=C$ approximately). This can only occur for $C=0$, and then we have a solution with period $2\pi/\lambda$ approximately. There is in fact a strictly periodic solution with period $2\pi/\lambda$ which is, for reasons which we shall give presently, unstable.

Returning to the case in which $|\dot{x}|$ is comparable with k in magnitude, we suppose first that $\dot{x}>\delta k$, where $\delta>0$ for a time of length D/k. Then x changes by at least $D\delta$, and this is excluded by (5) if $D\delta>2B$. Similarly $\dot{x}$ is not less than $-\delta k$ for an interval of time greater than D/k, for if it is x runs outside the strip $|x|<B$.

As regards the transitions, if $|1-x^2|>\delta>0$ and $|\dot{x}|$ is large, the second term in (1) is much more important than x or $b\ k\lambda\ \cos(\lambda t+\alpha)$, and so $\ddot{x}$ has the same sign as $\dot{x}$ in $|x|<1-\delta$ and the opposite if $|x|>1+\delta$, (provided that $|\dot{x}|$ is large and k is large). Hence any small but significant deviation from X_1 or X_3 is at once corrected, whereas a small but significant deviation from X_2 causes $|\dot{x}|$ to increase rapidly. In the latter case $|\dot{x}|$ cannot decrease again until x approaches either the X_1 or X_3 curve which corresponds.

Finally near $x=\pm 1$ the term $bk\lambda\cos(\lambda t+\alpha)$ dominates except when $\lambda t+\alpha$ is near $n\pi+1/2\pi$. The dips of X_3 towards $x=1$ and crests of X_1 toward $x=-1$ do in fact occur in these intervals, and a complete theory of the behavior of solutions near these points is very complicated. However, in spite of that we can now form a fairly good general picture of the behavior of solutions. They settle above $x=1$ into a long descent in waves of the form $x=X_3(t,C)$ approximately, dipping a little lower each time until they reach the neighborhood of $x=1$. There they have three alternatives: (1) another wave $x=X_3$ just above $x=1$, (2) an unstable wave $x=X_2$ just below $x=1$, or (3) a rush down to the corresponding X_1 which, as may be seen from figure 1, is near $x=-2$. The stable oscillations naturally follow the first or third alternative, and have period $(2n+1)2\pi/\lambda$ or $(2n-1)2\pi/\lambda$ according as they have $n+1/2$ or $n-1/2$ waves above $x=1$. Separating them there are many types of unstable motion following an X_2 curve which begins and ends on $x=1$ for part or the whole of the way (or a similar X_2 curve after a long ascent near $x=-1$). From an X_2 curve they may pull up sharply to X_1 or rush down to X_3 at any stage. All types starting near $x=1$ finally plunge down to the X_1 curve, and perform a corresponding long ascent to $x=-1$, the whole phenomenon for $x<0$ corresponding to that for $x>0$. All this can be rigorously established, and moreover the relative positions of solutions approximating to $X_3(t,C_1)$ and $X_3(t,C_2)$ remain the same throughout a long descent unless C_1 and C_2 differ by something which is extremely small for large k, such as $e^{-k^{1/2}}$.

We now return to the proof of theorem 1. The preceding analysis depended to a large extent on the fact that $1-x^2$ changes sign twice; in the work which follows the significant point is that the coefficient of $\dot{x}$ is positive for large x and that the function $g(x)$ in (2) has the sign of x. Physicists may consider it intuitive that a system with a restoring force and positive damping for large x should have bounded solutions, and I hope to show that this is also intuitive by mathematical commonsense. Incidentally the lemmas give a good deal of other information about the solutions. I shall as usual refer to t as the time, and say that t_1 is before or after t_2 according as $t_1<t_2$ or $t_1>t_2$. The constants B are independent of k and t, and are not necessarily the same in each place unless a suffix is attached, and, as we said earlier $k>1$.

We first ensure that all solutions eventually come fairly near $x=0$.

Lemma 1. *A solution of (1) cannot have absolute value greater than $3^{1/2}$ for all large t.*

Suppose that this is not so, and that $x\geq 3^{1/2}$ for $t\geq t_1$. Integrating from t_1 where $x=x_1$, $\dot{x}=\dot{x}_1$, we have

$$\dot{x}-\dot{x}_1+k\left(\frac{x^3}{3}-x-\frac{x_1^3}{3}+x_1\right)+\int_{t_1}^{t}xdt=bk[\sin(\lambda t+\alpha)-\sin\alpha],$$

and so

$$3^{1/2}(t-t_1)\leq\int_{t_1}^{t}xdt=-\dot{x}+kx\left(1-\frac{x^2}{3}\right)+O(1)$$

as $t\to\infty$, where the constant implied depends on k. The lefthand side tends to ∞, and so $x\to-\infty$, but this implies that $x\to-\infty$, which contradicts $x\geq 3^{1/2}$. Hence $x\leq 3^{1/2}$ for arbitrarily large t, and similarly $x\geq -3^{1/2}$ for some large t.

We next establish that as long as $|x|$ is not too large the value of $|\dot{x}|$ cannot increase too much.

Lemma 2. *If $|x|\leq 3^{1/2}$ on an arc PQ, then*

$$|\dot{x}_Q|<|\dot{x}_P|+B_1k,$$

and, if the arc lasts a time longer than $4/k$, $|\dot{x}_Q|\leq 2$. More generally if $|x|\leq b_0$ on an arc PQ, then

$$|\dot{x}_Q|<|\dot{x}_P|+B_1(b_0)k.$$

If $|x|\leq 3^{1/2}$ and $\dot{x}>k$ on an arc, it can only last a time at most $2.3^{1/2}/k<4/k$. For if it lasts longer, the solution travels a distance more than $2.3^{1/2}$ and therefore cannot remain in the strip. The same is true if $\dot{x}<-k$ on an arc in $|x|\leq 3^{1/2}$.

Let P_1 be the last point before Q at which $|\dot{x}|\leq k$, or P itself, whichever is the latest. Suppose first that $\dot{x}_{P_1}>0$, then $\dot{x}>0$ on the arc P_1Q. For, if not, $\dot{x}=0$ at some point of P_1Q and P_1 is *not* the last point at which $|\dot{x}|\leq k$. By the integrated equation, since $|x_Q|<3^{1/2}, |x_{P_1}|<3^{1/2}$,

$$\dot{x}_Q-\dot{x}_{P_1}\leq B_1k-\int_{t_1}^{t}x\,dt\leq B_1k,$$

where $B_1\geq 1$ depends on b, which gives the result. Similarly if $\dot{x}_{P_1}<0$, we have $\dot{x}_{P_1}-\dot{x}_Q\leq B_1k$. If the time is greater than $4k$, $|\dot{x}_{P_1}|\leq k$, and we have the second form of the result. The result for $|x|\leq b_0$ follows by the same method.

The next two lemmas show that the height of an arc QR outside the strip $|x|\leq 3^{1/2}$, and the time taken to describe it are bounded by numbers depending on $\dot{x}_Q$; in other words the velocity with which it emerges from the strip.

Lemma 3. *If the arc QR lies above $x=3^{1/2}$ and begins at Q on $x=3^{1/2}$, the greatest height h satisfies*

$$h<\frac{\dot{x}_Q}{2k}+B_2.$$

When $x=h=3^{1/2}+h_1, \dot{x}=0$. Integrating from the point Q to the point H at which $x=h$, we have

$$0=\dot{x}_Q-k\int_{3^{1/2}}^{3^{1/2}+h_1}(x^2-1)\,dx$$

$$-\int_0^t x\,dt+bk[\sin(\lambda t+\alpha)-\sin\alpha].$$

Since $x^2-1\geq 2$ on QR,

$$0<\dot{x}_Q-2kh_1+Bk$$

and the result follows for h_1 and so for h.

Lemma 4. *If QR is an arc above $x=3^{1/2}$ beginning at Q on $x=3^{1/2}$, then the time t taken to describe QR is less than $B_3\dot{x}_Q$, provided that $\dot{x}_Q>k$.*

Suppose that $\dot{x}_Q>k$, and that R is on $x=3^{1/2}$ so that $x_Q=x_R=3^{1/2}$. On QR it is easy to see that

$$\dot{x}<\dot{x}_Q+Bk-\int_0^t x\,dt$$

$$<B\dot{x}_Q-3^{1/2}t$$

because $\dot{x}_Q>k$. Also

$$0=x_R-x_Q=\int_0^t\dot{x}\,dt<B\dot{x}_0t-\frac{3^{1/2}}{2}t^2.$$

and so $t<B_3\dot{x}_Q$.

The reduction in energy over any sufficiently high arc is established in lemma 5 which gives effect to the remarks we made about (4′). It is much the most difficult part of the proof.

Lemma 5. *If QR is an arc above $x=3^{1/2}$ beginning at Q on $x=3^{1/2}$ and ending at R on $x=3^{1/2}$, for a given $B_1\geq 1$ there exists a $B_4\geq B_1\geq 1$ such that if $\dot{x}_Q>B_4k$,*

$$\dot{x}_R^2<\dot{x}_Q^2-4B_1k\dot{x}_Q.$$

The energy eq 4 for the arc QR is

$$\dot{x}_R^2-\dot{x}_Q^2=-2k\int_0^t(x^2-1)\dot{x}^2dt+2bk\lambda\int_0^t\dot{x}\sin(\lambda t+\alpha)dt.$$

Let

$$J=k\int_0^t(x^2-1)\dot{x}^2dt\geq k\int_0^t\dot{x}^2dt. \tag{8}$$

Then

$$\dot{x}_R^2-\dot{x}_Q^2\leq -2J+2bk\lambda\int_0^t|\dot{x}|dt$$

$$\leq -2J+Bkt^{1/2}\left(\int_0^t|\dot{x}|^2dt\right)^{1/2}$$

by Cauchy's inequality. So by lemma 4 and (8)

$$\dot{x}_R^2-\dot{x}_Q^2\leq -2J+B_5k^{1/2}\dot{x}_Q^{1/2}J^{1/2}$$

$$\leq -2J\left[1-\tfrac{1}{2}B_5\left(\frac{k\dot{x}_Q}{J}\right)^{1/2}\right]$$

$$<-J<-B_5^2k\dot{x}_Q,$$

provided that $J\geq B_5^2k\dot{x}_Q$, where B_5 depends on B_3 and $\dot{x}_Q\geq k$. We may obviously choose $B_5^2>4B_1$, and we have the result except for the case in which $J<B_5^2k\dot{x}_Q$.

Suppose now that $J<B_5^2k\dot{x}_Q$, and integrate from Q until $\dot{x}=\frac{1}{2}\dot{x}_Q$ or $x=2B_5^2+3^{1/2}$, whichever comes first. Then $\dot{x}\geq\frac{1}{2}\dot{x}_Q>0$. Hence x is increasing on this arc and

$$\int_0^t\sin(\lambda t+\alpha)\dot{x}dt=\int_{3^{1/2}}^{x}\sin(\lambda t+\alpha)dx<\int_{3^{1/2}}^{x}dx\leq 2B_5^2.$$

Hence

$$\dot{x}^2-\dot{x}_Q^2=-2k\int_0^t(x^2-1)\dot{x}^2dt-kb\lambda\int_0^x\sin(\lambda t+\alpha)dx-B$$
$$\geq -2J-kBB_5^2-B$$
$$\geq -2kB_5^2\dot{x}_Q-kB\geq -\frac{3}{4}\dot{x}_Q^2,$$

provided that $\dot{x}_Q>kB_4$. It follows that $\dot{x}^2>\frac{1}{4}\dot{x}_Q^2$ and therefore $\dot{x}>\frac{1}{2}\dot{x}_Q$, so that x reaches $2B_5^2+3^{1/2}$ first. Now since $x^2-1\geq 2$ on the arc,

$$J\geq 2k\int_{3^{1/2}}^{2B_5^2+3^{1/2}}|\dot{x}|dx\geq k\dot{x}_Q\cdot 2B_5^2,$$

and we have a contradiction. Hence the result of the lemma is true.

It remains to combine the results of lemmas 2 and 5.

Lemma 6. *If Q is a point on $x=3^{1/2}$ such that $\dot{x}_Q>B_4k>0$, then the solution returns to the strip $|x|\leq 3^{1/2}$ at R and emerges again at S with $|\dot{x}_S|<|\dot{x}_Q|-B_1k$.*

By lemma 2 with R and S in place of P and Q

$$|\dot{x}_S|^2<|\dot{x}_R|^2+2B_1k|\dot{x}_R|+B_1^2k^2.$$

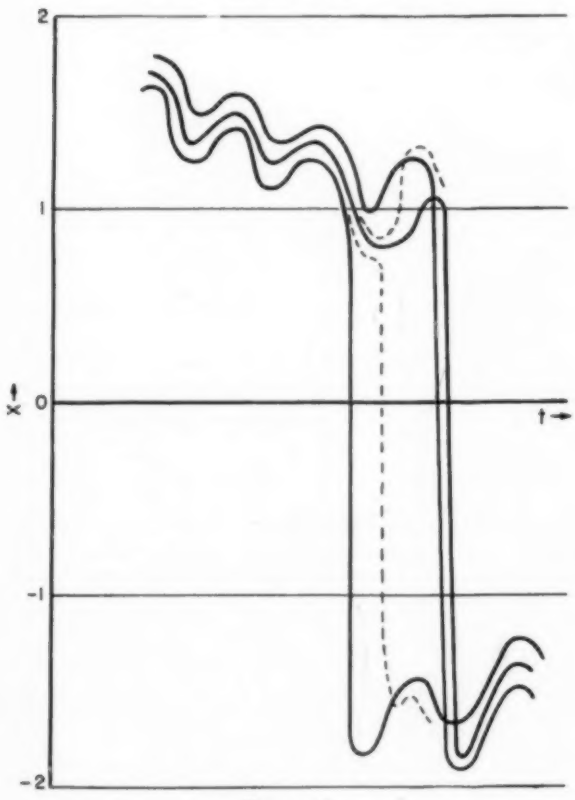

FIGURE 3.

Using lemma 5 in the form stated and also in the weaker form $|\dot{x}_R|\leq|\dot{x}_Q|$, we have

$$|\dot{x}_S|^2<|\dot{x}_Q|^2-4B_1k|\dot{x}_Q|+2B_1k|\dot{x}_R|+B_1^2k$$
$$=(|\dot{x}_Q|-B_1k)^2,$$

From which the result follows. For $\dot{x}_Q>B_4k\geq B_1k$.

We now have the result stated in theorem 1. For by lemma 1 the solution must enter the strip $|x|\leq 3^{1/2}$, and by the second part of lemma 2 $|\dot{x}|\leq B_1k$, if it stays there. If on the other hand it emerges at Q with $|\dot{x}_Q|\leq B_4k$, the height (or depth) of the subsequent arc outside the strip is less than B_4+B_2. For by symmetry all the lemmas for $x-\geq 3^{1/2}$ have strictly corresponding forms for $x\leq -3^{1/2}$. But by lemma 6 if $|\dot{x}_Q|>B_4k$, the solution emerges the next time at S with $|\dot{x}_S|<|\dot{x}_Q|-B_1k$, so that it must either stay in the strip or emerge eventually with $|\dot{x}_Q|\leq B_4k$, and then by the second part of lemma 2, $|x|\leq B_4+B_2$ for all subsequent t.

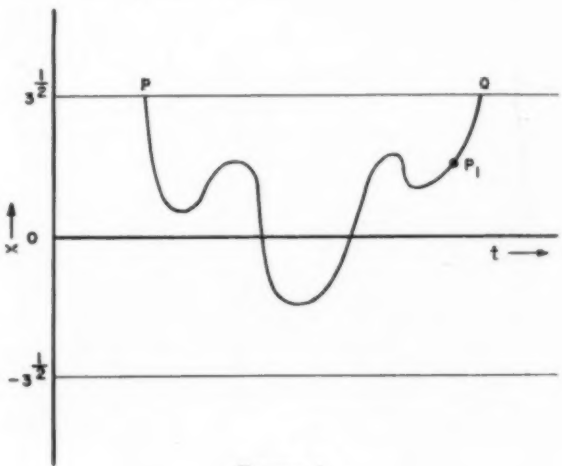

FIGURE 4.

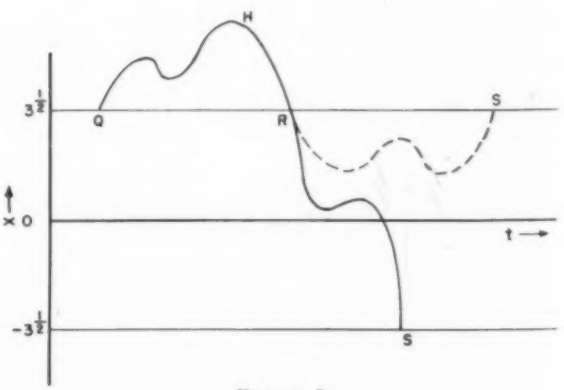

FIGURE 5.

LOS ANGELES, December 16, 1949.

Index to Volume 45

A

Page

Absorption of near-infrared energy by glasses, RP2118 121
Accelerometers, response to transient accelerations, RP2138 303
Acidity and alkalinity, pH standards, RP2153 418
Airplane mapping cameras, calibration, RP2108 1
Allshouse, Charles C., Jack M. Florence, Francis W. Glaze, Clarence H. Hahner, Absorption of near-infrared energy by certain glasses, RP2118 121
Aluminates, barium, action of water on, RP2149 381
Aluminum alloys, fatigue strength, RP2157 449
American Petroleum Institute-National Bureau of Standards hydrocarbons, freezing points and purity, and American Petroleum Institute-Standard, RP2122 173
4-Aminobenzophenone, dissociation constants, RP2162 489
Appel, William D., Florence H. Forziati, Walter K. Stone, John E. Rowen, Cotton powder for infrared transmission measurements, RP2116 109
Arsenic, arc spectrum, RP2144 346
Attenuators, cascade-connected, RP2129 231
Aitrod, Benjamin M., Martha A. Sherman, Strength of heat-resistant laminated plastics up to 300° C, RP2114 65

B

Baker, James L., John A. Pennett, Effects of prior static and dynamic stresses on the fatigue strength of aluminum alloys, RP2157 449
Ball, Anne F., Defoe C. Ginnings, Thomas B. Douglas, Heat capacity of sodium between 0° and 900° C, the triple point and heat of fusion, RP2110 23
Barium aluminates, action of water on, RP2149 381
Bates, Roger G., Gladys D. Pinching, Second dissociation constant of succinic acid from 0° to 50° C, RP2142 322
—, —, *Edgar R. Smith,* pH standards of high acidity and high alkalinity and the practical scale of pH, RP2153 418
—, —, First dissociation constant of succinic acid from 0° to 50° C and related thermodynamic quantities, RP2156 444
Beatty, Robert W., Cascade-connected attenuators, RP2129 231
Bennett, John A., James L. Baker, Effects of prior static and dynamic stresses on the fatigue strength of aluminum alloys, RP2157 449
Bernstein's polynomials, generalized to the infinite interval, RP2131 239
Beryllia porcelains, properties, RP2147 366
Black, Mason H., Donald Hubbard, Gerald F. Rynders, Electrode function (pH response), hygroscopicity, and chemical durability of soda-lead-oxide-silica glasses, RP2154 430
Blum, Joseph, A problem in precision cam design, RP2164 502
Bogue, R. H., W. C. Taylor, A sulfate susceptibility test for portland cements, RP2128 218
Boiling point of hydrocarbons, RP2151 406
Boiling points of aqueous solutions of dextrose, RP2158 458
Bone char, sieve analysis, RP2143 328
Boundary value problems, numerical solution, RP2132 245
Bower, Vincent E., John L. Torgesen, Edgar R. Smith, Boiling points of aqueous solutions of dextrose within the pressure range of 200 to 1,500 millimeters, RP2158 458
Bowman, Horace A., Determination of very small changes in rate over intervals of several days in mechanical timepieces, RP2127 218
Bridged-tee network for wide-range phase control, RP2123 193
Burdick, Milton D., Stewart M. Lang, Laurel H. Maxwell, Porcelains within the beryllia field of the system beryllia-alumina-zirconia, RP2147 366

C

Calorimeter, modified Bunsen ice, description, RP2110 23
Cam design, precision, RP2164 502
Cameras, airplane mapping, calibration, RP2108 1
Camin, David L., Alphonse F. Forziati, Frederick D. Rossini, Density, refractive index, boiling point, and vapor pressure of eight monoolefin (1-alkene), six pentadiene, and two cyclomonoolefin hydrocarbons, RP2151 406
Capillary tubes, metallic, measurement of internal diameters, RP2134 283
Carbon monoxide, and dioxide mass spectra, RP2135 288
Carbon monoxide, formed during oxygen absorption by alkaline pyrogallol, RP2112 43
Carlson, Elmer T., Thomas J. Chaconas, Lansing S. Wells, Study of the system barium oxide-aluminum oxide-water at 30° C, RP2149 381
Carpenter, Frank G., Victor R. Deitz, Methods of sieve analysis with particular reference to bone char, RP2143 328
Cartwright, Mary L., Forced oscillations in nonlinear systems, RP2166 514
Carwile, Nesbit L., Glenn W. Geil, Tensile properties of ingot iron at low temperatures, RP2119 129
Case, Frank A., Francis E. Washer, Calibration of precision airplane mapping cameras, RP2108 1
Cathodic protection, RP2148 373
Cement, portland, heat of hydration, RP2152 411
Cement, portland, sulfate susceptibility test, RP2128 223
Chaconas, Thomas J., Elmer T. Carlson, Lansing S. Wells, Study of the system barium oxide-aluminum oxide-water at 30° C, RP2149 381
Chemical durability of soda-lead-oxide-silica glasses, RP2154 430
Chlorofluoromethane, infrared spectrum, RP2125 204
Collagen and leather, compressibility, RP2160 468
Collett, Charles T., John C. Hughes, Francis C. Morey, Measurement of the internal diameters of metallic capillary tubes, RP2134 283
Copper, high-purity, creep, RP2121 153
Combustion efficiency, determination of by exhaust gas analysis, RP2117 113
Compressibility of leather and collagen, RP2160 468
Cotton powder, infrared transmission measurements, RP2116 109

D

Page

Dahl, Andrew I., Ernest F. Fiock, Response characteristics of temperature-sensing elements for use in the control of jet engines, RP2136 292
Dean, Helen M., Fred L. Mohler, Laura Williamson, Total ionization of hydrocarbons from mass spectral data, RP2130 235
Deitz, Victor R., Frank G. Carpenter, Methods of sieve analysis with particular reference to bone char, RP2143 328
Density of hydrocarbons, RP2151 406
Deuteromethanes, mass spectra, RP2155 441
Dextrose and sucrose solutions, dielectric constants, RP2137 299
Dextrose, boiling points of aqueous solutions, RP2158 458
Dextrose, stability at varying pH, RP2124 200
Diameter, internal, of metallic capillary tubes, measurement, RP2134 283
Dibeler, Vernon H., Fred L. Mohler, Edmund J. Wells, Jr., Robert M. Reese, Mass spectra of some simple isotopic molecules, RP2135 288
—, —, Mass spectra of the deuteromethanes, RP2155 441
Dielectric constants of solutions of dextrose and sucrose, RP2137 299
Diethylbenzenes, use as test mixtures, RP2140 315
Digges, Thomas G., William D. Jenkins, Creep of high-purity copper RP2121 153
Diolefins, density, refractive index, boiling point and vapor pressure, RP2151 140
Dirichlet systems L-series, real roots of, RP2165 505
Dissociation constant of succinic acid:
RP2142 322
RP2156 444
Dissociation constants of 4-aminobenzophenone, RP2162 489
Distillation method for determination of water in rubber, RP2146 362
Distillation test mixtures, RP2140 315
Douglas, Thomas B., Defoe C. Ginnings, Anne F. Ball, Heat capacity of sodium between 0° and 900° C, the triple point and heat of fusion, RP2110 23

E

Eigenvalue problems, numerical solution:
RP2132 245
RP2133 255
Electrode deterioration in transmit-receive tubes, RP2139 310
Electrode function of soda-lead-oxide-silica glasses, RP2154 430
Engine fuels, effect of pressure on octane rating, RP2120 148
Exhaust gas, gravimetric analysis, RP2117 113

F

Fatigue strength of aluminum alloys, RP2157 449
Feder, Donald P., Tracing of Skew rays, RP2113 61
Fiock, Ernest F., Andrew I. Dahl, Response characteristics of temperature-sensing elements for use in the control of jet engines, RP2136 292
Florence, Jack M., Charles C. Allshouse, Francis W. Glaze, Clarence H. Hahner, Absorption of near-infrared energy by certain glasses, RP2118 121
Forziati, Alphonse F., David L. Camin, Frederick D. Rossini, Density, refractive index, boiling point, and vapor pressure of eight monoolefin (1-alkene), six pentadiene, and two cyclomonoolefin hydrocarbons, RP2151 406
Forziati, Florence H., Walter K. Stone, John W. Rowen, William D. Appel, Cotton powder for infrared transmission measurements, RP2116 109
Freezing points and purity of API-Standard and API-NBS hydrocarbons, RP2122 173
French, Judson C., Electrode deterioration in transmit-receive tubes, RP2139 310
Fuels, engine, effect of pressure on octane rating, RP2120 148
Fur skin, deterioration studies, RP2141 317

G

Galvanic couples, electrical relations in, RP2148 373
Gas analysis, formation of carbon monoxide during oxygen absorption by alkaline pyrogallol, RP2112 43
Gas turbine combustion chambers analysis of exhaust gas, RP2117 113
Geil, Glenn W., Nesbit L. Carwile, Tensile properties of ingot iron at low temperatures, RP2119 129
Ginnings, Defoe C., Thomas B. Douglas, Anne F. Ball, Heat capacity of sodium between 0° and 900° C, the triple point and heat of fusion, RP2110 23
Glass wool and other porous media, permeability, RP2150 398
Glasses, soda-lead-oxide-silica, RP2154 430
Glaze, Francis W., Jack M. Florence, Charles C. Allshouse, Clarence H. Hahner, Absorption of near-infrared energy by certain glasses, RP2118 121

H

Hahner, Clarence H., Jack M. Florence, Charles C. Allshouse, Francis W. Glaze, Absorption of near-infrared energy by certain glasses, RP2118 121
Halpern, Carl, Willmer W. Ruegg, Gravimetric analysis of exhaust gas from gas turbine combustion chambers, RP2117 113
Hardwood fibers, resin bonding in offset papers, RP2126 208
Heat capacity of sodium, RP2110 23
Heat of hydration of portland cement, RP2152 411
Heat-resistant laminated plastics, strength, RP2114 65
Holler, H. D., Some electrical relations in galvanic couples, RP2148 373
Houterman, Elizabeth R., Edward T. Steiner, Aging of Karakul and seal fur skins, RP2141 317
Hubbard, Donald, Mason H. Black, Gerald F. Rynders, Electrode function (pH response), hygroscopicity, and chemical durability of soda-lead-oxide-silica glasses, RP2154 430

Page

Hughes, John C., Charles T. Collett, Francis C. Morey, Measurement of the internal diameters of metallic capillary tubes, RP2134 ... 283
Humidity, apparatus for producing known, RP2145 ... 357
Hydrocarbons, density, refractive index, boiling point, and vapor pressure, RP2151 ... 406
Hydrocarbons, ionization of, from mass spectral data, RP2130 ... 235
Hydrogens, isotopic, mass spectra, RP2135 ... 288
Hygrometers, testing, RP2145 ... 357

I

Ierall, Arthur S., Attenuation of oscillatory pressures in instrument lines, RP2115 ... 85
—, Permeability of glass wool and other highly porous media, RP2150 ... 398
Infrared energy absorption by certain glasses, RP2118 ... 121
Infrared spectrum of chlorofluoromethane, RP2125 ... 204
Ingot iron, tensile properties, RP2119 ... 129
Ionization constant of succinic acid:
RP2142 ... 322
RP2156 ... 444
Ionization of hydrocarbons from mass spectral data, RP2130 ... 235
Iron oxide and manganese, X-ray study, RP2111 ... 35

J

Janes, M. Elizabeth, Anton J. Streiff, Laurel F. Soule, Charlotte M. Kennedy, Vincent A. Sedlak, Charles B. Willingham, Frederick D. Rossini, Purification, purity, and freezing points of 29 hydrocarbons of the API-Standard and API-NBS series, RP2122 ... 173
Jenkins, William D., Thomas G. Digges, Creep of high-purity copper, RP2121 ... 153
Jet engines, control of temperature, RP2136 ... 292

K

Karakul and seal fur aging studies, RP2141 ... 317
Kennedy, Charlotte M., Anton J. Streiff, Laurel F. Soule, M. Elizabeth Janes, Vincent A. Sedlak, Charles B. Willingham, Frederick D. Rossini, Purification, purity, and freezing points of 29 hydrocarbons of the API-Standard and API-NBS series, RP2122 ... 173
Kilday, Marthada V., A quantitative study of the carbon monoxide formed during the absorption of oxygen by alkaline pyrogallol, RP2112 ... 43
Knock rating, effect of pressure and other variables, RP2120 ... 148
Kroll, Wilhelmina D., Samuel Levy, Response of accelerometers to transient accelerations, RP2138 ... 303

L

Lamb, Mary A., Earle K. Plyler, Infrared spectrum of chlorofluoromethane, RP2125 ... 204
Laminated plastics, flexural properties, RP2114 ... 65
Lanczos, Cornelius, An iteration method for the solution of the eigenvalue problem of linear differential and integral operators, RP2133 ... 255
Lang, Stewart M., Laurel H. Maxwell, Milton D. Burdick, Porcelains, within the beryllia field of the system beryllia-alumina-zirconia, RP2147 ... 366
Latin square, use in radioactivity measurements, RP2163 ... 496
Leather and collagen, compressibility, RP2160 ... 468
Lenses, prism effect in, RP2108 ... 1
Leredahl, William J., Effects of pressure and other variables on determinations of octane number, RP2120 ... 148
Levy, Samuel, Wilhelmina D. Kroll, Response of accelerometers to transient accelerations, RP2138 ... 303
Low temperatures, tensile properties of ingot iron at, RP2119 ... 129

M

Magnetic testing, permeameter for, RP2109 ... 17
Malmberg, Cyrus G., Arthur A. Maryott, Dielectric constants of aqueous solutions of dextrose and sucrose, RP2137 ... 299
Manganese and iron oxide, X-ray study, RP2111 ... 35
Mapping cameras, airplane, calibration, RP2108 ... 1
Maryott, Arthur A., Cyrus G. Malmberg, Dielectric constants of aqueous solutions of dextrose and sucrose, RP2137 ... 299
Mass spectra of isotopic molecules, RP2135 ... 288
Mass spectra of the deuteromethanes, RP2155 ... 441
Mass spectral data, total ionization of hydrocarbons from, RP2130 ... 235
Mauer, Floyd A., H. F. McMurdie, Barbara M. Sullivan, High-temperature X-ray study of the system Fe_2O_3—Mn_2O_3, RP2111 ... 35
Maxwell, Laurel H., Stewart M. Lang, Milton D. Burdick, Porcelains within the beryllia field of the system beryllia-alumina-zirconia, RP2147 ... 366
McDonald, Emma J., Stability of dextrose solutions of varying pH, RP2124 ... 200
McMurdie, H. F., Barbara M. Sullivan, Floyd A. Mauer, High-temperature X-ray study of the system Fe_2O_3—Mn_2O_3, RP2111 ... 35
Meggers, William F., Allen G. Shenstone, Charlotte E. Moore, First spectrum of arsenic, RP2144 ... 346
—, *Bourdon F. Scribner*, Arc and spark spectra of technetium, RP2161 ... 476
Milne, W. E., Numerical determination of characteristic numbers, RP2132 ... 245
Missimer, Joshua K., Merle B. Shaw, Martin J. O'Leary, Resin bonding of hardwood fibers in offset papers, RP2126 ... 208
Mohler, Fred L., Laura Williamson, Helen M. Dean, Total ionization of hydrocarbons from mass spectral data, RP2130 ... 235
—, *Vernon H. Dibeler, Edmund J. Wells, Jr., Robert M. Reese*, Mass spectra of some simple isotopic molecules, RP2135 ... 288
—, —, Mass spectra of the deuteromethanes, RP2155 ... 441
Moisture in rubber, determination, RP2146 ... 362
Molecules, isotopic, mass spectra, RP2135 ... 288
Moore, Charlotte, William F. Meggers, Allen G. Shenstone, First spectrum of arsenic, RP2144 ... 346
Morey, Francis C., Charles T. Collett, John C. Hughes, Measurement of the internal diameters of metallic capillary tubes, RP2134 ... 283

N

Page

Newman, Edwin S., A study of the determination of the heat of hydration of portland cement, RP2152 ... 411
Nonlinear systems, forced oscillations in, RP2166 ... 514
Numerical methods, determination of characteristic numbers:
RP2132 ... 245
RP2133 ... 255

O

Octane number, effect of pressure and other variables, RP2120 ... 148
Offset papers, resin bonding of hardwood fibers in, RP2126 ... 208
O'Leary, Martin J., Merle B. Shaw, Joshua K. Missimer, Resin bonding of hardwood fibers in offset papers, RP2126 ... 208
Olefins, density, refractive index, boiling point, and vapor pressure, RP2151 ... 406
Oscillations, forced, in nonlinear systems, RP2166 ... 514
Oscillatory pressures, attentuation of, in instrument lines, RP2115 ... 85
Oxygen analysis, formation of carbon monoxide with alkaline pyrogallol, RP2112 ... 43

P

Papers, offset, resin bonding of hardwood fibers in, RP2126 ... 208
Pyrogallol, alkaline, carbon monoxide formation during absorption of oxygen by, RP2112 ... 43
Pawley, Myron G., Wide-range phase control attentuation by adjustable impedance in a resistance-loaded bridged-tee network, RP2123 ... 193
Permeability of glass wool and other porous media, RP2150 ... 398
Permeameter, magnetic testing, RP2109 ... 17
Peters, C. Wilbur, Earle K. Plyler, Wavelengths for calibration of prism spectrometers, RP2159 ... 462
pH standards of acidity and alkalinity, RP2153 ... 418
Phase control, wide-range, RP2123 ... 193
Pinching, Gladys D., Rober G. Bates, Second dissociation constant of succinic acid from 0° to 50° C, RP2142 ... 322
—, —, *Edgar R. Smith*, pH standards of high acidity and high alkalinity and the practical scale of pH, RP2153 ... 418
—, —, First dissociation constant of succinic acid from 0° to 50° C and related thermodynamic quantities, RP2156 ... 444
Plastics, laminated, heat resistant, strength, RP2114 ... 65
Plyler, Earle K., Mary A. Lamb, Infrared spectrum of chlorofluoromethane, RP2125 ... 204
—, *C. Wilbur Peters*, Wavelengths for calibration of prism spectrometers, RP2159 ... 462
Polynomials, Bernstein's, generalized to the infinite interval, RP2131 ... 239
Porcelains, oxide, properties, RP2147 ... 366
Portland cement, heat of hydration, RP2152 ... 411
Portland cements, sulfate susceptibility test, RP2128 ... 223
Pressures, oscillatory, attenuation of, in instrument lines, RP2115 ... 85
Prism spectrometers, wavelengths for calibration, RP2159 ... 462

R

Radioactivity, standard calibration, RP2163 ... 496
Reese, Robert M., Vernon H. Dibeler, Fred L. Mohler, Edmund J. Wells, Jr., Mass spectra of some simple isotopic molecules, RP2135 ... 288
Refractive index of hydrocarbons, RP2151 ... 406
Resin bonding of hardwood fibers in offset papers, RP2126 ... 208
Roots, real, of dirichlet L-series, RP2165 ... 505
Rosser, J. Barkley, Real roots of real dirichlet L-series, RP2165 ... 505
Rossini, Frederick D., Anton J. Streiff, Laurel F. Soule, Charlotte M. Kennedy, M. Elizabeth Janes, Vincent A. Sedlak, Charles B. Willingham, Purification, purity, and freezing points of 29 hydrocarbons of the API-Standard and API-NBS series, RP2122 ... 173
—, *Alphonse F. Forziati, David L. Camin*, Density, refractive index, boiling point, and vapor pressure of eight monoolefin (1-alkene), six pentadiene, and two cyclomonoolefin hydrocarbons, RP2151 ... 406
Rowen, John W., Florence H. Forziati, Walter K. Stone, William D. Appel, Cotton powder for infrared transmission measurements, RP2116 ... 109
Rubber, analysis for water, RP2146 ... 362
Ruegg, Willmer W., Carl Halpern, Gravimetric analysis of exhaust gas from gas turbine combustion chambers, RP2117 ... 113
Rynders, Gerald F., Donald Hubbard, Mason H. Black, Electrode function (pH response), hygroscopicity, and chemical durability of soda-lead-oxide-silica glasses, RP2154 ... 430

S

Sager, Elizabeth E., Iris J. Siewers, Dissociation constant of 4-aminobenzophenone calculated from ultraviolet spectra at several temperatures, RP2162 ... 489
Sanford, Raymond L., Philip H. Winter, A permeammeter for magnetic testing at magnetizing forces up to 300 oersteds, RP2109 ... 17
Screen analysis, bone char, RP2143 ... 328
Scribner, Bourdon F., William F. Meggers, Arc and spark spectra of technetium, RP2161 ... 476
Seal and Karakul fur aging studies, RP2141 ... 317
Sedlak, Vincent A., Anton J. Streiff, Laurel F. Soule, Charlotte M. Kennedy, M. Elizabeth Janes, Charles B. Willingham, Frederick D. Rossini, Purification, purity, and freezing points of 29 hydrocarbons of the API-Standard and API-NBS series, RP2122 ... 173
—, *Charles B. Willingham*, Test mixtures for distillation at atmospheric and reduced pressure, RP2140 ... 315
Seliger, Howard H., A new method of radioactive standard calibration, RP2163 ... 496
Shaw, Merle B., Martin J. O'Leary, Joshua K. Missimer, Resin bonding of hardwood fibers in offset papers, RP2126 ... 208
Sherman, Martha A., Benjamin M. Axilrod, Strength of heat-resistant laminated plastics up to 300° C, RP2114 ... 65
Shenstone, Allen G., William F. Meggers, Charlotte E. Moore, First spectrum of arsenic, RP2144 ... 346
Sieve analysis, with reference to bone char, RP2143 ... 328

Page

Siewers, Iris J., Elizabeth E. Sager, Dissociation constants of 4-aminobenzophenone, calculated from ultraviolet spectra at several temperatures, RP2162 ... 489
Skew rays, tracing, RP2113 ... 61
Smith, Edgar R., Roger G. Bates, Gladys D. Pinching, pH standards of high acidity and high alkalinity and the practical scale of pH, RP2153 ... 418
—, *John L. Torgesen, Vincent E. Bower*, Boiling points of aqueous solutions of dextrose within the pressure range of 200 to 1,500 millimeters, RP2158 ... 458
Soda-lead-oxide-silica glasses, electrode function, RP2154 ... 430
Sodium, heat capacity, RP2110 ... 23
Soule, Laurel F., Anton J. Streiff, Charlotte M. Kennedy, M. Elizabeth Janes, Vincent A. Sedlak, Charles B. Willingham, Frederick D. Rossini, Purification, purity, and freezing points of 29 hydrocarbons of the API-Standard and API-NBS series, RP2122 ... 173
Spectra, arc and spark, of technetium, RP2161 ... 476
Spectra, mass, of deuteromethanes, RP2155 ... 441
Spectra, mass, of isotopic molecules, RP2135 ... 288
Spectral data, mass, total ionization of hydrocarbons from, RP2130 ... 235
Spectrometers, prism, wavelengths for calibration, RP2159 ... 462
Spectrum, arsenic, RP2144 ... 346
Standard, radioactive, calibration of, RP2163 ... 496
Standards, pH, of acidity and alkalinity, RP2153 ... 418
Steiner, Edward T., Elizabeth R. Hostermann, Aging of Karakul and seal fur skins, RP2141 ... 317
Stone, Walter K., Florence H. Forziati, John W. Rowen, William D. Appel, Cotton powder for infrared transmission measurements, RP2116 ... 109
Streiff, Anton J., Laurel F. Soule, Charlotte M. Kennedy, M. Elizabeth Janes, Vincent A. Sedlak, Charles B. Willingham, Frederick D. Rossini, Purification, purity, and freezing points of 29 hydrocarbons of the API-Standard and API-NBS series, RP2122 ... 173
Stress, prior static and dynamic, effect on the fatigue strength of aluminum alloys, RP2157 ... 449
Succinic acid, second dissociation constant:
RP2142 ... 322
RP2156 ... 444
Sucrose and dextrose solutions, dielectric constants, RP2137 ... 299
Sulfate susceptibility test for portland cements, RP2128 ... 223
Sullivan, Barbara M., H. F. McMurdie, Floyd A. Mauer, High-temperature X-ray study of the system Fe_2O_4-Mn_3O_4, RP2111 ... 35
Szasz, Otto, Generalization of S. Bernstein's polynomials to the infinite interval, RP2131 ... 239

T

Taylor, W. C., R. H. Pogue, A sulfate susceptibility test for portland cements, RP2128 ... 218
Technetium, arc and spark spectra, RP2161 ... 476
Temperature control in jet engines, RP2136 ... 292
Tensile properties of ingot iron, RP2119 ... 129
Thermocouples, response rates, RP2136 ... 292
Thermodynamic constants of succinic acid, RP2156 ... 444
Timepieces, mechanical, rate of drift, RP2127 ... 218
Toluene, determination of moisture in rubber by distillation with, RP2146 ... 362
Torgesen, John L., Vincent E. Bower, Edgar R. Smith, Boiling points of aqueous solutions of dextrose with the pressure range of 200 to 1,500 millimeters, RP2158 ... 458
Transmit-receive tubes, electrode deterioration, discharge, RP2139 ... 310
Transmittance of near-infrared by glasses, RP2118 ... 121
Tryon, Max, An improved apparatus for determining moisture in rubber by distillation with toluene, RP2146 ... 362
Tubes, metallic capillary, measurement of internal diameters, RP2134 ... 283
Turbine, gas, analysis of exhaust gas, RP2117 ... 113

U

Ultraviolet absorption spectra of some benzophenones, RP2162 ... 489

V

Vapor pressure of hydrocarbons, RP2151 ... 406
Vapor pressures of aqueous solutions of dextrose, RP2158 ... 458

W

Washer, Francis E., Frank A. Case, Calibration of precision airplane mapping cameras, RP2108 ... 1
Water in rubber, distillation method for determination, RP2146 ... 362
Weir, Charles E., High-pressure apparatus for compressibility studies and its application to measurements on leather and collagen, RP2160 ... 468
Wells, Edmund J., Jr., Vernon H. Dibeler, Fred L. Mohler, Robert M. Reese, Mass spectra of some simple isotopic molecules, RP2150 ... 398
Wells, Lansing S., Elmer T. Carlson, Thomas J. Chaconas, Study of the system barium oxide-aluminum oxide-water at 30° C, RP2149 ... 381
Werler, Arnold, Recirculating apparatus for testing hygrometers, RP2145 ... 357
Williamson, Lewis, Fred L. Mohler, Helen M. Dean, Total ionization of hydrocarbons from mass spectral data, RP2130 ... 235
Willingham, Charles B., Anton J. Streiff, Laurel F. Soule, Charlotte M. Kennedy, M. Elizabeth Janes, Vincent A. Sedlak, Frederick D. Rossini, Purification, purity, and freezing points of 29 hydrocarbons of the API-Standard and API-NBS series, RP2122 ... 173
—, *Vincent A. Sedlak*, Test mixtures for distillation at atmospheric and reduced pressure, RP2140 ... 315
Winter, Philip H., Raymond L. Sanford, A permeammeter for magnetic testing at magnetizing forces up to 300 oersteds, RP2109 ... 17

X

X-ray diffraction study of manganese and iron oxide, RP2111 ... 35

eering
rary
RP
JAN 3

Journal of Research

of the

National Bureau of Standards

US

DECEMBER 1950

VOLUME 45 NUMBER 6

U. S. DEPARTMENT OF COMMERCE
Charles Sawyer, Secretary
NATIONAL BUREAU OF STANDARDS
E. U. Condon, Director

DECEMBER 1950
VOLUME 45
NUMBER 6

JOURNAL OF RESEARCH

of the

NATIONAL BUREAU OF STANDARDS

PERIODICALS OF THE NATIONAL BUREAU OF STANDARDS

As the principal agency of the Federal Government for fundamental research in physics, chemistry, mathematics, and engineering, the National Bureau of Standards conducts projects in fourteen fields: electricity, optics, metrology, heat and power, atomic and radiation physics, chemistry, mechanics, organic and fibrous materials, metallurgy, mineral products, building technology, applied mathematics, electronics, and radio propagation. The Bureau has custody of the national standards of measurement and conducts research leading to the improvement of scientific and engineering standards and of techniques and methods of measurement. Testing methods and instruments are developed; physical constants and properties of materials are determined; and technical processes are investigated.

JOURNAL OF RESEARCH

Internationally known as a leading scientific periodical, the Journal presents research papers by authorities in the specialized fields of physics, mathematics, chemistry, and engineering. Complete details of the work are presented, including laboratory data, experimental procedures, and theoretical and mathematical analyses. Each of the monthly issues averages 85 two-column pages; illustrated. Annual subscription: domestic, $4.50; foreign, $5.50.

TECHNICAL NEWS BULLETIN

Summaries of current research at the National Bureau of Standards are published each month in the Technical News Bulletin. The articles are brief, with emphasis on the results of research, chosen on the basis of their scientific or technologic importance. Lists of all Bureau publications during the preceding month are given, including Research Papers, Handbooks, Applied Mathematics Series, Building Materials and Structures Reports, and Circulars. Each issue contains 12 or more two-column pages; illustrated. Annual subscription: domestic, $1.00; foreign, $1.35.

BASIC RADIO PROPAGATION PREDICTIONS

The Predictions provide the information necessary for calculating the best frequencies for communication between any two points in the world at any time during the given month. The data are important to all users of long-range radio communications and navigation, including broadcasting, air line, steamship, and wireless services, as well as to investigators of radio propagation and ionosphere. Each issue, covering a period of one month, is released three months in advance and contains 16 large pages, including pertinent charts, drawings, and tables. Annual subscription: domestic, $1.00; foreign, $1.25.

Order all publications from the Superintendent of Documents,
U. S. Government Printing Office, Washington 25, D. C.

The printing of this publication has been approved by the Director of the Bureau of the Budget, April 5, 1950

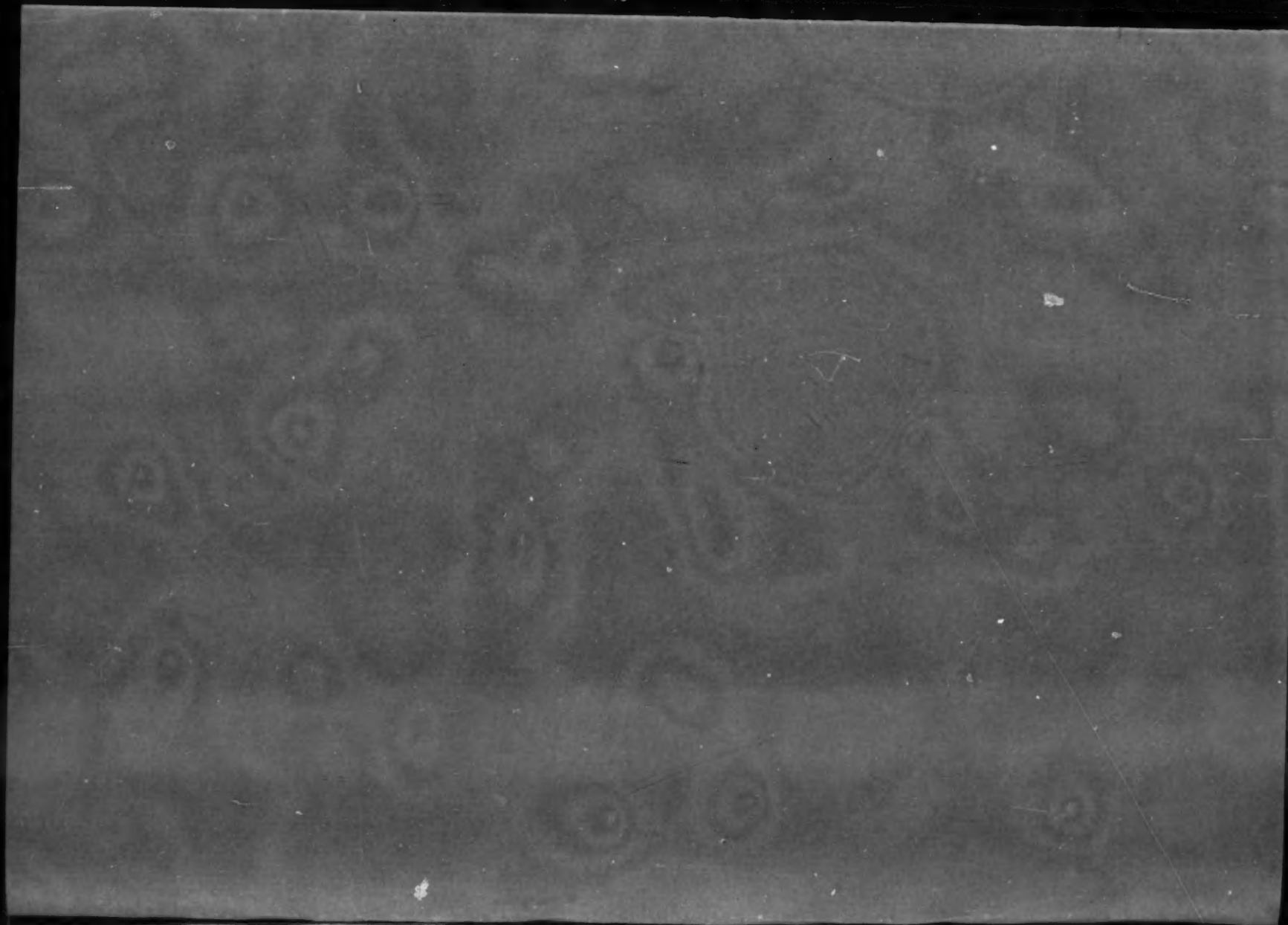

Journal of Research of the National Bureau of Standards Vol. 45, No. 6 December 1950

Contents

	Page
Mass spectra of the deuteromethanes. Vernon H. Dibeler and Fred L. Mohler. RP2155	441
First dissociation constant of succinic acid from 0° to 50° C, and related thermodynamic quantities. Gladys D. Pinching and Roger G. Bates. RP2156	444
Effects of prior static and dynamic stresses on the fatigue strength of aluminum alloys. John A. Bennett and James L. Baker. RP2157	449
Boiling points of aqueous solutions of dextrose within the pressure range of 200 to 1,500 millimeters. John L. Torgesen, Vincent E. Bower, and Edgar R. Smith. RP2158	458
Wavelengths for calibration of prism spectrometers. Earle K. Plyler and C. Wilbur Peters. RP2159	462
High-pressure apparatus for compressibility studies and its application to measurements on leather and collagen. Charles E. Weir. RP2160	468
Arc and spark spectra of technetium. William F. Meggers and Bourdon F. Scribner. RP2161	476
Dissociation constants of 4-aminobenzophenone calculated from ultraviolet spectra at several temperatures. Elizabeth E. Sager and Iris J. Stewers. RP2162	489
A new method of radioactive standard calibration. Howard H. Seliger. RP2163	496
A problem in precision cam design. Joseph Blum. RP2164	502
Real roots of real dirichlet L-series. J. Barkley Rosser. RP2165	505
Forced oscillations in nonlinear systems. Mary L. Cartwright. RP2166	514
Index to volume 45 (July to December 1950, Research Papers RP2108 to 2166)	519

The above Research Papers may be obtained from the Superintendent of Documents, Government Printing Office, Washington 25, D. C. as follows: RP2155, 10¢; RP2156, 10¢; RP2157, 10¢; RP2158, 10¢; RP2159, 10¢; RP2160, 10¢; RP2161, 10¢; RP2162, 10¢; RP2163, 10¢; RP2164, 10¢; RP2165, 10¢; RP2166, 10¢.

For sale by the Superintendent of Documents, U. S. Government Printing Office, Washington 25, D. C. Price 75 cents
$4.50 per year on subscription

UNITED STATES GOVERNMENT PRINTING OFFICE, WASHINGTON : 1950